

ANALYTICAL MODELING OF FUEL CONSUMPTION
AND REGULATED EXHAUST EMISSION RATES FOR
TRUCKS

BY

SALAH AHMED MOHAMED ELMOSELHY
ELMAGHAZY

INTERNATIONAL ISLAMIC UNIVERSITY MALAYSIA

2014

ANALYTICAL MODELING OF FUEL
CONSUMPTION AND REGULATED EXHAUST
EMISSION RATES FOR TRUCKS

BY

SALAH AHMED MOHAMED ELMOSELHY
ELMAGHAZY

A thesis submitted in fulfilment of the requirement for
the degree of Doctor of Philosophy in Engineering

Kulliyyah of Engineering
International Islamic University Malaysia

MAY 2014

ABSTRACT

Climate change due to greenhouse gas emissions led to new vehicle emissions standards which in turn led to a call for vehicle technologies to meet these standards. Modeling of vehicle fuel consumption and emissions emerged as an effective tool to help developing and assessing such technologies. Although vehicle analytical models are favourable in many cases due to describing the physical phenomena associated with vehicle operation based on the principles of physics and with explainable mathematical trends and with extendable modeling to other vehicle types, no analytical model has been developed and experimentally validated as yet of diesel fuel consumption and exhaust emissions rate. The present study analytically models diesel fuel consumption rate microscopically for the accelerating, cruising and decelerating modes of driving a vehicle and models diesel regulated emissions rate for the cruising mode of driving a vehicle. In order to make these models, an analytical model of the following subsystems has been made: (i) intake manifold taking the flexibility of crankshaft and air density into account, (ii) supercharging diesel centrifugal compressor, (iii) multi-cylinder supercharged diesel engine, (iv) diesel fuel system and engine power, (vi) exhaust system and the percentage of unburned fuel. Sensitivity analysis has been conducted for simplifying the models in order to fit the INTEGRATION software and traffic simulator. The models have been validated experimentally against field data. For the rate of diesel fuel mass flow, the average percentage of deviation was 1.8% for all standard cycles outperforming widely recognized models such as the CMEM and VT-Micro. The simulated results have been analyzed statistically for the rate of diesel fuel mass flow with coefficient of determination and relative error of 96% and 1.2%, respectively. The average percentage of deviation of 7% 1.7%, 1.9%, 2%, and 10.6% for the diesel engine power, CO emission, NO_x emission, HC emission, and percentage of unburned fuel respectively, for all Freeway cycles outperforming widely recognized models such as the CMEM and VT-Micro. The simulated results have been analyzed statistically as well with coefficient of determination of 73%, 99%, 99%, 83%, and 70% respectively. The corresponding relative error has been 7%, 3%, 1.7%, 2%, and 10.6% respectively. Moreover, the developed analytical models of the intake manifold gas speed dynamics, in-cylinder gas speed dynamics, supercharging compressor power, supercharging compressor mechanical efficiency, and supercharged air density have been experimentally validated using case studies with an average of deviation from field data of 12.6%, 11%, 3%, 8%, and 3.7%, respectively. The simulated results have been analyzed statistically as well with relative error of 12.6%, 11%, 3%, 8%, and 3.7%, respectively. In addition to devising two new classifications, which are the formulation approach-based modelling and main input variable-based modelling, the models developed in this study are (a) widely valid models which are not restricted to a specific dataset, (b) an effective tool to quickly judge whether the related experimental measurements make sense or not, (c) show which chemical reaction within the powertrain kinetically influences significantly emissions rate.



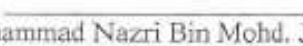
Keywords: Vehicle Fuel Consumption; Vehicle Regulated Emissions; Modeling; Diesel Powertrain

ملخص البحث

تغير المناخ بسبب انبعاث غازات الاحتباس الحراري أدى إلى وضع معايير جديدة للمعدل المسموح به لانبعاث الغازات من السيارات ، الأمر الذي أدى بدوره إلى الدعوة لتطوير تقنيات أنظمة محركات السيارات لتلبية هذه المعايير. ظهرت نمذجة استهلاك الوقود وانبعاثات المركبات باعتبارها أداة فعالة لتطوير وتقييم هذه التقنيات. على الرغم من أن النماذج التحليلية مفضلة في حالات عديدة ، لكونها تمكن من توصيف الظواهر الفيزيائية المرتبطة بنظام حركة السيارة على نحو شامل على أساس مبادئ الفيزياء مع ميزة وضوح التفسير الرياضي لنتائج النمذجة ، إلا أنه لم يتم حتى الآن عمل نموذج تحليلي والتأكد من صحته باستخدام النتائج المعملية لمعدل استهلاك الوقود ومعدل انبعاث الغازات من السيارات التي تعمل بوقود الديزل. في هذه الدراسة تم عمل نموذج تحليلي لنمذجة نظام محرك السيارات التي تعمل بوقود الديزل ولنمذجة معدل استهلاك وقود السيارات على المستوى المجهرى لحالات قيادة السيارة أثناء التسارع وتحرك السيارة بسرعة ثابتة والتباطؤ ولنمذجة معدل انبعاث الانبعاثات على المستوى المجهرى أثناء تحرك السيارة بسرعة ثابتة. من أجل عمل هذه النماذج التحليلية تم عمل النماذج التحليلية للأجزاء التالية: (1) مشعب السحب لتوليد القوة الديزل ذات الشحن الإضافي للهواء مع أخذ مرونة العمود المرفقي وكثافة الهواء في الاعتبار، (2) شاحن الهواء الإضافي لمحرك الديزل والذي يعمل بالطرد المركزي وبه مشنت ذو دوارات ريش ، (3) محرك الديزل ذو الشحن الإضافي للهواء ومتعدد الأسطوانات ، (4) نظام وقود الديزل وقوة المحرك ، (5) نظام العادم للمحركات التي تعمل بوقود الديزل ونسبة الوقود الغير محترق. ولقد تم اجراء تحليل حساسية للنماذج التي تم عملها لمعدل استهلاك وقود الديزل ومعدلات انبعاث العادم للتغير في قيم المتغيرات الموجودة في النموذج التحليلي من أجل تبسيطه بحيث يمكن استخدامه في نموذج المحاكاة المسمى " INTEGRATION " . وقد تم التحقق من صحة النماذج التحليلية المقدمة باستخدام النتائج المعملية. بالنسبة لمعدل استهلاك وقود الديزل كان متوسط النسبة المئوية للانحراف 1.8% لجميع دورات التشغيل المعتمدة فائقة في الأداء أداء نماذج علمية واسعة الانتشار مثل نموذج " CMEM " و نموذج " VT-Micro " . ولقد تم تحليل نتائج المحاكاة احصائيا وكان معامل التحديد والخطأ النسبي المناظر لتلك النتائج 96% و 1.2% على الترتيب. كذلك كان متوسط النسبة المئوية للانحراف 7% ، 1.7% ، 1.9% ، 2% ، و 10.6% لقوة المحرك ، ولمعدل انبعاث CO ، ولمعدل انبعاث NOx ، ولمعدل انبعاث HC ، ولنسبة الوقود الغير محترق ، على الترتيب وذلك لجميع دورات التشغيل المعتمدة باسم الطريق الحر فائقة في الأداء أداء نماذج علمية واسعة الانتشار مثل نموذج " CMEM " و نموذج " VT-Micro " . ولقد تم كذلك تحليل نتائج المحاكاة احصائيا وكان معامل التحديد 73% ، 99% ، 99% ، 83% ، 70% على الترتيب. كذلك كان الخطأ النسبي المناظر لتلك النتائج 7% ، 3% ، 1.7% ، 2% ، 10.6% على الترتيب. بالإضافة لهذا فقد تم التحقق من صحة النماذج التحليلية لمعدل تسارع سرعة الغاز في مشعب السحب ، لمعدل تسارع سرعة الغاز في مشعب السحب داخل اسطوانة محرك الديزل ، للقوة المطلوبة لتشغيل شاحن الهواء الإضافي لمحرك الديزل والذي يعمل بالطرد المركزي وبه مشنت ذو دوارات ريش ، للكفاءة الميكانيكية لتشغيل شاحن الهواء الإضافي لمحرك الديزل والذي يعمل بالطرد المركزي وبه مشنت ذو دوارات ريش ، ولكثافة الهواء المضغوط وتم ذلك باستخدام بيانات معملية عن طريق دراسات حالة وكان متوسط النسبة المئوية للانحراف 12.6% ، 11% ، 3% ، 8% ، 3.7% ، على الترتيب. ولقد تم كذلك تحليل نتائج المحاكاة احصائيا وكان الخطأ النسبي المناظر لتلك النتائج 12.67% ، 11% ، 3% ، 8% ، 3.7% على الترتيب. بالإضافة الى ابتكار تصنيفين جديدين لنمذجة معدل استهلاك الوقود و معدل اخراج العادم للسيارات ، وهما النمذجة حسب أسلوب الصياغة والنمذجة حسب المدخلات الرئيسية ، فان النماذج التحليلية التي تم عملها في هذه الدراسة تتميز بأنها: (أ) صالحة على نطاق واسع لا تقتصر صلاحيتها على مجموعة بيانات محدودة ومحددة ، (ب) وسيلة سريعة وغير مكلفة وذات كفاءة لتحديد معدل استهلاك الوقود و معدل اخراج العادم للسيارات التي تعمل بوقود الديزل كأداة فعالة للحكم على ما إذا كانت القياسات المعملية منطقية وصحيحة أم لا ، (ج) تظهر أي من التفاعلات الكيميائية داخل محرك الديزل يؤثر تفاعليا على معدل الانبعاثات بشكل أكبر.

APPROVAL PAGE

The thesis of Salah Ahmed Mohamed Elmoselhy Elmaghazy has been approved by the following:


Waleed Fekry Faris
Supervisor
Hesham Ahmed Rakha
Co-Supervisor, Virginia Polytechnic Institute and State University
Mirghani I. Ahmed
Internal Examiner
Mohammad Nurul Alam Hawlader
Internal Examiner
Mohammad Nazri Bin Mohd. Jaafar
External Examiner
Mohamad Fauzan Noordin
Chairman

DECLARATION

I hereby declare that this dissertation is the result of my own investigations, except where otherwise stated. I also declare that it has not been previously or concurrently submitted as a whole for any other degrees at IIUM or other institutions.

Salah Ahmed Mohamed Elmoselhy Elmaghazy

Signature



Date 15th of April 2014

INTERNATIONAL ISLAMIC UNIVERSITY MALAYSIA

**DECLARATION OF COPYRIGHT AND
AFFIRMATION OF FAIR USE OF UNPUBLISHED
RESEARCH**

Copyright © 2014 by International Islamic University Malaysia.
All rights reserved.

**ANALYTICAL MODELLING OF FUEL CONSUMPTION AND
REGULATED EMISSION RATES FOR TRUCKS**

I hereby affirm that the International Islamic University Malaysia (IIUM) holds all rights in the copyright of this Work and henceforth any reproduction or use in any form or by means whatsoever is prohibited without the written consent of IIUM. No part of this unpublished research may be reproduced, stored in a retrieval system, or transmitted, in any form or by means, electronic, mechanical, photocopying, recording or otherwise without prior written permission of the copyright holder.

Affirmed by Salah Ahmed Mohamed Elmoselhy Elmaghazy.



Signature

15th of April 2014
Date

ACKNOWLEDGEMENTS

First and foremost, praise be to Allah, the Most Merciful and Most Compassionate, for helping me in completing this research work. Professor Waleed F. Faris is thanked for his supervision and for his help in coordinating this research between the IIUM and Virginia Tech. Professor Hesham A. Rakha is thanked as well for his helpful supervision and valuable guidance. I would like to thank as well Dr Raed M. Kafafy, Dr Moumen Idris, and the IIUM. The financial support provided by the IIUM for this research under research grant # RMGS 09-10 is thankfully acknowledged. The technical support provided by the Center for Sustainable Mobility at Virginia Polytechnic Institute and State University (Virginia Tech) is thankfully acknowledged as well. I would like as well to thank all the members of my family for everything they have done for me asking Allah to bless them and to reward them the best reward.

Salah Elmoselhy

TABLE OF CONTENTS

Abstract.....	ii
Abstract in Arabic.....	iii
Approval Page.....	iv
Declaration Page.....	v
Copyright Page.....	vi
Acknowledgement.....	vii
List of Tables.....	xiii
List of Figures.....	xvii
List of Abbreviations	xviii
CHAPTER 1: INTRODUCTION.....	1
1.1. Overview	1
1.2. Background.....	2
1.3. Problem Statement.....	3
1.4. Significance of Problem Statement.....	3
1.5. Research Philosophy.....	5
1.6. Research Objectives.....	5
1.7. Research Methodology	6
1.8. Research Scope	7
1.9. Dissertation Layout	7
CHAPTER 2: LITERATURE REVIEW.....	8
2.1 Overview	8
2.2. Vehicle Fuel Consumption and Emissions Modelling	8
2.2.1 Scale of the Input Variables-based Modeling	9
2.2.1.1 Microscopic Models	9
2.2.1.2 Macroscopic Models	12
2.2.1.3 Mesoscopic Models	15
2.2.2 Formulation Approach-based Modeling	17
2.2.2.1 Analytical models	17
2.2.2.2 Empirical models	21
2.2.2.3 Statistical models	23
2.2.2.4 Graphical models	25
2.2.3 Main Input Variable-based Modelling	28
2.2.3.1 Average speed models	28
2.2.3.2 Instantaneous speed models	30
2.2.3.3 Specific power models	33
2.2.4 State Variable Value-based Modelling	34
2.2.4.1 Crank-angle resolution-based models	35
2.2.4.2 Mean value-based models	36
2.2.5 Number of Dimensions-based Modelling	39
2.2.5.1 Zero/one dimensional/single zone models	39

2.2.5.2 Quasi dimensional models	41
2.2.5.3 Multi dimensional/multi zone models	43
2.3. Research Gap and Summary of Literature Review.....	45
CHAPTER 3: DIESEL POWERTRAIN INTAKE MANIFOLD ANALYTICAL MODEL.....	51
3.1. Overview.....	51
3.2. Intake Manifold Dynamic Pressure	51
3.3. Mass Flow Rate of Air Goes Into Cylinders.....	52
3.4. Mass Flow Rate of Air Goes Into Cylinders With a Flexible Crankshaft.....	57
3.5. Mass Flow Rate at the Throat of the Intake Manifold and Intake Manifold Dynamic Pressure	62
3.6. In-cylinder Gas Speed Formulation	72
3.7. Analytical Model of Intake Manifold Gas Speed Dynamics.....	74
3.7.1. The net forces.....	75
3.7.2. The rate of change of momentum within the control volume...	76
3.7.3. The net flow of momentum across the control volume surface	77
3.7.4. The total momentum.....	78
3.8. Analytical Model of the Supercharged Air Density.....	79
CHAPTER 4: SUPERCHARGING DIESEL CENTRIFUGAL COMPRESSOR WITH VANES-BASED DIFFUSER ANALYTICAL MODEL.....	81
4.1. Overview.....	81
4.2. Analytical Sub-model of Power Required to Drive Supercharging Diesel Centrifugal Compressor with Vanes-based Diffuser.....	82
4.3. Analytical Sub-model of Velocities at the Diffuser of the Supercharging Diesel Centrifugal Compressor.....	90
4.4. Analytical Sub-model of Efficiency of Supercharging Diesel Centrifugal Compressor with Vanes-based Diffuser.....	95
CHAPTER 5: DIESEL ENGINE ANALYTICAL MODEL.....	99
5.1. Overview.....	99
5.2. In-cylinder Gas Speed Dynamics	99
5.2.1. The net forces.....	100
5.2.2. The rate of change of momentum within the control volume.....	101
5.2.3. The net flow of momentum across the control volume surface.....	102
5.2.4. The total momentum.....	102
5.3. Fuel Mass Flow Rate in the Diesel Engine Fuel System.....	103
5.3.1. Analytical modeling of the steady speed-based fuel mass actual flow rate in diesel engines.....	103
5.3.2. Analytical modeling of the acceleration-based fuel mass	105

actual flow rate in diesel powertrain fuel system.....	
5.4. Brake Power in the Diesel Engine.....	108
CHAPTER 6: DIESEL POWERTRAIN EXHAUST SYSTEM AND REGULATED EMISSIONS RATE ANALYTICAL MODEL.....	111
6.1. Overview.....	111
6.2. Analytical Model of Pressure Drop and Instantaneous Speed Across Diesel Exhaust System.....	112
6.3. Analytical Model of Percentage of Unburned Fuel in Diesel Powertrains.....	114
6.4. Analytical Model of Steady Speed Exhaust Emission Rate of Carbon Monoxide Diesel Exhaust Emissions	117
6.4.1. Analytical model of the rate of the steady speed-based CO exhaust emissions that result from CO ₂ dissociation.....	118
6.4.2. Analytical model of the rate of the steady speed-based CO exhaust emissions that result from the Water-Gas-Shift reaction.....	120
6.5. Analytical Model of Steady Speed Exhaust Emission Rate of NO _x Diesel Exhaust Emissions	122
6.5.1. Analytical model of Zeldovich mechanism to form NO.....	123
6.5.2. Analytical model of extended Zeldovich mechanism to form NO.....	125
6.5.3. Analytical model of super extended Zeldovich mechanism to form NO.....	127
6.5.4. Analytical model of the mechanism to form NO ₂	130
6.6. Analytical Model of Steady Speed Exhaust Emission Rate of HC Diesel Exhaust Emissions	132
CHAPTER 7: SENSITIVITY ANALYSIS OF THE DEVELOPED MODELS.....	134
7.1. Overview.....	134
7.2. Sensitivity Analysis of the Intake Manifold Gas Speed Dynamics Model.....	135
7.3. Sensitivity Analysis of the Model of the Power Required to Drive the Supercharging Diesel Centrifugal Compressor.....	137
7.4. Sensitivity Analysis of the Model of the Efficiency of the Supercharging Diesel Centrifugal Compressor.....	138
7.5. Sensitivity Analysis of the Model of the Supercharged Air Density....	140
7.6. Sensitivity Analysis of the Model of the In-cylinder Gas Speed Dynamics.....	141
7.7. Sensitivity Analysis of the Model of the Diesel Fuel Consumption Rate	143
7.8. Sensitivity Analysis of the Model of the Brake Power of Diesel Engine.....	145
7.9. Sensitivity Analysis of the Model of the Percentage of Unburned Diesel Fuel	146
7.10. Sensitivity Analysis of the Model of the Rate of Diesel Exhaust CO	148

Emission	148
7.10.1. Sensitivity analysis of the model of $R_{COSSCO+O_2}$	148
7.10.2. Sensitivity analysis of the model of $R_{COSSCO+H_2O}$	150
7.11. Sensitivity Analysis of the Model of the Rate of Diesel Exhaust NOx Emission	152
7.11.1. Sensitivity analysis of the model of R_{NOSSZM}	152
7.11.2. Sensitivity analysis of the model of $R_{NOSS EZM}$	154
7.11.3. Sensitivity analysis of the model of $R_{NOSS SEZM}$	156
7.11.4. Sensitivity analysis of the model of $R_{NO_2 SS}$	158
7.12. Sensitivity Analysis of the Model of the Rate of Diesel Exhaust HC Emission	160
CHAPTER 8: SIMULATED RESULTS AND DISCUSSION OF THE EXPERIMENTAL VALIDATION	162
8.1. Overview	162
8.2. Statistical Analysis	163
8.3. Simulation and Validation of the Model of the Diesel Fuel Consumption Rate	164
8.4. Simulation and Validation of the Model of the Rate of Diesel Exhaust CO Emission	172
8.5. Simulation and Validation of the Model of the Rate of Diesel Exhaust NOx Emission	176
8.6. Simulation and Validation of the Model of the Rate of Diesel Exhaust HC Emission	181
8.7. Simulation and Validation of the Model of the Percentage of Unburned Diesel Fuel	183
8.8. Simulation and Validation of the Model of the Brake Power of Diesel Engine	185
8.9. Simulation and Validation of the Intake Manifold Gas Speed Dynamics Model	187
8.10. Simulation and Validation of the Model of the Power Required to Drive the Supercharging Diesel Centrifugal Compressor	190
8.11. Simulation and Validation of the Model of the Efficiency of the Supercharging Diesel Centrifugal Compressor	191
8.12. Simulation and Validation of the Model of the Supercharged Air Density.....	193
8.13. Simulation and Validation of the Model of the In-cylinder Gas Speed Dynamics	194
CHAPTER 9: CONCLUSIONS AND FUTURE WORK	197
9.1 Summary and Conclusion	197
9.2. Major Contributions.....	200
9.3. Suggestions for Future Work.....	201

REFERENCES.....	203
APPENDIX A: INTERFACE FACILITY AND PROGRAMMING CODE ON THE DIESEL FUEL CONSUMPTION RATE MODEL.....	218
APPENDIX B: INTERFACE FACILITY AND PROGRAMMING CODE ON THE DIESEL CO EMISSION RATE MODEL	223
APPENDIX C: INTERFACE FACILITY AND PROGRAMMING CODE ON THE DIESEL NO _x EMISSION RATE MODEL	227
APPENDIX D: INTERFACE FACILITY AND PROGRAMMING CODE ON THE UNBURNED DIESEL HYDROCARBON MODEL.....	232
APPENDIX E: INTERFACE FACILITY AND PROGRAMMING CODE ON THE DIESEL HC EMISSION RATE MODEL	235
APPENDIX F: COMPARISONS BETWEEN THE SUBCATEGORIES OF EACH OF THE MODELLING CLASSIFICATIONS.....	237
APPENDIX G: THE FOUNDATION OF A PROPOSED LAW OF THERMODYNAMICS ON THE ENTHALPY OF GASEOUS PURE SUBSTANCES IN THERMODYNAMIC EQUILIBRIUM.....	255
APPENDIX H: LIST OF SPOTTED FLAWS IN CORRESPONDING MODELS DEVELOPED IN KEY REFERENCES.....	257
APPENDIX I: LIST OF PUBLICATIONS.....	258

LIST OF TABLES

<u>Table No.</u>		<u>Page No.</u>
7.1	Sensitivity analysis of the analytical model of \dot{c}_{im}	136
7.2	Sensitivity analysis of the analytical model of \dot{w}_c	138
7.3	Sensitivity analysis of the analytical model of η_{CM}	139
7.4	Sensitivity analysis of the analytical model of ρ	140
7.5	Sensitivity analysis of the analytical model of \dot{c}_{Cyl}	142
7.6	Sensitivity analysis of the analytical model of \dot{m}_{AFSS}	144
7.7	Sensitivity analysis of the analytical model of Γ_B	146
7.8	Sensitivity analysis of the analytical model of $R_{Unburned}$	147
7.9	Sensitivity analysis of the analytical model of $R_{COSSCO+O_2}$	149
7.10	Sensitivity analysis of the analytical model of $R_{COSSCO+H_2O}$	151
7.11	Sensitivity analysis of the analytical model of R_{NOSSZM}	153
7.12	Sensitivity analysis of the analytical model of $R_{NOSSSEZM}$	155
7.13	Sensitivity analysis of the analytical model of $R_{NOSSSEZM}$	157
7.14	Sensitivity analysis of the analytical model of R_{NO_2SS}	159
7.15	Sensitivity analysis of the analytical model of R_{HCSS}	161
8.1	Comparison of the simulated results with field data on \dot{m}_{AFSS}	166
8.2	Comparison of the simulated results with field data on \dot{m}_{NLSAF}	166
8.3	Comparison of the simulated results with field data on \dot{m}_{NHSFAF}	167
8.4	Comparison of the simulated results with field data on \dot{m}_{P1LSAF}	167
8.5	Comparison of the simulated results with field data on $\dot{m}_{P1HSFAF}$	168

8.6	Comparison of the simulated results with field data on \dot{m}_{P2LSAF} at $a_{VS} = 1.5 \text{ m/s}^2$	168
8.7	Comparison of the simulated results with field data on \dot{m}_{P2LSAF} at $a_{VS} = 1.8 \text{ m/s}^2$	169
8.8	Comparison of the simulated results with field data on \dot{m}_{P2HSAF} at $a_{VS} = 1.5 \text{ m/s}^2$	169
8.9	Comparison of the simulated results with field data on \dot{m}_{P2HSAF} at $a_{VS} = 1.8 \text{ m/s}^2$	170
8.10	Summary of the statistical analysis on \dot{m}_{AFSS} , \dot{m}_{NLSAF} , \dot{m}_{NHSAF} , \dot{m}_{P1LSAF} , \dot{m}_{P1HSAF} , \dot{m}_{P2LSAF} , and \dot{m}_{P2HSAF}	170
8.11	Experimental validation of the analytical model of $R_{CO SST}$ for all Freeway low speed cycles	174
8.12	Experimental validation of the analytical model of $R_{CO SST}$ for all Freeway high speed cycles	175
8.13	Summary of the statistical analysis on $R_{CO SST}$, $R_{COSSCO+O_2}$, and $R_{COSSCO+H_2O}$	175
8.14	Experimental validation of the analytical model of $R_{NOx SST}$, $R_{NO_2 SS}$, and $R_{NO SST}$ for all Freeway low speed cycles	179
8.15	Experimental validation of the analytical model of $R_{NOx SST}$, $R_{NO_2 SS}$, and $R_{NO SST}$ for all Freeway high speed cycles	180
8.16	Summary of the statistical analysis on $R_{NOx SST}$, $R_{NO_2 SS}$, and $R_{NO SST}$	180
8.17	Experimental validation of the analytical model of $R_{HC SS}$ for low speed Freeway cycles	182
8.18	Experimental validation of the analytical model of $R_{HC SS}$ for high speed Freeway cycles	182

8.19	Summary of the statistical analysis on R_{HCSS}	183
8.20	Experimental validation of the analytical model of $R_{Unburned}$	184
8.21	Summary of the statistical analysis on $R_{Unburned}$	184
8.22	Experimental validation of the analytical model of Γ_B	186
8.23	Summary of the statistical analysis on Γ_B	187
8.24	Field data of a case study conducted on \dot{c}_{im}	188
8.25	Summary of the statistical analysis on \dot{c}_{im}	189
8.26	Field data of a case study conducted on \dot{w}_c	190
8.27	Summary of the statistical analysis on \dot{w}_c	191
8.28	Field data of a case study conducted on η_{CM}	192
8.29	Summary of the statistical analysis on η_{CM}	192
8.30	Field Data of a Case Study conducted on \dot{c}_{Cyl}	195
8.31	Summary of the statistical analysis on \dot{c}_{Cyl}	195
F.I	The main assumptions and limitations in the scale of the input variable-based modelling classification	238
F.II	The main assumptions and limitations in the formulation approach-based modelling classification	239
F.III	The main assumptions and limitations in the main input variable-based modelling classification	241
F.IV	The main assumptions and limitations in the state variable value-based modelling classification	241
F.V	The main assumptions and limitations in the number of dimensions-based modelling classification	242
F.VI	The merits and drawbacks of the scale of the input variable-based modelling classification	243

F.VII	The merits and drawbacks of the formulation approach-based modelling classification	244
F.VIII	The merits and drawbacks of the main input variable-based modelling classification	245
F.IX	The merits and drawbacks of the state variable value-based modelling classification	245
F.X	The merits and drawbacks of the number of dimensions-based modelling classification	246
F.XI	The characteristic parameters of and data collection technique in the scale of the input variable-based modelling classification	247
F.XII	The characteristic parameters of and data collection technique in the formulation approach-based modelling classification	248
F.XIII	The characteristic parameters of and data collection technique in the main input variable-based modelling classification	249
F.XIV	The characteristic parameters of and data collection technique in the state variable value-based modelling classification	250
F.XV	The characteristic parameters of and data collection technique in the number of dimensions-based modelling classification	251
F.XVI	The accuracy and relevance to road traffic in the scale of the input variable-based modelling classification	252
F.XVII	The accuracy and relevance to road traffic in the scale of the formulation approach-based modelling classification	252
F.XVIII	The accuracy and relevance to road traffic in the main input variable-based modelling classification	253
F.XIX	The accuracy and relevance to road traffic in the state variable value-based modelling classification	253
F.XX	The accuracy and relevance to road traffic in the number of dimensions-based modelling classification	254

LIST OF FIGURES

<u>Figure No.</u>		<u>Page No.</u>
2.1	The inter-connections between thesis chapters and the research objectives	50
3.1	Geometry of cylinder, piston, connecting rod, and crankshaft	55
3.2	Geometry of cylinder, piston, connecting rod, and flexible crankshaft	58
3.3	Air flow throttling	63
3.4	Control volume in diesel intake manifold for one-dimensional flow analysis	74
4.1	Schematic diagram of supercharging diesel centrifugal compressor with vanes-based diffuser	83
4.2	The velocity diagram of the diesel centrifugal compressor at the entrance of impeller with pre-whirl	83
4.3	The velocity diagram of the diesel centrifugal compressor at the exit of diffuser	83
4.4	T-S diagram of the supercharging diesel centrifugal compressor with vanes-based diffuser	89
5.1	Control volume in diesel engine cylinder for one-dimensional flow analysis	100
6.1	Exhaust system main components	113

LIST OF ABBREVIATIONS

\dot{P}_i	dynamic pressure inside the intake manifold
\dot{T}_i	dynamic temperature inside the intake manifold
\dot{m}_i	air mass flow rate inside the intake manifold
$\dot{m}_{Throttle}$	actual mass flow rate of air goes from supercharger compressor and electronic throttle control into intake manifold, i.e. at the entrance of the intake manifold
\dot{m}_{AllCyl}	mass flow rate of air goes from intake manifold to all the cylinders of the engine
ρ_{Cyl}	density of air goes into cylinder
η_V	volumetric efficiency of filling in the cylinder
$\dot{V}_{CylTheoretical}$	theoretical air volumetric flow into cylinder
\dot{m}_{Cyl}	mass flow rate of air goes from intake manifold to one cylinder
a_p	instantaneous acceleration of the piston
a	crank length
ρ	density of air inside the intake manifold
$\dot{m}_{Throttle Theo}$	theoretical mass flow rate of air goes from supercharger compressor and electronic throttle control into intake manifold
$A_{0 Min}$	minimum cross sectional area of the throat at the entrance of the intake manifold
$A_{0 Mean}$	mean cross sectional area of a frictionless throat at the entrance of the intake manifold
τ_w	flow shear stress per unit area
ζ	flow friction coefficient
\dot{c}_{im}	air acceleration in the intake manifold in ($\mu\text{m/s}^2$)
P_2	pressure at the exit of the supercharging compressor (N/m^2)

T_2	temperature at the exit of the supercharging compressor (K)
$\eta_{Intercooler}$	intercooler efficiency which depends on the range of temperature of inlet air flow
Γ_I	indicated power of the engine (W)
W_{WS}	work done per working stroke (N.m.)
N_{WS}	number of working strokes per second
F_{Piston}	induced force on the piston due to the pressure resulted from the internal combustion
Γ_{IME}	indicated mean effective pressure of the engine (N.m ⁻²)
Ω_I	indicated torque of the engine (N.m)
V_{d-rad}	total displaced volume of the engine in (m ³ /rad)
η_{EM}	mechanical efficiency of the engine
$\dot{m}_{fuelactual}$	actual mass flow rate of fuel
$T_{Equator}$	yearly average temperature at equator (i.e. 27°C) (°C)
$L_{Latitude}$	absolute value of the given latitude (°)
$A_{Altitude}$	the given altitude (km)
ρ_{In-Cyl}	in-cylinder gas density (kg/m ³)
L_{Stroke}	length of the engine stroke (m)
ζ_{In-Cyl}	coefficient of flow friction in the cylinder
c_{Cyl}	gas flow speed in the cylinder (m/s)
D_{Cyl}	diameter of the cylinder (m)
Φ	equivalence ratio
$R_{F-A\ stoichiometric}$	stoichiometric fuel/air ratio which is constant and readily computable from the stoichiometric equation of chemical reaction of fuel with air
L_{Stroke}	piston stroke (m)
V_S	vehicle speed (m/s)
G_t	gear ratio at the engine transmission

G_d	gear ratio in the final drive (i.e. in the differential)
r_{wr}	vehicle tire rolling radius (m)
Γ_B	brake power of the engine (W)
Ω_B	brake torque of the engine (N.m)
Ω_{LB}	brake load torque applied to the engine (N.m)
Γ_{LB}	brake load power applied to the engine (W)
$n_{i \text{ Reactants}}$	number of moles of species i in the reactants per unit mass of working fluid
$\Delta h_{f,i \text{ Reactants}}$	the standard enthalpy of formation of species i in the reactants per unit mass of working fluid (J/M) at ambient temperature since the dominating largest portion of reactants enters the cylinder of the engine at quasi-ambient conditions
$n_{i \text{ Products}}$	number of moles of species i in the products per unit mass of working fluid
$\Delta h_{f,i \text{ Products}}$	the standard enthalpy of formation of species i in the products per unit mass of working fluid (J/M) at ambient temperature since the pressure drop in the exhaust occurs instantaneously when the exhaust valve opens and the exhaust pressure becomes then atmospheric
Q_{LHV}	Lower heating value of diesel fuel no. 2 (J/kg)
$E_{Combustion}$	power consumed/released during combustion (J/s)
E_{Fuel}	total power that can be generated from diesel fuel (J/s)
$\dot{m}_{exhaustSS}$	actual mass flow rate of exhaust in diesel engines under the condition of steady speed
$M_{CO \text{ molar}}$	molar mass of CO (kg/mol)
K_{CO+O_2}	the reaction constant of the CO ₂ dissociation at the average temperature of exhaust gas along the exhaust system 587°C at equilibrium (M ⁻¹ .s ⁻¹)
$[CO_2]$	the molar concentration of CO ₂ at the average temperature of exhaust gas along the exhaust system 587°C at equilibrium (M)
$M_{fuel \text{ molar}}$	the molar mass of diesel fuel (kg/mol)
K_{CO+H_2O}	the reaction constant of the Water-Gas-Shift reaction at the exhaust

	average temperature of 587°C at equilibrium ($M^{-1}.s^{-1}$)
$[H_2]$	the molar concentration of H_2 at the average temperature of exhaust gas along the exhaust system 587°C at equilibrium (M)
$R_{COinCO+O2permole}$	the rate of emission of CO per one mole of fuel in the CO_2 dissociation ($kg.s^{-1}.mol^{-1}$)
$\dot{m}_{fuelactualSS}$	steady speed-based fuel mass flow rate (kg/s)
a_{avg}	the average acceleration of trucks and light duty vehicles, i.e. $1 m/s^2$
$R_{COinCO+H2Opermole}$	the rate of emission of CO per one mole of fuel in the water-gas-shift reaction ($kg.L^{-1}.s^{-1}$)
$M_{NO molar}$	the molar mass of NO (kg/mol)
$R_{Unburned}$	the percentage of unburned fuel in the diesel engine
$K_{N_2+O_2}$	the reaction constant of Zeldovich mechanism at the average temperature of exhaust gas along the exhaust system 587°C at equilibrium ($M^{-1}s^{-1}$)
$[N_2]$	the molar concentration of N_2 at the average temperature of exhaust gas along the exhaust system 587°C at equilibrium (M)
$[O_2]$	the molar concentration of O_2 at the average temperature of exhaust gas along the exhaust system 587°C at equilibrium (M)
K_{N+OH}	the reaction constant of the extended Zeldovich mechanism at the average temperature of exhaust gas along the exhaust system 587°C at equilibrium ($M^{-1}s^{-1}$)
$[N]$	the molar concentration of N at the average temperature of exhaust gas along the exhaust system 587°C at equilibrium (M)
$[OH]$	the molar concentration of OH at the average temperature of exhaust gas along the exhaust system 587°C at equilibrium (M)
K_{N_2O+H}	the reaction constant of the super extended Zeldovich mechanism at the average temperature of exhaust gas along the exhaust system 587°C at equilibrium ($M^{-1}s^{-1}$)
$[N_2O]$	the molar concentration of N_2O at the average temperature of exhaust gas along the exhaust system 587°C at equilibrium (M)
$[H]$	the molar concentration of H at the average temperature of exhaust gas along the exhaust system 587°C at equilibrium (M)

$M_{NO_2 \text{ molar}}$	the molar mass of NO ₂ (kg/mol)
K_{NO+O_2}	the reaction constant of the oxidization of NO to form NO ₂ at the average temperature of exhaust gas along the exhaust system 587°C at equilibrium (M ⁻¹ s ⁻¹)
$[NO]$	the molar concentration of NO at the average temperature of exhaust gas along the exhaust system 587°C at equilibrium (M)
$R_{NO \text{ in } N_2+O_2 \text{ permole}}$	the rate of emission of NO per one mole of fuel in the Zeldovich mechanism of forming NO (kg.s ⁻¹ .L ⁻¹ .mol ⁻¹)
$V_{mixture}$	the volume of mixture of exhaust gases (L)
w	engine crankshaft rotational speed (rad/s)
Δ	a collision partner collectively represents all molecules present
$R_{NO \text{ in } N+OH \text{ permole}}$	the rate of emission of NO per one mole of fuel in the extended Zeldovich mechanism of forming NO (kg.s ⁻¹ .L ⁻¹ .mol ⁻¹)
$R_{NO \text{ in } N_2O+H \text{ permole}}$	the rate of emission of NO per one mole of fuel in the super extended Zeldovich mechanism of forming NO (kg.s ⁻¹ .L ⁻¹ .mol ⁻¹)
$R_{NO_2 \text{ permole}}$	the rate of emission of NO ₂ per one mole of fuel in the mechanism of NO ₂ formation (kg ^{0.5} .s ⁻¹ .L ^{-0.5} .mol ⁻¹)
$v_{DependentChanges}$	Value of the dependent variable in the analytical model with the increment/decrement of change
$v_{DependentBaseline}$	Baseline value of the dependent variable in the analytical model
$v_{IndependentChanges}$	Value of the independent variable in the analytical model with the increment/decrement of change
$v_{IndependentBaseline}$	Baseline value of the independent variable in the analytical model
a_{VS}	vehicle acceleration (m/s ²)
Q_{im}	the volumetric flow rate of air in the intake manifold at wide-open throttle, which is the state at which diesel engines mostly operate
$\frac{D}{L}$	the ratio of the diameter of plenum of intake manifold to the length of intake manifold
η_{CM}	mechanical efficiency of the compressor
\dot{W}_C	power required to drive the supercharging diesel centrifugal compressor (W)

\dot{m}_{air}	mass flow rate of air in the supercharging compressor
Q_{Cyl}	volumetric flow rate of air in the cylinder at maximum in-cylinder pressure
$\frac{D_{Cyl}}{L_{Stroke}}$	the ratio of the diameter of cylinder to the length of the stroke
δW	the mass-specific work done infinitesimally by/on the system
n_{mol}	the number of molecules in substance
a_{vw}	Van der Waals' coefficient which accounts for the intermolecular attractive interactions between molecules
b_{vw}	Van der Waals' coefficient which accounts for the actual molar volume of the molecules
N_{CM}	rotational speed of the rotor of the compressor (rpm)
r_{COD}	coefficient of determination
ε_R	relative error of the model
S_{xy}	the sample covariance
S_x	the standard deviation of the dataset of the interval variable x_i
S_y	the standard deviation of the dataset of the interval variable y_i
z_n	the number of the records in the sample
A	cross sectional area of the intake manifold
A_0	instantaneous cross sectional area of the throat at the entrance of the intake manifold
B	cylinder diameter
c	air speed (m/s)
c_p	gas specific heat at constant pressure, which is constant in the case of air is treated as an ideal gas
c_{r2}	the radial velocity of the air flow at the diffuser of the centrifugal compressor
D	diameter of the intake manifold (m)

E_{Kin}	kinetic energy per unit area
e_s	speed of sound (m/s)
E_{Total}	total energy of the air flow (J)
F_a	force generated due to the acceleration of the piston
F_{Moment}	force that generated this momentum within the control volume
F_{Press}	net pressure force within the control volume
F_{Shear}	net shear force within the control volume
g	gravitational acceleration (m/s^2)
h	gas enthalpy
h_{ref}	the vibrational and bonding energy at the system's temperature at the reference state, T_{ref}
I_C	moment of inertia of the compressor as an integrated system, i.e. of the compressor shaft, impeller, and diffuser collectively
L	length of intake manifold (m)
m_C	mass of the gas in the clearance volume of the engine cylinder, which equals the total mass of the gas in the engine cylinder before compression due to the principle of conservation of mass
m_{Cyl}	mass of air goes into cylinder
m_i	mass of air in the intake manifold (kg)
m_p	mass of the piston
n	number of crank revolutions for each power stroke per cylinder (two for 4-stroke cycles; one for 2-stroke cycles)
N_{Cyl}	number of the cylinders in the engine
N_m	crankshaft rotational speed (rpm)
N_s	crankshaft rotational speed (rps)
p	pressure of the air (N/m^2)
P_{Amb}	ambient pressure
P_{Atm}	atmospheric pressure in case of naturally aspirated engines and equals

	the compressor output pressure, $P_{\text{Compressor}}$, in case of supercharged engines which is adopted in this research
$P_{\text{Compressor}}$	pressure at the outlet of the supercharging compressor as stated in the compressor map corresponding to the maximum efficiency of the compressor and the required air flow rate
P_{Cyl}	pressure of air goes into cylinder which becomes P_i by the end of the intake stroke (N/m^2)
$P_{\text{Cyl Intake}}$	gas pressure inside the cylinder during the intake stroke
P_i	intake manifold pressure (N/m^2)
P_{ox}	stagnation pressure at state x at the centrifugal compressor
P_{oxs}	isentropic pressure at state x at the centrifugal compressor
P_{Peak}	peak pressure inside cylinders which is commercially set in the diesel engine catalogue for each category of diesel engines
P_{Vac}	vacuum pressure created in the cylinder during the intake stroke due to piston downward movement
P_x	static pressure at state x at the centrifugal compressor
q	specific heat flow
Q	heat flow
q_{i1}	amount of heat exists in the cylinder just before reaching state 1 in diesel cycle
q_{i2}	amount of heat exists in the cylinder just before reaching state 2 in diesel cycle
q_{i3}	amount of heat exists in the cylinder just before reaching state 3 in diesel cycle
q_{i4}	amount of heat exists in the cylinder just before reaching state 4 in diesel cycle
q_{o1}	amount of heat exists in the cylinder just after reaching state 1 in diesel cycle
q_{o2}	amount of heat exists in the cylinder just after reaching state 2 in diesel cycle
q_{o3}	amount of heat exists in the cylinder just after reaching state 3 in diesel cycle

q_{o4}	amount of heat exists in the cylinder just after reaching state 4 in diesel cycle
R	universal gas constant
r_C	compression ratio of the diesel engine
s	specific entropy of gas flow
S	absolute entropy of the gas flow
S_d	displacement of the piston
S_P	velocity of the piston
T_{Cyl}	temperature of air goes into cylinder
T_i	intake manifold temperature (K)
T_{i1}	gas temperature at the end of the exhaust stroke in diesel cycle
T_{i2}	gas temperature just before the beginning of the combustion process in diesel cycle
T_{i3}	gas temperature just after the end of the combustion process in diesel cycle
T_{i4}	gas temperature at the beginning of the exhaust stroke in diesel cycle
$T_{Inlet-Intercooler}$	intercooler inlet temperature (or post compressor temperature, i.e. T_2)
$T_{Intercooler}$	temperature at the outlet of the intercooler as stated in the intercooler catalogue
T_{Peak}	peak temperature inside cylinders which is commercially set in the diesel engine catalogue for each category of diesel engines
T_{ref}	the system's temperature at the reference state
$T_{Ref-Amb}$	ambient reference temperature
u	specific internal energy (J)
U	the tangential velocity of the rotor of the centrifugal compressor
U_2	the tangential velocity of the rotor at the diffuser of the centrifugal compressor

v	specific volume of the air (m^3)
V	total volume of air inside the engine cylinder
v_1	specific volume of gas in the engine at state 1
v_2	specific volume of gas in the engine at state 2
v_3	specific volume of gas in the engine at state 3
v_4	specific volume of gas in the engine at state 4
V_C	clearance volume of the engine cylinder
V_{Cyl}	volume of air goes into cylinder in the intake stroke
V_d	the total displaced volume of the engine ($\text{m}^3/\text{d-cycle}$)
$V_{d-\text{Cyl}}$	displaced volume per cylinder ($\text{m}^3/\text{d-cycle}$)
V_i	intake manifold volume (m^3)
V_P	volume of the piston
x_i	the interval variable that is the expected value analytically
y	vertical displacement of the rotating tip of the crank
Y	piston height
y_i	the interval variable that is the measured value, i.e. field dataset
z	potential altitude (m)
α_c	compressor rotational deceleration (rad/s^2)
θ	crankshaft rotational angle
θ_{IVC}	crankshaft rotational angle at which the intake valve closes
θ_{IVO}	crankshaft rotational angle at which the intake valve opens
ρ_P	density of the material of the piston which is usually aluminium alloy
ω_c	the angular speed of the rotor of the centrifugal compressor

CHAPTER 1

INTRODUCTION

1.1. OVERVIEW

The transportation sector is the third largest consumer of energy and the largest consumer of petroleum products and is one of the greatest contributors to air pollution worldwide (United Nations Economic and Social Council, 2009). Emissions from vehicles contribute to smog, low visibility, and various greenhouse gas emissions. About half of all air pollution and more than 80 percent of air pollution in cities are produced by the transportation sector worldwide (United Nations Economic and Social Council, 2009). Its energy consumption is growing faster than that of other sectors, driven by the rapid increase in motorization and strong transport demands from economic development. Meanwhile, the transport sector is the primary source of air pollution. These facts require the transport sector to take more efficient mitigation and adaptation measures to reduce energy consumption and emissions. A reduction in fuel consumption will lead to reduction in vehicle emissions (Yue, 2008). Therefore, automobile manufacturers are currently under pressure to produce more environmentally friendly vehicles (Fabian, 2010).

The transportation sector is the source of 41 percent of the Hydrocarbon (HC) emissions, 79 percent of carbon monoxide (CO) emissions, and 51 percent of Oxides of Nitrogen (NOx) emissions (Environmental Protection Agency, 1996). Highway motor vehicles generate 29 percent of HC emissions, 60 percent of CO emissions, and 31 percent of NOx emissions (Yue, 2008). Since trucks generally operate at low fuel economy and efficiency, the share of diesel vehicles in total CO₂ jumps to 72%

(Fabian, 2010). Since the majority of trucks are powered by diesel engines, this research addresses fuel consumption and emissions of diesel powertrains.

1.2. BACKGROUND

Vehicle fuel consumption and emission models are currently the primary tools for evaluating the regional impacts of transportation projects and in evaluating new hardware in the field of Intelligent Transportation System (ITS). In typical applications, a transportation planning model such as TRANPLAN (National Research Council, 1995), MINUTP (Yue, 2008) or EMME/2 (Environmental Protection Agency, 1996) is first used to determine the average speed and total vehicle-miles of travel for the network or facility being considered. Then, a fuel consumption and emissions model such as MOBILE6 (Fabian, 2010) or EMFAC (The Urban Analysis Group, 1992) is used to compute the average fuel consumption and emissions rates for the facility. Within this step, a base emissions rate reflecting fuel consumption and emissions measurements that were gathered in a laboratory using pre-defined test drive cycles is first selected for the facility considered. This base rate is then modified to account for differences in average speeds between the laboratory and real-world cycles, as well as for differences in temperature, vehicle load, fleet composition, accrued mileage of vehicles within the fleet, type of fuel used, and vehicle operating conditions. Total fuel consumption and emissions are finally obtained by multiplying the resulting rates by the estimated vehicle miles traveled on the facility (The Seider Group, 1997). Macroscopically, single fuel consumption rate and single emission rate are produced for each average speed input. These rates are produced under the assumptions that all vehicles pollute similarly for the same

average speed and vehicle-miles traveled and that variations in driver behavior can be neglected (INRO Consultants, 1996).

1.3. PROBLEM STATEMENT

Given that:

1. The share of diesel vehicles in CO₂ emissions jumps to 72% (Fabian, 2010);
2. Automobile manufacturers are currently under pressure to produce more environmentally friendly vehicles in an endeavor to mitigate the issue of global warming (Fabian, 2010);
3. The majority of trucks are powered by diesel engines (Fabian, 2010);
4. Gear-shifting-based modeling is sought because the model parameters can be adjusted to reflect different driving conditions without the need for gathering field data (Rakha, et al., 2012).

Therefore, there is a call for devising a cost-effective, widely valid, and gear-shifting-based microscopic model of diesel powertrain fuel consumption and emissions (Rakha, et al., 2012). Such a microscopic model should help in:

1. Evaluating the current/new diesel powertrain technologies;
2. Evaluating instantaneous fuel consumption and emission rate.

1.4. SIGNIFICANCE OF PROBLEM STATEMENT

The state-of-the-art emission models such as MOBILE6 developed by the US Environmental Protection Agency (EPA) and EMFAC7F developed by the California Air Resources Board (CARB) attempt to model vehicle emission rate accounting for

travel-related factors such as distance and number of trips, weather-related factors and vehicle-related factors such as engine size (Ahn, et al., 2002). However, these models generally fail to capture the effect of roadway related factors such as road grade and driver related factors such as driver's behavior and driving cycle on vehicle emissions. These models use average speed to estimate vehicle emissions whereas in each facility average speed there is implicitly a driving cycle (Ahn, et al., 2002). Thus, the current state-of-the-art emission models are unsuitable for evaluating the environmental impact of change in facility's operational-level (Ahn, et al., 2002). Although there have been statistical and empirical models developed to overcome the shortcomings of the state-of-the-art models by quantifying roadway and driver related factors on vehicle emissions and by using vehicle's instantaneous speed and acceleration, such as INTEGRATION, such models are only valid for the set of data based on which they have been developed.

Vehicle power losses can currently only be written as empirical regression expressions because of the lack of a physics-based model in this regard (Hendricks, 1997). In addition, the effect of diesel combustion cycle on engine model needs to be analytically investigated (Hendricks and Sorenson, 1990). Moreover, the exhaust manifold of diesel engines needs to be analytically investigated as well (Biteus, 2002). Largely, there is a need for analytical modeling of the diesel powertrain components for which no analytical models have been developed as yet (Biteus, 2002). Modeling of fuel consumption and emission of vehicles operating under a non-stoichiometric condition is particularly problematic (Greenwood, 2003). Therefore, an instantaneous, physics principles-based and widely valid model of diesel powertrains is sought. Therefore, the research problem is significant and the approach proposed to solve this problem is unprecedented.

1.5. RESEARCH PHILOSOPHY

The adopted research philosophy in this research consists of three pillars:

1. Developing an analytical model for each relevant component to fuel consumption and emission in diesel powertrain;
2. Developing an aggregate analytical model of diesel fuel consumption and emission rates;
3. Developing a simplified version of the developed aggregate analytical model to fit the INTEGRATION software of Virginia Tech.

1.6. RESEARCH OBJECTIVES

This dissertation aims to develop a microscopic diesel powertrain fuel consumption and emission rate model. The research objectives are as follows:

1. Developing an instantaneous, gear-shifting-based and microscopic analytical model to simulate the diesel powertrain fuel consumption rate under accelerating, cruising and decelerating driving conditions and regulated emissions rate under cruising driving condition for trucks in order to fit the INTEGRATION software package of Virginia Polytechnic Institute and State University (Virginia Tech);
2. Validating the simulation results against experimental results;
3. Developing an interface facility to give instantaneous fuel consumption and regulated emissions rate of trucks.

1.7. RESEARCH METHODOLOGY

This research is quantitative research based on a theoretical approach employing exploratory and descriptive techniques to analytically model diesel fuel consumption and regulated emissions rate. The experimental data for validation have been collected from literature namely a previous research work done by our research partner at Virginia Tech based on the Oak Ridge National Laboratory (ORNL) and the US Environmental Protection Agency (EPA) field data. In an endeavor to conduct this research, the following research procedure and operational framework has been followed:

1. Conducting thorough literature review in order to make sure the research problem significantly exists;
2. Coming up with specific research questions which fully address the research problem based on the literature review;
3. Establishing analytical framework and devising analytical models;
4. Conducting simulation based on the devised analytical models using readily available field data and MATLAB in order to check the suitability of the developed analytical models for being fitted into the ‘INTEGRATION’ traffic simulation software that is developed by Virginia Tech since this proposed research is a collaborative research project between the International Islamic University Malaysia and Virginia Tech;
5. Carrying out validation through comparison between the results of the developed analytical models and the corresponding field data.

The research assumptions in this research include the following assumptions: (i) as to field data that can be used for research validation, all vehicles pollute similarly for the

same average speed and vehicle-miles traveled; (ii) standard deviation in recorded speeds is small, and thus can be negligible.

1.8. RESEARCH SCOPE

This research lies within the borders of the bio-environmental engineering research area. Specifically, the scope of this study is limited to the intersection between the following specific research areas:

1. Analytical Modeling;
2. Supercharged diesel powertrains;
3. Diesel fuel consumption rate evaluation;
4. Steady speed diesel exhaust regulated emissions rate evaluation.

The models developed in this study are limited to diesel trucks and light duty vehicles fuelled by diesel fuel no. 2.

1.9. DISSERTATION LAYOUT

The dissertation commences with a literature review and identification of the research gap as indicated in Chapter 2. Chapter 3 presents an analytical model of diesel powertrain intake manifold. An analytical model of supercharging diesel centrifugal compressor with vanes-based diffuser is presented in Chapter 4. Chapter 5 elucidates an analytical model of diesel engine. An analytical model of diesel powertrain exhaust system and regulated emissions rate follows in Chapter 6. Sensitivity analysis of the developed models is presented in Chapter 7. Chapter 8 demonstrates the simulated results and experimental validation. Chapter 9 presents the conclusions of this study and future work.

CHAPTER 2

LITERATURE REVIEW

2.1 OVERVIEW

The present work reviews the vehicle fuel consumption and emissions modeling and key models. It classifies vehicle fuel consumption and emissions modeling into five classifications and presents the relevant models to each of them. These models are then compared with regard to assumptions, limitations, merits, drawbacks, characteristic parameters, data collection technique, accuracy, relevance to road traffic, and validation. A summary then follows on these models and comparisons highlighting the key points.

2.2. VEHICLE FUEL CONSUMPTION AND EMISSIONS MODELING

Several approaches have been developed in order to estimate vehicle fuel consumption and emission rate. They can be classified into five categories of classification: (1) Scale of the input variables-based modeling, (2) Formulation approach-based modeling, (3) Type of explanatory variable-based modeling, (4) State variable value-based modeling, (5) Number of dimensions-based modeling. Based on the scale of the input variables the current state-of-the-art and current state-of-practice models can be divided into three categories: microscopic, mesoscopic, and macroscopic models. The subcategories of the formulation approach-based modeling classification, i.e. the way of building model-based modeling classification, are analytical, empirical, statistical, and graphical models. In the explanatory variable-

based modeling classification, there are three subcategories: average speed, instantaneous speed, and specific power models. The state variable value-based modeling classification can be divided into crank-angle resolution-based models and mean value-based models. The subcategories of the number of dimensions-based modeling classification are zero/one dimensional/single zone, quasi dimensional, and multi dimensional/multi zone modeling.

2.2.1 Scale of the Input Variables-based Modeling

Let us start with investigating the scale of the input variables-based modeling classification that is divided into: microscopic models, mesoscopic models, and macroscopic models, as suggested by Yue (Yue, 2008). Microscopic models use instantaneous speed and acceleration data to estimate vehicle fuel consumption and emission rates. The fuel consumption and emission estimates from microscopic models are instantaneous rates as well. Macroscopic models use aggregate network-based parameters to estimate network-wide fuel consumption and emissions rates. Mesoscopic models use scales that lie in-between the macroscopic scale and microscopic scale, such as link-based estimates (Yue, 2008). All of these three categories can be called modal models if they account for different standard operating modes. These three categories are reviewed in the following three subsections respectively.

2.2.1.1 *Microscopic models*

Microscopic models estimate instantaneous vehicle fuel consumption and emission

rates that are then aggregated to estimate network-wide measures of effectiveness. Instantaneous fuel consumption models are derived from a relationship between fuel consumption rates and instantaneous vehicle power. Second-by-second vehicle characteristics and road conditions are required in order to estimate fuel consumption in these models. Due to the disaggregate characteristics of the fuel consumption data, these models are usually used to evaluate individual transportation projects. Instantaneous fuel consumption models can be used in microscopic traffic simulation packages to estimate fuel consumption based on instantaneous speeds and accelerations of individual vehicles (Yue, 2008). The key microscopic models include: (1) Comprehensive Modal Emission Model (CMEM), (2) VT-Microscopic Model, (3) VERSIT^{micro}, (4) PHEM, (5) VeTESS, (6) NetSim, (7) EMIT, (8) MOVES, (9) Vehicle Dynamics Models. These microscopic models will be highlighted in the following subsections.

An and Barth (An and Barth, 1997) developed a modal emissions model, called Comprehensive Modal Emission Model (CMEM), which is based on a simple parameterized empirical approach and consists of six modules that predict engine power, engine speed, air/fuel ratio, fuel use, engine-out emissions, and catalyst pass fraction. Three dynamic variables (acceleration, Air/Fuel equivalence ratio, and fuel rate), second-by-second speed, road grade angle, and accessory use (such as air conditioning) are used as the input operating variables. The instantaneous emission is the key output. The main limitation of CMEM is that it is unable to estimate emissions from heavy duty vehicles such as trucks and buses. The CMEM is utilized in the PARAMICS microscopic simulator.

Rakha and Ahn developed a microscopic vehicle fuel consumption and emission model called VT-Micro based on instantaneous speed and acceleration

(Rakha and Van Aerde, 2000; Ahn, 2002). The inputs to the VT-Micro are the instantaneous speed and acceleration and the outputs are instantaneous fuel consumption and emission rates of individual vehicles (Yue, 2008). The model estimates vehicle fuel consumption to within 2.5 percent of actual measured field values. The VT-Micro model has been incorporated within INTEGRATION, a microscopic traffic simulation package. INTEGRATION appears to have the highest probability of success in real world transportation applications (Tapani, 2005). Although the VT-Micro model seems to be the leading model in predicting instantaneous fuel consumption and emission rates, it is based on empirical formulae and thus provides unexplainable mathematical trends.

The VERSIT+^{micro} was developed in the Netherlands by TNO to simulate the traffic emissions of CO₂, NO_x and PM₁₀ as well as energy use factors as outputs on the basis of the instantaneous velocity and acceleration of a vehicle as inputs. The VERSIT+^{micro} is unique in yielding consistent results on national, regional and local scales so that it is positioned at par with the INTEGRATION model. The key drawback of the VERSIT+^{micro} is the linear dependence of the emission estimates on the velocity of the vehicle which limits the effect of the velocity on the emission estimates (Smit et al., 2007). The VERSIT+^{micro} is adopted by AIMSUN (Advanced Interactive Microscopic Simulator for Urban and Non-urban Networks) software.

The Passenger car and Heavy duty Emissions Model (PHEM) uses an emissions map as a look-up table in terms of the engine operating parameters to estimate emissions microscopically. There are not yet sufficient quantitative validation data for this model. The model provides predictions of aggregate emissions that are less accurate than the predictions of the INTEGRATION model. The PHEM is utilized in the VISSIM software.

VeTESS (Vehicle Transient Emissions Simulation Software) is another microscopic emission model like PHEM that adopts a quasi steady state modeling approach by taking into account the dynamic behaviour of the engine. The model's inputs are driving pattern, gradient, and vehicle specifications. The model's outputs are the engine power and emission rate. The VeTESS estimates for fuel consumption and emissions have generally an accuracy within 10 to 20%. VeTESS is utilized in the CORSIM (CORridor microscopic SIMulation) software. Similarly, EMIT model evaluates emissions depending on vehicle speed and acceleration. EMIT has been used to evaluate the environmental impact of technologies (Sommer et al., 2011).

MOtor Vehicle Emission Simulator (MOVES) is an emission model that is based on vehicle's instantaneous speed and acceleration. Albeit its good estimation of vehicle's emission rates, MOVES model is relatively time-consuming. The MOVES is utilized in the Transportation Analysis and SIMulation System (TRANSIMS) software. Vehicle dynamics or gear-shifting modeling approach is better because the model parameters can be adjusted to reflect different weather, tire, and roadway surface conditions without the need for gathering any field data. Research is currently needed to characterize analytically the relationships, if any, between the driver's throttle input and the vehicle conditions, roadway conditions, and surrounding traffic conditions (Rakha et al., 2010). Now, let us turn to investigate the second category of the scale of the input variables-based modeling classification.

2.2.1.2 Macroscopic models

Macroscopic models use average aggregate network parameters to estimate network-wide energy consumption and emission rates. The key models in the macroscopic

vehicle fuel consumption and emissions modeling subcategory include: (1) MOBILE, (2) EMFAC, (3) CORFLO, (4) Watson model, (5) COPERT. The following subsections will elaborate on these macroscopic models.

The MOBILE source emission factor model estimates are a function of the vehicle's average speed, vehicle's technology, vehicle's age, ambient temperature, fuel parameters, and vehicle's operating mode (National Research Council (NRC), 1995). Eight pollutants can be estimated by MOBILE6 model: HC, CO, NO_x, CO₂, PM, SO₂, NH₃, and six hazardous air pollutants (HAP). The CO₂ emission estimate from MOBILE6 is unlike other MOBILE6 emission estimates. This CO₂ emission rate estimate is based on vehicle type only and is not affected by speed, temperature, and gasoline type. In this model, basic emission rates are derived from emissions tests conducted under standard conditions such as temperature, fuel, and driving cycle. Speed Correction Factor (SCF) is then used when vehicle average travel speed is different from the average travel speed derived from the standard testing drive cycle. The SCF is derived based on emission rates from a specific number of testing driving cycles (Yue, 2008). Yet, MOBILE6 can not estimate fuel consumption and thus has been officially replaced by MOVES2010 model in the US.

The Emission FACTors (EMFAC) model is another vehicle emission model that has been widely used. The EMFAC emission rate estimates are as well a function of vehicle average speed. The EMFAC2007 can be used to estimate HC, CO, NO_x, CO₂, PM, SO_x, pb, and fuel consumption. Adjustments are used in this model for different temperatures, gasoline types, humidity, etc., after evaluating the basic emission rates that are derived from emissions tests conducted under standard conditions. Albeit the EMFAC model is good for estimating emission rates, it ignores the impact of intelligent transportation systems strategies, such as traffic signal

coordination, and therefore has been officially replaced by MOVES2010 model in the US.

CORFLO is a macroscopic traffic model and traffic simulation software that was developed by the Federal Highway Administration, USA. CORFLO's macroscopic modeling approach allows for fast simulation times and analysis of design control scenarios. The model is based on the energy conservation law and a dynamic speed density equation. Although it can run on inexpensive computers, CORFLO lacks the capability to simulate most ITS applications and does not account for dynamic route guidance modeling (Boxill and Yu, 2000).

Waston and Milkins (1980) used average speed to develop a fuel consumption model. The model incorporates the changes in the positive kinetic energy during acceleration as a predictor variable. When the average speeds are high enough, the aerodynamic effects on fuel consumption become significant. This usually occurs at average speeds over 55 km/h (Evans and Herman, 1976). The model helps in showing that it is easier to achieve steady-state speed requirement under highway driving conditions. The model's inputs are average speed, final speed, initial speed, and total section length. The model's output is fuel consumption. Although Waston's model is good for estimating fuel consumed, the accuracy of its estimation is less than that of instantaneous speed-based models.

The COmputer Program to compute Emissions from Road Transport (COPERT) is an average speed based macroscopic emission model. The model's input is the vehicle average speed and the model's output is the emission rate. The model was developed based upon the principle that the average emission factor for a certain pollutant and a given type of vehicle varies according to the average speed during a trip. However, in modeling the emission rates of heavy duty vehicles,

COPERT model is inherently unreliable at speeds above 100 km h⁻¹ (Int Panis et al., 2007). Having seen this, the third category of the scale of the input variables-based modeling classification will be presented in the next subsection.

2.2.1.3 Mesoscopic models

The input variables to mesoscopic model are more disaggregate than macroscopic model and more aggregate than microscopic model. Generally, mesoscopic models use a few explanatory variables to estimate vehicle fuel consumption and emissions (Yue, 2008). The key models in the mesoscopic vehicle fuel consumption and emissions modeling subcategory include: (1) Elemental model, (2) CONTRAM, (3) MEASURE model.

The elemental model, which is based on average speed, was proposed by Herman (Chang and Evans, 1981; Evans and Herman, 1978). It is a simple theoretically-based model expressing fuel consumption in urban conditions as a linear function of the average trip time per unit distance, i.e. reciprocal of average speed. In average speed models, fuel consumption rates is basically the model's output and trip time, trip distance and average speed are the model's inputs. Since these models do not adequately take into account aerodynamic drag resistance at high speeds, they should only be used for average speeds of less than 55 km/h in most cases (Akcelik, 1985). The Elemental model is adopted in the SIDRA INTERSECTION software that was developed by Akcelik (Akcelik, 1985) and that is widely used in transportation applications in Australia. The main drawback of this model is that it does not capture transient changes in vehicle's speed and acceleration.

The CONTinuous TRaffic Assignment Model (CONTRAM) is a mesoscopic model and simulator that is concerned with the dynamics of the flow of heavy traffic

using aggregated speed-density functions to model the behavior of that flow (Sommer et al., 2011). The core of CONTRAM is a dynamic assignment model that predicts traffic routes, link flows and queues and delays at intersections as they evolve over time. CONTRAM is thus capable of accurately representing time varying network conditions. Though CONTRAM model deal with multiple classes of vehicles, it lacks the ability to output measures of performance such as travel times and speeds nor does it seem to be able to model all the relevant ITS functions, e.g. it lacks the capability to model incidents or driver information systems (Boxill and Yu, 2000).

The Mobile Emission Assessment System for Urban and Regional Evaluation (MEASURE) was developed by researchers at The Georgia Institute of Technology. The MEASURE model is a Geographic Information System GIS-based modal emissions model process that predicts modal vehicle operations and generates mesoscopic estimates of HC, CO, and NO_x emissions (Bachman and Sarasua, 1996; Bachman and Sarasua, 2000). This model includes two major modules: start emission module and on-road emission module. Emission rates are modelled based on a refined tree-based regression analysis of vehicle emission test data from the US EPA and CARB. Emission rates are a function of vehicle model year, vehicle fuel delivery technology, high or normal emitter vehicle, and modal variables. The MEASURE model is compatible with most of the traditional microscopic traffic simulation packages and models. Outputs from microscopic traffic simulation package or travel demand forecasting models along with roadway conditions, traffic control conditions, traffic conditions, and facility type are used as the input into the regression analysis to calibrate the model. The vehicle activity data, fleet composition characteristics, operating conditions, and emission rates are then used as the model's inputs in order to get emissions estimates (Yue, 2008). This concludes the scale of the input

variables-based modeling classification. Let us now investigate the second classification.

2.2.2 Formulation Approach-based Modeling

Based on the formulation approach-based modeling, i.e. the way of building the vehicle model, fuel consumption and emission rates models can be divided into four categories: analytical, empirical, statistical, and graphical modeling. The analytical modeling of a vehicle models the vehicle in terms of mathematical formulae which describe the relationships between the vehicle subsystems based entirely on the principles of physics. Empirical modeling is an approach that uses observations and the trial-and-error method to model a system. Statistical modeling is an approach that solely uses data and statistical methodologies to model a system. Graphical modeling is an approach that uses graphical tools and graphical methods to model the subsystems of a system as unified objects connected with each other. These subcategories of the second classification of models will be presented in this section, respectively.

2.2.2.1 Analytical models

Analytical modeling has been adopted in several research papers in order to model vehicle powertrains. For example, Lavoie and Blumberg proposed a thermodynamics-based model to predict fuel consumption, and emissions as a function of engine design parameters and operating conditions (Lavoie and Blumberg, 1980). Albeit the validation of that model proved its reliability in predicting fuel consumption, it is valid only for spark ignition engines.

Metallidis and Natsiavas proposed non-linear models of the dynamics of single- and multi-cylinder reciprocating engines, which may involve torsional flexibility in the crankshaft (Metallidis and Natsiavas, 2003). These models took into account the torsional flexibility in the crankshaft and the dependence of the engine moment of inertia on the crankshaft rotation. A linearised version of the models was presented to acquire insight into some aspects of the system dynamics such as determining the steady-state response and investigating the effect of engine misfire on fuel consumption and emission rates. Yet, these models need relatively long computational time.

Harris and Pearce (Harris and Pearce, 1990) developed a mathematical model of the performance of a governed diesel engine using the following concept. At any throttle setting, and as torque is increased, the speed of a diesel engine will decrease from its value at zero torque and if torque increases further, the engine then operates along the locus of these points where the fuel delivery is a maximum. That model is simple enough to model and to indirectly measure tractor engine performance. Albeit it helps in evaluating the fuel consumption rate of tractor engines, the model does not account for estimating the emission rates of tractor engines.

Khayyam (Khayyam, et al., 2008) developed an analytical model of fuel consumption (AMFC) to coordinate the driving power and to manage the overall fuel consumption for an internal combustion engine vehicle. Their model effectively evaluates the different loads applied on the vehicle including road-slope, road-friction, wind-drag, accessories, and mechanical losses. However, the model needs relatively long computational time.

Zargari and Khan (Zargari and Khan, 2003) presented a model for the estimation of fuel consumption for bus operation on transitways/busways serving

major travel corridors. That bus fuel consumption model is developed for standard and articulated buses. Yet, the model lacks simplicity and can not be easily integrated into modern automobile control systems without simplification which in turn may lead to modeling errors.

Oberg (Oberg, 2001) extended previously developed analytical models for four cylinder turbocharged diesel engine that has no throttling developed by Karlsson (Karlsson, 2001) and by Nyberg (Nyberg and Sutte, 2004). In addition, Oberg presented the diesel engine combustion model and exhaust model developed by Butschek (Butschek, 2000). Oberg made extensions to the pumping and turbo submodels of these already developed diesel engines models and developed a model for both Exhaust Gas Recirculation (EGR) and Variable Nozzle Turbine turbocharger (VNT) of the diesel engine. Albeit these models give insight into what influence the rate of fuel consumption, Oberg reported that the EGR, and the VNT have been difficult to be analytically modeled satisfactorily.

Hillion (Hillion, et al., 2008) proposed a model-based control strategy to adapt the fuel injection settings according to the intake manifold condition on a diesel Homogeneous Charge Compression Ignition (HCCI) engine. For that purpose, the start of injection is adjusted based on the Knock Integral Model and intake manifold condition. The Knock Integral Model, originally developed by Livengood and Wu (Livengood and Wu, 1995), is a widely used model that gives an implicit relation between the start of injection crankshaft angle, start of combustion crankshaft angle, and the physical in-cylinder parameters such as cylinder pressure, cylinder temperature, in-cylinder burned gas rate, and the fuel/air ratio.

Kulkarni (Kulkarni, et al., 1992) reported that a turbo charged diesel engine without any governor or controller of fuel pump is normally represented by a fourth

order model. They used a model order reduction technique. The reduced order model was validated through simulation using typical data. They concluded that a simplified model, obtained by neglecting the manifold volumes, would give erroneous results.

Yang and Sorenson (Yang and Sorenson, 1992) developed a physical model for the diesel fuel injection electronic unit injector and the electronic distributor pump system. The model incorporates a simplified characteristic line method for determining the hydraulic transients in high pressure fuel lines and a transmission line analogy method for modeling magnetic processes in the solenoid. Yet, it is relatively calculation intensive.

Xia and Oh (Xia and Oh, 1999) developed a physical dynamic torque converter model to reduce fuel consumption. This model satisfies the energy conservation law and dynamic torque balance for all converter elements. The model was validated successfully and the results showed that converter dynamics has a significant effect on vehicle launch performance and thus on fuel economy. However, it needs to be simplified in order to be easily integrated into vehicle control applications.

Wu and Moin (Wu and Moin, 2008) reported that enthalpy (fuel mass fraction and/or temperature) fluctuations in the oncoming mixture have important impacts on premixed combustion and in particular on combustion instability. An analytical model for premixed combustion was derived from the reactive Navier-Stokes equations by using large-activation-energy analysis (AEA) that introduced the concept of flamelets to help in understanding laminar flames. The model gives insight into the premixed combustion, but is not suitable for vehicle control applications because of its complexity.

Ni and Henclewood presented the Bernoulli model of internal combustion engines for Vehicle Infrastructure Integration-enabled in-vehicle applications of high accuracy (Ni and Henclewood, 2008). The proposed model provides insight into the relation between engine power and the rate of fuel consumption, and it was validated successfully using empirical data. Yet, the model is not simple enough to be suitable for control and transportation applications. Having seen this, let us investigate the second subcategory of the formulation approach-based modeling classification.

2.2.2.2 Empirical models

Empirical modeling, or sometimes called phenomenological modeling, has been adopted in several research papers in the field of powertrain modeling and control. Hrovat and Sun presented linear internal combustion engine models and control design methodologies for the idle speed control (ISC) application (Hrovat and Sun, 1997). They reported that the application of modern idle speed control techniques, such as sensitivity tuning controls, has led to improved engine performance at idle speed. They highlighted the criticality of controlling the transition from/to the idle speed control mode. Though the models that are presented in that research paper give insight into the relation between the idle speed and the rate of fuel consumption, they are valid only for the idling operating condition.

Lindhjem et al. (2004) presented the Physical Emission Rate Estimator (PERE) which has been developed to complement the Motor Vehicle Emission Simulator (MOVES) GreenHouse Gas (GHG) emissions model for increasing the level of accuracy in estimating on-road vehicle emissions. They proposed under the sponsorship of the US EPA the PERE as an empirical model that is partly based on

the principles of physics to estimate on-road vehicle emissions. Yet, that proposed model is valid only for the range of data based on which it was built.

Cook and Powell (1987) reviewed the nonlinear modeling of internal combustion engines literature and presented a fundamental nonlinear model of an internal combustion engine. They found that nonlinear dynamic models are suitable for wide speed and load operating ranges. Rakha et al. (2010) hence developed a simple vehicle driveline model that can be integrated with car-following models within microscopic traffic simulation software. That model is calibrated using engine and driveline parameters that are publicly available without the need for field data collection. The model demonstrated the capability to produce vehicle acceleration, speed, position, and fuel consumption estimates that are consistent with field observations.

Powell et al. (1998) presented the mathematical modeling, analysis, and simulation of a dynamic automatic transmission and manual dry clutch combination powertrain model. Both the conventional powertrain model and hybridized powertrain model were simulated and validated using experimental test data. The model gives insight into what influence the rate of fuel consumption, but it does not provide explainable mathematical trends.

Eriksson (2007) proposed a component-based modeling methodology for turbocharged engines. Using this methodology, Eriksson, developed models for the engine turbocharger compressor efficiency, compressor flow, and turbine flow. It was concluded in that research these models could be used in observer design and air/fuel ratio control of SI engines, as well as in control design of direct injection engines with variable geometry turbine (VGT) and EGR. However these models do not provide explainable mathematical trends.

Filipi and Assanis (2001) developed a transient, non-linear, single-cylinder turbocharged diesel engine model for predictions of instantaneous engine speed and torque. That research models the diesel engine as a non-linear, dynamic system and provides an insight into the relation between the rate of fuel consumption, engine speed, and torque. Yet, the model is valid only for the range of data based on which it is developed.

Watson et al. (1980) developed an empirical correlation simulating the turbocharged diesel engine's combustion process (heat release) via a mathematical expression whose governing parameters are linked to in-cylinder conditions. The proposed fundamental model provides the combustion information at the operating point and has become a key model in modeling combustion in diesel engines providing insight into what influence the rate of fuel consumption (Kim et al., 2002). Yet, it is valid only for the range of data based on which it was developed.

Shaver et al. (2006) reported that due to dilution limits, the HCCI engines will need to switch to a conventional spark ignition (SI) or diesel mode at very low and high load conditions. Thus, they developed a simple control-oriented model of a single-cylinder multi-mode HCCI engine using exhaust reinduction. The model helps in controlling exhaust emissions but it does not provide explainable mathematical trends. This concludes the second category of the formulation approach-based modeling classification. Let us now investigate the third category in this classification.

2.2.2.3 Statistical models

Many researchers have preferred statistical modeling to other types of modeling for vehicle powertrain modeling. Lindhjem et al. (2004) presented the Motor Vehicle

Emission Simulator (MOVES) GreenHouse Gas (GHG) emissions model for on-road vehicle emissions. They proposed under the sponsorship of the US EPA a statistical model for modeling the on-road vehicle emissions. In that model, key vehicle operating parameters, such as engine speed, road grade, and vehicle weight are incorporated. Yet, that model is valid only for the range of data based on which it was built.

Cacciari and Piancastelli (2001) presented a lumped mass model that is able to estimate velocity, acceleration and fuel consumption using aerodynamic, inertia and thermodynamic data of the vehicle. The model is then used along with a Genetic Algorithm (GA) to optimize the engine choice and the gearbox speeds distribution. That model is the base for their proposed robotized manual gearbox. However, it does not provide explainable mathematical trends.

Ouladsine et al. (2004) presented a neural network-based model of a turbocharged diesel engine. The model is composed of three interconnected neural sub-models, each of them constituting a nonlinear Multi-Input Single-Output Output Error model. In that model, the parameter estimation is done based on data gathered from a real diesel engine or on static mapping. Albeit the model gives insight into what influence the rate of fuel consumption, it requires recalibration with each dataset.

Wahlstrom (2005) developed a model of an internal combustion engine equipped with VGT and EGR. It was reported that the torque produced by this engine's model demonstrates some model errors probably because of the difficulty of modeling the nonlinearity of the engine VGT and EGR and of capturing the effect of changing the engine speed on the VGT and EGR and thus on exhaust emission rates.

Zito and Dor'e Landau (2005) developed a high pressure direct injection (HDI) variable geometry turbocharged diesel engine model with VGT and without

EGR. The proposed model is based on a nonlinear black-box identification procedure that is in turn based on a polynomial NARMAX representation for modeling nonlinearities. Yet, it requires recalibration with each dataset.

Daw et al. (2009) extended an iterated-map model that relates masses of air and fuel, lumped on a cycle basis, with feedback from cycle-to-cycle via the cylinder residual gases to spark assisted HCCI combustion. This extended model combines diluent-limited flame propagation (SI) and temperature-dependent, residual gas driven combustion (HCCI) to compute a combustion extent and integrated heat release for each cycle. However, mapping-based modeling is sometimes not satisfactory because emission maps can be highly sensitive to the driving cycle. Let us now investigate the fourth and last category in the formulation approach-based modeling classification.

2.2.2.4 Graphical models

Graphical modeling has been widely chosen in numerous research papers to model vehicle powertrains. Butler et al. (1999) presented ‘V-Elph’ vehicle engine model that is composed of four components: electric motors, internal combustion engines, batteries, and support components that can be integrated into a model and can simulate drive-trains. V-Elph was written in the SIMULINK graphical simulation language and is portable to most computer platforms. The model is meant to predict vehicle fuel consumption and vehicle emissions. However, the accuracy of prediction of that model is not high.

Gao et al. (2007) presented a Resistive Companion Form technique and Bond Graph method for modeling powertrain components. They presented as well the modeling and simulation capabilities of existing tools such as Powertrain System Analysis Toolkit (PSAT), ADvanced VehIcle SimulatOR (ADVISOR), PSIM, and

Virtual Test Bed. These modeling methods and tools are helpful in predicting fuel consumption and emission rates. However, the models that these tools provide do not provide explainable mathematical trends.

Grossi et al. (2009) modelled an internal combustion engine using the Power-Oriented Graphs (POG) technique with analogy between engine description and electrical circuit. They found that there is modeling correspondence between the engine components and variables (e.g. throttle valve, cylinder, and inertial flows) and electrical counterparts (e.g. current, voltage, resistance). Albeit the model gives insight into what influence the rate of fuel consumption, its accuracy is not high.

Silverlind (2001) presented the Modelica software package which is a library of basic and flexible components suitable for developing mean value engine models and control algorithms for the evaluation of new hardware on the systems-level, such as the fuel injection system in the internal combustion engines. The Modelica software package provides a structured means to develop a mean value engine model and is originally developed for DaimlerChrysler. Stankovic (2000) presented ‘Modelica’ as a standardized, object-oriented, and multi-domain modeling language for modeling the automotive engines thermodynamic subsystems, such as the fuel injection sub-system. Stankovic, A., analyzed the performance of Modelica in automotive engine applications. It was identified that the modeling principle in Modelica is based on the connector applied, i.e. the interaction between the components, for the description of engine components. Elmqvist et al. (2004) described typical modeling and real-time simulation issues that occur in vehicle powertrain dynamics modeling. In addition, they demonstrated the powerful real-time capabilities of Dymola and the Modelica modeling languages and their symbolic processing of the model equations. Yet, these models do not provide explainable mathematical trends.

Kim and Kim (1999) developed a computational fluid dynamics model of a large diesel engine using the WAVE software package to predict combustion heat release rate from user-specified fuel injection rate and injector geometry. The model was simulated and verified by experimental data of heat release rate and NOx emission for Hyundai Heavy Industries Co., Ltd. Yet, that model does not provide explainable mathematical trends.

Mukherjee and Karmakar (2000) presented the modeling and simulation of physical dynamic systems through Bondgraphs portraying systems in terms of power bonds. They presented bond graph as a graphical representation of a physical dynamic system, such as vehicle engines, with the major difference from block diagrams that the arcs in bond graphs represent bi-directional exchange of physical energy, while those in block diagrams and signal-flow graphs represent uni-directional flow of information. The engine model is generated using a modeling environment that supports hierarchical structuring by means of bond graphs (Louca et al., 2001). Gissinger et al. (1989) described a graphical approach for the complete modeling of a diesel engine. They used Bond graphs to model and simulate the behaviour of a turbocharged six cylinder Diesel engine. The program handles the various non-linearities such as the non-linearity of the rate of fuel consumption, the various coolants, the heat transfers within the cylinder head and the ignition delays. Yet, these models do not provide explainable mathematical trends.

SIMULINK is a similar multidomain simulation and modeling software package called that was developed by Mathworks Inc., and has become a widespread engine modeling tool in industry (The MathWorks Inc., 2000; Eriksson et al., 2010). Its primary interface is a graphical block diagramming tool and a customizable set of block libraries that let designers model a variety of time-varying systems. The

platform provides reusable generic components in a library for developing engine models setting standardized rules for modeling dynamic systems, such as the fuel injection pump of internal combustion engines. Assanis et al. (2000) developed a SIMULINK integrated model of vehicle systems composed of turbocharged, intercooled diesel engine, driveline and vehicle dynamics modules. The engine model features the thermodynamics of the in-cylinder processes with transient capabilities to ensure high fidelity predictions and was validated successfully. However, it does not provide explainable mathematical trends. Having concluded the second classification, the next section presents the third classification of powertrain modeling.

2.2.3 Main Input Variable-based Modeling

Modeling of vehicle fuel consumption and emissions rates can be categorized as well based on the main input independent variable. In this type of categorization there are three subcategories: (1) Modeling based on average speed as the main input independent variable, (2) Modeling based on instantaneous speed as the main input independent variable, (3) Modeling based on specific power as the main input independent variable.

2.2.3.1 Average speed models

Average speed is the most widely used independent input variable in vehicle fuel consumption and emission rates modeling. Numerous research papers adopted average speed as the main independent input variable in vehicle fuel consumption and emission rates modeling. Ding and Rakha (2004) identified recent state-of-practice for estimating vehicle emissions based on average speed only. They found that research

has demonstrated that although the EPA MOBILE5 model would indicate that a slowing of traffic typically increases emissions, empirical research indicates the opposite in many cases. They proposed statistical models for estimating fuel consumption and emissions using these critical variables that include the average speed. Though these models were validated successfully, they require recalibration with each dataset.

Guensler et al. (1993) further explored adopting average speed as the main independent input variable in vehicle fuel consumption and emission rates modeling. They proposed disaggregate speed correction factor (SCF) modeling technique to estimate relationships between average speed and vehicle emissions. Yet, the results indicate that additional data should be collected and that additional independent variables should be included. Thus, they found that average vehicle speed as the single explanatory variable is insufficient for modeling emissions.

Taylor (2003) presented CONTRAM which is a computer model of time-varying traffic in road networks that takes as input the network definition and time-varying demand for travel between a set of origin and destination zones, and delivers as outputs the resulting network flows, routes and travel times. The paper detailed the central method used in this model which is the time-dependent queuing. In addition, it presented an empirical fuel consumption and emissions model based on Overall's function of average speed and fuel consumption. Although, this average speed model is helpful in estimating aggregate emissions inventories and highly relevant to road traffic, it ignores the effect of transient changes in vehicle speed and acceleration.

Rizzotto et al. (1995) presented a data-based fuzzy logic bus fuel consumption model. The results of fuel consumption measurements in that research were correlated to a set of independent variables which represent the vehicle average speed, number of

passengers on board, and the actual elevation of the road. They reported that fuzzy logic is more efficient in correlating measured data than traditional mathematical method such as least squares. Yet, the model does not provide explainable mathematical trends.

Liao and Machemehl (1998) suggested an average speed-based analytical fuel consumption model (AFCM) to estimate the effects of signal timing on fuel consumption at signalized intersections. In that research, results of numerical experiments conducted using the AFCM were compared with results from the TEXAS simulation model with 10 percent error. However, the AFCM does not account for the significant effect of speed variability on vehicle fuel consumption and emissions rates. Having investigated this, let us now elucidate the second category in the main input variable-based modeling classification.

2.2.3.2 Instantaneous speed models

Instantaneous speed is the second most widely used independent input variable in vehicle fuel consumption and emission rates modeling. Several research papers adopted instantaneous speed as the main independent input variable in vehicle fuel consumption and emission rates modeling. Rakha and Ahn (2004) proposed that average speed is insufficient to fully capture the environmental impacts of ITS. They found that for the same average speed, one can observe widely different instantaneous speed and acceleration profiles, each of which results in very different fuel consumption and emission levels. Thus, they developed a software package called INTEGRATION model that combines car-following, vehicle dynamics, lane changing, energy, and emission models to estimate mobile source emissions from

instantaneous speed and acceleration levels. The validity of the model was demonstrated using sample test scenarios that include traveling at a constant speed, traveling at variable speeds, stopping at a stop sign, and traveling along a signalized arterial. Ahn et al. (2002) for the INTEGRATION development proposed statistical regression models that predict vehicle fuel consumption and emission rates with key input variables of instantaneous vehicle speed and acceleration measurements. The energy and emission models described in that paper utilized data collected at the Oak Ridge National Laboratory (ORNL) that included fuel consumption and emission rate measurements (CO, HC, and NOx) for five light-duty vehicles and three light-duty trucks as a function of the vehicle's instantaneous speed and acceleration levels. The fuel consumption and emission models developed in that research were found to be relatively accurate as compared to the ORNL data, with coefficients of determination ranging from 0.92 to 0.99. The study indicated that since these models utilize the vehicle's instantaneous speed and acceleration levels as independent variables, they are capable of evaluating the environmental impacts of operational-level projects including ITSs. Yet, these models require recalibration with each dataset.

Rakha and Van Aerde (2000) for the INTEGRATION development as well proposed a series of multivariate fuel consumption and emission prediction models that are applicable both to be used within a traffic simulation model of a signalized arterial and directly to instantaneous speed and acceleration data from floating cars traveling down a similar signalized arterial. That study indicated that the application of these instantaneous models has been more practical in terms of both their absolute magnitude and their relative trends than of average speed-based models.

Panis et al. (2006) modeled the traffic emissions caused by acceleration and deceleration of vehicles based on an instantaneous emission model integrated with a

microscopic traffic simulation model. Their proposed integrated model captures the second-by-second speed and acceleration of individual vehicles. However, it is very labour intensive in conducting inventory analysis.

Zweiri et al. (2001) developed a detailed non-linear dynamic model for single-cylinder diesel engines. The model describes clearly the dynamic behavior and inter-relationships between fuelling and engine speed. Albeit the model captures the second-by-second variations in the speed of the engine, it is relatively time consuming.

Hung et al. (2005) developed a data-based model of vehicular fuel consumption and emissions as a function of instantaneous speed and driving mode. They proposed piecewise interpolation functions for each non-idling driving mode in that model. Although this instantaneous speed-based model can capture transient changes in a vehicle speed as it travels on a highway network, and is more accurate in estimating vehicle emissions than average speed models, it is very labour intensive in conducting inventory analysis.

Froschhammer (2009; 2006) presented cost-effective component-based SIMPACK real-time engine models used by the BMW Group. The term 'component-based' refers to models which include individual components, such as valves, as opposed to using quasi-static look-up tables to describe the engine characteristics. The models showed satisfactory performance, but they have relatively moderate computational efficiency.

dSPACE GmbH (2006) presented a dSPACE real time diesel engine model and HIL simulator implemented for Deutz AG. The presented model and simulator provides wide engine variants handling and easy engine test automation. Albeit the model was validated satisfactorily, it is relatively time consuming. This concludes the

second category in the main input variable-based modeling classification. Let us now investigate the third category in this classification.

2.2.3.3 Specific power models

Specific power is the third most widely used independent input variable in vehicle fuel consumption and emission rates modeling. Several researchers adopted specific power as the main independent input variable in vehicle fuel consumption and emission rates modeling. Frey et al. (2007) proposed a vehicle specific power-based approach to be used for modeling fuel consumption for diesel and hydrogen fuel cell buses. In that research, relative errors between trip fuel consumption estimates and actual fuel use were generally under 10% for all observations. Yet, the study recommended this vehicle specific power-based modeling approach if the relevant data were available.

Ran et al. (2007) presented a mean specific power-based model of hydrogen fueled spark-ignition internal combustion engines for design and sizing of such engines. The study concluded that the mean value based sizing and simulation model gives relatively satisfactory sizing results. However, the model is valid only for spark ignition engines.

Wang et al. (2008) presented a data-based Vehicle Specific Power VSP-based model of vehicle fuel consumption to estimate the influence of driving patterns on fuel consumption using a portable emissions measurement instrument. They found that fuel consumption increases significantly with acceleration. Although this specific power model has reasonable accuracy, it is valid only for the range of data based on which it was built.

Song et al. (2009) proposed a model for evaluating the effects of traffic management on fuel efficiency of light duty vehicles. The model captures the

relationships between the vehicle specific power, the real-world driving activities, and the corresponding fuel consumptions. However, that model needs availability of relevant specific power data.

Feng (2007) developed a new heavy-duty diesel vehicle load-based modal emission rate model that is called Heavy-Duty Diesel Vehicle Modal Emission Modeling (HDDV-MEM). The HDDV-MEM approach first predicts second-by-second engine power demand as a function of vehicle operating conditions and then applies brake-specific emission rates to these second-by-second engine power demand predictions. Albeit the model was validated satisfactorily, it is valid only for Diesel engines. Having investigated this, the fourth classification of modeling is elucidated in the next section.

2.2.4 State Variable Value-based Modeling

Another classification of modeling of vehicles fuel consumption and emissions is the state variable value-based modeling. This classification has two subcategories: crank-angle resolution-based models and mean value-based models, as suggested by Guzzella and Amstutz (1998). Cook et al. (2006) reported as well that diesel engine models can be classified into mean value modeling and cylinder-by-cylinder modeling, i.e. analytical modeling. The mean value modeling of diesel engines, its average value of states characteristic, and its simplicity and easiness of manipulation were presented and covered by Kao and Moskwa (1995). The cylinder-by-cylinder modeling, its crank angle resolution characteristic, and its explainable trends were presented and covered by Watson (Watson, 1984). It predicts the effects of mechanical and/or control system changes on vehicle powertrain output torque, fuel

consumption, and emission using the state of the crank-angle resolution. The mean value-based models predict these effects based on the mean value of the state variables within the vehicle powertrain system.

2.2.4.1 Crank-angle resolution-based models

Crank-angle resolution-based models have been used for long time for modeling vehicle powertrain fuel consumption and emission rates. Numerous researchers adopted this type of modeling for its accuracy. Guzzella and Amstutz (Guzzella and Amstutz, 1998) presented model-based controls of diesel engine torque and transient macroscopic pollutant emission. They identified the tendencies in the influence of control inputs into diesel engines on the brake specific fuel consumption and emissions. They found that adopting early start of injection as a control input results in good brake specific fuel consumption and reduced amount of particulates but at the expense of high NO_x emissions. They found as well that late start of injection results in reduced NO_x emissions but at the expense of an increase in brake specific fuel consumption and particulate emissions.

Streit and Borman (Streit and Borman, 1971) presented a crankshaft resolution model of multicylinder turbocharged diesel engines. The model for the cylinder includes instantaneous heat transfer, homogeneous combustion burning rates explaining their relation to the rate of fuel consumption, and a scavenging model which allows any intermediate mode between perfect scavenging and complete mixing. They developed as well a model for the compressor of the turbocharger. Upholding the research findings of that research, Heywood (Heywood, 1988) reported the existence of a radiative heat transfer component during combustion. Though these

models were validated satisfactorily, they require a relatively long computational time due to their complexity.

Winterbone et al. (1977) developed a crank angle resolution model of turbocharged diesel engines based on the “filling and emptying” technique and using empirical feedback to estimate their transient response. The experimentally validated model was then used to evaluate the linearized transfer function of the diesel engine for control studies, such as fuel consumption control. However, it needs to be simplified before being suitable for vehicle control applications.

Hillion et al. (2009) proposed linearization of the modified autoignition Knock Integral Model (KIM) for HCCI and a cool flame model in order to accurately control the end of the cool flame phenomenon and thus improving the stability of the combustion of HCCI engines during transients as well as improving the control on fuel consumption. The modified autoignition KIM for HCCI was originally proposed by Swan et al. (2006). The cool flame model models the combustion with a very low reaction rate during which several chemical processes occur simultaneously leading to the real combustion. Albeit these models demonstrated reasonable accuracy, they require a relatively long computational time for their complexity. Having elaborated on this, let us now turn to investigate the second category in the state variable value-based modeling classification.

2.2.4.2 Mean value-based models

The other subcategory of the state variable value-based modeling classification is the mean value-based modeling. Mean value-based models have been adopted extensively in modeling vehicle powertrain fuel consumption and emissions rates for its high computational efficiency. Hendricks (1986) reported that the detailed analytical

models of the internal processes in the engine are very accurate and very useful for detailed laboratory analysis of engine performance, but they require long computing times and exhibit large numbers of fitting parameters. Thus, Hendricks presented for the first time a model of the engine dynamics that is called Mean Value Engine Model (MVEM) to predict the effects of mechanical and/or control system changes on heavy duty diesel engines output torque. Hendricks (1997) further proposed a mean value diesel engine dynamics model that describes the transfers between inputs (e.g. the crankshaft angular speed and throttle valve angle) and the output (e.g. fuel mass flow). That model is derived partly from the principles of physics and thermodynamics and seeks to predict the mean values of heavy duty diesel engine variables (e.g. volumetric efficiency and exhaust manifold pressure).

Seykens et al. (2006) presented the extension of the steady state mean value DYNAmic engine MOdel (DYNAMO), proposed by Ewalds (2003), combining the compression release brake and an exhaust valve brake in order to predict engine brake torque, exhaust gas temperatures and air and fuel mass flow rates. The developed model has been used successfully to analyze the possibility to use the engine brake torque to make automatic gear switching smoother and faster. However, it is valid only for the range of data based on which it was built.

Moskwa and Hedrick (1992) presented a nonlinear dynamic engine model of a port fuel-injected engine, which can be used for control algorithm development. This engine model predicts the mean engine brake torque as a function of the engine controls such as throttle angle. Albeit this model was validated satisfactorily, it does not account for delays.

Sun et al. (2005) presented the fundamental system models of the Air-Fuel ratio and torque that are typically embedded into the engine control strategy for most

engines. They presented as well the key issues in electronic control of internal combustion engines and their solutions. The research findings of that research were upheld by the findings of Zhao et al. (1997). Sun reported that Assanis et al. (1999) proposed a predictive model of the wastegate of the turbocharger which consists of a spring-loaded diaphragm in the exhaust manifold. In addition, a mean value model of VGT diesel engines was developed by Kolmanovsky et al. (1997) for a diesel engine equipped with an EGR valve. Sun, et al., highlighted as well the research finding of Canova et al. (2010) that two-stage turbochargers are a recent solution to improve engine performance and to mitigate the turbo-lag phenomenon although their modeling is problematic because of their complexity.

Eriksson et al. (2010) presented semi-physical mean value nonlinear models of the dynamics and nonlinear behaviors of gas and energy flows in EGR/VGT equipped turbocharged diesel engines. They found that the EGR system and VGT which were introduced to reduce emissions are strongly coupled and are difficult to be optimized because of their overshoots, non-minimum phase behaviors, and sign reversals which is a conclusion upheld by the findings of Winge Vigild (2001).

Hendricks (2001) presented an adiabatic mean value model of spark ignition engines and diesel engines. The proposed adiabatic mean value model described the performance, such as the rates of fuel consumption and emission, and dynamics of the engines with EGR more accurately than the conventional isothermal mean value engine models. Yet, it does not account for delays. This concludes the state variable value-based modeling classification. Let us now investigate the last classification of powertrain modeling.

2.2.5 Number of Dimensions-based Modeling

The subcategories of the number of dimensions-based modeling classification are zero/one dimensional/single zone, quasi dimensional, and multi dimensional/multi zone modeling, as suggested by Jung and Assanis (2001). The zero/one dimensional/single zone modeling assumes that the cylinder charge is uniform in both composition and temperature, at all time during the cycle which results in high computational efficiency (Foster, 1985). Multi dimensional/multi zone models, such as KIVA, account for spatial variation in mixture composition and temperature, which are essential to predict exhaust emissions (Varnavas and Assanis, 1996). The quasi dimensional modeling is an intermediate step between zero-dimensional and multi-dimensional models and can provide the spatial information required to predict emission products and require significantly less computing resources compared to multi-dimensional models (Whitehouse and Sareen, 1974).

2.2.5.1 Zero/one dimensional/single zone models

When high computational efficiency becomes the first priority, Zero/one dimensional/single zone modeling is preferred to other types of modeling. Thus, several researchers opt for this type of modeling in order to model vehicle powertrain fuel consumption and emission rates. Oliver (2006) modeled the turbocharged diesel engines intake manifold in one dimension using WAVE software package in an endeavor to estimate CO and NO_x emissions. Oliver showed how injecting air into the manifold can greatly improve the transient response of the turbocharger. Schmitt et al. (2009) described how a zero-dimensional engine model can improve the engine control law design for a turbocharged diesel engine fitted with an EGR system.

Because of the simplicity of the zero-dimensional engine model, it proved to give a good estimate of the start of combustion with minimal computational time. This conclusion is supported by the findings of Aceves et al. (2001). That proposed model helps in developing diesel engine controllers to meet the Euro VI pollutant standard, while maintaining the fuel consumption advantage the diesel engines have compared to spark ignition engines.

Liu and Chen (2009) developed a zero-dimensional combustion model for SI engine knock optimization. The model helps in optimizing the rate of fuel consumption and fuel injection timing. It is based on a three-zone approach (i.e., unburned, burning, and burned zones). A modified version of Tanaka's reduced chemical kinetic model for a commercial gasoline fuel was applied in both burned and unburned zones incorporated with the LUCKS (Loughborough University Chemical Kinetics Simulation) code. In the burning zone, an equilibrium combustion thermodynamic model is used. Yet, its accuracy is relatively low.

Tirkey et al. (2010) developed a zero dimensional knock model, two-zone combustion model, and gas dynamic model to minimize engine emissions and safe knock limit by optimizing some operational and engine design parameters such as equivalence ratio. Therefore, the Nitric Oxide exhaust emission concentrations are then predicted using the rate kinetic model. Albeit the model was validated satisfactorily, the accuracy of this model is relatively low.

Barba et al. (2000) presented a phenomenological single-zone combustion model for high speed DI diesel engines with common rail injection to help in meeting the emissions requirements for this type of engines. The model focuses on result parameters like combustion noise and NO_x-emission which are affected by this fuel

split injection. Although the model is suitable for modeling and powertrain control applications and is highly relevant to road traffic, its accuracy is relatively low.

Shrivastava et al. (2002) developed a CFD optimization model for optimizing the design of a direct-injection diesel engine using a 1-D KIVA Genetic Algorithm (1-D-KIVA 3v-GA) computer code. The design fitness in this model was determined using a 1-D gas dynamics code model for the simulation of the gas exchange process, coupled with a 3-D code model of spray, combustion, and emissions formation. Though this model was validated satisfactorily, it does not account for the spatial variation in mixture composition and temperature in the cylinder charge. Having seen this, let us now investigate the second category of the number of dimensions-based modeling classification.

2.2.5.2 Quasi dimensional models

The second subcategory of the number of dimensions-based modeling classification is the quasi dimensional modeling. Quasi dimensional modeling strikes a balance between modeling accuracy and modeling computational efficiency. Many researchers hence preferentially adopt this type of modeling. Jung and Assanis (2001) developed a quasi-dimensional, multi-zone, direct injection (DI) diesel combustion model and implemented it in a full cycle simulation of a turbocharged engine. That combustion model accounts for transient fuel spray evolution, fuel-air mixing, ignition, combustion and NO_x, and soot pollutant formation. It was proved that the model is capable of predicting the rate of heat release and engine performance with high fidelity, but it can not predict NO_x and soot emissions satisfactorily.

Bazari (1994) presented a non-linear transient engine cycle simulation software integrated into a two-dimensional multi-zone combustion-emissions model

in order to predict exhaust emissions under transient operating conditions. They demonstrated using this combustion-emissions model the characteristics of engine transient operation. The model was validated satisfactorily, but it does not account for large spatial variations in mixture composition in the cylinder charge.

Patterson et al. (1994) developed three-dimensional KIVA code to study the effects of injection pressure and split injections on diesel engine performance and soot and NO_x emissions. The KIVA code included the following sub-models: a wave breakup atomization model, drop drag with drop distortion, spray/wall interaction with sliding, rebounding, and breaking-up drops, multi-step kinetics ignition and laminar-turbulent characteristic time combustion, wall heat transfer with unsteadiness and compressibility, Zeldovich NO_x formation, and soot formation with Nagle Strickland-Constable oxidation. Soot and NO_x emissions were found to be very sensitive to factors that influence the chamber gas temperatures such as crevice flow.

Arsie et al. (2007) proposed a semi-empirical two-zone thermodynamic model to optimize the control parameters of High Speed Direct Injection (HSDI) Diesel engines. The model facilitates the engine control design for commonrail Diesel engines with multiple injections, where the large number of control parameters requires a large experimental tuning effort. Yet, it does not account for large spatial variations in mixture composition and temperature in the cylinder charge. An optimization analysis based on that model was then performed aiming to minimize NO_x emissions with constraints on soot emissions and engine performance. The research findings of this study were supported by the research findings of Arsie et al. (2005; 2006).

Roy and Liu (2008) presented a quasi-dimensional model with eight Degrees Of Freedom (DOF) to simulate and to animate the response of a vehicle to different

road, traction, braking and wind conditions. The model was developed for vehicle suspension design and performance analysis. Its inputs are the engine throttle and starter, brake, transmission gear number, and clutch position. The model outputs are suspension parameters, such as rigidity and damping, and the longitudinal energy loss. Albeit the model was validated satisfactorily, it does not account for large spatial variations in mixture composition in the cylinder charge. Let us now investigate the third category of the number of dimensions-based modeling classification.

2.2.5.3 Multi dimensional/multi zone models

As the last subcategory of the number of dimensions-based modeling classification, multi dimensional/multi zone modeling is preferred when modeling accuracy is concerned. Several researchers adopt this type of modeling when they model the vehicle powertrain fuel consumption and emissions rates. Taklanti and Delhayé (1999) presented the methodologies of multi-dimensional modeling of the aerodynamic and combustion in Diesel engines developed at the PSA Peugeot Citroën. These methodologies are based on CFD and combustion simulation applications. Although the models developed using these methodologies are relatively accurate and give insight into what influence the rate of fuel consumption in Diesel engines, they require relatively long computational time so that they are not suitable for control applications without being simplified.

Easley et al. (2001) developed a multi-zone model of HCCI engines by coupling the first law of thermodynamics with detailed chemistry of hydrocarbon fuel oxidation and NO_x formation. This model is meant to be used in parametric studies to determine the effect of heat loss, crevice volume, temperature stratification, fuel-air equivalence ratio, engine speed, and boosting on HCCI engine operation. Though the

predictions that the model provides are satisfactorily accurate, they may vary according to the assumed initial or boundary conditions in these sub-models.

Aceves et al. (2000) developed a multi-zone model for prediction of the HCCI combustion and emissions and found that the hottest part of the mixture ignites first, and compresses the rest of the charge, which then ignites after a short time lag. They found that turbulence has little effect on HCCI combustion. The model was validated satisfactorily, but it requires relatively long computational time.

Komninos et al. (2005) presented a multi-zone phenomenological model for simulating the mass exchange between zones and the flow of the in-cylinder mixture in and out of the crevice region in HCCI engines. That experimentally validated model describes the combustion, heat and mass transfer processes for the closed part of the engine cycle, i.e. compression, combustion and expansion, helping in better understanding what influence the rate of fuel consumption. The findings of that study are further supported by the findings of Komninos and Hountalas (2008). Though the model demonstrated satisfactory predictions, it has relatively low computational efficiency.

Havstad et al. (2010) described CHEMKIN-based multi-zone model that simulates the expected combustion variations in a single-cylinder engine fueled with iso-octane as the engine transitions SI combustion to HCCI combustion. The model captures several important experimental trends, including stable SI combustion at low EGR (~10%), a transition to highly unstable combustion at intermediate EGR, and stable HCCI combustion at very high EGR (~75%). Albeit the model provides insight into what influence the rate of fuel consumption, the usually included phenomenological sub-models in such model result in having results that may vary according to the assumed initial or boundary conditions in these sub-models. This

concludes the classification of powertrain modeling and paves the way to compare them with each other. In an endeavor to provide further insight into the subcategories of each of the modeling classifications presented in this study, “Appendix F” presents comparisons between these subcategories with respect to assumptions, limitations, merits, drawbacks, characteristic parameters, data collection technique, accuracy, and relevance to road traffic.

2.3. RESEARCH GAP AND SUMMARY OF LITERATURE REVIEW

Modeling of vehicle fuel consumption and emissions emerged as an effective tool to help in developing and assessing vehicle technologies as well as to predict and to estimate aggregate vehicle fuel consumption and emissions. This study has reviewed the relevant literature to identify the current state of the art on vehicle fuel consumption and emissions modeling. The study has found that there are five types of modeling based on which the literature on vehicle fuel consumption and emissions can be categorised: (1) scale of the input variable-based modeling type, which was suggested by Yue (Yue, 2008), (2) formulation approach-based modeling type, (3) main input variable-based modeling type, (4) state variable value-based modeling type, which was suggested by Guzzella and Amstutz (Guzzella and Amstutz, 1998), (5) number of dimensions-based modeling type, which was suggested by Jung and Assanis (Jung and Assanis, 2001). The relevant main models in each of these categories to vehicle fuel consumption and emissions have been presented in this study.

The scale of the input variable-based modeling classification has been reviewed and its three subcategories have been explored which are microscopic, macroscopic, and mesoscopic models. The four subcategories in the formulation

approach-based modeling classification have been also reviewed which are analytical, empirical, statistical, and graphical modeling. In the main input variable-based modeling classification, the three subcategories in this classification have been reviewed as well which are average speed, instantaneous speed, and specific power models. The overview has presented as well the two subcategories in the state variable value-based modeling classification which are crank-angle resolution-based models and mean value-based models. The three subcategories in the number of dimensions-based modeling classification have been reviewed which are zero/one dimensional/single zone, quasi dimensional, and multi dimensional/multi zone modeling.

The review has revealed that the main input variables and parameters for vehicle fuel consumption and emissions modeling are vehicle average speed, vehicle average acceleration, crankshaft instantaneous speed, crankshaft instantaneous acceleration, and engine specific power. The other input variables and parameters for vehicle fuel consumption and emissions modeling which include engine torque, intake manifold pressure, engine displacement volume, road grade, vehicle weight, and loading condition such as accessory use. The reviewed models have been compared with regard to assumptions, limitations, merits, drawbacks, accuracy, relevance to road traffic, and data collection technique.

As to the scale of the input variable-based modeling type, it has been found that microscopic vehicle fuel consumption and emissions models can capture transient changes in a vehicle speed and acceleration level as it travels on a highway network, can capture the impact of intelligent transportation system strategies such as traffic signal coordination, and are more accurate in estimating vehicle fuel consumption and emissions than macroscopic models in terms of both their absolute magnitude and

their relative trends than of average speed-based models. In addition, macroscopic vehicle fuel consumption and emissions models have been found highly relevant to road traffic and most helpful in estimating aggregate emissions inventories.

It has been found that analytical modeling is the most accurate type of vehicle fuel consumption and emissions modeling and graphical modeling is the least accurate type of vehicle fuel consumption and emissions modeling in the formulation approach-based modeling type. In addition, it has been found that analytical models can describe the physical phenomena associated with vehicle operation and emissions productions and with explainable mathematical trends. They can be thus easily extended to other types of applications. It has been found as well that empirical models strike a balance between modeling accuracy and computational time effectiveness. Although Statistical models have been found requiring recalibration with each dataset and can not easily interpolate gaps in the dataset and can not easily extrapolate data beyond the bounds of the dataset, they have been found relatively easy to be made and the uncertainty in their results can be quantified. The least accurate type of formulation approach-based modeling is graphical models since they are simplification based on other types of modeling.

As to the main input variable-based modeling type, it has been found that average speed models result in modeling error of 57% in comparison with field data but they are most helpful in estimating aggregate emissions inventories and are highly relevant to road traffic. It has been found as well that instantaneous speed models are more accurate in estimating vehicle emissions than average speed models in terms of both their absolute magnitude and their relative trends. In addition, it has been found that specific power models are more suitable for heavy duty diesel vehicle engines.

In the state variable value-based type of modeling, it has been found that the crank-angle resolution-based models are the most accurate models in this classification although they usually require a relatively long computational time for their complexity so that they are less suitable for vehicle powertrain fuel consumption and emissions control applications and therefore are less relevant to road traffic than the mean value-based models. The mean value-based models strike a balance between modeling accuracy and computational efficiency and therefore are very suitable for vehicle powertrain fuel consumption and emissions control applications.

In the number of dimensions-based modeling type, it has been found that the zero/one dimensional/single zone models are the most computationally efficient models in this classification because of their simplicity and thus are most suitable for vehicle powertrain fuel consumption and emissions control applications and therefore are most relevant to road traffic. Yet, the zero/one dimensional/single zone models are the least accurate modeling subcategory in this classification. On the contrary, the multi dimensional/multi zone models are the most accurate modeling subcategory in this classification because they account for spatial variation in mixture composition and temperature in the cylinder charge. Yet, the multi dimensional/multi zone models require relatively long computational time and their usually included phenomenological sub-models result in having results that may vary according to the assumed initial or boundary conditions in these submodels. The quasi dimensional models subcategory lies somewhere in-between these two extremes since the quasi dimensional models strike a balance between modeling accuracy and computational efficiency.

A major challenge in this research area is to bridge the gap between the accuracy of microscopic modeling simulations and the scalability of macroscopic modeling

simulations. Scaling up microscopic modeling simulations to macro-scale allows engineers to address detailed research questions at a truly large scale helping in assessing and developing transportation applications accurately (Demers et al., 2009). Largely, there is a need for analytical microscopic modeling of the diesel powertrain components for which no analytical models have been developed as yet (Biteus, 2002). Analytically modeling of fuel consumption and emission of vehicles operating under a non-stoichiometric condition is particularly problematic (Greenwood, 2003). Therefore, this research presents an analytical microscopic model of diesel powertrain fuel consumption and emissions.

The proposed model analytically models the intake manifold of diesel powertrain in Chapters 3 and the supercharging compressor in Chapter 4 as the inlets to the diesel powertrain. The output of these developed models acts as the input into the analytical model of diesel engine as presented in Chapter 5. The output of the models developed in Chapters 3, 4 and 5 acts as the input into the analytical models developed in Chapter 5 on diesel powertrain fuel consumption rate and brake power. The output of the models developed in Chapters 3 and 5 acts as the input into the analytical model of diesel powertrain exhaust system and regulated emissions rate elucidated in Chapter 6. Figure 2.1 illustrates the inter-connections between these chapters and the research objectives.

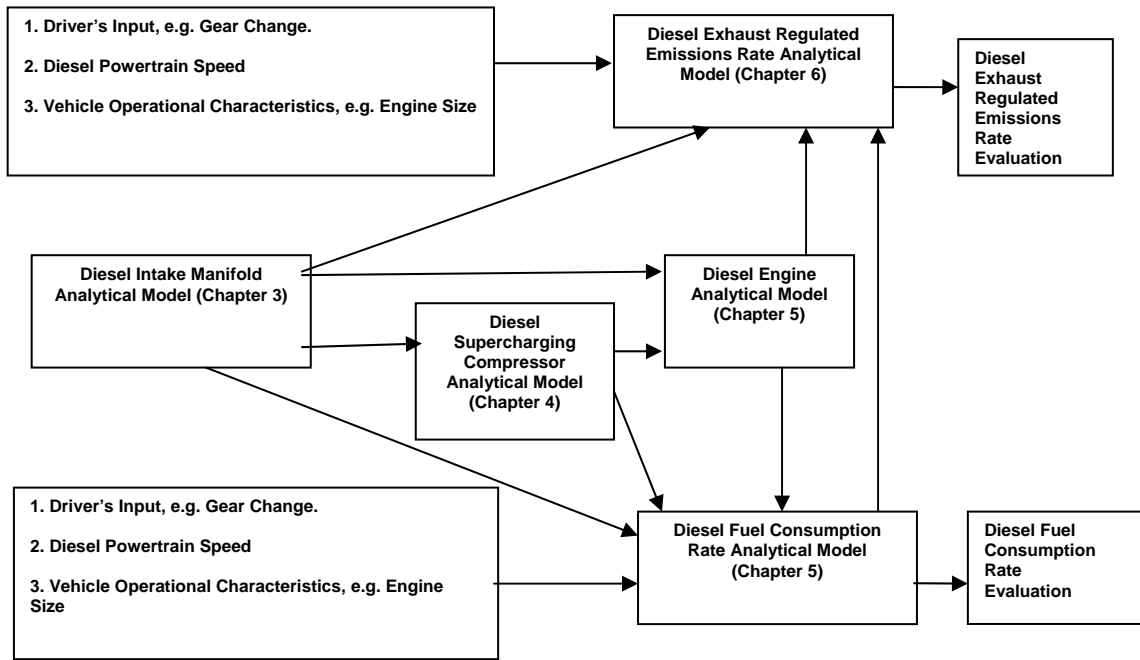


Figure 2.1

The inter-connections between thesis chapters and the research objectives

Chapter 7 presents the sensitivity analysis and the simplified models of the analytical models developed in Chapters 5 and 6 of diesel powertrain fuel consumption rate, engine power and regulated emissions rate. These simplified models are aimed to be fitted into the INTEGRATION software and traffic simulator. All of the analytical models presented in this study have been derived from the principles of physics as a way of validating these models.

CHAPTER 3

DIESEL POWERTRAIN INTAKE MANIFOLD ANALYTICAL MODEL

3.1. OVERVIEW

The highly promising features of diesel powertrains, such as high compression ratio, effective fuel consumption rate, high torque, and high output power, put continual demands on diesel powertrain development (Obert, 1973; Heywood, 1988; Taylor, 1985). The ITSs lie at the heart of the continual efforts of developing the diesel powertrains based on modeling. The pursuit of modeling diesel powertrain usually starts with modeling the intake manifold. Since no analytical model has been developed as yet of diesel powertrains, this chapter presents an analytical model of the intake manifold of a supercharged diesel powertrain, equipped with an electronic throttle control (ETC), as the inlet of the diesel powertrain with the aim of helping in analyzing analytically the performance of the diesel intake manifold. Following from principles of physics, Chapter 3 contributes to the implementation of the 1st pillar of the research philosophy adopted in this study in an endeavour to achieve the 1st objective in this research.

3.2. INTAKE MANIFOLD DYNAMIC PRESSURE

Since the intake manifold pressure is a key characteristic parameter in diesel intake manifold, let us firstly formulate analytically the intake manifold dynamic pressure. At no phase change, at relatively high temperature, and/or at relatively low pressure

air can be treated as an ideal gas. Since this is the case in the diesel engine intake manifold, it follows from the ideal gas law that (Obert, 1973):

$$P_i V_i = m_i R T_i \quad (3.1)$$

By establishing differentiation with respect to time on both sides of equation (3.1) in order to formulate the intake manifold pressure dynamics, given that the intake manifold volume is constant it follows that (Jung and Glover, 2003):

$$\dot{P}_i = \frac{R}{V_i} \left(m_i \dot{T}_i + T_i \dot{m}_i \right) \quad (3.2)$$

By combining equations (3.1) and (3.2) together, the following follows:

$$\dot{P}_i = \frac{R}{V_i} \left(\frac{P_i V_i}{R T_i} \dot{T}_i + T_i \dot{m}_i \right) \quad (3.3)$$

Simplifying equation (3.3) leads to the following:

$$\dot{P}_i = \frac{P_i}{T_i} \dot{T}_i + \frac{P_i}{m_i} \dot{m}_i \quad (3.4)$$

By applying the principle of conservation of mass on the intake manifold, the following follows from equation (3.4).

$$\dot{P}_i = P_i \frac{\dot{T}_i}{T_i} + \frac{R T_i}{V_i} \left(m_{Throttle} \dot{} - \dot{m}_{All Cyl} \right) \quad (3.5)$$

In order to resolve equation (3.5), the mass flow rate of air goes into cylinders has to be determined analytically first. Thus, the following subsection presents how the mass flow rate of air goes into cylinders, $\dot{m}_{All Cyl}$, can be determined analytically.

3.3. MASS FLOW RATE OF AIR GOES INTO CYLINDERS

In order to evaluate $\dot{m}_{All Cyl}$ of equation (3.5), the following follows from the

fundamental definition of the mass flow rate and from the fundamental definition of volumetric efficiency (Heywood, 1988; Sonntag et al., 2008; Ismail et al., 2009):

$$\dot{m}_{All\ Cyl} = \rho_{Cyl} \eta_V \dot{V}_{Cyl\ Theoretical} \quad (3.6)$$

Thus, by combining equation (3.6) with the definition of the theoretical air volumetric flow into cylinder, the following follows (Heywood, 1988):

$$\dot{m}_{Cyl} = \frac{\rho_{Cyl} \eta_V V_d N_s n}{N_{Cyl}} \quad (3.7)$$

Therefore, equation (3.7) can be rewritten as follows:

$$\dot{m}_{Cyl} = \frac{\rho_{Cyl} \eta_V V_d N_m n}{60 N_{Cyl}} \quad (3.8)$$

Considering the fundamental definition of density, it follows from equation (3.8) (Sonntag et al., 2008; Ismail et al., 2009):

$$\dot{m}_{Cyl} = \frac{m_{Cyl} \eta_V V_d N_m n}{60 N_{Cyl} V_{Cyl}} \quad (3.9)$$

Recalling the ideal gas law, it follows from combining equations (3.9) and (3.1) that:

$$\dot{m}_{Cyl} = \frac{\frac{P_{Cyl} V_{Cyl}}{R T_{Cyl}} \eta_V V_d N_m n}{60 N_{Cyl} V_{Cyl}} \quad (3.10)$$

T_{Cyl} equals T_i since the few microseconds which are the duration of the intake stroke are not sufficient to make significant heat transfer from the cylinder hot wall to the inducted fresh air charge into the cylinder since temperature rise takes time whereas pressure drop occurs instantaneously (Khummongkol et al., 2004). Thus, the following follows from equation (3.10):

$$\dot{m}_{Cyl} = \frac{P_{Cyl} \eta_V V_d N_m n}{60 N_{Cyl} R T_i} \quad (3.11)$$

For all of the four cylinders of the engine it follows from equation (3.11) that:

$$\dot{m}_{All\ Cyl} = \frac{P_{Cyl} \eta_V V_d N_m n}{60 R T_i} \quad (3.12)$$

Therefore, simplifying equation (3.12) leads to the following:

$$\dot{m}_{All\ Cyl} = \frac{\rho \eta_V V_d N_m n}{60} \quad (3.13)$$

In order to evaluate P_{Cyl} in equation (3.12), since pressure drop occurs instantaneously the cylinder pressure P_{Cyl} during the exhaust stroke and at the beginning of the intake stroke becomes ambient pressure (Obert, 1973; Taylor, 1985). However, due to the effect of accelerating the reciprocating piston, a slight pressure drop occurs in the cylinder due to the created vacuum pressure that results from the inertia and acceleration of the piston (Rama and Durgaiah, 2007). Thus, the cylinder pressure P_{Cyl} can be evaluated as follows:

$$P_{Cyl\ Intake} = P_{Atm} - P_{Vac} \quad (3.14)$$

By the end of the intake stroke, pressure equalizes throughout the intake manifold runners and thus P_{Cyl} becomes equating P_{in} . Therefore, P_{Cyl} can be evaluated as follows:

$$P_{Cyl} = \begin{cases} P_{Cyl\ Intake} & \theta_{IVO} \leq \theta < \theta_{IVC} \\ P_i & \theta = \theta_{IVC} \end{cases} \quad (3.15)$$

In order to evaluate P_{vac} in the diesel engine cylinder shown in Figure 3.1, the following follows from the fundamental definition of pressure (Rama and Durgaiiah, 2007):

$$P_{vac} = \frac{F_a}{\frac{\pi}{4} B^2} \quad (3.16)$$

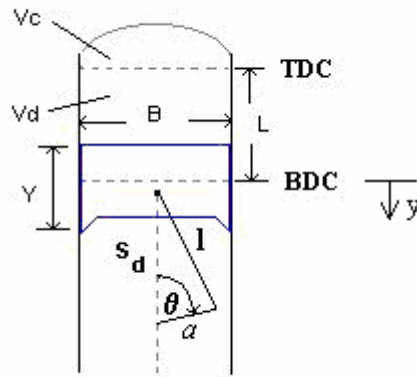


Figure 3.1

Geometry of cylinder, piston, connecting rod, and crankshaft

In order to evaluate F_a , it follows from the fundamental definition of force that

$$F_a = m_p a_p \quad (3.17)$$

In order to evaluate a_p , it follows from the fundamental definitions of displacement, velocity, and acceleration that

$$y = a - a \cos \theta \quad (3.18)$$

The crankshaft rotational speed in radians per second, w , can be expressed in terms of the crankshaft rotational speed in revolutions per minute, N_m , as follows:

$$w = 2\pi \frac{N_m}{60} \quad (3.19)$$

The instantaneous linear velocity of the piston, S_p , can be evaluated using equations (3.18) as follows:

$$S_p = \frac{dy}{dt} = w a \sin \theta \quad (3.20)$$

The linear acceleration of the piston, a_p , can be thus evaluated using equations (3.20) as follows:

$$a_p = \frac{d^2 y}{dt^2} = w^2 a \cos \theta \quad (3.21)$$

The mass of the piston, m_p , can be evaluated based on the fundamental definition of mass as follows (Ismail et al., 2009):

$$m_p = \rho_p V_p \quad (3.22)$$

Hence, the force generated due to the acceleration of the piston, F_a , can be evaluated by combining equations (3.17), (3.21), and (3.22) as follows given the fact that pistons are currently non-uniformly cylindrical in shape:

$$F_a = \rho_p V_p (w^2 a \cos \theta) \quad (3.23)$$

Substituting equation (3.23) in equation (3.16) leads to the following:

$$P_{Vac} = \frac{4 \rho_p V_p w^2 a \cos \theta}{\pi B^2} \quad (3.24)$$

Combining equations (3.19) and (3.24) leads to the following:

$$P_{Vac} = \frac{\pi \rho_p V_p a N_m^2 \cos \theta}{225 B^2} \quad (3.25)$$

Thus, by combining equations (3.14), (3.15), and (3.25), the pressure of air goes into cylinder P_{Cyl} can be evaluated as follows expressing N_s in terms of N_m :

$$P_{Cyl} = \begin{cases} P_{Atm} - \left(\frac{\pi \rho_p V_p a N_m^2 \cos \theta}{225 B^2} \right) & \theta_{IVO} \leq \theta < \theta_{IVC} \\ P_i & \theta = \theta_{IVC} \end{cases} \quad (3.26)$$

Therefore, by combining equations (3.12) and (3.26) the following follows:

$$\dot{m}_{All\ Cyl} = \begin{cases} \frac{\left(P_{Atm} - \left(\frac{\pi \rho_p V_p a N_m^2 \cos \theta}{225 B^2} \right) \right) \eta_v V_d N_m n}{60 R T_i} & \theta_{IVO} \leq \theta < \theta_{IVC} \\ \frac{P_i \eta_v V_d N_m n}{60 R T_i} & \theta = \theta_{IVC} \end{cases} \quad (3.27)$$

Flexibility of the crankshaft in diesel engines exhibits significant nonlinearities to the analysis of diesel powertrain intake manifold performance. Particularly, at crankshaft rotational speeds higher than 2000 rpm the influence of such flexibility on diesel powertrains performance becomes significant. Hence, the next subsection presents the mass flow rate of air goes into cylinders with a flexible crankshaft.

3.4. MASS FLOW RATE OF AIR GOES INTO CYLINDERS WITH A FLEXIBLE CRANKSHAFT

In order to evaluate $\dot{m}_{All\ Cyl}$ of equation (3.5) taking into account the flexibility of crankshaft, let us evaluate P_{Cyl} in equation (3.15) taking into account the flexibility of

crankshaft. Since pressure drop occurs instantaneously, the cylinder pressure P_{Cyl} during the exhaust stroke and at the beginning of the intake stroke becomes ambient pressure (Obert, 1973; Taylor, 1985). However, due to the effect of accelerating the reciprocating piston, a slight pressure drop occurs in the cylinder due to the created vacuum pressure that results from the inertia and acceleration of the piston (Rama and Durgaiah, 2007). Thus, the gas pressure inside the cylinder during the intake stroke $P_{Cyl\ Intake}$ can be evaluated as follows:

$$P_{Cyl\ Intake} = P_{Atm} - P_{Vac} \quad (3.28)$$

By the end of the intake stroke, pressure equalizes throughout the intake manifold runners and thus P_{Cyl} becomes equating P_{in} . The P_{Vac} in the diesel engine cylinder shown in Figure 3.2 can be evaluated from equation (3.16) the following from the fundamental definition of pressure. Also, the F_a can be evaluated from equation (3.17) following from the fundamental definition of force.

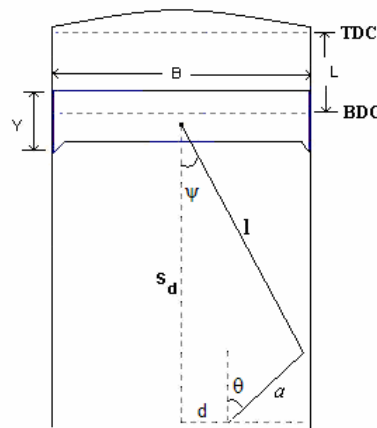


Figure 3.2

Geometry of cylinder, piston, connecting rod, and flexible crankshaft

In order to evaluate a_p , it follows from the fundamental definitions of displacement, velocity, and acceleration that

$$S_d = a \cos \theta + \sqrt{l^2 - d^2 - 2 d a \sin \theta - a^2 \sin^2 \theta} \quad (3.29)$$

The crankshaft rotational speed in radians per second, w , in terms of N_m can be evaluated from equation (3.19). The instantaneous linear velocity of the piston, S_p , can be evaluated using equation (3.29) as follows:

$$S_p = \frac{dS_d}{dt} = -a \sin \theta \frac{d\theta}{dt} + \frac{\left(-2 d a \cos \theta \frac{d\theta}{dt} - 2 a^2 \sin \theta \cos \theta \frac{d\theta}{dt} \right)}{2 \sqrt{l^2 - d^2 - 2 d a \sin \theta - a^2 \sin^2 \theta}} \quad (3.30)$$

Equation (3.30) can be rewritten as follows:

$$S_p = -a \left(\sin \theta + \frac{d a \cos \theta + a \sin \theta \cos \theta}{\sqrt{l^2 - d^2 - 2 d a \sin \theta - a^2 \sin^2 \theta}} \right) \frac{d\theta}{dt} \quad (3.31)$$

By combining equations (3.19) and (3.31) together, the following follows:

$$S_p = -\frac{2 a \pi N_m}{60} \left(\sin \theta + \frac{d a \cos \theta + a \sin \theta \cos \theta}{\sqrt{l^2 - d^2 - 2 d a \sin \theta - a^2 \sin^2 \theta}} \right) \quad (3.32)$$

The acceleration of the piston, a_p , can be thus evaluated using equations (3.32) as follows:

$$a_p = \frac{dS_p}{dt} = -\frac{2 a \pi N_m}{60} \left(\cos \theta \frac{d\theta}{dt} - \frac{(d a \cos \theta + a \sin \theta \cos \theta) \left(-2 d a \cos \theta \frac{d\theta}{dt} - 2 a^2 \sin \theta \cos \theta \frac{d\theta}{dt} \right)}{2 \left(l^2 - d^2 - 2 d a \sin \theta - a^2 \sin^2 \theta \right)^{\frac{3}{2}}} + \frac{-d \sin \theta \frac{d\theta}{dt} + \left(-a \sin^2 \theta \frac{d\theta}{dt} + a \cos^2 \theta \frac{d\theta}{dt} \right)}{\left(l^2 - d^2 - 2 d a \sin \theta - a^2 \sin^2 \theta \right)^{\frac{1}{2}}} \right) \quad (3.33)$$

By rearranging equation (3.33) the following follows:

$$a_p = -\frac{2a\pi N_m}{60} \left(\frac{\cos\theta - \frac{(da\cos\theta + a\sin\theta\cos\theta)(-2da\cos\theta - 2a^2\sin\theta\cos\theta)}{2(l^2 - d^2 - 2da\sin\theta - a^2\sin^2\theta)^{\frac{3}{2}}}}{\frac{-d\sin\theta - a\sin^2\theta + a\cos^2\theta}{(l^2 - d^2 - 2da\sin\theta - a^2\sin^2\theta)^{\frac{1}{2}}}} + \frac{d\theta}{dt} \right) \quad (3.34)$$

By combining equations (3.19) and (3.34) together, the following follows:

$$a_p = -\frac{a\pi^2 N_m^2}{900} \left(\frac{\cos\theta - \frac{(da\cos\theta + a\sin\theta\cos\theta)(-2da\cos\theta - 2a^2\sin\theta\cos\theta)}{2(l^2 - d^2 - 2da\sin\theta - a^2\sin^2\theta)^{\frac{3}{2}}}}{\frac{-d\sin\theta - a\sin^2\theta + a\cos^2\theta}{(l^2 - d^2 - 2da\sin\theta - a^2\sin^2\theta)^{\frac{1}{2}}}} + \right) \quad (3.35)$$

The mass of the piston, m_p , can be evaluated using equation (3.22) following from the fundamental definition of mass. Hence, the force generated due to the acceleration of the piston, F_a , can be evaluated by combining equations (3.17), (3.35), and (3.22) as follows:

$$F_a = \rho_p \left(\frac{\pi B^2 Y}{4} \right) \left(-\frac{a\pi^2 N_m^2}{900} \left(\frac{\cos\theta - \frac{(da\cos\theta + a\sin\theta\cos\theta)(-2da\cos\theta - 2a^2\sin\theta\cos\theta)}{2(l^2 - d^2 - 2da\sin\theta - a^2\sin^2\theta)^{\frac{3}{2}}}}{\frac{-d\sin\theta - a\sin^2\theta + a\cos^2\theta}{(l^2 - d^2 - 2da\sin\theta - a^2\sin^2\theta)^{\frac{1}{2}}}} + \right) \right) \quad (3.36)$$

Equation (3.36) can be simplified as follows:

$$F_a = \frac{\rho_p \pi^3 B^2 Y a N_m^2}{3600} \left(\frac{\cos\theta - \frac{(da\cos\theta + a\sin\theta\cos\theta)(-2da\cos\theta - 2a^2\sin\theta\cos\theta)}{2(l^2 - d^2 - 2da\sin\theta - a^2\sin^2\theta)^{\frac{3}{2}}}}{\frac{-d\sin\theta - a\sin^2\theta + a\cos^2\theta}{(l^2 - d^2 - 2da\sin\theta - a^2\sin^2\theta)^{\frac{1}{2}}}} + \right) \quad (3.37)$$

Substituting equation (3.37) in equation (3.16) leads to the following:

$$P_{vac} = \frac{\rho_p \pi^2 Y a N_m^2}{900} \left[\frac{\cos \theta - \frac{(d a \cos \theta + a \sin \theta \cos \theta)(-2 d a \cos \theta - 2 a^2 \sin \theta \cos \theta)}{2 (l^2 - d^2 - 2 d a \sin \theta - a^2 \sin^2 \theta)^{\frac{3}{2}}}}{-d \sin \theta - a \sin^2 \theta + a \cos^2 \theta} \frac{1}{(l^2 - d^2 - 2 d a \sin \theta - a^2 \sin^2 \theta)^{\frac{1}{2}}} + \right] \quad (3.38)$$

Thus, by combining equations (3.28), (3.15), and (3.38), the pressure of air goes into cylinder P_{Cyl} can be evaluated as follows:

$$P_{Cyl} = \begin{cases} P_{Atm} - \frac{\rho_p \pi^2 Y a N_m^2}{900} \left[\frac{\cos \theta - \frac{(d a \cos \theta + a \sin \theta \cos \theta)(-2 d a \cos \theta - 2 a^2 \sin \theta \cos \theta)}{2 (l^2 - d^2 - 2 d a \sin \theta - a^2 \sin^2 \theta)^{\frac{3}{2}}}}{-d \sin \theta - a \sin^2 \theta + a \cos^2 \theta} \frac{1}{(l^2 - d^2 - 2 d a \sin \theta - a^2 \sin^2 \theta)^{\frac{1}{2}}} + \right] & \theta_{IVO} \leq \theta < \theta_{IVC} \\ P_i & \theta = \theta_{IVC} \end{cases} \quad (3.39)$$

Therefore, by combining equations (3.22) and (3.39) the following follows:

$$\dot{m}_{All\ Cyl} = \begin{cases} \frac{\left(P_{Atm} - \frac{\rho_p \pi^2 Y a N_m^2}{900} \left[\frac{\cos \theta - \frac{(d a \cos \theta + a \sin \theta \cos \theta)(-2 d a \cos \theta - 2 a^2 \sin \theta \cos \theta)}{2 (l^2 - d^2 - 2 d a \sin \theta - a^2 \sin^2 \theta)^{\frac{3}{2}}}}{-d \sin \theta - a \sin^2 \theta + a \cos^2 \theta} \frac{1}{(l^2 - d^2 - 2 d a \sin \theta - a^2 \sin^2 \theta)^{\frac{1}{2}}} + \right] \right) \eta_v V_d N_m n}{60 R T_i} & \theta_{IVO} \leq \theta < \theta_{IVC} \\ \frac{P_i \eta_v V_d N_m n}{60 R T_i} & \theta = \theta_{IVC} \end{cases} \quad (3.40)$$

Now, the outstanding parameter to determine analytically the intake manifold dynamic pressure in equation (3.5) is the mass flow rate of air at the throat of the

intake manifold, $\dot{m}_{Throttle}$. Hence, the following subsection elucidates the analytical modeling of $\dot{m}_{Throttle}$.

3.5. MASS FLOW RATE AT THE THROAT OF THE INTAKE MANIFOLD AND INTAKE MANIFOLD DYNAMIC PRESSURE

Since air flow is a gas flow, the following follows: ‘Total energy equals the sum of the total energy associated with mass flow and work done.’ Given the fact that the total energy associated with mass flow comprises internal energy, kinetic energy, and potential energy, it therefore follows that

$$E_{Total} = \left(u + \frac{c^2}{2} + gz \right) + p v \quad (3.41)$$

It follows from the definition of the gas flow internal energy that:

$$h = u + pv \quad (3.42)$$

Thus, combining equations (3.41) and (3.42) together leads to the following:

$$E_{Total} = h + \frac{c^2}{2} + gz \quad (3.43)$$

By applying the first law of thermodynamics on the conservation of energy to stagnation due to throttling, as shown in Figure 3.3, the following follows for a couple of state points in the gas flow (1) and (0) (Obert, 1973):

$$h_o + \frac{c_o^2}{2} + gz_o = h_1 + \frac{c_1^2}{2} + gz_1 \quad (3.44)$$

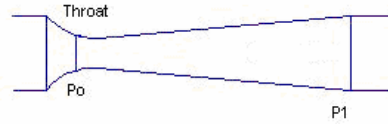


Figure 3.3

Air flow throttling

Since the difference in altitude between the points in the air flow within the intake manifold is relatively negligible, the assumption of the same altitude z is thus a valid assumption. It follows therefore from equation (3.44) that:

$$h_o + 0 + gz = h_1 + \frac{c_1^2}{2} + gz \quad (3.45)$$

By treating air in this case as an ideal gas as justified above, it follows that:

$$h = c_p T \quad (3.46)$$

Therefore, combining equations (3.45) and (3.46) leads to the following:

$$c_p T_o = c_p T_1 + \frac{c_1^2}{2} \quad (3.47)$$

Thus, equation (3.47) can be rewritten as:

$$T_o = T_1 + \frac{c_1^2}{2c_p} \quad (3.48)$$

Since the heat loss in the intake manifold is relatively negligible, it follows from the principles of the second and third laws of thermodynamics that (Bar–Meir, 2002):

$$ds = \frac{\delta q}{T} \quad (3.49)$$

By establishing integration in equation (3.49) between the couple of state points in the air flow (1) and (0):

$$s_o - s_1 = \int_1^0 \frac{\delta q}{T} \quad (3.50)$$

Recalling the first law of thermodynamics, it follows that (Obert, 1973):

$$\delta q = du + \delta w \quad (3.51)$$

Substituting equation (3.51) in equation (3.50):

$$s_o - s_1 = \int_1^0 \frac{du + \delta w}{T} \quad (3.52)$$

The non-flow process by definition is the process in which the working substance does not flow across its confining boundary during the state change (Johnston, 1992). Considering the intake manifold as a control system, the flow between the state points (1) and (0) indicated in Figure 3.3 does not flow across the confining boundary of the control system. Therefore, following from the definition of the work done, equation (3.52) can be rewritten as follows (Obert, 1973):

$$s_o - s_1 = \int_1^0 \frac{du + p dv}{T} \quad (3.53)$$

Combining equations (3.42) and (3.53) together:

$$s_o - s_1 = \int_1^0 \frac{(dh - p dv - v dp) + (p dv)}{T} \quad (3.54)$$

Thus, simplifying equation (3.54) leads to the following:

$$s_o - s_1 = \int_1^0 \frac{dh}{T} - \int_1^0 \frac{v dp}{T} \quad (3.55)$$

It follows from combining equation (3.1) and the definition of density that:

$$p = \rho R T \quad (3.56)$$

By combining equations (3.1), (3.55), and (3.56) together, the following follows based on specific quantities, i.e. per unit mass:

$$s_o - s_1 = \int_1^0 \frac{dh}{T} - \int_1^0 \frac{dP}{\rho T} \quad (3.57)$$

By combining equations (3.1), (3.46), and (3.57) together, the following follows:

$$s_o - s_1 = \int_1^0 c_p \frac{dT}{T} - \int_1^0 \frac{R dp}{p} \quad (3.58)$$

Hence, it follows mathematically from equation (3.58) that:

$$s_o - s_1 = c_p \ln \left(\frac{T_o}{T_1} \right) - R \ln \left(\frac{p_o}{p_1} \right) \quad (3.59)$$

Therefore, rearranging equation (3.59) leads to the following:

$$\frac{s_o - s_1}{R} = \frac{c_p}{R} \ln \left(\frac{T_o}{T_1} \right) - \ln \left(\frac{p_o}{p_1} \right) \quad (3.60)$$

It follows from equation (3.42) that:

$$dh = du + d(pv) \quad (3.61)$$

By combining equations (3.1) and (3.61), the following follows:

$$dh = du + R T \quad (3.62)$$

By dividing both sides of equation (3.62) by T and recalling equation (3.46) and recalling the similar equation to equation (3.46) for the specific heat at constant volume, it follows that:

$$c_p = c_v + R \quad (3.63)$$

Following from the definition of the ratio of specific heat, k , equation (3.63) can be rewritten as:

$$c_p = \frac{c_p}{k} + R \quad (3.64)$$

Thus, by rearranging equation (3.64) the following follows:

$$R = c_p \left(1 - \frac{1}{k} \right) \quad (3.65)$$

Hence, equation (3.65) can be rearranged as follows:

$$c_p = \frac{k R}{k - 1} \quad (3.66)$$

By substituting equation (3.66) in equation (3.60):

$$\frac{s_o - s_1}{R} = \frac{k}{k - 1} \ln \left(\frac{T_o}{T_1} \right) - \ln \left(\frac{p_o}{p_1} \right) \quad (3.67)$$

Since in the intake manifold no significant heat is transferred to or from the working fluid and the heat loss is negligible, the process can be assumed isentropic (Khummongkol et al., 2004; Holmgren, 2005). Therefore, the following follows from equation (3.67):

$$\ln\left(\frac{T_o}{T_1}\right) = \frac{k-1}{k} \ln\left(\frac{p_o}{p_1}\right) \quad (3.68)$$

By establishing an inverse logarithmic operation on both sides of equation (3.68) the following mathematically follows:

$$\frac{T_o}{T_1} = \left(\frac{p_o}{p_1}\right)^{\frac{k-1}{k}} \quad (3.69)$$

By substituting equation (3.66) in equation (3.48):

$$\frac{T_o}{T_1} = 1 + \frac{c_1^2}{2 T_1 k R} (k-1) \quad (3.70)$$

Since Mach number, M , by definition is defined as:

$$M = \frac{c}{e} \quad (3.71)$$

The speed of sound, e_s , by definition is evaluated using the following formula (Ni and Henclewood, 2008; Bar–Meir, 2002):

$$e_s = \sqrt{k R T} \quad (3.72)$$

Hence, by combining equations (3.70), (3.71), and (3.72) it follows that:

$$\frac{T_o}{T_1} = 1 + \frac{k-1}{2} M^2 \quad (3.73)$$

Equation (3.68) can be rearranged as follows:

$$\ln\left(\frac{p_o}{p_1}\right) = \frac{k}{k-1} \ln\left(\frac{T_o}{T_1}\right) \quad (3.74)$$

By establishing an inverse logarithmic operation on both sides of equation (3.74):

$$\frac{p_o}{p_1} = \left(\frac{T_o}{T_1} \right)^{\frac{k}{k-1}} \quad (3.75)$$

By substituting equation (3.69) in equation (3.73):

$$\left(\frac{p_o}{p_1} \right)^{\frac{k-1}{k}} = 1 + \frac{k-1}{2} M^2 \quad (3.76)$$

By establishing a logarithmic operation on both sides of equation (3.76):

$$\frac{k-1}{k} \ln \left(\frac{p_o}{p_1} \right) = \ln \left(1 + \frac{k-1}{2} M^2 \right) \quad (3.77)$$

By rearranging equation (3.77) and establishing an inverse logarithmic operation on both sides the following follows:

$$\frac{p_o}{p_1} = \left(1 + \frac{k-1}{2} M^2 \right)^{\frac{k}{k-1}} \quad (3.78)$$

In order to evaluate $\dot{m}_{Throttle}$ of equation (3.5), the following follows from the fundamental definition of the coefficient of discharge, C_D (Heywood, 1988):

$$\dot{m}_{Throttle} = C_D \dot{m}_{Throttle Theoretical} \quad (3.79)$$

The coefficient of discharge, C_D , can also be evaluated by definition as follows (Heywood, 1988):

$$C_D = \frac{A_{0 Min}}{A_{0 Mean}} \quad (3.80)$$

In order to evaluate $\dot{m}_{Throttle Theo}$ of equation (3.79), the following follows from the fundamental definition of the mass flow rate (Sonntag et al., 2008; Ismail et al., 2009):

$$\dot{m}_{Throttle Theo} = \rho c A_0 \quad (3.81)$$

By combining equations (3.56) and (3.81) together, the following follows:

$$\frac{\dot{m}_{Throttle Theo}}{A_0} = \frac{p}{RT} c \quad (3.82)$$

Equation (3.82) can be mathematically rearranged as follows:

$$\frac{\dot{m}_{Throttle Theo}}{A_0} = \frac{p}{p_0} \frac{p_0}{\sqrt{RT}} \frac{c}{\sqrt{k}} \frac{\sqrt{k}}{\sqrt{R}} \frac{\sqrt{T_0}}{\sqrt{T}} \frac{1}{\sqrt{T_0}} \quad (3.83)$$

Equation (3.83) can be further rearranged as follows:

$$\frac{\dot{m}_{Throttle Theo}}{A_0} = \frac{p}{p_0} \frac{p_0 c}{\sqrt{k RT}} \sqrt{\frac{k}{R}} \sqrt{\frac{T_0}{T}} \frac{1}{\sqrt{T_0}} \quad (3.84)$$

By combining equations (3.71), (3.72), and (3.84) together, the following follows:

$$\frac{\dot{m}_{Throttle Theo}}{A_0} = \frac{p_0}{\sqrt{T_0}} M \sqrt{\frac{k}{R}} \frac{p}{p_0} \sqrt{\frac{T_0}{T}} \quad (3.85)$$

Equation (3.75) can be rearranged as follows:

$$\frac{p}{p_0} = \left(\frac{T_0}{T} \right)^{\frac{-k}{k-1}} \quad (3.86)$$

For T equals T₁, combining equations (3.85), (3.86), and (3.73) together leads to the following:

$$\frac{\dot{m}_{Throttle Theo}}{A_0} = \frac{p_0}{\sqrt{T_0}} M \sqrt{\frac{k}{R}} \left(1 + \frac{k-1}{2} M^2 \right)^{\frac{-k}{k-1}} \left(1 + \frac{k-1}{2} M^2 \right)^{\frac{1}{2}} \quad (3.87)$$

Rearranging equation (3.87) leads to the following:

$$\frac{\dot{m}_{Throttle Theo}}{A_0 p_0 M} = \sqrt{\frac{k}{R T_0}} \left(1 + \frac{k-1}{2} M^2 \right)^{\frac{-k-1}{2(k-1)}} \quad (3.88)$$

Equation (3.88) can be rearranged as follows:

$$\frac{\dot{m}_{Throttle Theo}}{A_0 p_0 M} = \frac{\sqrt{k}}{\sqrt{k}} \sqrt{\frac{k}{R T_0}} \left(1 + \frac{k-1}{2} M^2 \right)^{\frac{-k-1}{2(k-1)}} \quad (3.89)$$

By combining equations (3.71), (3.72), and (3.89) the following follows:

$$\frac{\dot{m}_{Throttle Theo}}{A_0 p_0 \left(\frac{c}{\sqrt{k R T_0}} \right)} = \frac{k}{\sqrt{k R T_0}} \left(1 + \frac{k-1}{2} M^2 \right)^{\frac{-k-1}{2(k-1)}} \quad (3.90)$$

Equation (3.90) can be rearranged as follows:

$$\frac{\dot{m}_{Throttle Theo} k R T_0}{A_0 p_0 c} = k \left(1 + \frac{k-1}{2} M^2 \right)^{\frac{-k-1}{2(k-1)}} \quad (3.91)$$

By combining equations (3.71), (3.72), and (3.91) the following follows:

$$\dot{m}_{Throttle Theo} = \frac{A_0 k M p_0}{\sqrt{k R T_0}} \left(1 + \frac{k-1}{2} M^2 \right)^{\frac{-k-1}{2(k-1)}} \quad (3.92)$$

Equation (3.92) can be further mathematically simplified as follows:

$$\dot{m}_{Throttle\ Theo} = A_0 M p_0 \left(1 + \frac{k-1}{2} M^2 \right)^{\frac{-k-1}{2(k-1)}} \sqrt{\frac{k}{RT_0}} \quad (3.93)$$

Combining equations (3.79), (3.80), and (3.93) leads to the following:

$$\dot{m}_{Throttle} = \frac{A_{0\ Min}}{A_{0\ Mean}} \left(A_0 M p_0 \left(1 + \frac{k-1}{2} M^2 \right)^{\frac{-k-1}{2(k-1)}} \sqrt{\frac{k}{RT_0}} \right) \quad (3.94)$$

By combining equations (3.5), (3.27), and (3.94), the dynamic pressure inside the

intake manifold, \dot{p}_i , can be evaluated as follows:

$$\dot{p}_i = \begin{bmatrix} p_i \frac{\dot{T}_i}{T_i} + \frac{RT_i}{v_i} \left(\frac{A_{0\ Min} A_0 M p_0 \left(1 + \frac{k-1}{2} M^2 \right)^{\frac{-k-1}{2(k-1)}} \sqrt{\frac{k}{RT_0}}}{A_{0\ Mean}} \right. \\ \left. - \frac{\left(p_{Atm} - \left(\frac{\pi \rho_p V_p a N_m^2 \cos \theta}{225 B^2} \right) \right) \eta_v V_d N_m n}{60 RT_i} \right) & \theta_{IVO} \leq \theta < \theta_{IVC} \\ \\ p_i \frac{\dot{T}_i}{T_i} + \frac{RT_i}{v_i} \left(\frac{A_{0\ Min} A_0 M p_0 \left(1 + \frac{k-1}{2} M^2 \right)^{\frac{-k-1}{2(k-1)}} \sqrt{\frac{k}{RT_0}}}{A_{0\ Mean}} \right. \\ \left. - \frac{p_i \eta_v V_d N_m n}{60 RT_i} \right) & \theta = \theta_{IVC} \end{bmatrix} \quad (3.95)$$

Equation (3.40) can be used instead of equation (3.27) in this substitution to

analytically formulate \dot{p}_i if the flexibility of crankshaft is not negligible. Another key characteristic of the operation of diesel engines is the in-cylinder gas speed. In order to show analytically how the in-cylinder gas speed varies over time, the following subsection presents the analytical model of the in-cylinder gas speed.

3.6. IN-CYLINDER GAS SPEED FORMULATION

In order to formulate gas speed, c , in terms of instantaneous piston speed and engine parameters, the following follows from the fundamental definitions of mass flow rate and density as well as from equation (3.81) (Sonntag et al., 2008; Ismail et al., 2009; Heywood, 1988):

$$\dot{m}_{Throttle\ Theo} = \frac{m_C}{V} c A_{0Mean} \quad (3.96)$$

Rearranging equation (3.96) leads to the following:

$$c = \frac{\dot{m}_{Throttle\ Theo}}{m_C} \frac{V}{A_{0Mean}} \quad (3.97)$$

The theoretical mass flow rate of air goes from supercharger compressor and electronic throttle control into intake manifold, $\dot{m}_{Throttle\ Theo}$, can be expressed as follows following from the fundamental definition of mass flow rate (Sonntag et al., 2008; Ismail et al., 2009; Heywood, 1988):

$$\dot{m}_{Throttle\ Theo} = \rho \frac{dV}{dt} \quad (3.98)$$

The rate of change of V can be analytically formulated following from the fundamental definition of the rate of change of gas volume in reciprocating engines as follows (Heywood, 1988):

$$\frac{dV}{dt} = \frac{\pi B^2}{4} S_P \quad (3.99)$$

Thus, combining equations (3.97), (3.98), and (3.99) together leads to the following:

$$c = \frac{\rho \frac{\pi B^2}{4} S_p}{m_C} \frac{V}{A_{0Mean}} \quad (3.100)$$

Equation (3.100) can be rearranged as follows:

$$c = S_p \left(\frac{\left(\frac{\pi B^2}{4} \right)}{A_{0Mean}} \right) \left(\frac{\rho V}{m_C} \right) \quad (3.101)$$

Hence, equation (3.101) can be rewritten as follows:

$$c = S_p \left(\frac{\left(\frac{\pi B^2}{4} \right)}{A_{0Mean}} \right) \left(\frac{V}{V_C} \right) \quad (3.102)$$

Thus, equation (3.102) can be rewritten as follows:

$$c = \frac{S_p \pi B^2 r_C}{4 A_{0Mean}} \quad (3.103)$$

In order to express the instantaneous piston speed, S_p , in terms of engine parameters, the following follows from combining equation (3.18), (3.19), and (3.20):

$$S_p = \frac{\pi N_m a}{30} \sin \theta \quad (3.104)$$

Therefore, the speed of gas, c , can be analytically formulated as follows by combining equations (3.103) and (3.104):

$$c = \frac{\pi^2 B^2 r_C N_m a}{120 A_{0Mean}} \sin \theta \quad (3.105)$$

Analytically modeling the speed of gas, c , paves the way to analytically model the intake manifold gas speed dynamics.

3.7. ANALYTICAL MODEL OF INTAKE MANIFOLD GAS SPEED DYNAMICS

In order to evaluate the intake manifold gas dynamic speed, the momentum conservation is taken into consideration. Considering the control volume in the intake manifold shown in Figure 3.4, since the area change over the infinitesimal length of the intake manifold, dx , in the intake manifold is small, the flow is thus assumed to be quasi one dimensional flow.

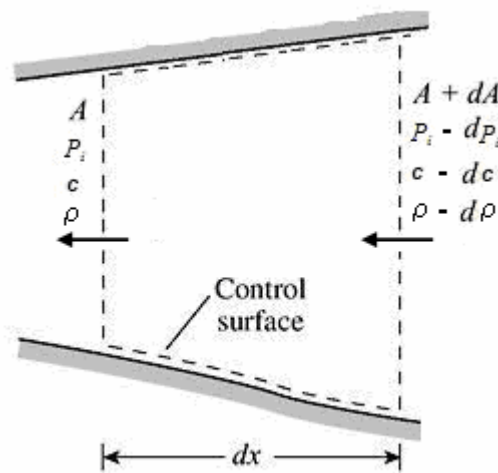


Figure 3.4

Control volume in diesel intake manifold for one-dimensional flow analysis

The momentum conservation equation states that the net pressure forces plus the wall shear force acting on the control volume surface equal the rate of change of momentum within the control volume plus the net flow of momentum out of the control volume (Heywood, 1988). Thus, the net forces, the rate of change of

momentum within the control volume, the net flow of momentum across the control volume surface, and the total momentum are presented respectively in this section.

3.7.1. The net forces

The net forces in the control volume shown in Figure 3.4 consist of pressure force and shear force. The net pressure force, F_{Press} , can be evaluated as follows:

$$F_{\text{Press}} = P_i A - \left(P_i - \frac{\partial P_i}{\partial x} dx \right) \left(A + \frac{dA}{dx} dx \right) + P_i \frac{dA}{dx} dx \quad (3.106)$$

By rearranging equation (3.106), the following follows:

$$F_{\text{Press}} = P_i A - P_i A - P_i \frac{dA}{dx} dx + A \frac{\partial P_i}{\partial x} dx + \frac{\partial P_i}{\partial x} dx \frac{dA}{dx} dx + P_i \frac{dA}{dx} dx \quad (3.107)$$

By simplifying equation (3.107) and ignoring the term of trivial value which is the term $\left(\frac{\partial P_i}{\partial x} dx \frac{dA}{dx} dx \right)$, the following follows from equation (3.107):

$$F_{\text{Press}} = A \frac{\partial P_i}{\partial x} dx \quad (3.108)$$

The net shear force, F_{Shear} , can be evaluated as follows:

$$F_{\text{Shear}} = -\tau_w (\pi D dx) \quad (3.109)$$

By definitions of the flow shear stress and flow friction coefficient, the following follows (Heywood, 1988):

$$\tau_w = \zeta E_{\text{Kin}} \quad (3.110)$$

The kinetic energy per unit area, E_{Kin} , can be evaluated by definition as follows (Heywood, 1988):

$$E_{Kin} = \rho \frac{c^2}{2} \quad (3.111)$$

Therefore, combining equations (3.109), (3.110), and (3.111) the following follows:

$$F_{Shear} = -\frac{\zeta \rho c^2 \pi D}{2} dx \quad (3.112)$$

Having analytically formulated the net forces, let us now have a look at the rate of change of momentum within the control volume.

3.7.2. The rate of change of momentum within the control volume

The rate of change of momentum within the control volume in the intake manifold shown in Figure 3.4, M_{Moment} , can be evaluated from the fundamental definition of momentum and force as follows (Heywood, 1988):

$$M_{Moment} = \frac{\partial}{\partial t} (c F_{Moment}) \quad (3.113)$$

The force that generated this momentum, F_{Moment} , can be evaluated from its fundamental definition as follows (Heywood, 1988):

$$F_{Moment} = \rho V_i \quad (3.114)$$

Thus, combining equations (3.113) and (3.114) together leads to the following:

$$M_{Moment} = \frac{\partial}{\partial t} (c \rho A dx) \quad (3.115)$$

Now, let us investigate the net flow of momentum across the control volume surface.

3.7.3. The net flow of momentum across the control volume surface

The net flow of momentum across the control volume surface in the intake manifold shown in Figure 3.4, M_{Net} , can be evaluated from the fundamental definition of momentum as follows (Heywood, 1988):

$$M_{Net} = \left(\rho - \frac{\partial \rho}{\partial x} dx \right) \left(c - \frac{\partial c}{\partial x} dx \right)^2 \left(A + \frac{dA}{dx} dx \right) - \rho c^2 A \quad (3.116)$$

Equation (3.116) can be rearranged as follows:

$$M_{Net} = \left(\rho - \frac{\partial \rho}{\partial x} dx \right) \left(c^2 + \frac{\partial^2 c}{\partial x^2} d^2 x - 2c \frac{\partial c}{\partial x} dx \right) \left(A + \frac{dA}{dx} dx \right) - \rho c^2 A \quad (3.117)$$

Equation (3.117) can be further rearranged as follows:

$$M_{Net} = \left(\begin{aligned} &\rho c^2 + \rho \frac{\partial^2 c}{\partial x^2} d^2 x - 2\rho c \frac{\partial c}{\partial x} dx - c^2 \frac{\partial \rho}{\partial x} dx \\ &- \frac{\partial \rho}{\partial x} dx \frac{\partial^2 c}{\partial x^2} d^2 x + 2c \frac{\partial c}{\partial x} dx \frac{\partial \rho}{\partial x} dx \end{aligned} \right) \left(A + \frac{dA}{dx} dx \right) - \rho c^2 A \quad (3.118)$$

Equation (3.118) can be further rearranged as follows:

$$\begin{aligned} M_{Net} = & A \rho c^2 + A \rho \frac{\partial^2 c}{\partial x^2} d^2 x - 2 A \rho c \frac{\partial c}{\partial x} dx - A c^2 \frac{\partial \rho}{\partial x} dx - A \frac{\partial \rho}{\partial x} dx \frac{\partial^2 c}{\partial x^2} d^2 x + 2 A c \frac{\partial c}{\partial x} dx \frac{\partial \rho}{\partial x} dx \\ & + \rho c^2 \frac{dA}{dx} dx + \rho \frac{\partial^2 c}{\partial x^2} d^2 x \frac{dA}{dx} dx - 2 \rho c \frac{\partial c}{\partial x} dx \frac{dA}{dx} dx - c^2 \frac{\partial \rho}{\partial x} dx \frac{dA}{dx} dx \\ & - \frac{\partial \rho}{\partial x} dx \frac{\partial^2 c}{\partial x^2} d^2 x \frac{dA}{dx} dx + 2 c \frac{\partial c}{\partial x} dx \frac{\partial \rho}{\partial x} dx \frac{dA}{dx} dx - \rho c^2 A \end{aligned} \quad (3.119)$$

By simplifying, ignoring mathematically trivial terms, and rearranging equation (3.119), the following follows:

$$M_{Net} = \frac{-\partial}{\partial x} (\rho c^2 A) dx + \rho c^2 \frac{dA}{dx} dx - 2 A \rho c \frac{\partial c}{\partial x} dx \quad (3.120)$$

Having investigated the net flow of momentum across the control volume surface, let us turn to investigate the total momentum.

3.7.4. The total momentum

Following from the fundamental definition of the momentum conservation and by combining equations (3.108), (3.112), (3.115), and (3.120), it therefore follows that:

$$A \frac{\partial P_i}{\partial x} dx - \zeta \frac{\rho c^2}{2} \pi D dx = \frac{\partial}{\partial t} (\rho A c dx) - 2 A \rho c \frac{\partial c}{\partial x} dx - c^2 A \frac{\partial \rho}{\partial x} dx + \rho c^2 \frac{dA}{dx} dx \quad (3.121)$$

By simplifying equation (3.121):

$$A \frac{\partial P_i}{\partial x} - \zeta \frac{\rho c^2}{2} \pi D = \frac{\partial}{\partial t} (\rho A c) - 2 A \rho c \frac{\partial c}{\partial x} - c^2 A \frac{\partial \rho}{\partial x} + \rho c^2 \frac{dA}{dx} \quad (3.122)$$

Equation (3.122) can be rewritten as follows:

$$A \frac{\partial P_i}{\partial x} - \zeta \frac{\rho c^2}{2} \pi D = \rho A \frac{\partial c}{\partial t} - 2 A \rho c \frac{\partial c}{\partial x} - A c^2 \frac{\partial \rho}{\partial x} + \rho c^2 \frac{dA}{dx} \quad (3.123)$$

Equation (3.123) can be rearranged as follows:

$$\rho A \frac{\partial c}{\partial t} = A \frac{\partial P_i}{\partial x} - \zeta \frac{\rho c^2}{2} \pi D + 2 A \rho c \frac{\partial c}{\partial x} + A c^2 \frac{\partial \rho}{\partial x} - \rho c^2 \frac{dA}{dx} \quad (3.124)$$

Equation (3.124) can be rearranged as follows:

$$\frac{\partial c}{\partial t} = \frac{1}{\rho} \frac{\partial P_i}{\partial x} - \zeta \frac{c^2}{2 A} \pi D + 2 c \frac{\partial c}{\partial x} + \frac{c^2}{\rho} \frac{\partial \rho}{\partial x} - \frac{c^2}{A} \frac{dA}{dx} \quad (3.125)$$

Thus, the intake manifold air dynamic speed can be expressed as follows following

from equation (3.125):

$$\dot{c}_{im} = \frac{1}{\rho} \left(\frac{\partial P_i}{\partial x} \right) - \zeta \frac{c^2 \pi D}{2 A} + 2 c \frac{\partial c}{\partial x} + \frac{c^2}{\rho} \frac{\partial \rho}{\partial x} - \frac{c^2}{A} \frac{dA}{dx} \quad (3.126)$$

By combining equations (3.105) and (3.126) together, the dynamic gas speed can be rewritten as:

$$\dot{c}_{im} = \frac{1}{\rho} \left(\frac{\partial P_i}{\partial x} \right) - \zeta \frac{c^2 \pi D}{2 A} + \frac{c^2}{\rho} \frac{\partial \rho}{\partial x} - \frac{c^2}{A} \frac{dA}{dx} \quad (3.127)$$

P_i , A , and ρ can be assumed constant with respect to x since a value of diameter can be assigned to the intake manifold as D (Sulaiman et al., 2010) and the intake manifold is relatively short in length. Hence, multiplying both sides of equation (3.127) by ' dx ' and establishing integration with respect to x :

$$\dot{c}_{im} = \frac{P_i}{\rho L} - \frac{2 \zeta c^2}{D} \quad (3.128)$$

Having seen this, let us now analytically model the supercharged air density in intake manifold.

3.8. ANALYTICAL MODEL OF THE SUPERCHARGED AIR DENSITY

In reality much of the compressor rotor exit kinetic energy pressure head is usually dissipated as a heat loss and is not converted into pressure rise (Heywood, 1988). Hence, it can follow that:

$$P_i = P_2 \quad (3.129)$$

$$T_i = T_2 - \eta_{Intercooler} (T_2 - T_{Ref\ Amb}) \quad (3.130)$$

The intercooler efficiency, $\eta_{Intercooler}$, is analytically formulated as follows:

$$\eta_{Intercooler} = \frac{T_{Inlet-Intercooler} - T_{Intercooler}}{T_{Inlet-Intercooler} - T_{Ref-Amb}} \quad (3.131)$$

Due to the fact that the supercharged air density in the intake manifold, ρ , varies with both latitude and altitude, this variation should be reflected in the present analytical model. Due to variation in the angle of incidence of the sun's rays at the surface of earth, the yearly average temperature varies as well with latitude. The yearly average

temperature over the equator is 27°C whereas the same over the poles is -20°C (Kottek, et al., 2006). In other words, an overall difference of 47°C spreads over 90 degrees of latitude. Thus, a decrement of 0.522°C/degree latitude naturally exists for latitude varies from -90° to 90° away from the equator at which the latitude is 0°. In addition, Hess (Hess, 1979) discovered that for the Troposphere, i.e. altitude ranges from sea level to 10,769 km, the temperature naturally decreases at a constant rate of 6.5 K/km (Greenwood, 2003). Therefore, the reference ambient temperature in K, $T_{Ref-Amb}$, indicated in equations (3.130) and (3.131), is related to the yearly average temperature over the equator at sea level in °C, $T_{Equator}$, as follows:

$$T_{Ref-Amb} = (T_{Equator} - 0.522 L_{Latitude} - 0.0065 A_{Altitude}) + 273.15 \quad (3.132)$$

Substituting equation (3.132) into equation (3.131), the intercooler efficiency, $\eta_{Intercooler}$, can be now analytically formulated for a given latitude and altitude as follows:

$$\eta_{Intercooler} = \frac{T_{Inlet-Intercooler} - T_{Intercooler}}{T_{Inlet-Intercooler} - T_{Equator} + 0.522 L_{Latitude} + 0.0065 A_{Altitude} - 273.15} \quad (3.133)$$

Hence, substituting equation (3.132) into equation (3.130), the intake manifold temperature, T_i , can be analytically modeled as follows:

$$T_i = T_2 - \eta_{Intercooler} (T_2 - T_{Equator} + 0.522 L_{Latitude} + 0.0065 A_{Altitude} - 273.15) \quad (3.134)$$

Thus, substituting equations (3.129) and (3.134) into equation (3.56), the supercharged air density in the intake manifold, ρ , can be expressed analytically as follows:

$$\rho = \frac{P_2}{R [T_2 - \eta_{Intercooler} (T_2 - T_{Equator} + 0.522 L_{Latitude} + 0.0065 A_{Altitude} - 273.15)]} \quad (3.135)$$

CHAPTER 4

SUPERCHARGING DIESEL CENTRIFUGAL COMPRESSOR WITH VANES-BASED DIFFUSER ANALYTICAL MODEL

4.1. OVERVIEW

In diesel powertrains, a compressor may be required by the engine either for good scavenging in 2-stroke engines, or as a means of raising the power output in 4-stroke engines (Obert, 1973). As the key tool to develop diesel powertrains, modeling of diesel supercharging compressors has a key role in diesel powertrain development. This research presents an analytical model of the power required to drive the rotor, of the velocities at the diffuser, and of the efficiency of a supercharging diesel centrifugal compressor with vanes-based diffuser. This chapter presents an analysis of the fluid flow through the compressor and elucidates an analytical model developed entirely based on the principles of physics. Since air can be treated as non-viscous fluid, the flow in diesel engines is therefore non-viscous and the gas flow can thus be conveniently treated as one-dimensional flow (Smits, 2006). Hence, a one-dimensional analysis of air flow is adopted in this chapter and hence one vector can represent all particles of the air stream throughout the compressor. The model developed in this chapter is limited to centrifugal compressors. In the analysis of air flow throughout the compressor, the following assumptions are made in this study (Obert, 1973):

1- Since there is no change in phase in the air flow throughout the compressor and the minimum temperature of the air flow throughout the compressor is far above the critical point of atmospheric air, air is thus treated as an ideal gas;

- 2- Since the air flow into the compressor is turbulent and the change in the flow rate of momentum through the rotor of the compressor equals the resultant of the forces acting upon the stream of air, therefore the air flow is steady and the rotor velocity is uniform based on average speed;
- 3- There is no leakage of air from the compressor, i.e. the principle of conservation of mass is applied to air flow.

The models developed in this chapter address and correct flaws in models presented in key references in this research area such as [Heywood, 1988; Taylor, 1985]. Following from principles of physics, Chapter 4 contributes to the implementation of the 1st pillar of the research philosophy adopted in this study in an endeavour to achieve the 1st objective in this research.

4.2. ANALYTICAL SUB-MODEL OF POWER REQUIRED TO DRIVE SUPERCHARGING DIESEL CENTRIFUGAL COMPRESSOR WITH VANES-BASED DIFFUSER

The particular type of supercharging diesel compressor under investigation in this study, i.e. the supercharging diesel centrifugal compressor with vanes-based diffuser, is schematically shown in Figure 4.1. The velocity diagrams of the diesel centrifugal compressor at the inlet of impeller with pre-whirl and at the exit of diffuser are shown in Figure 4.2 and Figure 4.3, respectively.

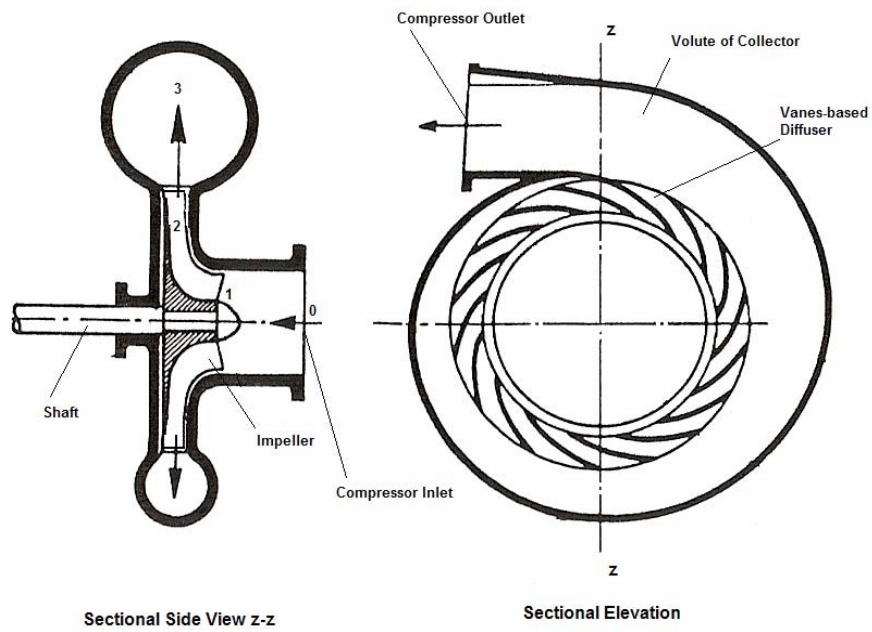


Figure 4.1
Schematic diagram of supercharging diesel centrifugal compressor with vanes-based diffuser

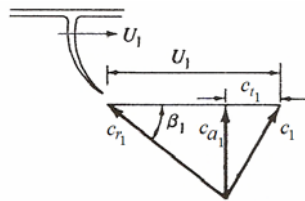


Figure 4.2
The velocity diagram of the diesel centrifugal compressor at the entrance of impeller with pre-whirl

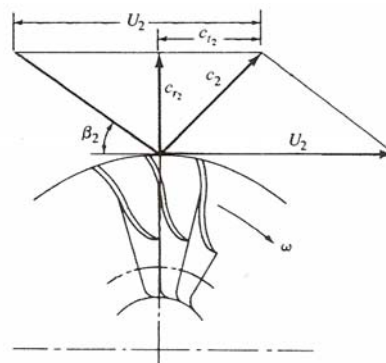


Figure 4.3
The velocity diagram of the diesel centrifugal compressor at the exit of diffuser

Since the forces acting upon the rotor of the compressor must be in balance with the change in momentum flow rate, the following equation follows infinitesimally neglecting body forces, such as the weight of air charge:

$$d F_{RW} - d (p A) = \dot{m}_{air} dc \quad (4.1)$$

By applying equation (4.1) to the states at the entrance and exit of the rotor of the compressor, i.e. states 1 and 2 on Figure 4.1, the following follows:

$$F_{RW} - (p_2 A_2 - p_1 A_1) = \dot{m}_{air} (c_2 - c_1) \quad (4.2)$$

Each pressure-area vector has three components: (a) an axial force, denoted by subscript 'a' in Figure 4.2, causing end thrust, (b) a radial force, denoted by subscript 'r' in Figure 4.2 and Figure 4.3, causing compressive stresses, (c) a tangential component, denoted by subscript 't' in Figure 4.2 and Figure 4.3, yet this component vanishes in the rotor since the net pressure force in the tangential direction is zero (Obert, 1973). Since the axial and radial components of air flow velocities produce thrusts which result in no displacements, the only component of air flow velocities that contributes to energy transfer in the compressor is the tangential component. Therefore, the resultant force of the rotor on the air flow in the tangential direction can be modelled as follows following from equation (4.2):

$$F_{RW} = \dot{m}_{air} (c_{t2} - c_{t1}) \quad (4.3)$$

Thus, following from Newton's third law of motion, the reaction exerted by the air flow to this force, R_a , becomes:

$$R_a = \dot{m}_{air} (c_{t1} - c_{t2}) \quad (4.4)$$

Since moments about the axis of the rotor must balance as well following from the principle of the conservation of angular momentum, equation (4.4) hence leads to the following:

$$T_C = \dot{m}_{air} (c_{t1} r_1 - c_{t2} r_2) \quad (4.5)$$

Thus, the thermodynamic power required to drive the rotor of the compressor, \dot{W}_C , can be modeled as follows following from equation (4.5):

$$\dot{W}_C = \dot{m}_{air} \varpi_c (c_{t1} r_1 - c_{t2} r_2) \quad (4.6)$$

In order to investigate analytically the relation between T_C and \dot{W}_C modeled in equations (4.5) and (4.6), respectively, and the velocity components illustrated in Figure 4.2 and Figure 4.3, let us investigate the analytical relation between the angular speed of the rotor, ω_c , and the tangential velocity of the rotor, U :

$$U = \varpi_c r \quad (4.7)$$

Thus, by combining equations (4.5) and (4.7), the developed analytical model of T_C can be rewritten as:

$$T_C = \frac{\dot{m}_{air}}{\varpi_c} (c_{t1} U_1 - c_{t2} U_2) \quad (4.8)$$

Likewise, by combining equations (4.6) and (4.7), the developed analytical model of

\dot{W}_C can be rewritten as:

$$\dot{W}_C = \dot{m}_{air} (c_{t1} U_1 - c_{t2} U_2) \quad (4.9)$$

Equations (4.8) and (4.9) represent the thermodynamic torque and power required to

drive the rotor of the compressor based on the velocity diagrams indicated in Figure 4.2 and Figure 4.3 without taking into account the bearing friction losses and fanning losses. This is particularly true in light of the fact that the velocity at the exit of the rotor, i.e. at state 2, reflects the effect of losses due to heat transfer and due to fluid friction. Since the inlet velocity to the rotor is axial, the tangential velocity component at state 1 in Figure 4.1, i.e. c_{t1} , becomes zero. Thus, the developed analytical model of the thermodynamic torque required to drive the rotor, T_C , indicated in equation (4.8) can be rewritten as:

$$T_C = - \frac{\dot{m}_{air} c_{t2} U_2}{\omega_c} \quad (4.10)$$

Likewise, the developed analytical model of \dot{W}_C in equation (4.9) can be rewritten as:

$$\dot{W}_C = - \dot{m}_{air} c_{t2} U_2 \quad (4.11)$$

Since the radial velocity of the air flow at the diffuser, c_{r2} , is relatively easier to be measured than the tangential velocity of the air flow at the diffuser, c_{t2} , for instance using a miniature X-wire probe (Ahmed, 2010), equations (4.10) and (4.11) can be rewritten as functions of c_{r2} rather than c_{t2} using the trigonometric relations in the velocity diagrams shown in Figure 4.3. It can be conceived from Figure 4.3 that

$$U_2 - c_{t2} = c_{r2} \cot \beta_2 \quad (4.12)$$

Hence, equation (4.12) can be rearranged as follows:

$$c_{t2} = U_2 \left(1 - \frac{c_{r2}}{U_2} \cot \beta_2 \right) \quad (4.13)$$

Now, by combining equations (4.13) and (4.10), the developed analytical model of the

thermodynamic torque required to drive the rotor, T_C , indicated in equation (4.10) can be rewritten as:

$$T_C = - \frac{\dot{m}_{air} U_2^2}{\varpi_c} \left(1 - \frac{c_{r2}}{U_2} \cot \beta_2 \right) \quad (4.14)$$

Likewise, by combining equations (4.13) and (4.11) the developed analytical model of the thermodynamic power required to drive the rotor, \dot{W}_C , indicated in equation (4.11) can be rewritten as:

$$\dot{W}_C = - \dot{m}_{air} U_2^2 \left(1 - \frac{c_{r2}}{U_2} \cot \beta_2 \right) \quad (4.15)$$

If the slip of the fluid becomes negligible by sufficiently increasing the number of the blades of the impeller, i.e. the relative velocity of the air flow to the rotor becomes entirely in the radial direction as dictated by the blade shape characterised by the impeller blade angle, β_1 , which is indicated in Figure 4.2, the tangential velocity of the air flow at the diffuser, c_{t2} , equals then the tangential velocity of the rotor at the diffuser, U_2 . Therefore, the developed analytical model of the thermodynamic torque required to drive the rotor, T_C , indicated in equation (4.10) can be rewritten as a function of the compressor air mass flow rate, the tangential velocity of the rotor at the diffuser, and the rotor angular speed as follows:

$$T_C = - \frac{\dot{m}_{air} U_2^2}{\varpi_c} \quad (4.16)$$

Likewise, the developed analytical model of the thermodynamic power required to drive the rotor of the compressor, \dot{W}_C , in equation (4.11) can be rewritten as a function of the compressor air mass flow rate and the tangential velocity of the rotor at

the diffuser as follows:

$$\dot{W}_C = -\dot{m}_{air} U_2^2 \quad (4.17)$$

By applying the principle of conservation of energy to the compressor, i.e. the first law of thermodynamics, to a control volume around the compressor, the steady flow energy equation on this system is

$$\dot{Q}_C - \dot{W}_C = \dot{m}_{air} \left[\left(h + \frac{c^2}{2} + g z \right)_{out} - \left(h + \frac{c^2}{2} + g z \right)_{in} \right] \quad (4.18)$$

Since the change in altitude between inlet and outlet in diesel centrifugal compressor is negligible, the term ‘gz’ is thus negligible in equation (4.18). Due to the fact that the enthalpies referred to in equation (4.18) are measured in compressor passages in which the velocity is considerable, rather than in large tanks for instance, their stagnation values should thus be used (Taylor, 1985). The stagnation or total pressure is defined as the pressure attained if the gas is isentropically brought to rest (Heywood, 1988). Hence, it follows from equation (4.18) that:

$$\dot{Q}_C - \dot{W}_C = \dot{m}_{air} [(h_0)_2 - (h_0)_1] \quad (4.19)$$

Since the air flows throughout the compressor is treated as an ideal gas, equation (4.19) can be rewritten as follows following from Figure 4.4:

$$\dot{Q}_C - \dot{W}_C = \dot{m}_{air} c_p [T_{02} - T_{01}] \quad (4.20)$$

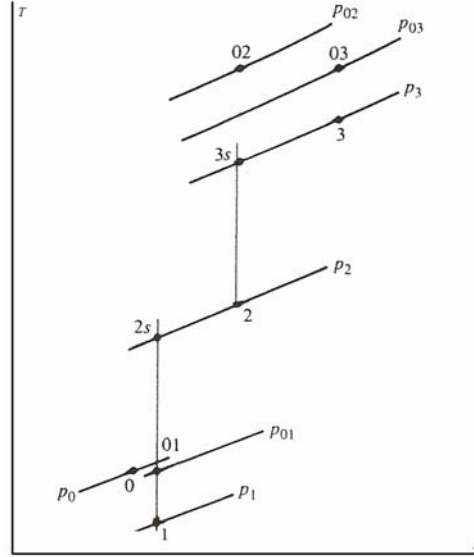


Figure 4.4

T-S diagram of the supercharging diesel centrifugal compressor with vanes-based diffuser

By recalling the analytical isentropic relation between temperature and pressure, equation (4.20) can be rewritten as:

$$\dot{Q}_C - \dot{W}_C = \dot{m}_{air} c_p T_{01} \left[\left(r_p \right)^{\frac{k-1}{k}} - 1 \right] \quad (4.21)$$

Since the heat transfer mode in the compressor is forced convection, the thermodynamic power required to drive the rotor of the compressor, \dot{W}_C , can be therefore modeled as a function of the compressor air mass flow rate, temperature, and pressure ratio following from equation (4.21) as follows:

$$\dot{W}_C = h_C (T_{02} - T_W) + \dot{m}_{air} c_p T_{01} \left[1 - \left(r_p \right)^{\frac{k-1}{k}} \right] \quad (4.22)$$

Thus, the thermodynamic torque required to drive the rotor, T_C , can also be modelled as a function of the compressor air mass flow rate, temperature, and pressure ratio

following from equation (4.22) as follows:

$$T_C = \frac{1}{\varpi_c} \left[h_c (T_{02} - T_W) + \dot{m}_{air} c_p T_{01} \left[1 - (r_p)^{\frac{k-1}{k}} \right] \right] \quad (4.23)$$

Since the kinetic energy that generates velocities at the diffuser of the supercharging diesel centrifugal compressor is key to estimate the thermodynamic power required to drive the rotor of the compressor, \dot{W}_C , an analytical sub-model of the velocities at the diffuser of the supercharging diesel centrifugal compressor with vanes-based diffuser is presented in the next section.

4.3. ANALYTICAL SUB-MODEL OF VELOCITIES AT THE DIFFUSER OF THE SUPERCHARGING DIESEL CENTRIFUGAL COMPRESSOR

In order to analytically model c_2 , c_{r2} , and c_{t2} as a function of the diesel centrifugal compressor input parameters and characteristic parameters, let us revisit the trigonometric relations between the velocities indicated in Figure 4.2.

Trigonometrically, it can be conceived from Figure 4.2 that:

$$c_{r1}^2 = c_{a1}^2 + (U_1 - c_{t1})^2 \quad (4.24)$$

Equation (4.24) can be rewritten as:

$$c_{r1}^2 = (c_{a1}^2 + c_{t1}^2) + (U_1^2 - 2U_1 c_{t1}) \quad (4.25)$$

Following from the trigonometric relations between the velocities indicated in Figure 4.2, equation (4.25) can be simplified as:

$$c_{r1}^2 = c_1^2 + U_1^2 - 2U_1 c_{t1} \quad (4.26)$$

Similarly, the following holds true at the exit of the rotor:

$$c_{r_2}^2 = c_2^2 + U_2^2 - 2U_2 c_{t_2} \quad (4.27)$$

Substituting equations (4.26) and (4.27) into equation (4.9) leads to:

$$\dot{W}_C = \frac{\dot{m}_{air}}{2} \left[(c_1^2 - c_2^2) + (c_{r_2}^2 - c_{r_1}^2) + (U_1^2 - U_2^2) \right] \quad (4.28)$$

If the slip of the fluid becomes negligible by sufficiently increasing the number of the blades of the impeller, the tangential velocity of the air flow at the diffuser, c_{t2} , equals then the tangential velocity of the rotor at the diffuser, U_2 , and thus equation (4.28) can be rewritten as:

$$\dot{W}_C = \frac{\dot{m}_{air}}{2} \left[(c_1^2 - c_2^2) + (c_{r_2}^2 - c_{r_1}^2) + (U_1^2 - c_{t2}^2) \right] \quad (4.29)$$

Now, in order to analytically formulate the radial velocity of the air flow at the diffuser, c_{r2} , let us combine equations (4.29) and (4.22) together as follows:

$$c_{r_2} = \sqrt{\frac{2}{\dot{m}_{air}} \left[h_C (T_{02} - T_W) + \dot{m}_{air} c_P T_{01} \left[1 - (r_P)^{\frac{k-1}{k}} \right] \right]} \quad (4.30)$$

$$+ c_{r_1}^2 - (c_1^2 - c_2^2) - (U_1^2 - c_{t2}^2)$$

Let us now combine equations (4.15) and (4.22) together as follows:

$$c_{r_2} = \frac{1}{\dot{m}_{air} c_{t2} \cot \beta_2} \left[h_C (T_{02} - T_W) + \dot{m}_{air} c_P T_{01} \left[1 - (r_P)^{\frac{k-1}{k}} \right] \right] + \frac{c_{t2}}{\cot \beta_2} \quad (4.31)$$

The absolute velocity of air flow at the exit of the diffuser, c_2 , can be thus analytically formulated by combining equations (4.30) and (4.31) together as pointed out next:

$$\begin{aligned}
c_2^2 = & \frac{1}{\dot{m}_{air}^2 c_{t2}^2 \cot^2 \beta_2} \left[h_C (T_{02} - T_W) + \dot{m}_{air} c_P T_{01} \left[1 - (r_P)^{\frac{k-1}{k}} \right] \right]^2 + \frac{c_{t2}^2}{\cot^2 \beta_2} \\
& + \frac{2}{\dot{m}_{air} \cot^2 \beta_2} \left[h_C (T_{02} - T_W) + \dot{m}_{air} c_P T_{01} \left[1 - (r_P)^{\frac{k-1}{k}} \right] \right] - \frac{2}{\dot{m}_{air}} \left[h_C (T_{02} - T_W) + \dot{m}_{air} c_P T_{01} \left[1 - (r_P)^{\frac{k-1}{k}} \right] \right] - c_{r1}^2 \\
& + (U_1^2 - c_{t2}^2) + c_1^2
\end{aligned} \tag{4.32}$$

Since the following can be conceived from the trigonometric relations between the velocities indicated in Figure 4.2:

$$c_2^2 = c_{t2}^2 + c_{r2}^2 \tag{4.33}$$

It follows thus from combining equations (4.32), (4.33), and (4.31) that:

$$\begin{aligned}
& \frac{1}{\dot{m}_{air}^2 c_{t2}^2 \cot^2 \beta_2} \left[h_C (T_{02} - T_W) + \dot{m}_{air} c_P T_{01} \left[1 - (r_P)^{\frac{k-1}{k}} \right] \right]^2 + \frac{c_{t2}^2}{\cot^2 \beta_2} + \frac{2}{\dot{m}_{air} \cot^2 \beta_2} \left[h_C (T_{02} - T_W) + \dot{m}_{air} c_P T_{01} \left[1 - (r_P)^{\frac{k-1}{k}} \right] \right] \\
& - \frac{2}{\dot{m}_{air}} \left[h_C (T_{02} - T_W) + \dot{m}_{air} c_P T_{01} \left[1 - (r_P)^{\frac{k-1}{k}} \right] \right] - c_{r1}^2 + (U_1^2 - c_{t2}^2) + c_1^2 \\
= & c_{t2}^2 + \frac{1}{\dot{m}_{air}^2 c_{t2}^2 \cot^2 \beta_2} \left[h_C (T_{02} - T_W) + \dot{m}_{air} c_P T_{01} \left[1 - (r_P)^{\frac{k-1}{k}} \right] \right]^2 + \frac{c_{t2}^2}{\cot^2 \beta_2} + \frac{2}{\dot{m}_{air} \cot^2 \beta_2} \left[h_C (T_{02} - T_W) + \dot{m}_{air} c_P T_{01} \left[1 - (r_P)^{\frac{k-1}{k}} \right] \right]
\end{aligned} \tag{4.34}$$

Hence, simplifying equation (4.34) leads to the following analytical formulation of the tangential velocity of the air flow at the diffuser, c_{t2} :

$$c_{t2} = \sqrt{\frac{U_1^2 + c_1^2 - c_{r1}^2}{2} - \frac{h_C (T_{02} - T_W)}{\dot{m}_{air}} - c_P T_{01} \left[1 - (r_P)^{\frac{k-1}{k}} \right]} \tag{4.35}$$

By substituting equations (4.35) in (4.31):

$$\begin{aligned}
c_{r2} = & \sqrt{\frac{U_1^2 + c_1^2 - c_{r1}^2}{2} - \frac{h_C (T_{02} - T_W)}{\dot{m}_{air}} - c_P T_{01} \left[1 - (r_P)^{\frac{k-1}{k}} \right]} \left[\frac{1}{\dot{m}_{air} \left(\frac{U_1^2 + c_1^2 - c_{r1}^2}{2} - \frac{h_C (T_{02} - T_W)}{\dot{m}_i} - c_P T_{01} \left[1 - (r_P)^{\frac{k-1}{k}} \right] \right) \cot \beta_2} \right. \\
& \left. \left[h_C (T_{02} - T_W) + \dot{m}_{air} c_P T_{01} \left[1 - (r_P)^{\frac{k-1}{k}} \right] \right] + \frac{1}{\cot \beta_2} \right]
\end{aligned} \tag{4.36}$$

By substituting equations (4.36) in (4.33):

$$c_2 = \sqrt{\left[\frac{\left(\frac{U_1^2 + c_1^2 - c_{r_1}^2}{2} - \frac{h_c (T_{02} - T_w)}{\dot{m}_{air}} - c_p T_{01} \left[1 - (r_p)^{\frac{k-1}{k}} \right] \right)}{1 + \left[\frac{\left(\frac{U_1^2 + c_1^2 - c_{r_1}^2}{2} - \frac{h_c (T_{02} - T_w)}{\dot{m}_{air}} - c_p T_{01} \left[1 - (r_p)^{\frac{k-1}{k}} \right] \right) \cot \beta_2}{\left[h_c (T_{02} - T_w) + \dot{m}_{air} c_p T_{01} \left[1 - (r_p)^{\frac{k-1}{k}} \right] \right] + \frac{1}{\cot \beta_2}} \right]^2} \right]} \quad (4.37)$$

As a matter of fact supercharging compressors do not change the mass flow rate goes into intake manifold and cylinders due to the conservation of mass (Taylor, 1985; Omran et al., 2007). The performance of these compressors is usually presented in terms of a map of air mass flow rate versus pressure ratio with showing lines of constant efficiency and constant compressor impeller speed (Wahlstrom and Eriksson, 2011). Therefore, the present research proposes that instead of using an empirical formula for estimating the compressor air mass flow rate, an analytical model of the mass flow rate of air is used that was analytically derived from the first principles of physics in another research paper by linking the intake manifold to the engine cylinders rather than to the supercharging compressor. Hence, for a given intercooler efficiency, $\eta_{Intercooler}$, and for a given volumetric efficiency of the engine, η_V , the air mass flow rate, \dot{m}_{air} , can be analytically modelled as follows similar to equation (3.12):

$$\dot{m}_{air} = \frac{P_i \eta_V V_d N_m n}{60 R T_i} \quad (4.38)$$

Since in reality much of the compressor rotor exit kinetic energy pressure head, i.e. $(P_{02} - P_2)$, is usually dissipated as a heat loss and is not converted into pressure rise

and because the stagnation enthalpy at state 2, h_{02} , equals the stagnation enthalpy at state 3, h_{03} , the following follows (Heywood, 1988):

$$P_i = P_2 \quad (4.39)$$

$$T_i = T_2 - \eta_{Intercooler} (T_2 - T_{Ref\ Amb}) \quad (4.40)$$

Therefore, substituting equations (4.39) and (4.40) into equation (4.38) leads to the following:

$$\dot{m}_{air} = \frac{P_2 \eta_V V_d N_m n}{60 R (T_2 - \eta_{Intercooler} (T_2 - T_{Ref\ Amb}))} \quad (4.41)$$

Now, by substituting equation (4.41) into (4.35), c_{t2} can be rewritten to analytically formulate the tangential velocity of the air flow at the diffuser as:

$$c_{t2} = \sqrt{\frac{U_1^2 + c_1^2 - c_{r1}^2}{2} - \frac{60 R h_C (T_2 - \eta_{Intercooler} (T_2 - T_{Ref\ Amb})) (T_{02} - T_W)}{P_2 \eta_V V_d N_m n} - c_P T_{01} \left[1 - (r_P)^{\frac{k-1}{k}} \right]} \quad (4.42)$$

Similarly, by substituting equation (4.41) into (4.36), c_{r2} can be rewritten to analytically formulate the radial velocity of the air flow at the diffuser as:

$$c_{r2} = \sqrt{\frac{U_1^2 + c_1^2 - c_{r1}^2}{2} - \frac{60 R h_C (T_2 - \eta_{Intercooler} (T_2 - T_{Ref\ Amb})) (T_{02} - T_W)}{P_2 \eta_V V_d N_m n} - c_P T_{01} \left[1 - (r_P)^{\frac{k-1}{k}} \right]} \left[\frac{1}{\dot{m}_{air} \left(\frac{U_1^2 + c_1^2 - c_{r1}^2}{2} - \frac{60 R h_C (T_2 - \eta_{Intercooler} (T_2 - T_{Ref\ Amb})) (T_{02} - T_W)}{P_2 \eta_V V_d N_m n} - c_P T_{01} \left[1 - (r_P)^{\frac{k-1}{k}} \right] \right) \cot \beta_2} \right] \left[h_C (T_{02} - T_W) + \left(\frac{P_2 \eta_V V_d N_m n}{60 R (T_2 - \eta_{Intercooler} (T_2 - T_{Ref\ Amb}))} \right) c_P T_{01} \left[1 - (r_P)^{\frac{k-1}{k}} \right] \right] + \frac{1}{\cot \beta_2} \quad (4.43)$$

Likewise, by substituting equation (4.41) into (4.37), c_2 can be rewritten to analytically formulate the absolute velocity of the air flow at the exit of the diffuser as:

$$c_2 = \left[\left[\left(\frac{U_1^2 + c_1^2 - c_{r_1}^2}{2} - \frac{60 R h_c (T_2 - \eta_{Intercooler} (T_2 - T_{Ref Amb})) (T_{02} - T_W)}{P_2 \eta_V V_d N_m n} - c_P T_{01} \left[1 - (r_p)^{\frac{k-1}{k}} \right] \right) \right. \right. \\ \left. \left. \left[\left(\frac{1}{\dot{m}_{air} \cot \beta_2} \right) \right. \right. \right. \\ \left. \left. \left. 1 + \left(\frac{1}{\left(\frac{U_1^2 + c_1^2 - c_{r_1}^2}{2} - \frac{60 R h_c (T_2 - \eta_{Intercooler} (T_2 - T_{Ref Amb})) (T_{02} - T_W)}{P_2 \eta_V V_d N_m n} - c_P T_{01} \left[1 - (r_p)^{\frac{k-1}{k}} \right] \right)} \right) \right. \right. \right. \\ \left. \left. \left. \left[h_c (T_{02} - T_W) + \left(\frac{P_2 \eta_V V_d N_m n}{60 R (T_2 - \eta_{Intercooler} (T_2 - T_{Ref Amb}))} \right) c_P T_{01} \left[1 - (r_p)^{\frac{k-1}{k}} \right] \right] + \frac{1}{\cot \beta_2} \right] \right] \right] \right] \quad (4.44)$$

Since efficiency plays a key role in accurately estimating the thermodynamic power required to drive the rotor of the compressor, \dot{W}_C , the following section presents the third and last sub-model in this chapter that investigates analytically the efficiency of supercharging diesel centrifugal compressor with vanes-based diffuser.

4.4. ANALYTICAL SUB-MODEL OF EFFICIENCY OF SUPERCHARGING DIESEL CENTRIFUGAL COMPRESSOR WITH VANES-BASED DIFFUSER

In order to account for the bearing friction losses and fanning losses in the compressor, the efficiency of the compressor is modelled analytically as well in this study. The compressor total-to-total isentropic efficiency, η_{CTT} , is by definition given as follows following from the second law of thermodynamics (Heywood, 1988; Watson and Janota, 1982):

$$\eta_{CTT} = \frac{\text{reversible thermodynamic power requirement}}{\text{actual thermodynamic power requirement}} \quad (4.45)$$

Thus, following from equation (4.22), equation (4.45) can be rewritten as:

$$\eta_{CTT} = \frac{h_{02s} - h_{01}}{h_C (T_{02} - T_W) + \dot{m}_{air} c_P T_{01} \left[1 - \left(\frac{p_{02}}{p_{01}} \right)^{\frac{k-1}{k}} \right]} \quad (4.46)$$

Hence, equation (4.46) can be rewritten as:

$$\eta_{CTT} = \frac{c_P (T_{02s} - T_{01})}{h_C (T_{02} - T_W) + \dot{m}_{air} c_P T_{01} \left[1 - \left(\frac{p_{02}}{p_{01}} \right)^{\frac{k-1}{k}} \right]} \quad (4.47)$$

For the isentropic process between states 01 and 02s, equation (4.47) can be rewritten as follows by recalling the derived analytical isentropic relation between temperature and pressure from another research paper:

$$\eta_{CTT} = \frac{c_P T_{01} \left(\left(\frac{p_{02}}{p_{01}} \right)^{\frac{k-1}{k}} - 1 \right)}{h_C (T_{02} - T_W) + \dot{m}_{air} c_P T_{01} \left[1 - \left(\frac{p_{02}}{p_{01}} \right)^{\frac{k-1}{k}} \right]} \quad (4.48)$$

Since the compressor in supercharged diesel powertrains feeds the engine through a large manifold, much of the rotor exit kinetic energy pressure head, i.e. $(P_{02} - P_2)$, is usually dissipated as a heat loss and is not converted into pressure rise (Heywood, 1988). Therefore, equation (4.48) should be rewritten as follows in order to reflect this fact:

$$\eta_{CTT} = \frac{c_P T_{01} \left(\left(\frac{p_2}{p_{01}} \right)^{\frac{k-1}{k}} - 1 \right)}{h_C (T_{02} - T_W) + \dot{m}_{air} c_P T_{01} \left[1 - \left(\frac{p_{02}}{p_{01}} \right)^{\frac{k-1}{k}} \right]} \quad (4.49)$$

By incorporating the influence of η_{CCT} on the thermodynamic power required to drive the rotor of the compressor, \dot{W}_C , equations (4.49) and (4.22) should be combined together as follows:

$$\dot{W}_C = \frac{\left(h_C (T_{02} - T_W) + \dot{m}_{air} c_P T_{01} \left[1 - \left(\frac{p_{02}}{p_{01}} \right)^{\frac{k-1}{k}} \right] \right)^2}{c_P T_{01} \left(\left(\frac{p_2}{p_{01}} \right)^{\frac{k-1}{k}} - 1 \right)} \quad (4.50)$$

In order to analytically evaluate the total power required to drive the compressor, \dot{W}_{CT} , the mechanical efficiency of the compressor, η_{CM} , should be incorporated into equations (4.50) as elucidated next:

$$\dot{W}_{CT} = \frac{\left(h_C (T_{02} - T_W) + \dot{m}_{air} c_P T_{01} \left[1 - \left(\frac{p_{02}}{p_{01}} \right)^{\frac{k-1}{k}} \right] \right)^2}{c_P T_{01} \left(\left(\frac{p_2}{p_{01}} \right)^{\frac{k-1}{k}} - 1 \right) \eta_{CM}} \quad (4.51)$$

In order to analytically model the mechanical efficiency of the compressor, η_{CM} , indicated in equation (4.51), let us recall the definition of mechanical efficiency in its mathematical form (Heywood, 1988):

$$\eta_{CM} = 1 - \frac{P_{CF}}{\dot{W}_C} \quad (4.52)$$

In order to analytically model the power loss due to friction in compressor, P_{CF} , indicated in equation (4.52), let us draw on the fundamental relation between the power loss due to friction in compressor, P_{CF} , and the total friction mean effective pressure in compressor, P_{CTFME} (Heywood, 1988):

$$P_{CTFME} = \frac{P_{CF} n}{V_{Cd} \omega_c} \quad (4.53)$$

The angular speed of the rotor of the compressor in revolution per minute, N_{CM} , can be expressed in terms of the angular speed of the rotor of the compressor in radians per second, ω_c , as follows:

$$\omega_c = \frac{2\pi}{60} N_{CM} \quad (4.54)$$

The total friction mean effective pressure in compressor, P_{CTFME} , by definition is given by the following expression (Harari and Sher, 1995):

$$P_{CTFME} = \frac{2\pi I_C \alpha_C}{V_{Cd}} \quad (4.55)$$

By combining equations (4.50), (4.53), and (4.55), equation (4.52) can be rewritten as:

$$\eta_{CM} = 1 - \frac{\pi^2 I_C \alpha_C N_{CM}}{15 n \dot{W}_C} \quad (4.56)$$

CHAPTER 5

DIESEL ENGINE ANALYTICAL MODEL

5.1. OVERVIEW

Since the most contributing part of the diesel powertrain to diesel exhaust is the diesel engine (Bala showry and Sita Rama Raju, 2010.), modeling diesel engines has received increasing attention. This chapter presents an analytical model of supercharged diesel engines, equipped with ETC, as the heart of the diesel powertrain. In this chapter, the in-cylinder gas speed dynamics, the fuel mass flow rate in the diesel engine fuel system, the brake power in the diesel engine are formulated analytically. Following from principles of physics, Chapter 5 contributes to the implementation of the 1st and 2nd pillars of the research philosophy adopted in this study with respect to the analytical modeling of the diesel powertrain fuel consumption rate in an endeavour to achieve the 1st objective in this research. In addition, this Chapter contributes to achieving the 1st objective of this research with respect to the analytical modeling of the diesel powertrain fuel consumption rate.

5.2. IN-CYLINDER GAS SPEED DYNAMICS

In order to evaluate the in-cylinder gas dynamic speed, \dot{c}_{Cyl} , in terms of instantaneous piston speed and engine parameters, the momentum conservation is taken into consideration. Considering the control volume in the diesel engine cylinder shown in Figure 5.1, since there is no area change over the infinitesimal length of the engine

cylinder, dx , in the engine cylinder, the flow is thus assumed to be quasi one-dimensional flow.

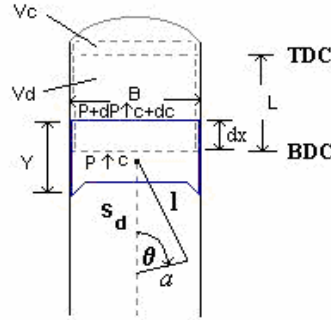


Figure 5.1

Control volume in diesel engine cylinder for one-dimensional flow analysis

The momentum conservation equation states that the net pressure forces plus the wall shear force acting on the control volume surface equal the rate of change of momentum within the control volume plus the net flow of momentum out of the control volume (Heywood, 1988). Thus, the net forces in the control volume shown in Figure 5.1, the rate of change of momentum within the control volume, the net flow of momentum across the control volume surface, and the total momentum are investigated in this section, respectively.

5.2.1. The Net Forces

The net forces in the control volume shown in Figure 5.1 consist of pressure force and shear force. The net pressure force, F_{Press} , can be evaluated as follows:

$$F_{Press} = P_{Cyl} A_{Cyl} - \left(P_{Cyl} + \frac{\partial P_{Cyl}}{\partial x} dx \right) (A_{Cyl}) \quad (5.1)$$

By rearranging Equation (5. 1), the following follows:

$$F_{Press} = -A_{Cyl} \frac{\partial P_{Cyl}}{\partial x} dx \quad (5.2)$$

The net shear force, F_{Shear} , can be evaluated as follows:

$$F_{Shear} = -\tau_w (\pi D_{Cyl} dx) \quad (5.3)$$

By definitions of the flow shear stress and flow friction coefficient, the following follows (Heywood, 1988):

$$\tau_w = \zeta_{In-Cyl} E_{Kin} \quad (5.4)$$

The kinetic energy per unit area, E_{Kin} , can be evaluated by definition as follows (Heywood, 1988):

$$E_{Kin} = \rho_{Cyl} \frac{c_{Cyl}^2}{2} \quad (5.5)$$

Therefore, combining Equations (5.3), (5.4), and (5.5) the following follows:

$$F_{Shear} = -\frac{\zeta_{In-Cyl} \rho_{Cyl} c_{Cyl}^2 \pi D_{Cyl}}{2} dx \quad (5.6)$$

5.2.2. The Rate of Change of Momentum Within the Control Volume

The rate of change of momentum within the control volume in the engine cylinder shown in Figure 5.1, M_{Moment} , can be evaluated from the fundamental definition of momentum and force as follows (Heywood, 1988):

$$M_{Moment} = \frac{\partial}{\partial t} (c_{Cyl} F_{Moment}) \quad (5.7)$$

The force that generated this momentum, F_{Moment} , can be evaluated from its fundamental definition as follows (Heywood, 1988):

$$F_{Moment} = \rho_{Cyl} V_{Cyl} \quad (5.8)$$

Thus, combining Equations (5.7) and (5.8) together leads to the following:

$$M_{Moment} = \frac{\partial}{\partial t} (c_{Cyl} \rho_{Cyl} A_{Cyl} dx) \quad (5.9)$$

5.2.3. The Net Flow of Momentum Across the Control Volume Surface

The net flow of momentum across the control volume surface in the engine cylinder shown in Figure 5.1, M_{Net} , can be evaluated from the fundamental definition of momentum as follows (Heywood, 1988):

$$M_{Net} = \left(\rho_{Cyl} + \frac{\partial \rho_{Cyl}}{\partial x} dx \right) \left(c_{Cyl} + \frac{\partial c_{Cyl}}{\partial x} dx \right)^2 (A_{Cyl}) - \rho_{Cyl} c_{Cyl}^2 A_{Cyl} \quad (5.10)$$

By simplifying, ignoring mathematically trivial terms, and rearranging Equation (5.10), the following follows:

$$M_{Net} = \frac{\partial}{\partial x} (\rho_{Cyl} c_{Cyl}^2 A_{Cyl}) dx \quad (5.11)$$

5.2.4. The Total Momentum

Therefore following from the fundamental definition of the momentum conservation and by combining Equations (5.2), (5.6), (5.9), and (5.11) the following follows:

$$-A_{Cyl} \frac{\partial P_{Cyl}}{\partial x} dx - \zeta_{In-Cyl} \frac{\rho_{Cyl} c_{Cyl}^2}{2} \pi D_{Cyl} dx = \rho_{Cyl} A_{Cyl} \frac{\partial c_{Cyl}}{\partial t} dx + \rho_{Cyl} A_{Cyl} \frac{\partial c_{Cyl}^2}{\partial x} dx \quad (5.12)$$

Thus, the in-cylinder gas dynamic velocity can be expressed as follows following from simplifying and rearranging Equation (5.12):

$$\dot{c}_{Cyl} = -2c_{Cyl} \left(\frac{\partial c_{Cyl}}{\partial x} \right) - \frac{1}{\rho_{Cyl}} \left(\frac{\partial P_{Cyl}}{\partial x} \right) - 2\zeta_{In-Cyl} \frac{c_{Cyl}}{D_{Cyl}} \quad (5.13)$$

By recalling the in-cylinder gas speed analytical formula (3.105) and combining this formula with Equation (5.13), the dynamic gas speed can be represented analytically as follows:

$$\dot{c}_{Cyl} = -\frac{1}{\rho_{Cyl}} \left(\frac{\partial P_{Cyl}}{\partial x} \right) - 2\zeta_{In-Cyl} \frac{c_{Cyl}^2}{D_{Cyl}} \quad (5.14)$$

Since a value of diameter, D_{Cyl} , can be assigned to the cylinder and the length of the stroke, L_{Stroke} , is relatively short \dot{c}_{Cyl} , P_{Cyl} , c_{Cyl} , and ρ_{Cyl} can be considered constants with respect to x (Sulaiman, et al., 2010). Hence, establishing integration on equation (5.14) with respect to x leads to the following:

$$\dot{c}_{Cyl} = -\frac{P_{Cyl}}{\rho_{Cyl} L_{Stroke}} - 2\zeta_{In-Cyl} \frac{c_{Cyl}^2}{D_{Cyl}} \quad (5.15)$$

5.3. FUEL MASS FLOW RATE IN THE DIESEL ENGINE FUEL SYSTEM

The direct injection common rail diesel fuel system that is widely adopted in vehicular diesel technology consists mainly of the following components: (i) fuel tank, (ii) fuel filter, (iii) fuel pump, (iv) pressure sensor, (v) common rail, (vi) governor, (vii) injectors. The fuel mass actual flow rate of this diesel fuel system under both steady speed and acceleration-based operating conditions will be analytically modelled in this section, respectively.

5.3.1. Analytical Modeling of the Steady Speed-based Fuel Mass Actual Flow Rate in Diesel Engines

In diesel engine testing, the fuel consumption is measured in terms of the fuel mass

flow rate. In order to analytically model the fuel mass flow rate in diesel engines, let us apply a control volume to the fuel pump in the diesel fuel system. Let us first recall the definition of the actual fuel-to-air ratio, $R_{F-A \text{ actual}}$, (Obert, 1973) under steady speed condition:

$$\dot{m}_{AFSS} = R_{F-A \text{ actual}} \dot{m}_{All \text{ Cyl}} \quad (5.16)$$

By combining the definition of equivalence ratio, Φ , with equation (5.16), it follows that (Obert, 1973):

$$\dot{m}_{AFSS} = \Phi R_{F-A \text{ stoich}} \dot{m}_{All \text{ Cyl}} \quad (5.17)$$

Taking into consideration that in diesel engines the actual mass flow rate of air primarily equals the theoretical mass flow rate of air since what primarily varies with load and accelerator pedal position is the mass flow rate of fuel, it thus follows from substituting equation (3.13) into equation (5.17) that:

$$\dot{m}_{AFSS} = \Phi R_{F-A \text{ stoichiometric}} \frac{\rho_{Cyl} \eta_V V_d N_m n}{60} \quad (5.18)$$

The engine crankshaft rotational speed in (rad/s), w , can be as well analytically formulated as follows (Guensler et al., 2005):

$$w = \frac{V_S G_t G_d}{r_{wr}} \quad (5.19)$$

Thus, following from equation (5.19), the actual mass flow rate of fuel in the diesel engine under the steady speed condition in (kg/s), \dot{m}_{AFSS} , indicated in equation (5.18) can be analytically reformulated as follows:

$$\dot{m}_{AFSS} = \Phi R_{F-A \text{ stoich}} \frac{\rho_{Cyl} \eta_V V_d V_S G_t G_d n}{2\pi r_{wr}} \quad (5.20)$$

The V_d term in equation (5.20) can be rewritten in terms of the number of cylinders of the engine as follows:

$$V_d = V_{d-Cyl} N_{Cyl} \quad (5.21)$$

Substituting equation (5.21) into equation (5.20) leads to the final formulation of the actual mass flow rate of fuel in the diesel engine under the steady speed condition in (kg/s), \dot{m}_{AFSS} :

$$\dot{m}_{AFSS} = \Phi R_{F-A \text{ stoich}} \frac{\rho_{Cyl} \eta_V V_{d-Cyl} N_{Cyl} V_S G_t G_d n}{2 \pi r_{wr}} \quad (5.22)$$

The key explanatory variable in equation (5.22) is V_S . Analytically modeling the steady speed-based fuel mass actual flow rate in diesel engines paves the way for analytically modeling the acceleration-based fuel mass actual flow rate in diesel powertrain fuel system.

5.3.2. Analytical Modeling of the Acceleration-based Fuel Mass Actual Flow Rate in Diesel Powertrain Fuel System

As a matter of fact, the speed and acceleration data on the majority of trucks and light duty commercial vehicles are based on steady state conditions and acceleration ranges from - 0.3 m/s² to 0.3 m/s² (Rakha, et al., 2003). Following from the analytical modeling of the \dot{m}_{AFSS} , this section thus will present the analytical models of the actual mass flow rate of fuel in diesel engines under negative acceleration ranges from -1.5 m/s² up to 0 m/s² for both low speed cycles, \dot{m}_{NLSAF} , and high speed cycles, $\dot{m}_{NHS AF}$. It is noteworthy that the low speed cycles are the standard cycles of speed of less than or equal to half of the average speed of the maximum speed cycle which is the Freeway High Speed Cycle. This section will also present the actual mass flow

rate of fuel in diesel engines under positive acceleration ranges from 0.1 m/s^2 up to 0.9 m/s^2 for both low speed cycles, \dot{m}_{P1LSAF} , and high speed cycles, \dot{m}_{P1HSAF} . This section will present as well the actual mass flow rate of fuel in diesel engines under positive acceleration ranges from 1 m/s^2 up to 2 m/s^2 , for both low speed cycles \dot{m}_{P2LSAF} , and high speed cycles, \dot{m}_{P2HSAF} .

Under the acceleration-based operating condition, the influence of the number of power strokes per cycle becomes more noticeable on the rate of fuel consumption. In addition, it has been recently found that the acceleration-based actual rate of vehicle fuel consumption is exponentially proportional to vehicle acceleration (Rakha, et al., 2003). The exponential function, e^x , can be considered basically dimensionless since the basic representation of e^x in the mathematical expansion of e^x is “1” which is a dimensionless quantity. Therefore, the actual mass flow rate of fuel in diesel engines under negative acceleration ranges from -1.5 m/s^2 up to 0 m/s^2 for low speed cycles, \dot{m}_{NLSAF} , and for high speed cycles, \dot{m}_{NHSAF} , can be formulated as follows following from equation (5.22):

$$\dot{m}_{NLSAF} = \Phi R_{F-A \text{ stoich}} \frac{\rho_{Cyl} \eta_V V_{d-Cyl} N_{Cyl} V_S G_t G_d n^{1.19}}{2\pi r_{wr}} e^{\frac{a_{VS} V_S}{(n)^{4.8}}} \quad (5.23)$$

The key explanatory variables in equation (5.23) are V_S and a_{VS} . Equation (5.23) is dimensionally correct which supports the validity of this developed model. In a similar fashion, \dot{m}_{NHSAF} can be formulated as follows:

$$\dot{m}_{NHSAF} = \Phi R_{F-A \text{ stoich}} \frac{\rho_{Cyl} \eta_V V_{d-Cyl} N_{Cyl} V_S G_t G_d n^{1.19}}{2\pi r_{wr}} e^{\frac{a_{VS} V_S}{(n)^{5.2}}} \quad (5.24)$$

The key explanatory variables in equation (5.24) are V_s and a_{VS} . Equation (5.24) is dimensionally correct which supports the validity of this developed model.

The actual mass flow rate of fuel in diesel engines under positive acceleration ranges from 0.1 m/s^2 up to 0.9 m/s^2 for low speed cycles, \dot{m}_{P1LSAF} , and for high speed cycles, \dot{m}_{P1HSAF} , can also be formulated following from equation (5.22) as follows:

$$\dot{m}_{P1LSAF} = \Phi R_{F-A \text{ stoich}} \frac{\rho_{Cyl} \eta_V V_{d-Cyl} N_{Cyl} V_s G_t G_d n^{0.78}}{2\pi r_{wr}} e^{a_{VS} + 0.25} \quad (5.25)$$

The key explanatory variables in equation (5.25) are V_s and a_{VS} . Equation (5.25) is dimensionally correct which supports the validity of this developed model. Similarly, \dot{m}_{P1HSAF} can be analytically modeled as follows:

$$\dot{m}_{P1HSAF} = \Phi R_{F-A \text{ stoich}} \frac{\rho_{Cyl} \eta_V V_{d-Cyl} N_{Cyl} V_s G_t G_d n^{0.78}}{2\pi r_{wr}} e^{a_{VS} + 0.5} \quad (5.26)$$

The key explanatory variables in equation (5.26) are V_s and a_{VS} . Equation (5.26) is dimensionally correct which supports the validity of this developed model.

The actual mass flow rate of fuel in diesel engines under positive acceleration ranges from 1 m/s^2 up to 2 m/s^2 for low speed cycles, \dot{m}_{P2LSAF} , and for high speed cycles, \dot{m}_{P2HSAF} , can as well be modeled following from equation (5.22):

$$\dot{m}_{P2LSAF} = \Phi R_{F-A \text{ stoich}} \frac{\rho_{Cyl} \eta_V V_{d-Cyl} N_{Cyl} V_s G_t G_d n^{0.78}}{2\pi r_{wr}} e^{a_{VS}} \quad (5.27)$$

The key explanatory variables in equation (5.27) are V_s and a_{VS} . Equation (5.27) is dimensionally correct which supports the validity of this developed model. In a similar fashion, \dot{m}_{P2HSAF} can be analytically modeled as follows:

$$\dot{m}_{P2HSAF} = \Phi R_{F-A \text{ stoich}} \frac{\rho_{Cyl} \eta_V V_{d-Cyl} N_{Cyl} V_S G_t G_d n^{0.78}}{2 \pi r_{wr}} e^{(n)^{0.25} a_{VS}} \quad (5.28)$$

The key explanatory variables in equation (5.28) are V_S and a_{VS} . Equation (5.28) is dimensionally correct which supports the validity of this developed model.

5.4. BRAKE POWER IN THE DIESEL ENGINE

It follows from the fundamental definition of the indicated power of the diesel engine that (Ganesan, 2008):

$$\Gamma_I = W_{WS} N_{WS} \quad (5.29)$$

The term W_{WS} in equation (5.29) can be analytically figured out as follows:

$$W_{WS} = F_{Piston} L_{Stroke} N_{Cyl} \quad (5.30)$$

Also, the term N_{WS} in equation (5.29) can be analytically figured out as follows:

$$N_{WS} = \frac{N_S}{n} \quad (5.31)$$

Further, the term F_{Piston} in equation (5.30) can be analytically formulated as follows:

$$F_{Piston} = \Gamma_{IME} A_{Piston} \quad (5.32)$$

Recalling the definition of $\dot{V}_{CylTheoretical}$ in terms of N_S and V_d :

$$N_S = \frac{\dot{V}_{CylTheoretical}}{V_d} \quad (5.33)$$

The term Γ_{IME} in equation (5.32) can thus be analytically formulated similar to the definition of $\dot{V}_{CylTheoretical}$ indicated in equation (5.33):

$$\Gamma_{IME} = \frac{\Omega_I}{V_{d-rad}} \quad (5.34)$$

The term V_{d-rad} in equation (5.34) can be analytically formulated as follows for four-stroke engines:

$$V_{d-rad} = \frac{V_d}{4\pi} \quad (5.35)$$

The term V_d in equation (5.35) can be analytically formulated as follows:

$$V_d = A_{Piston} L_{Stroke} N_{Cyl} \quad (5.36)$$

Substituting equation (5.36) into equation (5.35), equation (5.35) into equation (5.34), equation (5.34) into equation (5.32), equation (5.32) into equation (5.30), and equations (5.31) and (5.30) into equation (5.29), equation (5.29) can be rewritten as follows:

$$\Gamma_I = \frac{4\pi \Omega_I N_S}{n} \quad (5.37)$$

For four-stroke engines, equation (5.37) can be simplified as follows:

$$\Gamma_I = 2\pi \Omega_I N_S \quad (5.38)$$

The brake power (Γ_B) and brake torque (Ω_B) of the engine can be analytically formulated as follows following from the definition of the diesel engine mechanical efficiency, η_{EM} , respectively:

$$\Gamma_B = \eta_{EM} \Gamma_I - \Gamma_{LB} \quad (5.39)$$

$$\Omega_B = \eta_{EM} \Omega_I - \Omega_{LB} \quad (5.40)$$

Substituting equations (5.39) and (5.40) into (5.38), Γ_B in (W) can be analytically formulated as follows:

$$\Gamma_B = 2\pi (\Omega_B + \Omega_{LB}) N_S - \Gamma_{LB} \quad (5.41)$$

Substituting equation (5.19) into equation (5.41) leads to the analytical formulation of the brake power (Γ_B) of the four-stroke engine:

$$\Gamma_B = \frac{V_S G_t G_d}{r_{wr}} (\Omega_B + \Omega_{LB}) - \Gamma_{LB} \quad (5.42)$$

CHAPTER 6

DIESEL POWERTRAIN EXHAUST SYSTEM AND REGULATED EMISSIONS RATE ANALYTICAL MODEL

6.1. OVERVIEW

Vehicle emission rate models are currently the primary tool for evaluating the regional impacts of transportation projects and in evaluating developed transportation technologies. This chapter presents and validates an analytical model of diesel exhaust system and regulated emissions rate. It commences with exploring the key components of diesel exhaust system. Then, an analytical model of the energy available in the exhaust of supercharged diesel powertrains is presented. The pressure difference and instantaneous speed across diesel exhaust system are analytically modelled after that. An analytical model of the percentage of unburned fuel in diesel powertrains is then presented. The proportions of main species of diesel exhaust emission are presented after that. Since Carbon dioxide (CO_2) naturally exists in fresh air, catalytic converters usually convert Carbon monoxide (CO) into CO_2 , key vehicle emissions models such as INTEGRATION do not count CO_2 among harmful vehicle emissions, key vehicle emissions models focus on CO when it comes to CO_x (Masterton and Huley, 2009; Rakha, et al., 2003). Thus, the steady speed diesel exhaust emission rate of CO is then analytically modelled. An analytical model of the steady speed diesel exhaust emission rate of Nitric oxides is developed after that. Finally, the steady speed diesel exhaust emission rate of hydrocarbons (HC) is then analytically modelled. Following from principles of physics, Chapter 6 contributes to the implementation of the 1st and 2nd pillars of the research philosophy adopted in this study with respect to the analytical modeling of the diesel regulated emissions rate in

an endeavour to achieve the 1st objective in this research. In addition, this Chapter contributes to achieving the 1st objective of this research with respect to the analytical modeling of the diesel regulated emissions rate.

6.2. ANALYTICAL MODEL OF PRESSURE DROP AND INSTANTANEOUS SPEED ACROSS DIESEL EXHAUST SYSTEM

Exhaust system components specifications, e.g. the pipe diameter, component length, catalytic converter size, muffler size, and exhaust manifold design are engineered to provide proper exhaust flow to reduce power losses due to pumping, to provide proper silencing, and to provide proper emission levels on a particular engine (Usan, 2005). This is particularly true in light of the fact that passing of exhaust gases more freely lowers the back pressure, which is inherent in the exhaust system (Usan, 2005). Thus, this section investigates the instantaneous speed and pressure difference across the diesel exhaust system. Let us start with the instantaneous speed across the diesel exhaust system. The exhaust flow that comes out from all the cylinders of a multi-cylinder engine is considered steady-flow (Obert, 1973). Thus, following from the principle of continuity of fluid flow, it follows for each component j in the diesel exhaust system indicated in Figure 6.1 that:

$$\dot{m}_{Exhaust} = \rho_{Exhaust} A_{Exhaust\ j} v_{Exhaust\ j} \quad (6.1)$$

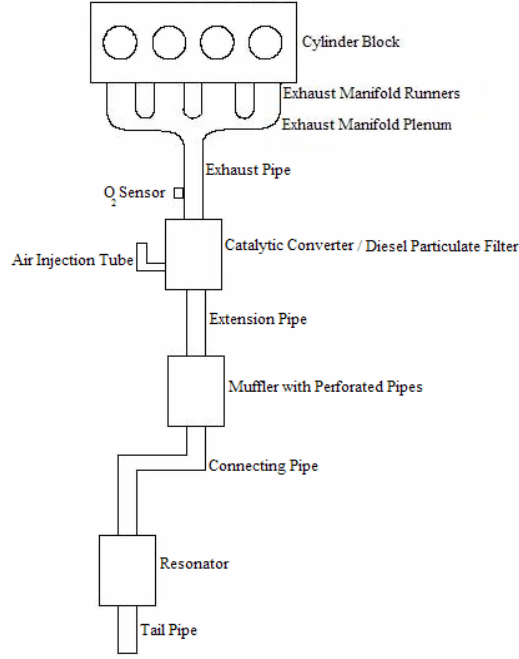


Figure 6.1

Exhaust system main components

Combining the principle of conservation of mass at the time of opening the exhaust valve with equation (6.1) leads to the following (Obert, 1973):

$$v_{Exhaust\ j} = \frac{\dot{m}_{All\ Cyl} + \dot{m}_{fuel\ actual}}{A_{Exhaust\ j} \left[\left(\frac{\dot{m}_{All\ Cyl}}{\dot{m}_{All\ Cyl} + \dot{m}_{fuel}} \right) \rho_{Cyl} + \left(\frac{\dot{m}_{fuel}}{\dot{m}_{All\ Cyl} + \dot{m}_{fuel}} \right) \rho_{fuel} \right]} \quad (6.2)$$

By simplifying equation (6.2), the exhaust flow local velocity at component j in the diesel exhaust system, $v_{Exhaust\ j}$, can be analytically modeled as follows:

$$v_{Exhaust\ j} = \frac{\left(\dot{m}_{All\ Cyl} + \dot{m}_{fuel} \right)^2}{A_{Exhaust\ j} \left[\dot{m}_{All\ Cyl} \rho_{Cyl} + \dot{m}_{fuel} \rho_{fuel} \right]} \quad (6.3)$$

For a given intercooler efficiency, $\eta_{Intercooler}$, and for a given volumetric efficiency of the engine, η_V , the \dot{m}_{AllCyl} is analytically formulated in equation (3.13). The ρ_{Cyl} indicated in equation (6.3) can be formulated analytically following from the ideal gas law as follows:

$$\rho_{Cyl} = \frac{P_i}{R T_i} \quad (6.4)$$

Now, let us investigate the pressure drop across the diesel exhaust system. Throughout the diesel exhaust system, Bernoulli's equation is applicable. Thus, the dynamic pressure drop at each of the nine components of the diesel exhaust system indicated in Figure 6.1, $\Delta P_{Exhaust\ j}$, is given as follows neglecting the negligible difference in altitude within the diesel exhaust system:

$$\Delta P_{Exhaust\ j} = \frac{1}{2} \rho_{fuel} v_{Exhaust\ j}^2 \quad (6.5)$$

Combining equations (6.3), (6.4) and (6.5), the total quasi-steady pressure loss due to friction across the diesel exhaust system, $\Delta P_{Exhaust\ friction}$, can be therefore analytically formulated as follows:

$$\Delta P_{Exhaust\ friction} = \sum_{j=1}^9 \frac{1}{2} \rho_{fuel} v_{Exhaust\ j}^2 \quad (6.6)$$

Having seen this, let us now investigate how much unburned fuel exists in the exhaust flow in diesel powertrains.

6.3. ANALYTICAL MODEL OF PERCENTAGE OF UNBURNED FUEL IN DIESEL POWERTRAINS

Among the drawbacks of diesel engines is that fuel droplets don't combust

quickly/completely compared to a premixed charge, with a sudden change of engine speed. Thus, diesel engines are preferably used in transportation devices which usually maintain a constant rpm, e.g. semi-trucks and trains, and are not typically used in automobiles which take on a lot of stop and go traffic (Usan, 2005). Unburned diesel fuel is an organic grouping detectable within an exhaust sample (Bramston-Cook, et al., 2000). In order to analytically model the percentage of unburned fuel without regeneration for a diesel engine, $R_{Unburned}$, let us first recall the relationship between the percentage of unburned fuel for a single cylinder engine, $R_{Unburned\ Cyl}$, and the percentage of burned fuel for a single cylinder engine, $R_{Burned\ Cyl}$, in diesel engines:

$$R_{Unburned\ Cyl} = n^5 (1 - R_{Burned\ Cyl}) \quad (6.7)$$

The percentage of burned fuel for a single cylinder engine, $R_{Burned\ Cyl}$, indicated in equation (6.7) in turn can be analytically formulated as follows:

$$R_{Burned\ Cyl} = \frac{E_{Combustion}}{E_{Fuel}} \quad (6.8)$$

The power consumed/released during combustion, $E_{Combustion}$, indicated in equation (6.8) can be analytically modeled following from the first law of thermodynamics on energy conservation as follows (Heywood, 1988):

$$E_{Combustion} = \frac{\dot{m}_{exhaust\ SS}}{N_{Cyl}} \left[\sum_{i\ Reac\ tants} n_i \Delta h_{f,i\ Reac\ tants} - \sum_{i\ Products} n_i \Delta h_{f,i\ Products} \right] \quad (6.9)$$

The total power that can be generated from diesel fuel, E_{Fuel} , indicated in equation (6.8) can be analytically modeled as follows (Heywood, 1988):

$$E_{Fuel} = \frac{\dot{m}_{AFSS}}{N_{Cyl}} Q_{LHV} \quad (6.10)$$

Substituting equations (6.9) and (6.10) into equation (6.8):

$$R_{Burned} = \frac{\dot{m}_{exhaust SS} \left[\sum_{i \text{ Reactants}} n_i \Delta h_{f,i \text{ Reactants}} - \sum_{i \text{ Products}} n_i \Delta h_{f,i \text{ Products}} \right]}{\dot{m}_{AFSS} Q_{LHV}} \quad (6.11)$$

Substituting equation (6.11) into equation (6.7):

$$R_{UnburnedCyl} = n^5 \left(1 - \left(\frac{1}{100} \right) \frac{\dot{m}_{exhaust SS} \left[\sum_{i \text{ Reactants}} n_i \Delta h_{f,i \text{ Reactants}} - \sum_{i \text{ Products}} n_i \Delta h_{f,i \text{ Products}} \right]}{\dot{m}_{AFSS} Q_{LHV}} \right) \quad (6.12)$$

Rearranging equation (6.12):

$$R_{UnburnedCyl} = n^5 \left(1 - \left(\frac{1}{100} \right) \left(\frac{\dot{m}_{exhaust SS}}{\dot{m}_{AFSS}} \right) \left[\frac{\sum_{i \text{ Reactants}} n_i \Delta h_{f,i \text{ Reactants}} - \sum_{i \text{ Products}} n_i \Delta h_{f,i \text{ Products}}}{Q_{LHV}} \right] \right) \quad (6.13)$$

It follows from the principle of conservation of mass that:

$$\dot{m}_{exhaust SS} = \dot{m}_{AFSS} + \dot{m}_{AllCyl} \quad (6.14)$$

The \dot{m}_{AllCyl} is analytically formulated in equation (3.13). The engine crankshaft rotational speed in (rad/s), w , is analytically formulated in equation (5.19).

Substituting equations (3.13) and (5.19) into equation (6.13):

$$R_{UnburnedCyl} = n^5 \left(1 - \left(\frac{1}{100} \right) \left(\frac{\rho_{Cyl} \eta_V V_d n V_S G_t G_d}{\dot{m}_{AFSS} 2 \pi r_{wr}} + 1 \right) \left[\frac{\sum_{i \text{ Reactants}} n_i \Delta h_{f,i \text{ Reactants}} - \sum_{i \text{ Products}} n_i \Delta h_{f,i \text{ Products}}}{Q_{LHV}} \right] \right) \quad (6.15)$$

For multi-cylinder diesel engines, the percentage of unburned fuel without regeneration in diesel engines, $R_{Unburned}$, in (ppm) can be analytically formulated following from equation (6.15) as follows:

$$R_{Unburned} = N_{Cyl} n^5 \left\langle 1 - \left[\frac{\rho_{Cyl} \eta_V V_d V_S G_t G_d n}{2 \pi r_{wr} \dot{m}_{AFSS}} + 1 \right] \left(\frac{\sum_{i \text{ Reactants}} n_i \Delta h_{f,i \text{ Reactants}} - \sum_{i \text{ Products}} n_i \Delta h_{f,i \text{ Products}}}{Q_{LHV}} \right) \right\rangle \quad (6.16)$$

For four-stroke multi-cylinder diesel engines, the percentage of unburned fuel without regeneration in diesel engines, $R_{Unburned}$, in (ppm) can be analytically formulated following from equation (6.16) as follows:

$$R_{Unburned} = 32 N_{Cyl} \left\langle 1 - \left[\frac{\rho_{Cyl} \eta_V V_d V_S G_t G_d n}{2 \pi r_{wr} \dot{m}_{AFSS}} + 1 \right] \left(\frac{\sum_{i \text{ Reactants}} n_i \Delta h_{f,i \text{ Reactants}} - \sum_{i \text{ Products}} n_i \Delta h_{f,i \text{ Products}}}{Q_{LHV}} \right) \right\rangle \quad (6.17)$$

The analytical modeling of the $R_{Unburned}$ paves the way to analytically model the steady speed exhaust emission rate of CO in diesel engines.

6.4. ANALYTICAL MODEL OF STEADY SPEED EXHAUST EMISSION RATE OF CARBON MONOXIDE DIESEL EXHAUST EMISSIONS

The rate of the steady speed-based total CO exhaust emissions in (kg/s), R_{COSS} , is the algebraic summation of the rate of the steady speed-based CO exhaust emissions that result from CO₂ dissociation in (kg/s), $R_{COSSCO+O2}$, and the rate of the steady speed-

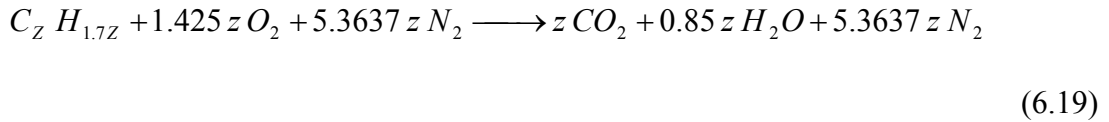
based CO exhaust emissions that result from the Water-Gas-Shift reaction in (kg/s), $R_{COSSCO+H_2O}$, which are both the key sources of generating CO in the exhaust system as indicated in equation (6.18):

$$R_{COSS} = R_{COSSCO+O_2} + R_{COSSCO+H_2O} \quad (6.18)$$

The analytical modeling of the $R_{COSSCO+O_2}$ and the $R_{COSSCO+H_2O}$ will be developed in this section. Let us first investigate the analytical modeling of the $R_{COSSCO+O_2}$ that is based on the CO₂ dissociation.

6.4.1. Analytical Model of the Rate of the Steady Speed-based CO Exhaust Emissions that Result from CO₂ Dissociation

The stoichiometric chemical reaction of the combustion of diesel fuel no. 2 in diesel engines that reflects the influence of fuel composition on combustion is given as follows:



As a matter of fact, the combustion in diesel engines is usually incomplete in reality. Hence, the equivalence ratio, Φ , which reflects the influence of the actual concentration of reactants, should appear in the chemical equation of the combustion of diesel fuel. In addition, the percentage of burned fuel with respect to total fuel supplied to the cylinder of the engine, i.e. $(1-R_{Unburned})$, should appear in the chemical equation of the combustion of diesel fuel as well. Therefore, the actual chemical reaction of the combustion of diesel fuel no. 2 in diesel engines is given as follows following from chemical equation (6.19):

$$\begin{aligned}
& (1-R_{Unburned})C_Z H_{1.7Z} + \frac{1.425 z (1-R_{Unburned})}{\phi} O_2 + \frac{5.3637 z (1-R_{Unburned})}{\phi} N_2 \\
& \longrightarrow z (1-R_{Unburned})CO_2 + 0.85 z (1-R_{Unburned})H_2O + 1.425 z (1-R_{Unburned}) \left(\frac{1}{\phi} - 1 \right) O_2 + \frac{5.3637 z (1-R_{Unburned})}{\phi} N_2
\end{aligned} \tag{6.20}$$

The CO_2 dissociation is therefore described in the following chemical reaction following from chemical equation (6.20):

$$z(1-R_{Unburned})CO_2 \Leftrightarrow z(1-R_{Unburned})CO + \frac{z(1-R_{Unburned})}{2}O_2 \tag{6.21}$$

The forward reaction rate at equilibrium, $R^+_{CO+O_2}$ in (s^{-1}), can be thus analytically formulated as follows:

$$R^+_{CO+O_2} = (1-R_{Unburned})K_{CO+O_2} [CO_2] \tag{6.22}$$

Applying the definition of the forward reaction rate at equilibrium, $R^+_{CO+O_2}$, to the CO_2 dissociation indicated in chemical equation (6.21) leads to:

$$R_{CO \text{ in } CO+O_2 \text{ per mole}} = M_{CO \text{ molar}} R^+_{CO+O_2} \tag{6.23}$$

The $R_{COSSCO+O_2}$ in (kg /s) can thus be analytically formulated following from equation (9) as follows:

$$R_{COSSCO+O_2} = \frac{\dot{m}_{fuel \text{ actual SS}} R_{CO \text{ in } CO+O_2 \text{ per mole}} V_S}{M_{fuel \text{ molar}} a_{avg}} \tag{6.24}$$

Equation (6.24) gives $R_{COSSCO+O_2}$ in (kg/s) in a dimensionally correct form. Hence, substituting equations (6.22) and (6.23) into equation (6.24) leads to:

$$R_{COSSCO+O_2} = \frac{\dot{m}_{fuel \text{ actual SS}} (M_{CO \text{ molar}} (1-R_{Unburned})K_{CO+O_2} [CO_2]) V_S}{M_{fuel \text{ molar}} a_{avg}} \tag{6.25}$$

The steady speed-based fuel mass flow rate, $\dot{m}_{fuel \text{ actual SS}}$, can be analytically formulated as follows [16]:

$$\dot{m}_{AFSS} = \Phi R_{F-A \text{ stoich}} \frac{\rho_{Cyl} \eta_V V_d V_S G_t G_d n}{2 \pi r_{wr}} \tag{6.26}$$

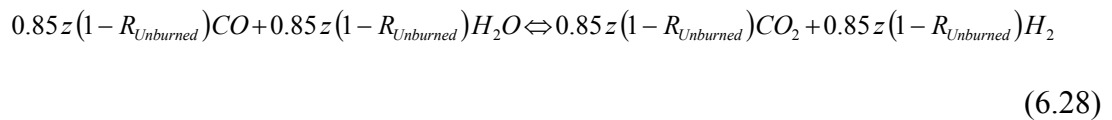
The CO₂ dissociation is sensitive to high temperature so that the influence of the number of power strokes per mechanical cycle becomes more apparent in CO₂ dissociation. The rate of the steady speed-based CO exhaust emissions that result from CO₂ dissociation for four-stroke diesel engines in (kg/s), $R_{COSSCO+O_2}$, can be hence analytically formulated following from substituting equation (6.26) into equation (6.25):

$$R_{COSSCO+O_2} = \Phi R_{F-A \text{ stoich}} \rho_{Cyl} \eta_V V_d (V_S)^2 G_t G_d n^{-12.2} \frac{(M_{CO \text{ molar}} (1 - R_{Unburned}) K_{CO+O_2} [CO_2])}{2\pi r_{wr} M_{fuel \text{ molar}}} \quad (6.27)$$

The key explanatory variable in equation (6.27) is V_S . Equation (6.27) is dimensionally correct which supports the validity of this developed model. Let us now turn to the analytical formulation of the rate of the steady speed-based CO exhaust emissions that result from the Water-Gas-Shift reaction in (kg/m), $R_{COSSCO+H_2O}$.

6.4.2. Analytical Model of the Rate of the Steady Speed-based CO Exhaust Emissions that Result from the Water-Gas-Shift Reaction

The chemical reaction of the water-gas-shift in the combustion of diesel fuel no. 2 in diesel engines is given following from chemical equation (6.20) as follows (Brown et al., 2009):



For low speed cycles, the reverse reaction rate at equilibrium, $R_{CO+H_2O}^-$ in (M.s⁻¹), can be thus analytically formulated as follows:

$$R_{CO+H_2O}^- = (1 - R_{Unburned}) K_{CO+H_2O} [CO_2] [H_2] \quad (6.29)$$

Applying the definition of the reverse reaction rate at equilibrium, $R_{CO+H_2O}^-$, to the water-gas-shift reaction indicated in chemical equation (6.28) leads to:

$$R_{CO \text{ in } CO+H_2O \text{ per mole}} = M_{CO \text{ molar}} R_{CO+H_2O}^- \quad (6.30)$$

The $R_{COSSCO+H_2O}$ in (kg.mol.L⁻¹.s⁻²) can thus be analytically formulated following from equation (6.30) as follows:

$$R_{COSSCO+H_2O} = \frac{\dot{m}_{fuel \text{ actual SS}} R_{CO \text{ in } CO+H_2O \text{ per mole}}}{M_{fuel \text{ molar}}} \quad (6.31)$$

The $R_{COSSCO+H_2O}$ in (kg.mol.L⁻¹.s⁻²) can hence be analytically formulated as follows by substituting equations (6.29) and (6.30) into equation (6.31):

$$R_{COSSCO+H_2O} = \frac{\dot{m}_{fuel \text{ actual SS}} M_{CO \text{ molar}} (1 - R_{Unburned}) K_{CO+H_2O} [CO_2] [H_2]}{M_{fuel \text{ molar}}} \quad (6.32)$$

In order to formulate $R_{COSSCO+H_2O}$ in (kg/s), equation (6.32) can be rewritten as follows:

$$R_{COSSCO+H_2O} = \frac{\dot{m}_{fuel \text{ actual SS}} (M_{CO \text{ molar}} (1 - R_{Unburned}) (K_{CO+H_2O})^2 [CO_2] [H_2]) V_s}{M_{fuel \text{ molar}} a_{avg} w} \quad (6.33)$$

Equation (6.33) gives $R_{COSSCO+H_2O}$ in (kg/s) in a dimensionally correct form. The engine crankshaft rotational speed, w , is analytically formulated in equation (5.19). Since the formation of the CO emission is highly sensitive to high temperature, the influence of the number of power strokes per cycle is noticeable on the CO emission rate. In addition, it has been recently found that vehicle speed has an exponential influence on the CO emission rate (Rakha, et al., 2003). Therefore, the rate of the steady speed-based CO exhaust emissions that result from the Water-Gas-Shift

reaction for low speed cycles in (kg/s), $R_{COSSCO+H_2O LS}$, for four-stroke diesel engines can be modeled as follows by substituting equations (6.26) and (5.19) into equation (6.33):

$$R_{COSSCO+H_2O LS} = \Phi R_{F-A stoich} \rho_{Cyl} \eta_V V_d V_S \left(n \right)^{\left(-1.7 - \frac{\log V_S}{\log 3.33} \right)} \frac{\left(M_{CO molar} (1 - R_{Unburned}) (K_{CO+H_2O})^2 [CO_2][H_2] \right)}{2 \pi M_{fuel molar}} \quad (6.34)$$

The rate of the steady speed-based CO exhaust emissions that result from the Water-Gas-Shift reaction for high speed cycles in (kg/s), $R_{COSSCO+H_2O HS}$, for four-stroke diesel engines can also be thus modeled as follows by substituting equations (6.26) and (5.19) into equation (6.33):

$$R_{COSSCO+H_2O HS} = \Phi R_{F-A stoich} \rho_{Cyl} \eta_V V_d V_S n^{-2.57} e^{\frac{V_S}{n^{5.01}}} \frac{\left(M_{CO molar} (1 - R_{Unburned}) (K_{CO+H_2O})^2 [CO_2][H_2] \right)}{2 \pi M_{fuel molar}} \quad (6.35)$$

The key explanatory variable in equations (6.34) and (6.35) is V_S . Equations (6.34) and (6.35) are dimensionally correct which supports the validity of this developed model. The next key component of diesel exhaust regulated emissions is NOx.

6.5. ANALYTICAL MODEL OF STEADY SPEED EXHAUST EMISSION

RATE OF NO_x DIESEL EXHAUST EMISSIONS

The rate of the steady speed-based total NO_x exhaust emission in (kg/s), $R_{NOx SST}$, is the algebraic summation of the rate of the steady speed-based NO exhaust emission, $R_{NO SST}$ and the rate of the steady speed-based NO₂ exhaust emission, $R_{NO_2 SS}$, as indicated in equation (6.36):

$$R_{NOx SST} = R_{NO SST} + R_{NO_2 SS} \quad (6.36)$$

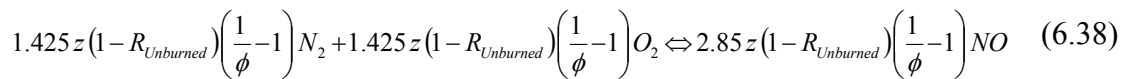
The R_{NOSS} is the algebraic summation of the rate of the steady speed-based NO emission that results from Zeldovich mechanism, R_{NOSSZM} (i.e. $N_2+O_2 \leftrightarrow 2NO$), the rate of the steady speed-based NO emission that results from extended Zeldovich mechanism, $R_{NOSS EZM}$ (i.e. $N+OH \leftrightarrow NO+H$), and the rate of the steady speed-based NO emission that results from super extended Zeldovich mechanism, $R_{NOSS SEZM}$ (i.e. $N_2O+H \leftrightarrow NO+NH$). This is indicated in equation (6.37):

$$R_{NOSS} = R_{NOSSZM} + R_{NOSS EZM} + R_{NOSS SEZM} \quad (6.37)$$

The analytical models of the R_{NOSSZM} in (kg/s) for both low speed cycles and high speed cycles, the $R_{NOSS EZM}$ in (kg/s) for both low speed cycles and high speed cycles, the $R_{NOSS SEZM}$ in (kg/s) for both low speed cycles and high speed cycles, and the R_{NO_2SS} in (kg/s) for both low speed cycles and high speed cycles will be developed in the next four sub-sections, respectively.

6.5.1. Analytical Model of Zeldovich Mechanism to Form NO

The Zeldovich mechanism to form NO is described in the following chemical reaction following from chemical equation (6.20) (Hong et al., 2006; Brown et al., 2009):



The forward reaction rate at equilibrium, $R^+_{N_2+O_2}$ in (mol.s⁻¹.L⁻¹), can be thus analytically formulated based on the law of mass action as follows:

$$R^+_{N_2+O_2} = (1-R_{Unburned})K_{N_2+O_2}[N_2][O_2] \quad (6.39)$$

Applying the definition of the forward reaction rate at equilibrium, $R^{+}_{N_2+O_2}$, to the Zeldovich mechanism of forming NO indicated in chemical equation (6.38) leads to:

$$R_{NO \text{ in } N_2+O_2 \text{ per mole}} = M_{NO \text{ molar}} R^{+}_{N_2+O_2} \quad (6.40)$$

The R_{NOSSZM} in (kg.mol/s) can thus be analytically formulated following from equation (6.40) as follows:

$$R_{NOSSZM} = \frac{\dot{m}_{AFSS} R_{NO \text{ in } N_2+O_2 \text{ per mole}} V_{mixture} V_S}{M_{fuel \text{ molar}} (a_{avg})} \quad (6.41)$$

Equation (6.41) gives R_{NOSSZM} in (kg.mol/s) in a dimensionally correct form. Hence, substituting equations (6.39) and (6.40) into equation (6.41) leads to:

$$R_{NOSSZM} = \frac{\dot{m}_{AFSS} (M_{NO \text{ molar}} (1 - R_{Unburned}) K_{N_2+O_2} [N_2][O_2]) V_{mixture} V_S}{M_{fuel \text{ molar}} (a_{avg})} \quad (6.42)$$

Equation (6.42) is dimensionally correct which supports the validity of this developed model. In order to formulate R_{NOSSZM} in (kg/s), equation (6.42) can be rewritten as follows:

$$R_{NOSSZM} = \frac{\dot{m}_{AFSS} (M_{NO \text{ molar}} (1 - R_{Unburned}) K_{N_2+O_2} [N_2][O_2]) K_{N_2+O_2} V_S}{M_{fuel \text{ molar}} (a_{avg}) w} \quad (6.43)$$

The engine crankshaft rotational speed, w , is analytically formulated in equation (5.19). Also, $\dot{m}_{fuel \text{ actual } SS}$ is analytically formulated in equation (5.22). Hence, R_{NOSSZM} in (kg/s) can be formulated as follows by substituting equations (5.19) and (5.22) into equation (6.43):

$$R_{NOSSZM} = \frac{\Phi R_{F-A \text{ stoich}} \rho_{Cyl} \eta_V V_d V_S n (M_{NO \text{ molar}} (1 - R_{Unburned}) (K_{N_2+O_2})^2 [N_2][O_2])}{2 \pi M_{fuel \text{ molar}}} \quad (6.44)$$

Since the formation of the Zeldovich mechanism-based NO emission is highly sensitive to high temperature, the influence of the number of power strokes per cycle is noticeable on the Zeldovich mechanism-based NO emission rate. In addition, it has been recently found that vehicle speed has an exponential influence on the NOx emission rate (Rakha et al. 2003). Therefore, R_{NOSSZM} in (kg/s) can be modeled as follows for low speed cycles, $R_{NOSSZMLS}$, following from equation (6.44):

$$R_{NOSSZMLS} = \frac{\Phi R_{F-A \text{ stoich}} \rho_{Cyl} \eta_V V_d V_S (n)^{-2.82} (M_{NO \text{ molar}} (1 - R_{Unburned}) (K_{N_2+O_2})^2 [N_2][O_2])}{2 \pi M_{fuel \text{ molar}}} e^{\left(\frac{V_S}{(n)^{3.7}}\right)} \quad (6.45)$$

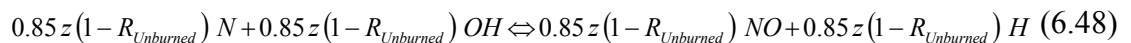
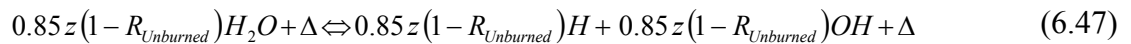
Also, R_{NOSSZM} in (kg/s) can thus be modeled as follows for high speed cycles, $R_{NOSSZMHS}$, following from equation (6.44):

$$R_{NOSSZMHS} = \frac{\Phi R_{F-A \text{ stoich}} \rho_{Cyl} \eta_V V_d V_S n^{-3.97} (M_{NO \text{ molar}} (1 - R_{Unburned}) (K_{N_2+O_2})^2 [N_2][O_2])}{2 \pi M_{fuel \text{ molar}}} e^{\left(\frac{V_S}{(n)^{3.55}}\right)} \quad (6.46)$$

The key explanatory variable in equations (6.45) and (6.46) is V_S . Let us now turn to the analytical formulation of the R_{NOSSZM} in (kg/s).

6.5.2. Analytical Model of Extended Zeldovich Mechanism to Form NO

The extended Zeldovich mechanism to form NO is described in the couple of chemical reactions presented in equations (6.47) and (6.48) following from equation (6.20) (Heywood, 1988; Lavoie et al., 1970):



The forward reaction rate at equilibrium, R_{N+OH}^+ in (mol.s⁻¹.L⁻¹), can be hence analytically formulated based on the law of mass action as follows:

$$R_{N+OH}^+ = (1 - R_{Unburned}) K_{N+OH} [N][OH] \quad (6.49)$$

Applying the definition of the forward reaction rate at equilibrium, R_{N+OH}^+ , to the extended Zeldovich mechanism of forming NO indicated in chemical equation (6.48) leads to:

$$R_{NO \text{ in } N+OH \text{ per mole}} = M_{NO \text{ molar}} R_{N+OH}^+ \quad (6.50)$$

The $R_{NOSS \text{ EZM}}$ in (kg.mol/s) can thus be analytically formulated following from equation (6.50) as follows:

$$R_{NOSS \text{ EZM}} = \frac{\dot{m}_{fuel \text{ actual SS}} R_{NO \text{ in } N+OH \text{ per mole}} V_{mixture} V_S}{M_{fuel \text{ molar}} (a_{avg})} \quad (6.51)$$

Equation (6.51) gives $R_{NOSS \text{ EZM}}$ in (kg.mol/s) in a dimensionally correct form.

Therefore, substituting equations (6.49) and (6.50) into equation (6.51) leads to:

$$R_{NOSS \text{ EZM}} = \frac{\dot{m}_{fuel \text{ actual SS}} (M_{NO \text{ molar}} (1 - R_{Unburned}) K_{N+OH} [N][OH]) V_{mixture} V_S}{M_{fuel \text{ molar}} (a_{avg})} \quad (6.52)$$

Equation (6.52) is dimensionally correct which supports the validity of this developed model. In order to formulate $R_{NOSS \text{ EZM}}$ in (kg/s), equation (6.52) can be rewritten as follows:

$$R_{NOSS \text{ EZM}} = \frac{\dot{m}_{fuel \text{ actual SS}} (M_{NO \text{ molar}} (1 - R_{Unburned}) K_{N+OH} [N][OH]) K_{N+OH} V_S}{M_{fuel \text{ molar}} (a_{avg}) w} \quad (6.53)$$

Hence, $R_{NOSS \text{ EZM}}$ in (kg/s) can be formulated as follows by substituting equations (5.19) and (5.22) into equation (6.53):

$$R_{NOSS \text{ EZM}} = \frac{\Phi R_{F-A \text{ stoich}} \rho_{Cyl} \eta_V V_d V_S n (M_{NO \text{ molar}} (1 - R_{Unburned}) (K_{N+OH})^2 [N][OH])}{2\pi M_{fuel \text{ molar}}} \quad (6.54)$$

Since the formation of the extended Zeldovich mechanism-based NO emission is highly sensitive to high temperature, the influence of the number of power strokes per cycle is noticeable on the extended Zeldovich mechanism-based NO emission rate. In addition, it has been recently found that vehicle speed has an exponential influence on the NOx emission rate (Rakha et al. 2003). Hence, $R_{NOSS EZM}$ in (kg/s) can be modeled as follows for low speed cycles, $R_{NOSS EZMLS}$, following from equation (6.54):

$$R_{NOSS EZMLS} = \frac{\Phi R_{F-A \text{ stoich}} \rho_{Cyl} \eta_V V_d V_S n^{-2.65} \left(M_{NO \text{ molar}} (1 - R_{Unburned}) (K_{N+OH})^2 [N][OH] \right) e^{\left(\frac{V_S}{(n)^{3.9}} \right)}}{2 \pi M_{fuel \text{ molar}}} \quad (6.55)$$

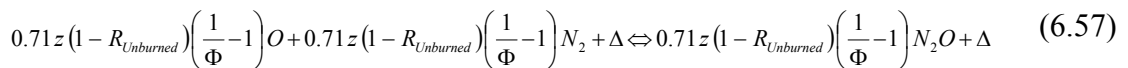
Also, $R_{NOSS EZM}$ in (kg/s) can thus be modeled as follows for high speed cycles, $R_{NOSS EZMHS}$, following from equation (6.54):

$$R_{NOSS EZMHS} = \frac{\Phi R_{F-A \text{ stoich}} \rho_{Cyl} \eta_V V_d V_S n^{-3.85} \left(M_{NO \text{ molar}} (1 - R_{Unburned}) (K_{N+OH})^2 [N][OH] \right) e^{\left(\frac{V_S}{(n)^{3.55}} \right)}}{2 \pi M_{fuel \text{ molar}}} \quad (6.56)$$

The key explanatory variable in equations (6.55) and (6.56) is V_S . Let us now explore the analytical formulation of the $R_{NOSS SEZM}$ in (kg/s).

6.5.3. Analytical Model of Super Extended Zeldovich Mechanism to Form NO

The super extended Zeldovich mechanism to form NO is described in the three chemical reactions presented in equations (6.57), (6.58) and (6.59) following from equation (6.20) (Dean and Bozzelli, 2000; Heywood, 1988; Miller et al., 1998; Polifke, 1995):



$$0.85 z(1 - R_{Unburned}) H_2O + \Delta \Leftrightarrow 0.85 z(1 - R_{Unburned}) H + 0.85 z(1 - R_{Unburned}) OH + \Delta \quad (6.58)$$

$$0.85 z(1 - R_{Unburned}) N_2O + 0.85 z(1 - R_{Unburned}) H \Leftrightarrow 0.85 z(1 - R_{Unburned}) NO + 0.85 z(1 - R_{Unburned}) NH \quad (6.59)$$

The forward reaction rate at equilibrium, $R^+_{N_2O+H}$ in (mol.s⁻¹.L⁻¹), can be hence analytically formulated based on the law of mass action as follows:

$$R^+_{N_2O+H} = (1 - R_{Unburned}) K_{N_2O+H} [N_2O][H] \quad (6.60)$$

Applying the definition of the forward reaction rate at equilibrium, $R^+_{N_2O+H}$, to the super extended Zeldovich mechanism of forming NO indicated in chemical equation (6.59) leads to:

$$R_{NO \text{ in } N_2O+H \text{ per mole}} = M_{NO \text{ molar}} R^+_{N_2O+H} \quad (6.61)$$

The $R_{NOSS \text{ SEZM}}$ in (kg.mol/s) can hence be analytically formulated following from equation (6.61) as follows:

$$R_{NOSS \text{ SEZM}} = \frac{\dot{m}_{fuel \text{ actual SS}} R_{NO \text{ in } N_2O+H \text{ per mole}} V_{mixture} V_S}{M_{fuel \text{ molar}} (a_{avg})} \quad (6.62)$$

Equation (6.62) gives $R_{NOSS \text{ SEZM}}$ in (kg.mol/s) in a dimensionally correct form. Hence, substituting equations (6.60) and (6.61) into equation (6.62) leads to:

$$R_{NOSS \text{ SEZM}} = \frac{\dot{m}_{fuel \text{ actual SS}} (M_{NO \text{ molar}} (1 - R_{Unburned}) K_{N_2O+H} [N_2O][H]) V_{mixture} V_S}{M_{fuel \text{ molar}} (a_{avg})} \quad (6.63)$$

Equation (6.63) is dimensionally correct which supports the validity of this developed model. In order to formulate $R_{NOSS \text{ SEZM}}$ in (kg/s), equation (6.63) can be rewritten as follows:

$$R_{NOSSSEZM} = \frac{\dot{m}_{fuel actual SS} (M_{NO molar} (1 - R_{Unburned}) K_{N_2O+H} [N_2O][H]) K_{N_2O+H} V_S}{M_{fuel molar} (a_{avg}) w} \quad (6.64)$$

Hence, $R_{NOSSSEZM}$ in (kg/s) can be formulated as follows by substituting equations (5.19) and (5.22) into equation (6.64):

$$R_{NOSSSEZM} = \frac{\Phi R_{F-A stoich} \rho_{Cyl} \eta_V V_d V_S n (M_{NO molar} (1 - R_{Unburned}) (K_{N_2O+H})^2 [N_2O][H])}{2 \pi M_{fuel molar}} \quad (6.65)$$

Since the formation of the super extended Zeldovich mechanism-based NO emission is highly sensitive to high temperature, the influence of the number of power strokes per cycle is noticeable on the super extended Zeldovich mechanism-based NO emission rate. In addition, it has been recently found that vehicle speed has an exponential influence on the NOx emission rate (Rakha et al. 2003). Hence, $R_{NOSSSEZM}$ in (kg/s) can be modeled as follows for low speed cycles, $R_{NOSSSEZMLS}$, following from equation (6.65):

$$R_{NOSSSEZMLS} = \frac{\Phi R_{F-A stoich} \rho_{Cyl} \eta_V V_d V_S n^{-2.82} (M_{NO molar} (1 - R_{Unburned}) (K_{N_2O+H})^2 [N_2O][H])}{2 \pi M_{fuel molar}} e^{\left(\frac{V_S}{(n)^{3.7}}\right)} \quad (6.66)$$

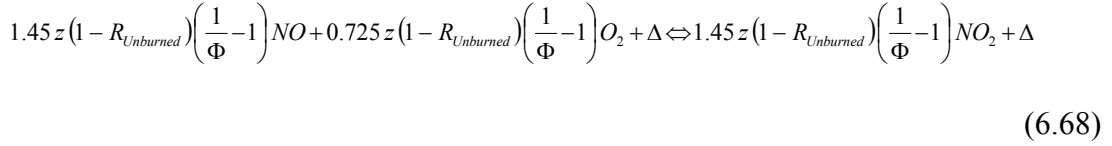
Also, $R_{NOSSSEZM}$ in (kg/s) can thus be modeled as follows for high speed cycles, $R_{NOSSSEZMHS}$, following from equation (6.65):

$$R_{NOSSSEZMHS} = \frac{\Phi R_{F-A stoich} \rho_{Cyl} \eta_V V_d V_S n^{-3.97} (M_{NO molar} (1 - R_{Unburned}) (K_{N_2O+H})^2 [N_2O][H])}{2 \pi M_{fuel molar}} e^{\left(\frac{V_S}{(n)^{3.55}}\right)} \quad (6.67)$$

The key explanatory variable in equations (6.66) and (6.67) is V_S . Let us now finally explore the principles of chemical physics on which the analytical model of the R_{NO2SS} is based.

6.5.4. Analytical Model of the Mechanism to Form NO₂

The formation NO₂ is described in the chemical reaction presented in equation (6.53) following from equation (6.20) (Heywood, 1988):



The forward reaction rate at equilibrium, $R^+_{NO+O_2}$ in (mol^{0.5}.s⁻¹.L^{-0.5}), can be therefore analytically formulated based on the law of mass action as follows:

$$R^+_{NO+O_2} = (1 - R_{Unburned}) K_{NO+O_2} [NO][O_2]^{0.5} \quad (6.69)$$

Applying the definition of the forward reaction rate at equilibrium, $R^+_{NO+O_2}$, to mechanism of NO₂ formation indicated in chemical equation (6.68) leads to:

$$R_{NO_2 \text{ per mole}} = M_{NO_2 \text{ molar}} R^+_{NO+O_2} \quad (6.70)$$

The $R_{NO_2 SS}$ in (kg.mol^{0.5}/s) can thus be analytically formulated following from equation (6.70) as follows:

$$R_{NO_2 SS} = \frac{\dot{m}_{fuel \text{ actual SS}} R_{NO \text{ in } NO+O_2 \text{ per mole}} V_{mixture}^{0.5} V_S}{M_{fuel \text{ molar}} (a_{avg})} \quad (6.71)$$

Equation (6.71) gives $R_{NO_2 SS}$ in (kg.mol^{0.5}/s) in a dimensionally correct form. Hence, substituting equations (6.69) and (6.70) in equation (6.71) leads to:

$$R_{NO_2 SS} = \frac{\dot{m}_{fuel \text{ actual SS}} (M_{NO_2 \text{ molar}} (1 - R_{Unburned}) K_{NO+O_2} [NO][O_2]^{0.5}) V_{mixture}^{0.5} V_S}{M_{fuel \text{ molar}} (a_{avg})} \quad (6.72)$$

Equation (6.72) is dimensionally correct which supports the validity of this developed model. In order to formulate $R_{NO_2 SS}$ in (kg/s), equation (6.72) can be rewritten as follows:

$$R_{NO_2 SS} = \frac{\dot{m}_{fuel actual SS} (M_{NO_2 molar} (1 - R_{Unburned}) K_{NO+O_2} [NO][O_2]^{0.5}) (K_{NO+O_2})^{0.5} V_S}{M_{fuel molar} (a_{avg}) w^{0.5}} \quad (6.73)$$

Hence, $R_{NO_2 SS}$ in (kg/s) can be formulated as follows by substituting equations (5.19) and (5.22) into equation (6.73):

$$R_{NO_2 SS} = \frac{\Phi R_{F-A stoich} \rho_{Cyl} \eta_V V_d V_S^{1.5} G_t^{0.5} G_d^{0.5} n (M_{NO_2 molar} (1 - R_{Unburned}) (K_{NO+O_2})^{1.5} [NO][O_2]^{0.5})}{2 \pi M_{fuel molar}} \quad (6.74)$$

Since the formation of the NO_2 emission is highly sensitive to high temperature, the influence of the number of power strokes per cycle is noticeable on the NO_2 emission rate. In addition, it has been recently found that vehicle speed has an exponential influence on the NO_x emission rate (Rakha et al. 2003). Hence, $R_{NO_2 SS}$ in (kg/s) can be modeled as follows for low speed cycles, $R_{NO_2 SSLS}$, following from equation (6.74):

$$R_{NO_2 SSLS} = \frac{\Phi R_{F-A stoich} \rho_{Cyl} \eta_V V_d V_S^{1.5} G_t^{0.5} G_d^{0.5} n^{-15.15} (M_{NO_2 molar} (1 - R_{Unburned}) (K_{NO+O_2})^{1.5} [NO][O_2]^{0.5})}{2 \pi (r_{wr})^{0.5} M_{fuel molar}} e^{\left(\frac{V_S}{(n)^{3.85}}\right)} \quad (6.75)$$

Also, $R_{NO_2 SS}$ in (kg/s) can hence be modeled as follows for high speed cycles,

$R_{NO_2 SSHS}$, following from equation (6.74):

$$R_{NO_2 SSHS} = \frac{\Phi R_{F-A stoich} \rho_{Cyl} \eta_V V_d V_S^{1.5} G_t^{0.5} G_d^{0.5} n^{-16.95} (M_{NO_2 molar} (1 - R_{Unburned}) (K_{NO+O_2})^{1.5} [NO][O_2]^{0.5})}{2 \pi (r_{wr})^{0.5} M_{fuel molar}} e^{\left(\frac{V_S}{(n)^{3.55}}\right)} \quad (6.76)$$

The key explanatory variable in equations (6.75) and (6.76) is V_s . Having explored the principles of chemical physics on which these analytical models are based, let us now turn to the experimental validation of these models.

6.6. ANALYTICAL MODEL OF STEADY SPEED EXHAUST EMISSION RATE OF HC DIESEL EXHAUST EMISSIONS

Hydrocarbon (HC) emissions are particulate-adsorbed combustion products result from unburned fuel, semi-volatile products of combustion, and gaseous combustion products, which are all organic groupings detectable within an exhaust sample (Bramston-Cook, et al., 2000). This section presents the analytical model, derivation of the model, and experimental validation of the model of the total HC exhaust emissions rate in diesel engines, respectively. It can follow from the definition of the rate of HC emission, R_{HCSS} , that:

$$R_{HCSS} = \dot{m}_{fuel actual} e^{R_{unburned}} \quad (6.77)$$

Since the influence of the number of power strokes per cycle becomes more apparent on the HC emission rate, the steady speed-based rate of HC emission for low-speed Freeway cycles, R_{HCSSL} , can thus be analytically formulated following from equation (6.77) as follows:

$$R_{HCSSL} = \dot{m}_{fuel actual} n^{-10.46} e^{R_{unburned}} \quad (6.78)$$

Also, the steady speed-based rate of HC emission for high-speed Freeway cycles, R_{HCSSH} , can thus be analytically formulated following from equation (6.77) as follows:

$$R_{HCSSHS} = \dot{m}_{fuel actual} n^{-9.97} e^{R_{t in burned}} \quad (6.79)$$

Equations (6.78) and (6.79) give R_{HCSS} in (g/s) in a dimensionally correct form which supports the validity of this developed model. The key explanatory variable in equations (6.78) and (6.79) is V_S since \dot{m}_{AFSS} is a function of V_S as proved in equation (5.22).

CHAPTER 7

SENSITIVITY ANALYSIS OF THE DEVELOPED MODELS

7.1. OVERVIEW

Modeling of vehicle fuel consumption levels initially had been based on coarse empirical data to produce fuel consumption models (de Weille, 1966). These models were then superseded by empirical studies that related vehicle fuel consumption to operating conditions, such as roughness, gradient, and vehicle speed (Greenwood, 2003; Rakha, et al., 2012). A currently sought approach is to develop gear-shifting-based analytical models for estimating vehicle fuel consumption and regulated emissions rate. This chapter thus presents a simplified version of the analytical models developed in this study on the diesel powertrain for use in a traffic simulation environment, such as the INTEGRATION model. The simplification conducted in this research is based on a sensitivity analysis on the developed analytical models. The sensitivity analysis relies on applying the sensitivity ratio, $R_{Sensitivity}$, formulation to each of the independent variables. While evaluating $R_{Sensitivity}$ for each independent variable, the values of the remaining independent variables remain unchanged from the baseline values. This $R_{Sensitivity}$ formulation is as follows (United States Environmental Protection Agency EPA, 2001):

$$R_{Sensitivity} = \frac{\frac{V_{Dependent\ Changes} - V_{Dependent\ Baseline}}{V_{Dependent\ Baseline}}}{\frac{V_{Independent\ Changes} - V_{Independent\ Baseline}}{V_{Independent\ Baseline}}} \quad (7.1)$$

Chapter 7 contributes to the implementation of the 3rd pillar of the research philosophy adopted in this study in an endeavour to achieve the 1st objective in this research. In

addition, this Chapter contributes to achieving the 1st objective of this research with respect to the analytical modeling of both the diesel powertrain fuel consumption rate and the diesel regulated emissions rate. The following subsections will present the simplified version of the developed analytical models of \dot{c}_{im} , \dot{W}_C , η_{CM} , ρ , \dot{c}_{Cyl} , \dot{m}_{AFSS} , \dot{m}_{NLSAF} , \dot{m}_{NHSFAF} , \dot{m}_{P1LSAF} , $\dot{m}_{P1HSFAF}$, \dot{m}_{P2LSAF} , $\dot{m}_{P2HSFAF}$, Γ_B , $R_{Unburned}$, $R_{COSSCO+O_2}$, $R_{COSSCO+H_2O}$, R_{NOSSZM} , $R_{NOSS EZM}$, $R_{NOSS SEZM}$, R_{NO_2SS} , R_{HCSS} , respectively.

7.2. SENSITIVITY ANALYSIS OF THE INTAKE MANIFOLD GAS SPEED DYNAMICS MODEL

The intake manifold air speed dynamics in diesel engines, \dot{c}_{im} , is analytically modeled in equation (3.128). The key explanatory variable in this model is c . The baseline value of c is 32 m/s. The sensitivity analysis of the analytical model of \dot{c}_{im} is presented in Table 7.1 following from equations (3.128) and (7.1).

Table 7.1
Sensitivity analysis of the analytical model of \dot{c}_{im}

	-50% Decrement Below Baseline Value	-25% Decrement Below Baseline Value	Baseline Value	+25% Increment Above Baseline Value	+50% Increment Above Baseline Value	Average Sensitivity Ratio on Each Independent Variable
\dot{c}_{im}	0.058	0.095	0.131 m/s ²	0.167	0.204	N/A
P_i	0.049*10 ⁶	0.074*10 ⁶	0.0985*10 ⁶ N/m ²	0.123*10 ⁶	0.148*10 ⁶	N/A
$R_{Sensitivity}$ on P_i	1.1	1.1	N/A	1.1	1.1	1.1
\dot{c}_{im}	0.276	0.179	0.131 m/s ²	0.102	0.083	N/A
ρ_{air}	0.85	1.275	1.7 kg/m ³	2.125	2.55	N/A
$R_{Sensitivity}$ on ρ_{air}	-2.2	-1.47	N/A	-0.9	-0.7	-1.3
\dot{c}_{im}	0.276	0.179	0.131 m/s ²	0.102	0.083	N/A
L	0.2	0.3	0.4 m	0.5	0.6	N/A
$R_{Sensitivity}$ on L	-2.2	-1.47	N/A	-0.9	-0.7	-1.3
\dot{c}_{im}	0.138	0.134	0.131 m/s ²	0.127	0.124	N/A
ζ	0.28	0.41	0.55	0.69	0.83	N/A
$R_{Sensitivity}$ on ζ	0	0	N/A	0	0	0
\dot{c}_{im}	0.117	0.126	0.131 m/s ²	0.134	0.136	N/A
D	0.040	0.060	0.080 m	0.100	0.120	N/A
$R_{Sensitivity}$ on D	0.21	0.2	N/A	0.1	0.1	0.2

Thus, \dot{c}_{im} is insensitive to the changes in the value of ζ . Hence, ζ should be considered a constant in the formulation of \dot{c}_{im} . Also, \dot{c}_{im} is sensitive to the changes in the value of P_i , ρ , L , and D . Hence, P_i , ρ , L , and D should not be considered a constant in the formulation of \dot{c}_{im} . The simplified analytical model of the intake

manifold air speed dynamics in diesel engines, \dot{c}_{im} , can be hence formulated as follows:

$$\dot{c}_{im} = \frac{P_i}{\rho L} - 1.1 \frac{c^2}{D} \quad (7.2)$$

7.3. SENSITIVITY ANALYSIS OF THE MODEL OF THE POWER REQUIRED TO DRIVE THE SUPERCHARGING DIESEL CENTRIFUGAL COMPRESSOR

The power required to drive the rotor, \dot{W}_C , is analytically modeled in equation (4.15).

The key explanatory variable in this model is U_2 . The baseline value of U_2 is 223 m/s. The sensitivity analysis of the analytical model of \dot{W}_C is presented in Table 7.2 following from equations (4.15) and (7.1).

Table 7.2

Sensitivity analysis of the analytical model of \dot{W}_C

	-50% Decrement Below Baseline Value	-25% Decrement Below Baseline Value	Baseline Value	+25% Increment Above Baseline Value	+50% Increment Above Baseline Value	Average Sensitivity Ratio on Each Independent Variable
\dot{W}_C	3.5	5.2	6.9 kW	8.7	10.4	N/A
\dot{m}_{air}	0.1	0.15	0.2 kg/s	0.25	0.3	N/A
$R_{Sensitivity, \text{ on } \dot{m}_{air}}$	1	1	N/A	1	1	1
\dot{W}_C	8.5	7.7	6.9 kW	6.2	5.4	N/A
c_{r2}	33.5	50.1	66.9 m/s	83.6	100.4	N/A
$R_{Sensitivity, \text{ on } c_{r2}}$	-0.5	-0.5	N/A	-0.41	-0.44	-0.5
\dot{W}_C	2.7	5.5	6.9 kW	7.9	8.7	N/A
β_2	22.5°	33.8°	45°	56.3°	67.5°	N/A
$R_{Sensitivity, \text{ on } \beta_2}$	1.2	0.8	N/A	0.6	0.52	0.8

Therefore, \dot{W}_C is sensitive to the changes in the value of \dot{m}_{air} , c_{r2} , and β_2 . Thus,

\dot{m}_{air} , c_{r2} , and β_2 should not be considered a constant in the formulation of \dot{W}_C .

Hence, the simplified analytical model of \dot{W}_C is equation (4.15).

7.4. SENSITIVITY ANALYSIS OF THE MODEL OF THE EFFICIENCY OF THE SUPERCHARGING DIESEL CENTRIFUGAL COMPRESSOR

The efficiency of the supercharging diesel centrifugal compressor, η_{CM} , is analytically modeled in equation (4.56). The key explanatory variable in this model is

α_C . The baseline value of α_C is 500 rad/s². The sensitivity analysis of the analytical model of η_{CM} is presented in Table 7.3 following from equations (4.56) and (7.1).

Table 7.3
Sensitivity analysis of the analytical model of η_{CM}

	-50% Decrement Below Baseline Value	-25% Decrement Below Baseline Value	Baseline Value	+25% Increment Above Baseline Value	+50% Increment Above Baseline Value	Average Sensitivity Ratio on Each Independent Variable
η_{CM}	0.90	0.84	0.79	0.74	0.69	N/A
I_C	1	1.5	2 kg.m ²	2.5	3	N/A
$R_{Sensitivity}$ on I_C	-0.3	-0.3	N/A	-0.3	-0.3	-0.3
η_{CM}	0.90	0.84	0.79	0.74	0.69	N/A
N_{CM}	2250	3375	4500 rpm	5625	6750	N/A
$R_{Sensitivity}$ on N_{CM}	-0.3	-0.3	N/A	-0.3	-0.3	-0.3
η_{CM}	0.58	0.72	0.79	0.83	0.86	N/A
\dot{W}_C	3.54*10 ⁶	5.31*10 ⁶	7.08*10 ⁶ N.m.ks ⁻¹	8.85*10 ⁶	10.62*10 ⁶	N/A
$R_{Sensitivity}$ on \dot{W}_C	0.53	0.4	N/A	0.2	0.2	0.33

Thus, η_{CM} is sensitive to the changes in the value of I_C , N_{CM} , and \dot{W}_C . Hence,

I_C , N_{CM} , and \dot{W}_C should not be considered a constant in the formulation of η_{CM} .

Therefore, the simplified analytical model of η_{CM} is equation (4.56).

7.5. SENSITIVITY ANALYSIS OF THE MODEL OF THE SUPERCHARGED AIR DENSITY

The supercharged air density in diesel engines, ρ , is analytically modeled in equation (3.135). The key explanatory variable in this model is P_2 . The baseline value of P_2 is 146450 N/m². The sensitivity analysis of the analytical model of ρ is presented in Table 7.4 following from equations (3.135) and (7.1).

Table 7.4
Sensitivity analysis of the analytical model of ρ

	-50% Decrement Below Baseline Value	-25% Decrement Below Baseline Value	Baseline Value	+25% Increment Above Baseline Value	+50% Increment Above Baseline Value	Average Sensitivity Ratio on Each Independent Variable
ρ	2.01	1.82	1.65 kg/m ³	1.54	1.43	N/A
T_2	186.5	279.8	373 K	466.3	559.5	N/A
$R_{Sensitivity}$ on T_2	-0.44	-0.41	N/A	-0.27	-0.27	-0.35
ρ	1.50	1.58	1.65 kg/m ³	1.77	1.87	N/A
$\eta_{Intercooler}$	0.36	0.54	0.72	0.9	1.08	N/A
$R_{Sensitivity}$ on $\eta_{Intercooler}$	0.2	0.2	N/A	0.29	0.27	0.24
ρ	1.63	1.65	1.65 kg/m ³	1.69	1.71	N/A
$L_{Latitude}$	18°	27°	36° North	45°	54°	N/A
$R_{Sensitivity}$ on $L_{Latitude}$	0.02	0	N/A	0.1	0.1	0.1
ρ	1.67	1.67	1.65 kg/m ³	1.67	1.67	N/A
$A_{Altitude}$	129.5	194.3	259 m above sea	323.8	388.5	N/A
$R_{Sensitivity}$ on $A_{Altitude}$	0	0	N/A	0	0	0

Thus, ρ is insensitive to the changes in the value of $A_{Altitude}$. Hence, $A_{Altitude}$ should be considered a constant in the formulation of ρ . Also, ρ is sensitive to the changes in the value of T_2 , $\eta_{Intercooler}$, and $L_{Latitude}$. Hence, T_2 , $\eta_{Intercooler}$, and $L_{Latitude}$ should not be considered a constant in the formulation of ρ . The simplified analytical model of ρ can be hence formulated as follows:

$$\rho = \frac{P_2}{287.058 [T_2 - \eta_{Intercooler} (T_2 + 0.522 L_{Latitude} - 298.4665)]} \quad (7.3)$$

7.6. SENSITIVITY ANALYSIS OF THE MODEL OF THE IN-CYLINDER GAS SPEED DYNAMICS

The in-cylinder gas speed dynamics in diesel engines, \dot{c}_{Cyl} , is analytically modeled in equation (5.15). The key explanatory variable in this model is c_{Cyl} . The baseline value of c_{Cyl} is 7 m/s. The sensitivity analysis of the analytical model of \dot{c}_{Cyl} is presented in Table 7.5 following from equations (5.15) and (7.1).

Table 7.5

Sensitivity analysis of the analytical model of \dot{c}_{Cyl}

	-50% Decrement Below Baseline Value	-25% Decrement Below Baseline Value	Baseline Value	+25% Increment Above Baseline Value	+50% Increment Above Baseline Value	Average Sensitivity Ratio on Each Independent Variable
\dot{c}_{Cyl}	-12.8	-19.2	-25.57 m/s ²	-32	-38.4	N/A
P_{Cyl}	20*10 ⁵	30*10 ⁵	40*10 ⁵ N/m ²	50*10 ⁵	60*10 ⁵	N/A
$R_{Sensitivity}$ on P_{Cyl}	1	1	N/A	1	1	1
\dot{c}_{Cyl}	-51.2	-34.1	-25.57 m/s ²	-20.5	-17.1	N/A
ρ_{Cyl}	0.85	1.275	1.7 kg/m ³	2.125	2.55	N/A
$R_{Sensitivity}$ on ρ_{Cyl}	-2	-1.3	N/A	-0.8	-0.7	-1.2
\dot{c}_{Cyl}	-47	-33.6	-25.57 m/s ²	-21.3	-18.1	N/A
L_{Stroke}	0.05	0.07	0.092 m	0.11	0.13	N/A
$R_{Sensitivity}$ on L_{Stroke}	-1.7	-1.3	N/A	-0.7	-0.6	-1.1
\dot{c}_{Cyl}	-25.58	-25.58	-25.57 m/s ²	-25.58	-25.58	N/A
ζ_{In-Cyl}	0.33	0.49	0.65	0.8	0.98	N/A
$R_{Sensitivity}$ on ζ_{In-Cyl}	0	0	N/A	0	0	0
\dot{c}_{Cyl}	-25.58	-25.58	-25.57 m/s ²	-25.58	-25.58	N/A
D_{Cyl}	0.044	0.066	0.088 m	0.110	0.132	N/A
$R_{Sensitivity}$ on D_{Cyl}	0	0	N/A	0	0	0

Thus, \dot{c}_{Cyl} is insensitive to the changes in the value of ζ_{In-Cyl} and D_{Cyl} . Hence,

ζ_{In-Cyl} and D_{Cyl} should be considered a constant in the formulation of \dot{c}_{Cyl} . Also,

\dot{c}_{Cyl} is sensitive to the changes in the value of P_{Cyl} , ρ_{Cyl} , and L_{Stroke} . Therefore,

P_{Cyl} , ρ_{Cyl} , and L_{Stroke} should not be considered a constant in the formulation of \dot{c}_{Cyl} .

The simplified analytical model of \dot{c}_{Cyl} can be thus formulated as follows:

$$\dot{c}_{Cyl} = -\frac{P_{Cyl}}{\rho_{Cyl} L_{Stroke}} - 14.77 \dot{c}_{Cyl}^2 \quad (7.4)$$

7.7. SENSITIVITY ANALYSIS OF THE MODEL OF THE DIESEL FUEL CONSUMPTION RATE

The actual mass flow rate of fuel in diesel engines under the steady speed condition, \dot{m}_{AFSS} , is analytically modeled in equation (5.22). The key explanatory variable in this model is V_s . The baseline value of V_s is 13.56 m/s. The sensitivity analysis of the analytical model of \dot{m}_{AFSS} is presented in Table 7.6 following from equations (5.22) and (7.1).

Table 7.6
Sensitivity analysis of the analytical model of \dot{m}_{AFSS}

	-50% Decrement Below Baseline Value	-25% Decrement Below Baseline Value	Baseline Value	+25% Increment Above Baseline Value	+50% Increment Above Baseline Value	Average Sensitivity Ratio on Each Independent Variable
Φ	0.35	0.525	0.7	0.875	1.05	N/A
\dot{m}_{AFSS} (kg/s)	$0.41 \cdot 10^{-3}$	$0.616 \cdot 10^{-3}$	$0.822 \cdot 10^{-3}$	$1.03 \cdot 10^{-3}$	$1.23 \cdot 10^{-3}$	N/A
$R_{Sensitivity \dot{m}_{AFSS} \text{ on } \Phi}$	1	1	N/A	1.01	1	1
η_V	0.45	0.675	0.9	1.125	1.35	N/A
\dot{m}_{AFSS} (kg/s)	$0.41 \cdot 10^{-3}$	$0.617 \cdot 10^{-3}$	$0.822 \cdot 10^{-3}$	$1.03 \cdot 10^{-3}$	$1.23 \cdot 10^{-3}$	N/A
$R_{Sensitivity \dot{m}_{AFSS} \text{ on } \eta_V}$	1	1	N/A	1	1	1
r_{wr} (m)	0.162	0.242	0.323	0.404	0.485	N/A
\dot{m}_{AFSS} (kg/s)	$1.64 \cdot 10^{-3}$	$1.1 \cdot 10^{-3}$	$0.822 \cdot 10^{-3}$	$0.657 \cdot 10^{-3}$	$0.547 \cdot 10^{-3}$	N/A
$R_{Sensitivity \dot{m}_{AFSS} \text{ on } r_{wr}}$	-2	-1.35	N/A	-0.8	-0.67	-1.2
ρ_{Cyl} (kg/m ³)	0.85	1.275	1.7	2.125	2.55	N/A
\dot{m}_{AFSS} (kg/s)	$0.411 \cdot 10^{-3}$	$0.617 \cdot 10^{-3}$	$0.822 \cdot 10^{-3}$	$1.03 \cdot 10^{-3}$	$1.23 \cdot 10^{-3}$	N/A
$R_{Sensitivity \dot{m}_{AFSS} \text{ on } \rho_{Cyl}}$	1	1	N/A	1	1	1
V_{d-Cyl} (m ³ /d-cycle)	0.000041	0.000062	0.0000825	0.000103	0.000124	N/A
\dot{m}_{AFSS} (kg/s)	$0.409 \cdot 10^{-3}$	$0.618 \cdot 10^{-3}$	$0.822 \cdot 10^{-3}$	$1 \cdot 10^{-3}$	$1.2 \cdot 10^{-3}$	N/A
$R_{Sensitivity \dot{m}_{AFSS} \text{ on } V_{d-Cyl}}$	1	1	N/A	1	1	1
N_{Cyl}	2	3	4	5	6	N/A
\dot{m}_{AFSS} (kg/s)	$0.41 \cdot 10^{-3}$	$0.62 \cdot 10^{-3}$	$0.822 \cdot 10^{-3}$	$1.03 \cdot 10^{-3}$	$1.23 \cdot 10^{-3}$	N/A
$R_{Sensitivity \dot{m}_{AFSS} \text{ on } N_{Cyl}}$	1	1	N/A	1	1	1
G_t	0.5	0.75	1	1.25	1.5	N/A
\dot{m}_{AFSS} (kg/s)	$0.41 \cdot 10^{-3}$	$0.61 \cdot 10^{-3}$	$0.822 \cdot 10^{-3}$	$1.03 \cdot 10^{-3}$	$1.23 \cdot 10^{-3}$	N/A
$R_{Sensitivity \dot{m}_{AFSS} \text{ on } G_t}$	1	1	N/A	1	1	1
G_d	1.25	1.875	2.5	3.125	3.75	N/A
\dot{m}_{AFSS} (kg/s)	$0.41 \cdot 10^{-3}$	$0.61 \cdot 10^{-3}$	$0.822 \cdot 10^{-3}$	$1.03 \cdot 10^{-3}$	$1.23 \cdot 10^{-3}$	N/A
$R_{Sensitivity \dot{m}_{AFSS} \text{ on } G_d}$	1	1	N/A	1	1	1

Therefore, the dependent variable, \dot{m}_{AFSS} , is sensitive to the changes in the value of the independent variables. The simplified analytical model of \dot{m}_{AFSS} is hence formulated in equation (5.22). Similarly, each of \dot{m}_{NLSAF} , \dot{m}_{NHSFAF} , \dot{m}_{P1LSAF} , $\dot{m}_{P1HSFAF}$, \dot{m}_{P2LSAF} and $\dot{m}_{P2HSFAF}$ is thus sensitive to the changes in the value of the respective independent variables indicated in equations (5.23), (5.24), (5.25), (5.26), (5.27) and (5.28), respectively. Hence, the simplified analytical model of \dot{m}_{NLSAF} , \dot{m}_{NHSFAF} , \dot{m}_{P1LSAF} , $\dot{m}_{P1HSFAF}$, \dot{m}_{P2LSAF} and $\dot{m}_{P2HSFAF}$ is formulated in equations (5.23), (5.24), (5.25), (5.26), (5.27) and (5.28), respectively.

7.8. SENSITIVITY ANALYSIS OF THE MODEL OF THE BRAKE POWER OF DIESEL ENGINE

The brake power of the four-stroke diesel engine, Γ_B , is analytically modeled in equation (5.42). The key explanatory variable in this model is V_S . The baseline value of V_S is 54 m/s, based on Chevrolet S-10 General Motors engine 262 in³ (4.3 L) 90° V6, at 4000 rpm. The sensitivity analysis of the analytical model of Γ_B is presented in Table 7.7 following from equations (5.42) and (7.1).

Table 7.7
Sensitivity analysis of the analytical model of Γ_B

	-50% Decrement Below Baseline Value	-25% Decrement Below Baseline Value	Baseline Value	+25% Increment Above Baseline Value	+50% Increment Above Baseline Value	Average Sensitivity Ratio on Each Independent Variable
Γ_B	$66*10^3$	$100*10^3$	$133*10^3$ W	$166*10^3$	$199*10^3$	N/A
Ω_B	159.5	239.3	319 N·m	398.8	478.5	N/A
$R_{Sensitivity}$ on Ω_B	1	1	N/A	1	1	1
Γ_B	$66*10^3$	$100*10^3$	$133*10^3$ W	$166*10^3$	$199*10^3$	N/A
G_t	0.5	0.75	1	1.25	1.5	N/A
$R_{Sensitivity}$ on G_t	1	1	N/A	1	1	1
Γ_B	$66*10^3$	$100*10^3$	$133*10^3$ W	$166*10^3$	$199*10^3$	N/A
G_d	1.25	1.875	2.5	3.125	3.75	N/A
$R_{Sensitivity}$ on G_d	1	1	N/A	1	1	1
Γ_B	$265*10^3$	$177*10^3$	$133*10^3$ W	$106*10^3$	$88*10^3$	N/A
r_{wr}	0.162	0.242	0.323 m	0.404	0.485	N/A
$R_{Sensitivity}$ on r_{wr}	-2	-1.3	N/A	-0.8	-0.7	-1.2

Thus, Γ_B is sensitive to the changes in the value of Ω_B , G_t , G_d , and r_{wr} . Hence,

Ω_B , G_t , G_d , and r_{wr} should not be considered a constant in the formulation of Γ_B .

The simplified analytical model of Γ_B is hence formulated in equation (5.42).

7.9. SENSITIVITY ANALYSIS OF THE MODEL OF THE PERCENTAGE OF UNBURNED DIESEL FUEL

The percentage of unburned fuel without regeneration in diesel engines, $R_{Unburned}$, in

(ppm) for four-stroke multi-cylinder diesel engines, $R_{Unburned}$, is analytically modeled in equation (6.17). The key explanatory variable in this model is V_S . The baseline value of V_S is 13.56 m/s. The sensitivity analysis of the analytical model of $R_{Unburned}$ is presented in Table 7.8 following from equations (6.17) and (7.1).

Table 7.8
Sensitivity analysis of the analytical model of $R_{Unburned}$

	-50% Decrement Below Baseline Value	-25% Decrement Below Baseline Value	Baseline Value	+25% Increment Above Baseline Value	+50% Increment Above Baseline Value	Average Sensitivity Ratio on Each Independent Variable
$R_{Unburned}$	125.2	123.91	122 ppm	121.4	120.09	N/A
V_d	0.0015	0.00225	0.0033 m ³ /cycle	0.00375	0.0045	N/A
$R_{Sensitivity}$ on V_d	0	0	N/A	0	0	0
$R_{Unburned}$	124.93	123.53	122 ppm	120.72	119.32	N/A
ρ_{Cyl}	0.85	1.275	1.7 kg/m ³	2.125	2.55	N/A
$R_{Sensitivity}$ on ρ_{Cyl}	0	0	N/A	0	0	0
$R_{Unburned}$	124.93	123.53	122 ppm	120.72	119.32	N/A
η_V	0.45	0.675	0.9	1.125	1.35	N/A
$R_{Sensitivity}$ on η_V	0	0	N/A	0	0	0
$R_{Unburned}$	116.5	120.3	122 ppm	123.26	123.98	N/A
$\dot{m}_{fuel\ actual\ SS}$	$0.41 \cdot 10^{-3}$	$0.62 \cdot 10^{-3}$	$0.822 \cdot 10^{-3}$ kg/s	$1.03 \cdot 10^{-3}$	$1.23 \cdot 10^{-3}$	N/A
$R_{Sensitivity}$ on $\dot{m}_{fuel\ actual\ SS}$	0	0	N/A	0	0	0.1
$R_{Unburned}$	116.5	120.25	122 ppm	123.26	123.98	N/A
r_{wr}	0.162	0.242	0.323 m	0.404	0.485	N/A
$R_{Sensitivity}$ on r_{wr}	0	0	N/A	0	0	0
$R_{Unburned}$	124.93	123.53	122 ppm	120.72	119.32	N/A
G_t	0.5	0.75	1	1.25	1.5	N/A
$R_{Sensitivity}$ on G_t	0	0	N/A	0	0	0
$R_{Unburned}$	124.93	123.53	122 ppm	120.72	119.32	N/A

Table 7.8 – Continued

G_d	1.25	1.875	2.5	3.125	3.75	N/A
$R_{Sensitivity}$ on G_d	0	0	N/A	0	0	0

Thus, $R_{Unburned}$ is insensitive to the changes in the values of ρ_{Cyl} , η_V , V_d , G_t , G_d , and r_{wr} . Hence, ρ_{Cyl} , η_V , V_d , G_t , G_d , and r_{wr} should be considered a constant in the formulation of $R_{Unburned}$. The simplified analytical model of $R_{Unburned}$ in (ppm) can be hence formulated as follows:

$$R_{Unburned} = 128 \left\langle 1 - \left[\left(\frac{0.0012 V_s}{m_{FASS}} + 1 \right) (0.21334) \right] \right\rangle \quad (7.5)$$

7.10. SENSITIVITY ANALYSIS OF THE MODEL OF THE RATE OF DIESEL EXHAUST CO EMISSION

The analytical model of diesel exhaust CO emission consists of a couple of sub-models: $R_{COSSCO+O_2}$ and $R_{COSSCO+H_2O}$. This section will present the sensitivity analysis of these two sub-models.

7.10.1. Sensitivity Analysis of the Model of $R_{COSSCO+O_2}$

The rate of the steady speed-based CO exhaust emissions that result from CO_2 dissociation for four-stroke diesel engines in (kg/s), $R_{COSSCO+O_2}$, is analytically modeled in equation (6.27). The key explanatory variable in this model is V_s . The baseline value of V_s is 13.56 m/s. The sensitivity analysis of the analytical model of $R_{COSSCO+O_2}$ is presented in Table 7.9 following from equations (6.27) and (7.1).

Table 7.9
Sensitivity analysis of the analytical model of $R_{COSS CO+O_2}$

	-50% Decrement Below Baseline Value	-25% Decrement Below Baseline Value	Baseline Value	+25% Increment Above Baseline Value	+50% Increment Above Baseline Value	Average Sensitivity Ratio on Each Independent Variable
$R_{COSS CO+O_2}$	4.77e-006	7.15e-006	9.54e-006 g/s	1.19e-005	1.43e-005	N/A
Φ	0.35	0.525	0.7	0.875	1.05	N/A
$R_{Sensitivity}$, on Φ	1	1	N/A	1	1	1
$R_{COSS CO+O_2}$	4.77e-006	7.15e-006	9.54e-006 g/s	1.19e-005	1.43e-005	N/A
ρ_{Cyl}	0.85	1.275	1.7 kg/m ³	2.125	2.55	N/A
$R_{Sensitivity}$, on ρ_{Cyl}	1	1	N/A	1	1	1
$R_{COSS CO+O_2}$	4.77e-006	7.15e-006	9.54e-006 g/s	1.19e-005	1.43e-005	N/A
η_V	0.45	0.675	0.9	1.125	1.35	N/A
$R_{Sensitivity}$, on η_V	1	1	N/A	1	1	1
$R_{COSS CO+O_2}$	4.34e-006	6.50e-006	9.54e-006 g/s	1.08e-005	1.30e-005	N/A
V_d	0.0015	0.00225	0.0033 m ³ /cycle	0.00375	0.0045	N/A
$R_{Sensitivity}$, on V_d	1.1	1.27	N/A	0.5	0.73	0.9
$R_{COSS CO+O_2}$	9.54e-006	9.54e-006	9.54e-006 g/s	9.54e-006	9.54e-006	N/A
$R_{Unburned}$	0.0000058	0.0000087	0.0000116	0.0000145	0.0000232	N/A
$R_{Sensitivity}$, on $R_{Unburned}$	0	0	N/A	0	0	0
$R_{COSS CO+O_2}$	4.77e-006	7.15e-006	9.54e-006 g/s	1.19e-005	1.43e-005	N/A
G_t	0.5	0.75	1	1.25	1.5	N/A
$R_{Sensitivity}$, on G_t	1	1	N/A	1	1	1
$R_{COSS CO+O_2}$	4.77e-006	7.15e-006	9.54e-006 g/s	1.19e-005	1.43e-005	N/A
G_d	1.25	1.875	2.5	3.125	3.75	N/A
$R_{Sensitivity}$, on G_d	1	1	N/A	1	1	1
$R_{COSS CO+O_2}$	1.90e-005	1.27e-005	9.54e-006 g/s	7.63e-006	6.35e-006	N/A
r_{wr}	0.162	0.242	0.323 m	0.404	0.485	N/A
$R_{Sensitivity}$, on r_{wr}	-2	-1.3	N/A	-0.8	-0.7	-1.2

Thus, $R_{COSS\ CO+O_2}$ is insensitive only to the changes in the value of $R_{Unburned}$. Hence, $R_{Unburned}$ should be considered a constant in the formulation of $R_{COSS\ CO+O_2}$. Therefore, the simplified analytical model of the $R_{COSS\ CO+O_2}$ in (kg/s) is formulated as shown in equation (7.6) using the following data: $R_{F-A\ stoich} = 0.069588$, $M_{fuel\ molar} = 0.0137$, $n = 2$, $R_{Unburned} = 0.0000116$, $M_{CO\ molar} = 0.028\ kg$, $K_{CO+O_2} = 0.0002\ M^{-1}.s^{-1}$, $[CO_2] = 0.0197\ M$.

$$R_{COSS\ CO+O_2} = 1.895471 * 10^{-11} \left(\frac{\Phi \rho_{Cyl} \eta_V V_d (V_S)^2 G_t G_d}{r_{wr}} \right) \quad (7.6)$$

7.10.2. Sensitivity Analysis of the Model of $R_{COSS\ CO+H_2O}$

The rate of the steady speed-based CO exhaust emissions that result from the Water-Gas-Shift reaction, $R_{COSS\ CO+H_2O}$, for four-stroke diesel engines is analytically modeled for both low-speed cycles and high-speed cycles in equations (6.34) and (6.35), respectively. The key explanatory variable in this model is V_S . The baseline value of V_S is 13.56 m/s. The sensitivity analysis of the analytical model of $R_{COSS\ CO+H_2O}$ is presented in Table 7.10 following from equations (6.34), (6.35) and (7.1).

Table 7.10
Sensitivity analysis of the analytical model of $R_{COSS CO+H_2O}$

	-50% Decrement Below Baseline Value	-25% Decrement Below Baseline Value	Baseline Value	+25% Increment Above Baseline Value	+50% Increment Above Baseline Value	Average Sensitivity Ratio on Each Independent Variable
$R_{COSS CO+H_2O}$	0.0021	0.0032	0.0042 g/s	0.0053	0.0063	N/A
Φ	0.35	0.525	0.7	0.875	1.05	N/A
$R_{Sensitivity}$, on Φ	1	1	N/A	1	1	1
$R_{COSS CO+H_2O}$	0.0021	0.0032	0.0042 g/s	0.0053	0.0063	N/A
ρ_{Cyl}	0.85	1.275	1.7 kg/m ³	2.125	2.55	N/A
$R_{Sensitivity}$, on ρ_{Cyl}	1	1	N/A	1	1	1
$R_{COSS CO+H_2O}$	0.0021	0.0032	0.0042 g/s	0.0053	0.0063	N/A
η_V	0.45	0.675	0.9	1.125	1.35	N/A
$R_{Sensitivity}$, on η_V	1	1	N/A	1	1	1
$R_{COSS CO+H_2O}$	0.0019	0.0029	0.0042 g/s	0.0048	0.0057	N/A
V_d	0.0015	0.00225	0.0033 m ³ /cycle	0.00375	0.0045	N/A
$R_{Sensitivity}$, on V_d			N/A			
$R_{COSS CO+H_2O}$	0.0042	0.0042	0.0042 g/s	0.0042	0.0042	N/A
$R_{Unburned}$	0.0000058	0.0000087	0.0000116	0.0000145	0.0000232	N/A
$R_{Sensitivity}$, on $R_{Unburned}$	0	0	N/A	0	0	0

Thus, $R_{COSS CO+H_2O}$ is insensitive only to the changes in the value of $R_{Unburned}$. Hence,

$R_{Unburned}$ should be considered a constant in the formulation of $R_{COSS CO+H_2O}$.

Therefore, the simplified analytical models of the $R_{COSS CO+H_2OLS}$ and $R_{COSS CO+H_2OHS}$ in (kg/s) are formulated as shown in equations (7.7) and (7.8) for low-speed cycles and high-speed cycles, respectively using the following data: $R_{F-A stoich} = 0.069588$,

$M_{fuel molar} = 0.0137$, $n = 2$, $R_{Unburned} = 0.0000116$, $M_{CO molar} = 0.028$ kg, $K_{CO+H_2O} = 2.25$, $[CO_2] = 0.008$ M, $[H_2] = 0.008$ M.

$$R_{COSSCO+H_2O_{LS}} = 7.333848 * 10^{-6} \left(\Phi \rho_{Cyl} \eta_V V_d V_S (2)^{\left(-1.7 - \frac{\log V_S}{\log 3.33}\right)} \right) \quad (7.7)$$

$$R_{COSSCO+H_2O_{HS}} = 1.235051 * 10^{-6} \left(\Phi \rho_{Cyl} \eta_V V_d V_S e^{\left(\frac{V_S}{2^{5.01}}\right)} \right) \quad (7.8)$$

7.11. SENSITIVITY ANALYSIS OF THE MODEL OF THE RATE OF DIESEL EXHAUST NO_x EMISSION

The analytical model of diesel exhaust NO_x emission consists of four sub-models:

R_{NOSSZM} , R_{NOSSZM} , R_{NOSSZM} and R_{NO_2SS} . This section will present the sensitivity analysis of these four sub-models.

7.11.1. Sensitivity Analysis of the Model of R_{NOSSZM}

The rate of the Zeldovich mechanism-based NO emission, R_{NOSSZM} , is analytically modeled in equations (6.45) and (6.46) for low-speed cycles and high-speed cycles, respectively. The key explanatory variable in this model is V_S . The baseline value of V_S is 13.56 m/s. The sensitivity analysis of the analytical model of R_{NOSSZM} is presented in Table 7.11 following from equations (6.45), (6.46) and (7.1).

Table 7.11
Sensitivity analysis of the analytical model of R_{NOSSZM}

	-50% Decrement Below Baseline Value	-25% Decrement Below Baseline Value	Baseline Value	+25% Increment Above Baseline Value	+50% Increment Above Baseline Value	Average Sensitivity Ratio on Each Independent Variable
R_{NOSSZM}	3.72e-010	5.57e-010	7.4e-010 g/s	9.29e-010	1.12e-009	N/A
Φ	0.35	0.525	0.7	0.875	1.05	N/A
$R_{Sensitivity}$, on Φ	1	1	N/A	1	1	1
R_{NOSSZM}	3.72e-010	5.57e-010	7.4e-010 g/s	9.29e-010	1.12e-009	N/A
ρ_{Cyl}	0.85	1.275	1.7 kg/m ³	2.125	2.55	N/A
$R_{Sensitivity}$, on ρ_{Cyl}	1	1	N/A	1	1	1
R_{NOSSZM}	3.72e-010	5.57e-010	7.4e-010 g/s	9.29e-010	1.12e-009	N/A
η_V	0.45	0.675	0.9	1.125	1.35	N/A
$R_{Sensitivity}$, on η_V	1	1	N/A	1	1	1
R_{NOSSZM}	3.38e-010	5.067e-010	7.4e-010 g/s	8.45e-010	1.0136e-009	N/A
V_d	0.0015	0.00225	0.0033 m ³ /cycle	0.00375	0.0045	N/A
$R_{Sensitivity}$, on V_d	1	1	N/A	1	1	1
R_{NOSSZM}	7.4e-010	7.4e-010	7.4e-010 g/s	7.4e-010	7.4e-010	N/A
$R_{Unburned}$	0.0000058	0.0000087	0.0000116	0.0000145	0.0000232	N/A
$R_{Sensitivity}$, on $R_{Unburned}$	0	0	N/A	0	0	0

Thus, R_{NOSSZM} is insensitive only to the changes in the value of $R_{Unburned}$. Hence, $R_{Unburned}$ should be considered a constant in the formulation of R_{NOSSZM} . Therefore, the simplified analytical models of $R_{NOSSZM LS}$ and $R_{NOSSZM HS}$ in (kg/s) for low-speed cycles and high-speed cycles, respectively, are indicated in equations (7.9) and (7.10) using the following data: $R_{F-A stoich} = 0.069588$, $M_{NO molar} = 0.030$, $M_{fuel molar} = 0.0137$, $n=2$, $R_{Unburned} = 0.0000116$, $K_{N_2+O_2} = 0.00001$, $[N_2] = 0.799$, $[O_2] = 0.199$.

$$R_{NOSSZMLS} = 5.45996 * 10^{-14} \left(\Phi \rho_{Cyl} \eta_V V_d V_S e^{\left(\frac{V_S}{(2)^{3.7}} \right)} \right) \quad (7.9)$$

$$R_{NOSSZMHS} = 2.46498 * 10^{-14} \left(\Phi \rho_{Cyl} \eta_V V_d V_S e^{\left(\frac{V_S}{(2)^{3.55}} \right)} \right) \quad (7.10)$$

7.11.2. Sensitivity Analysis of the Model of R_{NOSSZM}

The rate of the extended Zeldovich mechanism-based NO emission, R_{NOSSZM} , is analytically modeled in equations (6.55) and (6.56) for low-speed cycles and high-speed cycles, respectively. The key explanatory variable in this model is V_S . The baseline value of V_S is 13.56 m/s. The sensitivity analysis of the analytical model of R_{NOSSZM} is presented in Table 7.12 following from equations (6.55), (6.56) and (7.1).

Table 7.12
Sensitivity analysis of the analytical model of $R_{NOSS EZM}$

	-50% Decrement Below Baseline Value	-25% Decrement Below Baseline Value	Baseline Value	+25% Increment Above Baseline Value	+50% Increment Above Baseline Value	Average Sensitivity Ratio on Each Independent Variable
$R_{NOSS EZM}$	6.55e-004	9.8e-004	0.0013 g/s	0.0016	0.0020	N/A
Φ	0.35	0.525	0.7	0.875	1.05	N/A
$R_{Sensitivity}$ on Φ	1	1	N/A	1	1	1
$R_{NOSS EZM}$	6.55e-004	9.8e-004	0.0013 g/s	0.0016	0.0020	N/A
ρ_{Cyl}	0.85	1.275	1.7 kg/m ³	2.125	2.55	N/A
$R_{Sensitivity}$ on ρ_{Cyl}	1	1	N/A	1	1	1
$R_{NOSS EZM}$	6.55e-004	9.8e-004	0.0013 g/s	0.0016	0.0020	N/A
η_V	0.45	0.675	0.9	1.125	1.35	N/A
$R_{Sensitivity}$ on η_V	1	1	N/A	1	1	1
$R_{NOSS EZM}$	5.96e-004	8.9e-004	0.0013 g/s	0.0015	0.0018	N/A
V_d	0.0015	0.00225	0.0033 m ³ /cycle	0.00375	0.0045	N/A
$R_{Sensitivity}$ on V_d	1.1	1.26	N/A	0.62	0.77	0.94
$R_{NOSS EZM}$	0.0013	0.0013	0.0013 g/s	0.0013	0.0013	N/A
$R_{Unburned}$	0.0000058	0.0000087	0.0000116	0.0000145	0.0000232	N/A
$R_{Sensitivity}$ on $R_{Unburned}$	0	0	N/A	0	0	0

Thus, $R_{NOSS EZM}$ is insensitive only to the changes in the value of $R_{Unburned}$. Hence, $R_{Unburned}$ should be considered a constant in the formulation of $R_{NOSS EZM}$. Therefore, the simplified analytical models of the $R_{NOSS EZM LS}$ and $R_{NOSS EZM HS}$ in (kg/s) for low-speed cycles and high-speed cycles, respectively, are indicated in equations (7.11) and (7.12): $R_{F-A stoich} = 0.069588$, $M_{NO molar} = 0.030$, $M_{fuel molar} = 0.0137$, $n=2$, $R_{Unburned} = 0.0000116$, $K_{N+OH} = 0.015$, $[N] = 0.356$, $[OH] = 0.356$.

$$R_{NOSS EZM LS} = 1.101802 * 10^{-7} \left(\Phi \rho_{Cyl} \eta_V V_d V_S e^{\left(\frac{V_S}{(2)^{3.9}} \right)} \right) \quad (7.11)$$

$$R_{NOSS EZM HS} = 4.7958676 * 10^{-8} \left(\Phi \rho_{Cyl} \eta_V V_d V_S e^{\left(\frac{V_S}{(2)^{3.55}} \right)} \right) \quad (7.12)$$

7.11.3. Sensitivity Analysis of the Model of $R_{NOSS SEZM}$

The rate of the super extended Zeldovich mechanism-based NO emission, $R_{NOSS SEZM}$, is analytically modeled in equations (6.66) and (6.67) for low-speed cycles and high-speed cycles, respectively. The key explanatory variable in this model is V_S . The baseline value of V_S is 13.56 m/s. The sensitivity analysis of the analytical model of $R_{NOSS SEZM}$ is presented in Table 7.13 following from equations (6.66), (6.67) and (7.1).

Table 7.13
Sensitivity analysis of the analytical model of $R_{NOSS SEZM}$

	-50% Decrement Below Baseline Value	-25% Decrement Below Baseline Value	Baseline Value	+25% Increment Above Baseline Value	+50% Increment Above Baseline Value	Average Sensitivity Ratio on Each Independent Variable
$R_{NOSS SEZM}$	2.35e-006	3.5e-006	4.69e-006 g/s	5.86e-006	7.04e-006	N/A
Φ	0.35	0.525	0.7	0.875	1.05	N/A
$R_{Sensitivity}$, on Φ	1	1	N/A	1	1	1
$R_{NOSS SEZM}$	2.35e-006	3.5e-006	4.69e-006 g/s	5.86e-006	7.04e-006	N/A
ρ_{Cyl}	0.85	1.275	1.7 kg/m ³	2.125	2.55	N/A
$R_{Sensitivity}$, on ρ_{Cyl}	1	1	N/A	1	1	1
$R_{NOSS SEZM}$	2.35e-006	3.5e-006	4.69e-006 g/s	5.86e-006	7.04e-006	N/A
η_V	0.45	0.675	0.9	1.125	1.35	N/A
$R_{Sensitivity}$, on η_V	1	1	N/A	1	1	1
$R_{NOSS SEZM}$	2.13e-006	3.2e-006	4.69e-006 g/s	5.33e-006	6.4e-006	N/A
V_d	0.0015	0.00225	0.0033 m ³ /cycle	0.00375	0.0045	N/A
$R_{Sensitivity}$, on V_d	1.1	1.3	N/A	0.6	0.73	0.93
$R_{NOSS SEZM}$	4.69e-006	4.69e-006	4.69e-006 g/s	4.69e-006	4.69e-006	N/A
$R_{Unburned}$	0.0000058	0.0000087	0.0000116	0.0000145	0.0000232	N/A
$R_{Sensitivity}$, on $R_{Unburned}$	0	0	N/A	0	0	0

Thus, $R_{NOSS SEZM}$ is insensitive only to the changes in the value of $R_{Unburned}$. Hence, $R_{Unburned}$ should be considered a constant in the formulation of $R_{NOSS SEZM}$. Therefore, the simplified analytical models of the $R_{NOSS SEZM LS}$ and $R_{NOSS SEZM HS}$ in (kg/s) for low-speed cycles and high-speed cycles, respectively, are indicated in equations (7.13) and (7.14) using the following data: $R_{F-A stoich} = 0.069588$, $M_{NO molar} = 0.030$,

$M_{fuel\ molar}=0.0137$, $n=2$, $R_{Unburned} = 0.0000116$, $K_{N_2O+H} = 0.018$, $[N_2O]= 0.0176$,
 $[H]= 0.0176$.

$$R_{NO_{SS}SEZM\ LS}=3.446799*10^{-10}\left(\Phi\ \rho_{air}\ \eta_V\ V_d\ V_S\ e^{\left(\frac{V_S}{(2)^{3.7}}\right)}\right) \quad (7.13)$$

$$R_{NO_{SS}SEZM\ HS}=1.553214*10^{-10}\left(\Phi\ \rho_{air}\ \eta_V\ V_d\ V_S\ e^{\left(\frac{V_S}{(2)^{3.55}}\right)}\right) \quad (7.14)$$

7.11.4. Sensitivity Analysis of the Model of $R_{NO_2,SS}$

The rate of NO₂ emission, $R_{NO_2,SS}$, is analytically modeled in equations (6.75) and (6.76) for low-speed cycles and high-speed cycles, respectively. The key explanatory variable in this model is V_S . The baseline value of V_S is 13.56 m/s. The sensitivity analysis of the analytical model of $R_{NO_2,SS}$ is presented in Table 7.14 following from equations (6.75), (6.76) and (7.1).

Table 7.14
Sensitivity analysis of the analytical model of $R_{NO_2 SS}$

	-50% Decrement Below Baseline Value	-25% Decrement Below Baseline Value	Baseline Value	+25% Increment Above Baseline Value	+50% Increment Above Baseline Value	Average Sensitivity Ratio on Each Independent Variable
$R_{NO_2 SS}$	3.64e-004	5.46e-004	7.28e-004 g/s	9.1e-004	0.001	N/A
Φ	0.35	0.525	0.7	0.875	1.05	N/A
$R_{Sensitivity}$ on Φ	1	1	N/A	1	1	1
$R_{NO_2 SS}$	3.64e-004	5.46e-004	7.28e-004 g/s	9.1e-004	0.001	N/A
ρ_{Cyl}	0.85	1.275	1.7 kg/m ³	2.125	2.55	N/A
$R_{Sensitivity}$ on ρ_{Cyl}	1	1	N/A	1	1	1
$R_{NO_2 SS}$	3.64e-004	5.46e-004	7.28e-004 g/s	9.1e-004	0.001	N/A
η_V	0.45	0.675	0.9	1.125	1.35	N/A
$R_{Sensitivity}$ on η_V	1	1	N/A	1	1	1
$R_{NO_2 SS}$	3.31e-004	4.96e-004	7.28e-004 g/s	8.27e-004	9.92e-004	N/A
V_d	0.0015	0.00225	0.0033 m ³ /cycle	0.00375	0.0045	N/A
$R_{Sensitivity}$ on V_d	1.1	1.27	N/A	0.5	0.73	0.9
$R_{NO_2 SS}$	7.28e-004	7.28e-004	7.28e-004 g/s	7.28e-004	7.28e-004	N/A
$R_{Unburned}$	0.0000058	0.0000087	0.0000116	0.0000145	0.0000232	N/A
$R_{Sensitivity}$ on $R_{Unburned}$	0	0	N/A	0	0	0
$R_{NO_2 SS}$	5.15e-004	6.3e-004	7.28e-004 g/s	8.14e-004	8.91e-004	N/A
G_t	0.5	0.75	1	1.25	1.5	N/A
$R_{Sensitivity}$ on G_t	0.6	0.54	N/A	0.5	0.5	0.54
$R_{NO_2 SS}$	5.15e-004	6.30e-004	7.28e-004 g/s	8.14e-004	8.91e-004	N/A
G_d	1.25	1.875	2.5	3.125	3.75	N/A
$R_{Sensitivity}$ on G_d	0.6	0.54	N/A	0.5	0.5	0.54
$R_{NO_2 SS}$	0.001	8.41e-004	7.28e-004 g/s	6.51e-004	5.94e-004	N/A
r_{wr}	0.162	0.242	0.323 m	0.404	0.485	N/A
$R_{Sensitivity}$ on r_{wr}	-0.75	-0.62	N/A	-0.42	-0.4	-0.6

Thus, R_{NO_2SS} is insensitive only to the changes in the value of $R_{Unburned}$. Hence, $R_{Unburned}$ should be considered a constant in the formulation of R_{NO_2SS} . Therefore, the simplified analytical models of the R_{NO_2SSLS} and R_{NO_2SSHs} in (kg/s) for low-speed cycles and high-speed cycles, respectively, are indicated in equations (7.15) and (7.16) using the following data: $R_{F-A\ stoich} = 0.069588$, $M_{NO_2\ molar} = 0.046\text{ kg}$, $K_{NO+O_2} = 6\text{ M}^{-1}\text{s}^{-1}$, $[NO] = 0.0066\text{ M}$, $[O_2] = 0.0034\text{ M}$, $M_{fuel\ molar} = 0.0137$, $n=2$, $R_{Unburned} = 0.0000116$.

$$R_{NO_2SSLS} = 5.784856 * 10^{-9} \left(\frac{\Phi \rho_{air} \eta_V V_d V_S^{1.5} G_t^{0.5} G_d^{0.5}}{(r_{wr})^{0.5}} e^{\left(\frac{V_S}{(2)^{3.85}} \right)} \right) \quad (7.15)$$

$$R_{NO_2SSHs} = 1.661264 * 10^{-9} \left(\frac{\Phi \rho_{air} \eta_V V_d V_S^{1.5} G_t^{0.5} G_d^{0.5}}{(r_{wr})^{0.5}} e^{\left(\frac{V_S}{(2)^{3.55}} \right)} \right) \quad (7.16)$$

7.12. SENSITIVITY ANALYSIS OF THE MODEL OF THE RATE OF DIESEL EXHAUST HC EMISSION

The rate of HC emission, R_{HCSS} , is analytically modeled in equations (6.78) and (6.79) for low-speed cycles and high-speed cycles, respectively. The key explanatory variable in this model is V_S . The baseline value of V_S is 13.56 m/s. The sensitivity analysis of the analytical model of R_{HCSS} is presented in Table 7.15 following from equations (6.78), (6.79) and (7.1).

Table 7.15
Sensitivity analysis of the analytical model of R_{HCSS}

	-50% Decrement Below Baseline Value	-25% Decrement Below Baseline Value	Baseline Value	+25% Increment Above Baseline Value	+50% Increment Above Baseline Value	Average Sensitivity Ratio on Each Independent Variable
R_{HCSS}	0.00029	0.00044	0.00058 g/s	0.00073	0.00088	N/A
\dot{m}_{AFSS}	0.411	0.6165	0.822 g/s	1.028	1.233	N/A
$R_{Sensitivity}$ on \dot{m}_{AFSS}	1	1	N/A	1	1	1
R_{HCSS}	0.00058	0.00058	0.00058 g/s	0.00058	0.00058	N/A
$R_{Unburned}$	0.0000058	0.0000087	0.0000116	0.0000145	0.0000232	N/A
$R_{Sensitivity}$ on $R_{Unburned}$	0	0	N/A	0	0	0

Thus, R_{HCSS} is insensitive only to the changes in the value of $R_{Unburned}$. Hence,

$R_{Unburned}$ should be considered a constant in the formulation of R_{HCSS} . Therefore, the

R_{HCSSLS} and R_{HCSSHS} in (g/s) for low-speed cycles and high-speed cycles,

respectively, are indicated in equations (7.17) and (7.18) using the following data:

$$n=2, R_{Unburned} = 0.0000116.$$

$$R_{HCSSLS} = 0.00071 \dot{m}_{fuel actual} \quad (7.17)$$

$$R_{HCSSHS} = 0.0009971 \dot{m}_{fuel actual} \quad (7.18)$$

CHAPTER 8

SIMULATED RESULTS AND DISCUSSION OF THE EXPERIMENTAL VALIDATION

8.1. OVERVIEW

In an endeavour to validate the analytical models developed in the previous chapters, the field data of Oak Ridge National Laboratory (ORNL) and U.S. Environmental Protection Agency (EPA) have been utilized for comparison with the simulated results of the developed models of diesel fuel consumption rate, CO emission rate, NOx emission rate, unburned diesel hydrocarbon percentage, HC emission rate and brake power of diesel engines (Rakha, et al., 2003; West, et al., 1997; Brzezinski, et al., 1999; Rakha, et al., 2012). MATLAB has been used for developing an interface facility for the developed analytical models for the purpose of simulation. The MATLAB programming code and the interface facility developed in this study on diesel fuel consumption rate, CO emission rate, NOx emission rate, unburned diesel hydrocarbon and HC emission rate are provided in Appendix A, Appendix B, Appendix C, Appendix D and Appendix E. In addition, case studies have been utilized in order to validate the developed analytical models of \dot{c}_{im} , \dot{W}_C , η_{CM} , ρ , and \dot{c}_{Cyl} .

This chapter presents the experimental validation of the developed analytical models of \dot{m}_{AFSS} , \dot{m}_{NLSAF} , \dot{m}_{NHSAF} , \dot{m}_{PVLASF} , \dot{m}_{P1HSAF} , \dot{m}_{P2LSAF} , \dot{m}_{P2HSAF} , $R_{COSSCO+O_2}$,

$R_{COSSCO+H_2O}$, R_{NOSSZM} , $R_{NOSS EZM}$, $R_{NOSS SEZM}$, R_{NO_2SS} , $R_{Unburned}$, R_{HCSS} , Γ_B , \dot{c}_{im} , \dot{W}_C , η_{CM} , ρ and \dot{c}_{Cyl} , respectively. This Chapter achieves the 2nd objective of this

research that is to validate the simulation results against experimental results. The

MATLAB programming code and the interface facility developed in this study on diesel fuel consumption rate, CO emission rate, NOx emission rate, unburned diesel hydrocarbon and HC emission rate which are provided in Appendix A, Appendix B, Appendix C, Appendix D and Appendix E achieve the 3rd objective of this research.

8.2. STATISTICAL ANALYSIS

The statistical analysis for comparing the field data with the simulated results consists of a couple of measures: (i) coefficient of determination, r_{COD} , which should be close to ‘1’ (Keller, 2012), (ii) relative error of the model, ε_R , which should be close to ‘0%’ (Keller, 2012). The coefficient of determination, r_{COD} , can be evaluated as follows (Keller, 2012):

$$r_{COD} = \left(\frac{S_{xy}}{S_x S_y} \right)^2 \quad (8.1)$$

The standard deviation of the dataset of the interval variable x_i that is the expected value analytically, S_x , can be evaluated as follows (Keller, 2012):

$$S_x = \sqrt{\frac{\sum_{i=1}^{z_n} (x_i - \bar{x})^2}{z_n - 1}} \quad (8.2)$$

Similarly, the standard deviation of the field dataset of the interval variable y_i that is the measured value, S_y , can be evaluated as follows (Keller, 2012):

$$S_y = \sqrt{\frac{\sum_{i=1}^{z_n} (y_i - \bar{y})^2}{z_n - 1}} \quad (8.3)$$

The sample covariance, S_{xy} , can be evaluated as follows (Keller, 2012):

$$S_{xy} = \frac{\sum_{i=1}^{z_n} (x_i - \bar{x})(y_i - \bar{y})}{z_n - 1} \quad (8.4)$$

The relative error of the model, ε_R , can be evaluated as follows (Keller, 2012):

$$\varepsilon_R = \sum_{i=1}^{z_n} \left| \frac{y_i - x_i}{y_i} \right| \frac{100\%}{z_n} \quad (8.5)$$

The r_{COD} and ε_R will be utilized in this chapter as quantifiable measures of validation.

8.3. SIMULATION AND VALIDATION OF THE MODEL OF DIESEL FUEL CONSUMPTION RATE

The experimental validation in this study compares the simulated results of the analytical model of the steady speed-based fuel mass actual flow rate \dot{m}_{AFSS} following from equation (5.22) with the corresponding field data of Oak Ridge National Laboratory (ORNL) and U.S. Environmental Protection Agency (EPA) (Rakha, et al., 2003; West, et al., 1997; Brzezinski, et al., 1999). It compares as well the simulated results of the analytical models of the acceleration-based fuel mass actual flow rate \dot{m}_{NLSAF} , \dot{m}_{NHSFAF} , \dot{m}_{P1LSAF} , $\dot{m}_{P1HSFAF}$, \dot{m}_{P2LSAF} , and $\dot{m}_{P2HSFAF}$ following from equations (5.23), (5.24), (5.25), (5.26), (5.27), and (5.28), respectively, with the corresponding field data of ORNL and U.S. EPA (Rakha, et al., 2003; West, et al., 1997; Brzezinski, et al., 1999). The field data of ORNL and EPA are provided for the average speed of all the Freeway cycles (Rakha, et al., 2003; West, et al., 1997; Brzezinski, et al., 1999).

The data for making the calculations on the \dot{m}_{AFSS} analytical model results are based on the following data provided on diesel light trucks and light commercial vehicles with four-stroke engines under steady speed condition with Φ of 0.7, ρ of 1.7 kg/m^3 , η_V of 0.9, V_d of $0.00033 \text{ m}^3/\text{d-cycle}$, r_{wr} of 0.323 m, and $R_{F-A \text{ stoichiometric}}$ of 0.0696. The field data of ORNL and EPA are provided for the average speed of all cycles. The data on G_t and G_d vary with the cycles as follows: (i) G_t of 1.43 and G_d of 2.5 for Freeway LOS G cycle (vehicle average speed 20.96 km/hr), (ii) G_t of 1.43 and G_d of 2.5 for Freeway LOS F cycle (vehicle average speed 29.76 km/hr), (iii) G_t of 1 and G_d of 2.5 for Freeway LOS E cycle (vehicle average speed 48.8 km/hr), (iv) G_t of 1 and G_d of 2.5 for Freeway LOS D cycle (vehicle average speed 84.64 km/hr), (v) G_t of 1 and G_d of 2.5 for Freeway LOS A-C cycle (vehicle average speed 95.52 km/hr), (vi) G_t of 1 and G_d of 2.5 for Freeway High Speed cycle (vehicle average speed 101 km/hr) (Rakha, et al., 2003; West, et al., 1997; Brzezinski, et al., 1999). The value of the equivalence ratio, Φ , depends primarily on the mode of running the vehicle engine. Vehicle diesel engines normally operate at $\phi \leq 0.80$ (Heywood, 1988). For idling mode, accelerating mode, cruising mode, and decelerating mode the value of Φ is almost 0.55, 0.80, 0.70, and 0.60, respectively (Heywood, 1988; Kao and Moskwa, 1994; Gupta, 2006). This is in accord with the fact that as the value of Φ decreases, the fuel availability lost in exhaust stroke decreases; thus, engine efficiency increases which significantly interprets why the efficiency of diesel engines is relatively high (Heywood, 1988). The comparison of the simulated results with the field data on \dot{m}_{AFSS} is shown in Table 8.1 based on equation (5.22).

Table 8.1

Comparison of the simulated results with field data on \dot{m}_{AFSS}

Field Data	\dot{m}_{AFSS} Analytically (g/s)	\dot{m}_{AFSS} read from field data (g/s)	Percentage of Deviation
ORNL & EPA Freeway LOS G cycle (Average Speed 20.96 km/hr)	0.5	0.501	0.2 %
ORNL & EPA Freeway LOS F cycle (Average Speed 29.76 km/hr)	0.7	0.63	11 %
ORNL & EPA Freeway LOS E cycle (Average Speed 48.8 km/hr)	0.822	0.822	0 %
ORNL & EPA Freeway LOS D cycle (Average Speed 84.64 km/hr)	1.425	1.38	3.2 %
ORNL & EPA Freeway LOS A-C cycle (Average Speed 95.52 km/hr)	1.61	1.65	2.4 %
ORNL & EPA Freeway High Speed cycle (Average Speed 101 km/hr)	1.7	1.8	5.5 %
			Average Percentage of Deviation = 3.7 %

The comparisons of the simulated results with the field data on \dot{m}_{NLSAF} and \dot{m}_{NHSF} are shown in Tables 8.2 and 8.3 based on equations (5.23) and (5.24), respectively.

Table 8.2

Comparison of the simulated results with field data on \dot{m}_{NLSAF}

Field Data	\dot{m}_{NLSAF} Analytically kg/s	\dot{m}_{NLSAF} read from field data kg/s	Percentage of Deviation
ORNL & EPA Arterials/Collectors LOS E-F cycle (Average Speed 18.67 km/hr)	$0.332 \cdot 10^{-3}$	$0.333 \cdot 10^{-3}$	0.3 %
ORNL & EPA Local Roadways cycle (Average Speed 20.76 km/hr)	$0.358 \cdot 10^{-3}$	$0.359 \cdot 10^{-3}$	0.28 %
ORNL & EPA Arterials/Collectors LOS C- D cycle (Average Speed 30.9 km/hr)	$0.458 \cdot 10^{-3}$	$0.459 \cdot 10^{-3}$	0.22 %
ORNL & EPA Non-Freeway Urban Travel cycle (Average Speed 31.22 km/hr)	$0.461 \cdot 10^{-3}$	$0.46 \cdot 10^{-3}$	0.22 %
ORNL & EPA Arterials/Collectors LOS A- B cycle (Average Speed 39.91 km/hr)	$0.517 \cdot 10^{-3}$	$0.518 \cdot 10^{-3}$	0.19 %
			Average Percentage of Deviation = 0.242 %

Table 8.3

Comparison of the simulated results with field data on $\dot{m}_{NHS\text{AF}}$

Field Data	$\dot{m}_{NHS\text{AF}}$ Analytically kg/s	$\dot{m}_{NHS\text{AF}}$ read from field data kg/s	Percentage of Deviation
ORNL & EPA Freeway Ramps cycle (Average Speed 55.68 km/hr)	$0.488 \cdot 10^{-3}$	$0.488 \cdot 10^{-3}$	0 %
ORNL & EPA Freeway LOS D cycle (Average Speed 84.64 km/hr)	$0.534 \cdot 10^{-3}$	$0.534 \cdot 10^{-3}$	0 %
ORNL & EPA Freeway LOS A-C cycle (Average Speed 95.52 km/hr)	$0.533 \cdot 10^{-3}$	$0.533 \cdot 10^{-3}$	0 %
ORNL & EPA Freeway High Speed cycle (Average Speed 101 km/hr)	$0.53 \cdot 10^{-3}$	$0.53 \cdot 10^{-3}$	0 %
			Average Percentage of Deviation = 0 %

The comparisons of the simulated results with the field data on $\dot{m}_{PIL\text{SAF}}$ and $\dot{m}_{P1\text{HSAF}}$ are shown in Tables 8.4 and 8.5 based on equations (5.25) and (5.26), respectively.

Table 8.4

Comparison of the simulated results with field data on $\dot{m}_{PIL\text{SAF}}$

Field Data	$\dot{m}_{PIL\text{SAF}}$ Analytical kg/s	$\dot{m}_{PIL\text{SAF}}$ read from field data kg/s	Percentage of Deviation
ORNL & EPA Arterials/Collectors LOS E-F cycle (Average Speed 18.67 km/hr)	$1.39 \cdot 10^{-3}$	$1.42 \cdot 10^{-3}$	2.1 %
ORNL & EPA Local Roadways cycle (Average Speed 20.76 km/hr)	$1.55 \cdot 10^{-3}$	$1.6 \cdot 10^{-3}$	3.1 %
ORNL & EPA Arterials/Collectors LOS C-D cycle (Average Speed 30.9 km/hr)	$2.3 \cdot 10^{-3}$	$2.3 \cdot 10^{-3}$	0 %
ORNL & EPA Non-Freeway Urban Travel cycle (Average Speed 31.22 km/hr)	$2.33 \cdot 10^{-3}$	$2.4 \cdot 10^{-3}$	3 %
ORNL & EPA Arterials/Collectors LOS A-B cycle (Average Speed 39.91 km/hr)	$2.98 \cdot 10^{-3}$	$3 \cdot 10^{-3}$	0.7 %
			Average Percentage of Deviation = 1.78 %

Table 8.5

Comparison of the simulated results with field data on \dot{m}_{P1HSAF}

Field Data	\dot{m}_{P1HSAF} Analytically kg/s	\dot{m}_{P1HSAF} read from field data kg/s	Percentage of Deviation
ORNL & EPA Freeway Ramps cycle (Average Speed 55.68 km/hr)	3.73×10^{-3}	3.8×10^{-3}	1.8 %
ORNL & EPA Freeway LOS D cycle (Average Speed 84.64 km/hr)	5.67×10^{-3}	5.8×10^{-3}	2.2 %
			Average Percentage of Deviation = 2 %

The comparisons of the simulated results with the field data on \dot{m}_{P2LSAF} are shown in Tables 8.6 and 8.7 for a_{VS} of 1.5 m/s^2 and 1.8 m/s^2 , respectively, based on equation (5.27).

Table 8.6

Comparison of the simulated results with field data on \dot{m}_{P2LSAF} at $a_{VS} = 1.5 \text{ m/s}^2$

Field Data	\dot{m}_{P2LSAF} Analytically kg/s	\dot{m}_{P2LSAF} read from field data kg/s	Percentage of Deviation
ORNL & EPA Arterials/Collectors LOS E-F cycle (Average Speed 18.67 km/hr)	1.98×10^{-3}	2.02×10^{-3}	1.98 %
ORNL & EPA Local Roadways cycle (Average Speed 20.76 km/hr)	2.2×10^{-3}	2.242×10^{-3}	1.9 %
ORNL & EPA Arterials/Collectors LOS C-D cycle (Average Speed 30.9 km/hr)	3.27×10^{-3}	3.33×10^{-3}	1.8 %
ORNL & EPA Non-Freeway Urban Travel cycle (Average Speed 31.22 km/hr)	3.31×10^{-3}	3.37×10^{-3}	1.8 %
ORNL & EPA Arterials/Collectors LOS A-B cycle (Average Speed 39.91 km/hr)	4.23×10^{-3}	4.31×10^{-3}	1.86 %
			Average Percentage of Deviation = 1.86 %

Table 8.7

Comparison of the simulated results with field data on \dot{m}_{P2LSAF} at $a_{VS} = 1.8 \text{ m/s}^2$

Field Data	\dot{m}_{P2LSAF} Analytically kg/s	\dot{m}_{P2LSAF} read from field data kg/s	Percentage of Deviation
ORNL & EPA Arterials/Collectors LOS E-F cycle (Average Speed 18.67 km/hr)	2.67×10^{-3}	2.72×10^{-3}	1.8 %
ORNL & EPA Local Roadways cycle (Average Speed 20.76 km/hr)	2.97×10^{-3}	3.03×10^{-3}	1.98 %
ORNL & EPA Arterials/Collectors LOS C-D cycle (Average Speed 30.9 km/hr)	4.42×10^{-3}	4.5×10^{-3}	1.77 %
ORNL & EPA Non-Freeway Urban Travel cycle (Average Speed 31.22 km/hr)	4.46×10^{-3}	4.55×10^{-3}	1.98 %
ORNL & EPA Arterials/Collectors LOS A-B cycle (Average Speed 39.91 km/hr)	5.71×10^{-3}	5.8×10^{-3}	1.5 %
			Average Percentage of Deviation = 1.8 %

The comparisons of the simulated results with the field data on \dot{m}_{P2HSAF} are shown in Tables 8.8 and 8.9 for a_{VS} of 1.5 m/s^2 and 1.8 m/s^2 , respectively, based on equation (5.28).

Table 8.8

Comparison of the simulated results with field data on \dot{m}_{P2HSAF} at $a_{VS} = 1.5 \text{ m/s}^2$

Field Data	\dot{m}_{P2HSAF} Analytically kg/s	\dot{m}_{P2HSAF} read from field data kg/s	Percentage of Deviation
ORNL & EPA Freeway Ramps cycle (Average Speed 55.68 km/hr)	5.48×10^{-3}	5.58×10^{-3}	1.79 %
ORNL & EPA Freeway LOS D cycle (Average Speed 84.64 km/hr)	8.33×10^{-3}	8.48×10^{-3}	1.77 %
			Average Percentage of Deviation = 1.78 %

Table 8.9

Comparison of the simulated results with field data on \dot{m}_{P2HSAF} at $a_{VS} = 1.8 \text{ m/s}^2$

Field Data	\dot{m}_{P2HSAF} Analytically kg/s	\dot{m}_{P2HSAF} read from field data kg/s	Percentage of Deviation
ORNL & EPA Freeway Ramps cycle (Average Speed 55.68 km/hr)	$7.82 \cdot 10^{-3}$	$8 \cdot 10^{-3}$	1 %
ORNL & EPA Freeway LOS D cycle (Average Speed 84.64 km/hr)	$11.9 \cdot 10^{-3}$	$12.12 \cdot 10^{-3}$	1.8 %
			Average Percentage of Deviation = 1.4 %

The comparison of the field data with the simulated results of the developed models of

\dot{m}_{AFSS} , \dot{m}_{NLSAF} , \dot{m}_{NHSAF} , \dot{m}_{P1LSAF} , \dot{m}_{P1HSAF} , \dot{m}_{P2LSAF} , and \dot{m}_{P2HSAF} is statistically analyzed in Table 8.10. This statistical analysis is based on equations (8.1) through (8.5).

Table 8.10

Summary of the statistical analysis on \dot{m}_{AFSS} , \dot{m}_{NLSAF} , \dot{m}_{NHSAF} , \dot{m}_{P1LSAF} , \dot{m}_{P1HSAF} , \dot{m}_{P2LSAF} , and \dot{m}_{P2HSAF}

Table #	\bar{x}	\bar{y}	S_x	S_y	S_{xy}	r_{COD}	ϵ_R
Table 8.1	$1.127 \cdot 10^{-3} \text{ kg/s}$	$1.1305 \cdot 10^{-3} \text{ kg/s}$	$0.51 \cdot 10^{-3}$	$0.55 \cdot 10^{-3}$	$2.8 \cdot 10^{-7}$	0.996	4.3%
Table 8.2	0.425 g/s	0.426 g/s	0.077	0.077	0.0059	0.99	2.4%
Table 8.3	0.521 g/s	0.521 g/s	0.023	0.022	$0.497 \cdot 10^{-3}$	0.97	0%
Table 8.4	2.11 g/s	2.144 g/s	0.65	0.64	0.397	0.91	1.7%
Table 8.5	4.7 g/s	4.8 g/s	1.41	1.41	1.98	0.99	1.9%
Table 8.6	3 g/s	3.05 g/s	0.93	0.93	0.8	0.92	1.9%
Table 8.7	4.05 g/s	4.12 g/s	1.25	1.26	1.5	0.91	1.8%
Table 8.8	6.91 g/s	7.03 g/s	2.1	2.1	4.1	0.9	1.8%
Table 8.9	9.86 g/s	10.06 g/s	2.93	2.92	8.5	0.98	1.9%

The analytical modeling of the actual mass flow rate in diesel engines indicated in equations (5.22) through (5.28) shows that Φ , $R_{F-A \text{ stoich}}$, ρ_{Cyl} , η_V , V_{d-Cyl} , N_{Cyl} , V_S , G_t and G_d are directly proportional to the mass flow rate in diesel engines. This analytical modeling indicates as well that r_{wr} is inversely proportional to the mass flow rate in diesel engines. The model shows that the actual mass flow rate in diesel engines is directly influenced by the chemical composition of diesel fuel which is primarily Alkanes hydrocarbon compounds through the direct proportionality with $R_{F-A \text{ stoich}}$. Tables 8.1 and 8.10 point out that under the steady speed operating condition the average percentage of deviation of the simulated results from the corresponding field data is 3.7% for all Freeway cycles with 99% coefficient of determination and 4% relative error. Tables 8.2, 8.3, and 8.10 indicate that under the negative acceleration-based operating condition, the average percentage of deviation of the simulated results from the corresponding field data is 0.12 % for all standard cycles with 98% coefficient of determination and 1.2% relative error. Tables 8.4, 8.5, 8.6, 8.7, 8.8, 8.9, and 8.10 demonstrate that under the positive acceleration-based operating condition, the average percentage of deviation of the acceleration-based simulated results from the corresponding field data is 1.77 % for all standard cycles with 93.5% coefficient of determination and 1.8% relative error. The average deviation of the simulated results of these developed analytical models from field data outperforms for all standard cycles other widely recognized models such as the CMEM that shows deviation of more than 10% from field data and VT-Micro that shows deviation of about 2.5% from field data (Rakha, et al., 2003; Rakha, et al., 2012).

8.4. SIMULATION AND VALIDATION OF THE MODEL OF THE RATE OF DIESEL EXHAUST CO EMISSION

The evaluation of $R_{CO_{SST}}$ in the simulated results of the developed analytical models indicated in Tables 8.11 and 8.12 is based on the following data provided on diesel light trucks and light duty vehicles with four-stroke engines under steady speed condition: Φ , of 0.7, ρ of 1.7 kg/m³, η_v of 0.9, V_d of 0.00033 m³/d-cycle, r_{wr} of 0.323 m, and $R_{F-A \text{ stoichiometric}}$ of 0.0696. The field data of ORNL and EPA are provided for the average speed of all Freeway cycles. The data on G_t and G_d vary with the Freeway cycles as follows: (1) G_t of 1.43 and G_d of 2.5 for Freeway LOS G cycle (vehicle average speed 20.96 km/hr), (2) G_t of 1.43 and G_d of 2.5 for Freeway LOS F cycle (vehicle average speed 29.76 km/hr), (3) G_t of 1 and G_d of 2.5 for Freeway LOS E cycle (vehicle average speed 48.8 km/hr), (4) G_t of 1 and G_d of 2.5 for Freeway LOS D cycle (vehicle average speed 84.64 km/hr), (5) G_t of 1 and G_d of 2.5 for Freeway LOS A-C cycle (vehicle average speed 95.52 km/hr), (6) G_t of 1 and G_d of 2.5 for Freeway High Speed cycle (vehicle average speed 101 km/hr) (Rakha, et al., 2003; West, et al., 1997; Brzezinski, et al., 1999).

The evaluation of $R_{Unburned}$ in the simulated results is based on the following data provided on diesel light trucks and light duty vehicles with four-stroke four-cylinder engines: Φ of 0.7; the number of moles of diesel fuel no. 2 in the reactants per unit mass of working fluid, $n_{DF2 \text{ Reactants}}$, is 1; the standard enthalpy of formation of diesel fuel no. 2 in the reactants per unit mass of working fluid (in J/M) at ambient temperature, $\Delta h_{f, DF2 \text{ Reactants}}$, since the dominating largest portion of reactants enters the cylinder of the engine at quasi-ambient conditions, is 454.5*10³ J/M; the number

of moles of O₂ in the reactants per unit mass of working fluid, $n_{O_2 \text{ Reactants}}$, is 22.8; the standard enthalpy of formation of O₂ in the reactants per unit mass of working fluid (in J/M) at ambient temperature, $\Delta h_{f,O_2 \text{ Reactants}}$, is 0 J/M; the number of moles of N₂ in the reactants per unit mass of working fluid, $n_{N_2 \text{ Reactants}}$, is 85.82; the standard enthalpy of formation of N₂ in the reactants per unit mass of working fluid (in J/M) at ambient temperature, $\Delta h_{f,N_2 \text{ Reactants}}$, is 0 J/M; the number of moles of CO₂ in the products per unit mass of working fluid, $n_{CO_2 \text{ Products}}$, is 16; the standard enthalpy of formation of CO₂ in the products per unit mass of working fluid (in J/M) at ambient temperature, $\Delta h_{f,CO_2 \text{ Products}}$, since the pressure drop in the exhaust occurs instantaneously when the exhaust valve opens and the exhaust pressure becomes then atmospheric, is $393.5 \cdot 10^3$ J/M; the number of moles of H₂O in the products per unit mass of working fluid, $n_{H_2O \text{ Products}}$, is 13.6; the standard enthalpy of formation of H₂O in the products per unit mass of working fluid (in J/M) at ambient temperature, $\Delta h_{f,H_2O \text{ Products}}$, is $241.8 \cdot 10^3$ J/M; the number of moles of N₂ in the products per unit mass of working fluid, $n_{N_2 \text{ Products}}$, is 85.82; and the standard enthalpy of formation of N₂ in the products per unit mass of working fluid (in J/M) at ambient temperature, $\Delta h_{f,N_2 \text{ Products}}$, is 0 J/M (Rakha, et al., 2003; West, et al., 1997; Brzezinski, et al., 1999; Heywood, 1988).

The evaluation of $R_{CO_{SST}}$ in the simulated results is based on the following data: V_d of 3.3 L, and $M_{fuel \text{ molar}}$ of 0.0137 kg/mol, and $M_{CO \text{ molar}}$ of 0.028 kg. The evaluation of $R_{CO_{SSCO+O_2}}$ in the simulated results is based on the following data: K_{CO+O_2} of $0.0002 \text{ M}^{-1} \cdot \text{s}^{-1}$, and $[CO_2]$ of 0.0197 M. Also, the evaluation of

$R_{COSSCO+H_2O}$ in the simulated results is based on the following data: K_{CO+H_2O} of 2.25, $[CO_2]$ of 0.008 M, and $[H_2]$ of 0.008 M. Table 8.11 presents the experimental validation of the analytical models of the R_{COSS} for low speed cycles following from equations (6.18) and (7.6). It shows the comparison of the results of the developed analytical model against field data on the rate of CO total steady speed engine-out emissions for diesel fuel no. 2 for all Freeway low speed cycles.

Table 8.11
Experimental validation of the analytical model of R_{COSS} for all Freeway low speed cycles

Field Data	R_{COSS} Analytically (g/s)	$R_{COTotal}$ read from field data (g/s)	Percentage of Deviation
ORNL & EPA Freeway LOS G cycle (Average Speed 20.96 km/hr)	1.68×10^{-3}	1.65×10^{-3}	1.8 %
ORNL & EPA Freeway LOS F cycle (Average Speed 29.76 km/hr)	1.95×10^{-3}	1.95×10^{-3}	0 %
ORNL & EPA Freeway LOS E cycle (Average Speed 48.8 km/hr)	2.42×10^{-3}	2.5×10^{-3}	3.2 %
			Average of Deviation = 1.6 %

Table 8.12 presents the experimental validation of the analytical models of the R_{COSS} for high speed cycles following from equations (6.18), (7.7) and (7.8). It shows the comparison of the results of the developed analytical model against field data on the rate of CO total steady speed engine-out emissions for diesel fuel no. 2 for all Freeway high speed cycles.

Table 8.12

Experimental validation of the analytical model of R_{COSS} for all Freeway high speed cycles

Field Data	R_{COSS} Analytically (g/s)	R_{COSS} read from field data (g/s)	Percentage of Deviation
ORNL & EPA Freeway LOS D cycle (Average Speed 84.64 km/hr)	21.3×10^{-3}	20.05×10^{-3}	3.9 %
ORNL & EPA Freeway LOS A-C cycle (Average Speed 95.52 km/hr)	26.43×10^{-3}	26.5×10^{-3}	0.2 %
ORNL & EPA Freeway High Speed cycle (Average Speed 101 km/hr)	29.31×10^{-3}	29.7×10^{-3}	1.3 %
			Average of Deviation = 1.8 %

The comparison of the field data with the simulated results of the developed models of R_{COSS} , $R_{COSSCO+O_2}$, and $R_{COSSCO+H_2O}$ is statistically analyzed in Table 8.13. This statistical analysis is based on equations (8.1) through (8.5).

Table 8.13

Summary of the statistical analysis on R_{COSS} , $R_{COSSCO+O_2}$, and $R_{COSSCO+H_2O}$

Table #	\bar{x}	\bar{y}	S_x	S_y	S_{xy}	r_{COD}	ε_R
Table 8.11 and Table 8.12	13.8×10^{-3} g/s	13.725×10^{-3} g/s	12.82×10^{-3}	13.18×10^{-3}	1.686×10^{-4}	0.99	3%

The results of the developed analytical models indicated in equations (6.18), (7.6), (7.7) and (7.8) have been compared with field data provided by key experimental research authorities in this research area and the comparison shows good accuracy with ε_R of 3% which is close to the target of ε_R of 0% as indicated in Table 8.13. This comparison indicated in Tables 8.11 and 8.12 shows that the average percentage of deviation of the steady speed-based simulated results from the corresponding field data is 1.6% and 1.8% for all low speed Freeway cycles and for all high speed

Freeway cycles, respectively. The statistical analysis presented in Table 8.13 shows that the r_{COD} is as high as 99%. The average deviation of the simulated results of these developed analytical models from field data outperforms for all Freeway cycles its counterpart of other widely recognized models such as the CMEM and VT-Micro (Rakha, et al., 2012; Rakha, et al., 2003). The developed analytical models point out that R_{COSS} is directly proportional to V_d , G_t , ρ_{Cyl} and V_s . Equations (7.6), (7.7) and (7.8) imply that $R_{COSS CO+O_2}$ is considerably less than $R_{COSS CO+H_2O}$ as can be gathered from the values of K_{CO+O_2} and K_{CO+H_2O} .

8.5. SIMULATION AND VALIDATION OF THE MODEL OF THE RATE OF DIESEL EXHAUST NO_x EMISSION

The experimental validation of the developed analytical models of $R_{NOx SST}$, $R_{NOSS ZM}$, $R_{NOSS EZM}$, $R_{NOSS SEZM}$ and $R_{NO_2 SS}$ for both low speed cycles and high speed cycles is demonstrated in this section. The evaluation of the \dot{m}_{AFSS} in the simulated results of the developed analytical models indicated in Tables 8.14 and 8.15 is based on the following data provided on diesel light trucks and light commercial vehicles with four-stroke engines under the steady speed operating condition: Φ of 0.7, ρ of 1.7 kg/m³, η_v of 0.9, V_d of 0.00033 m³/d-cycle, r_{wr} of 0.323 m, and $R_{F-A stoichiometric}$ of 0.0696. The field data of ORNL and EPA are provided for the average speed of all Freeway cycles. The data on G_t and G_d vary with the Freeway cycles as follows: (1) G_t of 1.43 and G_d of 2.5 for Freeway LOS G cycle (vehicle average speed 20.96 km/hr), (2) G_t of 1.43 and G_d of 2.5 for Freeway LOS F cycle (vehicle average

speed 29.76 km/hr), (3) G_t of 1 and G_d of 2.5 for Freeway LOS E cycle (vehicle average speed 48.8 km/hr), (4) G_t of 1 and G_d of 2.5 for Freeway LOS D cycle (vehicle average speed 84.64 km/hr), (5) G_t of 1 and G_d of 2.5 for Freeway LOS A-C cycle (vehicle average speed 95.52 km/hr), (6) G_t of 1 and G_d of 2.5 for Freeway High Speed cycle (vehicle average speed 101 km/hr) (Rakha et al., 2003; West et al., 1997; Brzezinski et al., 1999).

The evaluation of the $R_{Unburned}$ is based on the following data provided on diesel light trucks and light commercial vehicles with four-stroke four-cylinder engines: Φ of 0.7; the number of moles of diesel fuel no. 2 in the reactants per unit mass of working fluid, $n_{DF2\text{ Reactants}}$, is 1; the standard enthalpy of formation of diesel fuel no. 2 in the reactants per unit mass of working fluid (in J/M) at ambient temperature, $\Delta h_{f,DF2\text{ Reactants}}$, since the dominating largest portion of reactants enters the cylinder of the engine at quasi-ambient conditions, is $454.5 \cdot 10^3$ J/M; the number of moles of O_2 in the reactants per unit mass of working fluid, $n_{O2\text{ Reactants}}$, is 22.8; the standard enthalpy of formation of O_2 in the reactants per unit mass of working fluid (in J/M) at ambient temperature, $\Delta h_{f,O2\text{ Reactants}}$, is 0 J/M; the number of moles of N_2 in the reactants per unit mass of working fluid, $n_{N2\text{ Reactants}}$, is 85.82; the standard enthalpy of formation of N_2 in the reactants per unit mass of working fluid (in J/M) at ambient temperature, $\Delta h_{f,N2\text{ Reactants}}$, is 0 J/M; the number of moles of CO_2 in the products per unit mass of working fluid, $n_{CO2\text{ Products}}$, is 16; the standard enthalpy of formation of CO_2 in the products per unit mass of working fluid (in J/M) at ambient temperature, $\Delta h_{f,CO2\text{ Products}}$, since the pressure drop in the exhaust occurs instantaneously when the exhaust valve opens and the exhaust pressure becomes then atmospheric, is $393.5 \cdot 10^3$

J/M; the number of moles of H₂O in the products per unit mass of working fluid, $n_{\text{H}_2\text{O Products}}$, is 13.6; the standard enthalpy of formation of H₂O in the products per unit mass of working fluid (in J/M) at ambient temperature, $\Delta h_{f, \text{H}_2\text{O Products}}$, is 241.8×10^3 J/M; the number of moles of N₂ in the products per unit mass of working fluid, $n_{\text{N}_2 \text{ Products}}$, is 85.82; and the standard enthalpy of formation of N₂ in the products per unit mass of working fluid (in J/M) at ambient temperature, $\Delta h_{f, \text{N}_2 \text{ Products}}$, is 0 J/M (Rakha et al., 2003; West et al., 1997; Brzezinski et al., 1999; Heywood, 1988).

The evaluation of $R_{\text{NO}_x \text{ SST}}$ in the simulated results is based on the following data: V_d of 3.3 L, and $M_{\text{fuel molar}}$ of 13.7 g/mol. The evaluation of $R_{\text{NO SST}}$ in the simulated results is based on the following data: $M_{\text{NO molar}}$ of 0.030 kg, $K_{\text{N}_2+\text{O}_2}$ of $0.00001 \text{ M}^{-1}\text{s}^{-1}$, $K_{\text{N}+\text{OH}}$ of $0.015 \text{ M}^{-1}\text{s}^{-1}$, $K_{\text{N}_2\text{O}+\text{H}}$ of $0.018 \text{ M}^{-1}\text{s}^{-1}$, $[\text{N}_2]$ of 0.799 M, $[\text{O}_2]$ of 0.199 M, $[\text{N}]$ of 0.356 M, $[\text{OH}]$ of 0.356 M, $[\text{N}_2\text{O}]$ of 0.0176 M, and $[\text{H}]$ of 0.0176 M. The evaluation of $R_{\text{NO}_2 \text{ SS}}$ in the simulated results is based on the following data: $M_{\text{NO}_2 \text{ molar}}$ of 0.046 kg, $K_{\text{NO}+\text{O}_2}$ of $6 \text{ M}^{-1}\text{s}^{-1}$, $[\text{NO}]$ of 0.0066 M, and $[\text{O}_2]$ of 0.0034 M.

Table 8.14 presents the experimental validation of the analytical models of $R_{\text{NO}_x \text{ SST}}$, $R_{\text{NO}_2 \text{ SS}}$, and $R_{\text{NO SST}}$, $R_{\text{NO SS ZM}}$, $R_{\text{NO SS EZM}}$ and $R_{\text{NO SS SEZM}}$ indicated in equations (6.36), (7.15), (6.37), (7.9), (7.11) and (7.13), respectively, for all Freeway low speed cycles. It shows the comparison of the simulated results of the developed analytical model with field data on the rate of NO_x total steady speed engine-out emission for diesel fuel no. 2 for all Freeway low speed cycles.

Table 8.14
Experimental validation of the analytical model of $R_{NOx SST}$, $R_{NO_2 SS}$, and $R_{NO SST}$ for all
Freeway low speed cycles

Field Data	$R_{NO_2 SS}$ Steady Speed Total Analytically (g/s)	$R_{NO SST}$ Steady Speed Total Analytically (g/s)	$R_{NOx SST} = R_{NO_2 SS} +$ $R_{NO SST}$ Steady Speed Total Analytically (g/s)	$R_{NOx SST}$ read from field data (g/s)	Percentage of Deviation
ORNL & EPA Freeway LOS G cycle (Average Speed 20.96 km/hr)	$0.143 \cdot 10^{-3}$	$0.337 \cdot 10^{-3}$	$0.48 \cdot 10^{-3}$	$0.5 \cdot 10^{-3}$	4 %
ORNL & EPA Freeway LOS F cycle (Average Speed 29.76 km/hr)	$0.287 \cdot 10^{-3}$	$0.563 \cdot 10^{-3}$	$0.85 \cdot 10^{-3}$	$0.85 \cdot 10^{-3}$	0 %
ORNL & EPA Freeway LOS E cycle (Average Speed 48.8 km/hr)	$0.728 \cdot 10^{-3}$	$1.559 \cdot 10^{-3}$	$2 \cdot 10^{-3}$	$1.95 \cdot 10^{-3}$	2.6 %
					Average Deviation = 2.2%

Table 8.15 presents the experimental validation of the analytical models of $R_{NOx SST}$, $R_{NO_2 SS}$, and $R_{NO SST}$, $R_{NO SS ZM}$, $R_{NO SS EZM}$ and $R_{NO SS SEZM}$ indicated in equations (6.36), (7.16), (6.37), (7.10), (7.12) and (7.14), respectively, for all Freeway high speed cycles. It shows the comparison of the simulated results of the developed analytical model with field data on the rate of NOx total steady speed engine-out emission for diesel fuel no. 2 for all Freeway high speed cycles.

Table 8.15
Experimental validation of the analytical model of $R_{NOx SST}$, $R_{NO_2 SS}$, and $R_{NO SST}$ for all
Freeway high speed cycles

Field Data	$R_{NO_2 SS}$ Steady Speed Total Analytically (g/s)	$R_{NO SST}$ Steady Speed Total Analytically (g/s)	$R_{NOx SST} = R_{NO_2 SS} +$ $R_{NO SST}$ Steady Speed Total Analytically (g/s)	$R_{NOx SST}$ read from field data (g/s)	Percentage of Deviation
ORNL & EPA Freeway LOS D cycle (Average Speed 84.64 km/hr)	$1.4 \cdot 10^{-3}$	$2.96 \cdot 10^{-3}$	$4.36 \cdot 10^{-3}$	$4.3 \cdot 10^{-3}$	0 %
ORNL & EPA Freeway LOS A-C cycle (Average Speed 95.52 km/hr)	$2.2 \cdot 10^{-3}$	$4.3 \cdot 10^{-3}$	$6.5 \cdot 10^{-3}$	$6.25 \cdot 10^{-3}$	4 %
ORNL & EPA Freeway High Speed cycle (Average Speed 101 km/hr)	$2.7 \cdot 10^{-3}$	$5.21 \cdot 10^{-3}$	$7.91 \cdot 10^{-3}$	$8 \cdot 10^{-3}$	1 %
					Average Deviation = 1.67%

The comparison of the field data with the simulated results of the developed models of $R_{NOx SST}$, $R_{NO_2 SS}$, and $R_{NO SST}$ is statistically analyzed in Table 8.16. This statistical analysis is based on equations (8.1) through (8.5).

Table 8.16
Summary of the statistical analysis on $R_{NOx SST}$, $R_{NO_2 SS}$, and $R_{NO SST}$

Table #	\bar{x}	\bar{y}	S_x	S_y	S_{xy}	r_{COD}	ϵ_R
Table 8.14 and Table 8.15	$3.675 \cdot 10^{-3}$ g/s	$3.6417 \cdot 10^{-3}$ g/s	$3.08 \cdot 10^{-3}$	$3.06 \cdot 10^{-3}$	$9.4 \cdot 10^{-6}$	0.999	1.75%

This comparison indicated in Tables 8.14 and 8.15 points out that the average percentage of deviation of the steady speed-based simulated results from the

corresponding field data is 2.2% and 1.67% for all low speed Freeway cycles and for all high speed Freeway cycles, respectively. The statistical analysis presented in Table 8.16 shows with r_{COD} of 99.9% that the ε_R is 1.75% which is close to the target of ε_R of 0%. The developed analytical models point out that $R_{NOx.SST}$ is proportional to ρ_{Cyl} , V_d and V_s . The developed models indicate that NO_2 emission rate is about one third of the NO emission rate. This is in accord with the fact that NO in the diesel exhaust is rapidly oxidized into NO_2 and it has been found experimentally that the final concentration of $[NO_2]$ at equilibrium is usually about half the concentration of NO (Gilbert et al., 2011; Brown et al., 2009; Villarba, 2013). The developed models indicate as well that the extended Zeldovich mechanism is the dominant reaction in the NO formation. The average deviation of the simulated results of these developed analytical models from field data outperforms for all Freeway cycles widely recognized models such as the CMEM and VT-Micro (Rakha et al., 2003; Rakha, et al., 2012).

8.6. SIMULATION AND VALIDATION OF THE MODEL OF THE RATE OF DIESEL EXHAUST HC EMISSION

The experimental validation of the analytical model of $R_{HC.SS}$ for both low speed cycles and high speed cycles is presented in this section, respectively. The field data were extracted from the following references (Rakha, et al., 2003; West, et al., 1997; Brzezinski, et al., 1999). Table 8.17 presents the experimental validation of the analytical models of the $R_{HC.SS}$ for low speed cycles indicated in equation (7.17) for four-stroke engines.

Table 8.17
Experimental validation of the analytical model of R_{HCSS} for low speed Freeway cycles

Field Data	Analytically (g/s)	read from field data (g/s)	Percentage of Deviation
ORNL & EPA Freeway LOS G cycle (Average Speed 20.96 km/hr)	$0.4 \cdot 10^{-3}$	$0.4 \cdot 10^{-3}$	0 %
ORNL & EPA Freeway LOS F cycle (Average Speed 29.76 km/hr)	$0.4 \cdot 10^{-3}$	$0.4 \cdot 10^{-3}$	0 %
ORNL & EPA Freeway LOS E cycle (Average Speed 48.8 km/hr)	$0.6 \cdot 10^{-3}$	$0.6 \cdot 10^{-3}$	0 %
			Average Percentage of Deviation = 0 %

Table 8.18 presents the experimental validation of the analytical models of the R_{HCSS} for high speed cycles indicated in equation (7.18).

Table 8.18
Experimental validation of the analytical model of R_{HCSS} for high speed Freeway cycles

Field Data	Analytically (g/s)	read from field data (g/s)	Percentage of Deviation
ORNL & EPA Freeway LOS D cycle (Average Speed 84.64 km/hr)	$1.4 \cdot 10^{-3}$	$1.3 \cdot 10^{-3}$	7.7 %
ORNL & EPA Freeway LOS A-C cycle (Average Speed 95.52 km/hr)	$1.7 \cdot 10^{-3}$	$1.7 \cdot 10^{-3}$	0 %
ORNL & EPA Freeway High Speed cycle (Average Speed 101 km/hr)	$1.8 \cdot 10^{-3}$	$1.9 \cdot 10^{-3}$	5 %
			Average Percentage of Deviation = 4 %

The comparison of the field data with the simulated results of the developed model of R_{HCSS} is statistically analyzed in Table 8.19. This statistical analysis is based on equations (8.1) through (8.5).

Table 8.19
Summary of the statistical analysis on R_{HCSS}

Table #	\bar{x}	\bar{y}	S_x	S_y	S_{xy}	r_{COD}	ε_R
Table 8.17 and Table 8.18	1.05×10^{-3} g/s	1.05×10^{-3} g/s	6.6×10^{-4}	6.7×10^{-4}	4×10^{-7}	0.83	2%

This comparison indicated in Tables 8.17 and 8.18 points out that the average percentage of deviation of the steady speed-based simulated results from the corresponding field data is 0% and 4% for all low speed Freeway cycles and for all high speed Freeway cycles, respectively. The statistical analysis presented in Table 8.19 shows with r_{COD} of 83% that the ε_R is 2% which is close to the target of ε_R of 0%. The developed analytical models indicated in equations (7.17), (7.18) and (5.22) point out that R_{HCSS} is proportional to ρ_{Cyl} , V_d and V_s . The average deviation of the simulated results of these developed analytical models from field data outperforms for all Freeway cycles widely recognized models such as the CMEM and VT-Micro (Rakha et al., 2003; Rakha, et al., 2012).

8.7. SIMULATION AND VALIDATION OF THE MODEL OF THE PERCENTAGE OF UNBURNED DIESEL FUEL

The experimental validation of the analytical model of $R_{Unburned}$ presented in equation

(7.5) is presented in Table 8.20 for four-stroke engines. The field data for experimental validation of this model were extracted from the following reference (Velmurugan and Loganathan, 2011).

Table 8.20
Experimental validation of the analytical model of $R_{Unburned}$

Field Data	$R_{Unburned}$ Analytically	$R_{Unburned}$ read from field data	Percentage of Deviation
At the Average Speed 20.96 km/hr of ORNL & EPA Freeway LOS G cycle	0.01254 %	0.0112 %	12 %
At the Average Speed 29.76 km/hr of ORNL & EPA Freeway LOS F cycle	0.012436 %	0.0111 %	12 %
At the Average Speed 48.8 km/hr of ORNL & EPA Freeway LOS E cycle	0.012516 %	0.0116 %	7.8 %
			Average Percentage of Deviation = 10.6 %

The comparison of the field data with the simulated results of the developed model of $R_{Unburned}$ is statistically analyzed in Table 8.21. This statistical analysis is based on equations (8.1) through (8.5).

Table 8.21
Summary of the statistical analysis on $R_{Unburned}$

Table #	\bar{x}	\bar{y}	S_x	S_y	S_{xy}	r_{COD}	ϵ_R
Table 8.20	0.012497 %	0.0113 %	0.000055 %	0.00027 %	6.8×10^{-9}	0.7	10.6%

This comparison indicated in Table 8.20 points out that the average percentage of deviation of the steady speed-based simulated results from the corresponding field data is 10.6% for all low speed Freeway cycles. The statistical analysis presented in

Table 8.21 shows with r_{COD} of 70% that the ε_R is 10.6% which is close to the target of ε_R of 0%. The developed analytical model indicated in equation (7.5) points out that $R_{Unburned}$ is proportional to N_{Cyl} .

8.8. SIMULATION AND VALIDATION OF THE MODEL OF THE BRAKE POWER OF DIESEL ENGINE

The experimental validation of the analytical model of Γ_B presented in equation (5.42) is presented in Table 8.22 for four-stroke engines. The field data for experimental validation of this model were mainly extracted from the following reference (Rakha, et al., 2012).

Table 8.22
Experimental validation of the analytical model of Γ_B

Vehicle	Engine Code	Engine Specifications		Reference	P_B read from engine specifications (under the idling condition)	P_B analytically (under the idling condition)	Deviation
Chevrolet S-10	General Motors engine 262 cu in (4.3 L) 90° V6	displaced volume	4.3 L	(GM Powertrain)	120 kW	133 kW (Based on efficiency of 90% (Rakha, et al., 2012), and that maximum torque occurs at 2400 rpm onwards (Heywood, 1988))	10.8 %
		maximum torque	319 N·m @ 2400 rpm				
		number of cylinders	6				
		number of strokes	4				
		brake power	120 kW (160 hp) @ 4000 rpm				
Ford Windstar	Ford engine 3.8 L Essex V6	displaced volume	3.8 L	(Ford Parts; Ford Essex V6 Engine; Ford Motors)	150 kW	163 kW (Based on efficiency of 90% (Rakha, et al., 2012), and that maximum torque occurs at 3000 rpm onwards (Heywood, 1988))	8.6 %
		maximum torque	312 N·m @ 3000 rpm				
		number of cylinders	6				
		number of strokes	4				
		brake power	150 kW (200 hp) @ 5000 rpm				
Chevy Blazer	General Motors Vortec Engine 4.3 L (262 cu in) 4300 90° V6 truck engine	displaced volume	4.3 L	(GM Powertrain)	149 kW	146.6 kW (Based on efficiency of 90% (Rakha, et al., 2012), and that maximum torque occurs at 2540 rpm onwards (Heywood, 1988))	1.5 %
		maximum torque	339 N·m @ 2540 rpm.				
		number of cylinders	6				
		number of strokes	4				
		brake power	149 kW (200 hp) @ 4130 rpm				
Average of Deviation = 6.9 %							

The comparison of the field data with the simulated results of the developed model of Γ_B is statistically analyzed in Table 8.23. This statistical analysis is based on equations (8.1) through (8.5).

Table 8.23
Summary of the statistical analysis on Γ_B

Table #	\bar{x}	\bar{y}	S_x	S_y	S_{xy}	r_{COD}	ε_R
Table 8.22	147.5 kW	139.7 kW	15.02	17.039	218.465	0.73	7%

This comparison indicated in Table 8.22 points out that the average percentage of deviation of the simulated results from the corresponding field data is 6.9%. The statistical analysis presented in Table 8.23 shows with r_{COD} of 73% that the ε_R is 7% which is close to the target of ε_R of 0%. The developed analytical model indicated in equation (5.42) points out that Γ_B is proportional to V_s , G_t and G_d . This analytical model indicates as well that Γ_B is inversely proportional to r_{wr} .

8.9. SIMULATION AND VALIDATION OF THE INTAKE MANIFOLD GAS SPEED DYNAMICS MODEL

The experimental validation of the analytical model of the air acceleration in intake manifold, \dot{c}_{im} , indicated in equation (7.2) is presented in this section. A case study has been conducted in this regard using the following field data presented in Table 8.24:

Table 8.24
Field data of a case study conducted on \dot{c}_{im}

Parameter	Value extracted from field data	Reference
\dot{c}_{im}	0.15 m/s ² , in average (i.e. $\frac{0+0.3}{2}$ m/s ²) for slow to medium acceleration of flow	(Ibrahim and Dunn, 2006)
P_i	0.0985*10 ⁶ N/m ²	(Sulaiman et al., 2010)
$\frac{D}{L}$	$\frac{80\text{ mm}}{400\text{ mm}}$, i.e. 0.2	(Edelbrock Pro-Flo XT EFI LS1 Chevy Intake Manifold Systems, 2013)
\dot{Q}_{im}	40*10 ⁻³ * N_{Cyl} m ³ /s	(Sulaiman et al., 2010)
ζ	0.55	(Sulaiman et al., 2010)
ρ	1.7 m/s ³	(Eaton M90 Supercharger)

An intercooler is usually used at the outlet of the supercharger compressor in order to maintain the air temperature drawn into the intake manifold to be below 35°C in average under heavy driving conditions (Holmgren, 2005). The maximum outlet pressure of the supercharger compressor is usually limited to 1.5 bar (Hiellier and Coomber, 2004). The value of P_i indicated in Table 8.24 is not the maximum outlet pressure of the supercharger compressor since the intercooler reduces the temperature of the supercharged higher density air so that the P_i is reduced according to the Ideal Gas Law. Following from and Table 8.24, \dot{c} indicated in equation (7.2) is thus evaluated as follows:

$$\dot{c} = \frac{\dot{Q}_{im}}{\frac{\pi}{4} D^2} \quad (8.6)$$

Following from equation (7.2), equation (8.6) and Table 8.24, the \dot{c}_{im} for four-cylinder Chevy engines is 131,000 $\mu\text{m/s}^2$. The positive sign of \dot{c}_{im} implies accelerated

flow. Since diesel engines are usually operated at wide-open throttle, the corresponding intake manifold air flow acceleration ranges from slow to medium acceleration of air flow. The comparison of the field data with the simulated results of the developed model of \dot{c}_{im} is statistically analyzed in Table 8.25. This statistical analysis is based on equation (8.5).

Table 8.25
Summary of the statistical analysis on \dot{c}_{im}

Table #	\bar{x}	\bar{y}	ε_R
Table 8.24	0.131 m/s ²	0.15 m/s ²	12.7%

Therefore, the ε_R of 12.7% on \dot{c}_{im} is an order of magnitude of deviation that is less than that of well known models in the field of ITS and vehicle powertrain modeling such as the CMEM (Rakha et al., 2012). Equation (7.2) has shown that the influence of P_i , ρ , and L on \dot{c}_{im} is significantly as much as 90%. Equation (7.2) has shown as well that the influence of ζ , c , and D is insignificantly as little as 10%. The developed analytical model of \dot{c}_{im} addresses flaws exist in corresponding models presented in key references in this research area, such as (Heywood, 1988).

8.10. SIMULATION AND VALIDATION OF THE MODEL OF THE POWER REQUIRED TO DRIVE THE SUPERCHARGING DIESEL CENTRIFUGAL COMPRESSOR

The experimental validation of the analytical model of the power required to drive the supercharging diesel centrifugal compressor, \dot{W}_C , indicated in equation (4.15) is presented in this section. A case study has been conducted in this regard using the following field data presented in Table 8.26:

Table 8.26
Field data of a case study conducted on \dot{W}_C

Parameter	Value extracted from field data	Reference
$\frac{P_{\text{Compressor}}}{P_{\text{Amb}}}$	1.45	(Eaton M90 Supercharger)
ρ	1.7 m/s ³	(Eaton M90 Supercharger)
Q_{im}	350 m ³ /hr, i.e. \dot{m}_i of 0.2 kg/s	(Eaton M90 Supercharger)
η_{CM}	85%	(Hill and Peterson, 1992)
$\frac{U_2}{e_s}$	0.65, i.e. U_2 of 223 m/s	(Hill and Peterson, 1992)
$\frac{c_{r2}}{U_2}$	0.3	(Hill and Peterson, 1992)
β_2	45°	(Hill and Peterson, 1992)
\dot{W}_C	9 hp, i.e. 6.7 kW	(Hill and Peterson, 1992; Lysholm Supercharger LYS 2300 AX)

Following from equation (4.15) and Table 8.26, \dot{W}_C for Eaton M90 Supercharger for Chevy engines is 6.9 kW. The comparison of the field data with the simulated results

of the developed model of \dot{W}_C is statistically analyzed in Table 8.27. This statistical analysis is based on equation (8.5).

Table 8.27
Summary of the statistical analysis on \dot{W}_C

Table #	\bar{x}	\bar{y}	ε_R
Table 8.26	6.9 kW	6.7 kW	3%

Therefore, the ε_R of 3% on \dot{W}_C is an order of magnitude of deviation that is less than that of well known models in the field of ITS and vehicle powertrain modeling such as the CMEM (Rakha et al., 2012). Equation (4.15) has shown that \dot{m}_{air} is directly proportional to \dot{W}_C . It has shown as well that c_{r2} is inversely proportional to \dot{W}_C . The developed analytical model of \dot{W}_C addresses flaws exist in corresponding models presented in key references in this research area, such as (Heywood, 1988).

8.11. SIMULATION AND VALIDATION OF THE MODEL OF THE EFFICIENCY OF THE SUPERCHARGING DIESEL CENTRIFUGAL COMPRESSOR

The experimental validation of the analytical model of the efficiency of the supercharging diesel centrifugal compressor, η_{CM} , indicated in equation (4.56) is presented in this section. A case study has been conducted in this regard using the following field data presented in Table 8.28:

Table 8.28
Field data of a case study conducted on η_{CM}

Parameter	Value extracted from field data	Reference
I_C	2 kg.m ²	(Spirig et al., 2002; Botros and Ganesan, 2008)
α_C	500 rad/s ²	(Rao, 2011)
N_{CM}	4500 rpm	(Eaton M90 Supercharger)
\dot{W}_C	9 hp, i.e. 6.7 kW	(Hill and Peterson, 1992)
η_{CM}	85%	(Eaton M90 Supercharger)

Following from equation (4.56) and Table 8.28, η_{CM} for Eaton M90 Supercharger for four-stroke Chevy engines is 78%. The comparison of the field data with the simulated results of the developed model of η_{CM} is statistically analyzed in Table 8.29. This statistical analysis is based on equation (8.5).

Table 8.29
Summary of the statistical analysis on η_{CM}

Table #	\bar{x}	\bar{y}	ε_R
Table 8.28	78%	85%	8%

Therefore, the ε_R of 8% on η_{CM} is an order of magnitude of deviation that is less than that of well known models in the field of ITS and vehicle powertrain modeling such as the CMEM (Rakha et al., 2012). Equation (4.56) has shown that \dot{W}_C is directly

proportional to η_{CM} . It has shown as well that I_C , α_C and N_{CM} are inversely proportional to η_{CM} .

8.12. SIMULATION AND VALIDATION OF THE MODEL OF THE SUPERCHARGED AIR DENSITY

In order to experimentally validate the analytical model of the supercharged air density in diesel engines, ρ , indicated in equations (7.3) and (3.135), the following actual values of the parameters indicated in equation (3.135) are used:

- (i) As to P_2 , the average value of actual pressure ratio in the performance map of the Eaton M90 Supercharger that is incorporated in GM Trucks is used, i.e. $1.45 P_{Ambient}$ where $P_{Ambient}$ is $0.101 \times 10^6 \text{ N/m}^2$ (Eaton M90 Supercharger);
- (ii) As to R , the value of $287.058 \text{ J.kg}^{-1}.\text{K}^{-1}$ is used;
- (iii) As to T_2 , the average value of the temperature at the exit of the supercharging compressor in the performance map of the Lysholm Supercharger LYS 2300 AX is used, i.e. 100°C (Lysholm Supercharger LYS 2300 AX);
- (iv) As to $\eta_{Intercooler}$, the average value of 0.72 is used (RB Racing RSR Intercoolers);
- (v) As to $T_{Equator}$, the value of 27°C is used (Kottek et al., 2006);
- (vi) As to $L_{Latitude}$, the value of 36° North for Oak Ridge National Laboratory (ORNL) in Oak Ridge, Tennessee, USA is used;
- (vii) As to $A_{Altitude}$, the value of 259 m above sea for Oak Ridge National Laboratory (ORNL) in Oak Ridge, Tennessee, USA is used.

By substituting these seven values in equation (3.135), the resulting value of ρ is 1.65 kg/m^3 . This resulting value of the supercharged air density in diesel engines, ρ ,

has been used in the experimental validation of the analytical formulation of the actual mass flow rate of fuel in diesel engines under the steady speed condition in (kg/s), \dot{m}_{AFSS} , of equation (5.22) indicated in Table 8.1 using the field data gathered at ORNL that were extracted from the following references (Rakha, et al., 2003; West, et al., 1997; Brzezinski, et al., 1999). Tables 8.1 and 8.10 show that under the steady speed operating condition the average percentage of deviation of the simulated results from the corresponding field data is 3.7% for all Freeway cycles with 99% coefficient of determination and 4% relative error. Therefore, the ε_R of 4% on ρ is an order of magnitude of deviation that is less than that of well known models in the field of ITS and vehicle powertrain modeling such as the CMEM (Rakha et al., 2012).

8.13. SIMULATION AND VALIDATION OF THE MODEL OF THE IN-CYLINDER GAS SPEED DYNAMICS

The experimental validation of the model of the in-cylinder gas speed dynamics is presented in this section. A case study has been conducted in this regard using the following field data indicated in Table 8.30 for maximum in-cylinder pressure, P_{Cyl} :

Table 8.30

Field data of a case study conducted on \dot{c}_{Cyl}

Parameter	Value extracted from field data	Reference
P_{Cyl}	$40 \cdot 10^5 \text{ N/m}^2$	(Dec, 2009)
$\frac{D_{Cyl}}{L_{Stroke}}$	$\frac{88 \text{ mm}}{92 \text{ mm}}$, i.e. 0.96	(Edelbrock Pro-Flo XT EFI LS1 Chevy Intake Manifold Systems)
Q_{Cyl}	$40 \cdot 10^{-3} \text{ m}^3/\text{s}$	(Sulaiman, 2010)
ζ_{In-Cyl}	0.55	(Sulaiman, 2010)
ρ_{Cyl}	1.7 m/s^3	(Eaton M90 Supercharger)
\dot{c}_{Cyl}	23 m/s^2 for highly accelerated flow	(Ibrahim and Dunn, 2006)

The \dot{c}_{Cyl} indicated in equations (5.15) and (7.4) can be thus evaluated using equation (8.6). Following from equation (5.15), equation (8.6) and Table 8.30, the \dot{c}_{Cyl} for Chevrolet S-10 2.2 L Isuzu Diesel I4 engine with Edelbrock Pro-Flo XT LS1 EF1 Intake Manifold is $-25,576,171 \mu\text{m/s}^2$. The negative sign of \dot{c}_{Cyl} implies decelerated flow. The comparison of the field data with the simulated results of the developed model of \dot{c}_{Cyl} is statistically analyzed in Table 8.31. This statistical analysis is based on equation (8.5).

Table 8.31

Summary of the statistical analysis on \dot{c}_{Cyl}

Table #	\bar{x}	\bar{y}	ε_R
Table 8.30	25.576 m/s^2	23 m/s^2	11%

Therefore, the ε_R of 11% on \dot{c}_{Cyl} is an order of magnitude of deviation that is less than that of well known models in the field of ITS and vehicle powertrain modeling such as the CMEM (Rakha et al., 2012). Equation (5.15) has shown that P_{Cyl} , ζ_{In-Cyl} and c_{Cyl} are directly proportional to \dot{c}_{Cyl} . It has shown as well that ρ_{Cyl} , L_{Stroke} and D_{Cyl} are inversely proportional to \dot{c}_{Cyl} . Equation (5.15) has shown that the influence of P_{Cyl} , L_{Stroke} and ρ_{Cyl} on \dot{c}_{Cyl} is significantly as much as 99%. Equation (5.15) has shown as well that the influence of ζ_{In-Cyl} , c_{Cyl} and D_{Cyl} on \dot{c}_{Cyl} is insignificantly as little as less than 1%. The developed analytical model of \dot{c}_{Cyl} addresses flaws exist in corresponding models presented in key references in this research area, such as (Heywood, 1988).

CHAPTER 9

CONCLUSIONS AND FUTURE WORK

9.1 SUMMARY AND CONCLUSION

This study has developed and experimentally validated an instantaneous, gear-shifting-based and microscopic analytical model to simulate the diesel powertrain fuel consumption rate under accelerating, cruising and decelerating driving conditions and regulated emissions rate under cruising driving condition for trucks. In order to get these 1st and 2nd objectives of research achieved, the study has developed a framework for this modeling which has been elucidated in the research philosophy indicated in Chapter 1. The 3rd and last objective of developing an interface facility to give instantaneous fuel consumption and regulated emissions rate of trucks has been achieved as well through developing a simplified version of the developed analytical models for fitting the INTEGRATION software package of Virginia Tech. This study has shown these three objectives are achievable and has achieved them.

The analytical model of diesel powertrain intake manifold has been developed in Chapter 3 which has contributed to the implementation of the 1st pillar of the research philosophy adopted in this study endeavouring to achieve the 1st objective in this research. The analytical model of the supercharging diesel centrifugal compressor with vanes-based diffuser has been developed in Chapter 4 which has contributed to the implementation of the 1st pillar of the research philosophy adopted in this study endeavouring to achieve the 1st objective in this research. In Chapter 5 the analytical model of multi-cylinder supercharged diesel engine has been developed contributing to the implementation of the 1st and 2nd pillars of the research philosophy adopted in

this study with respect to the analytical modeling of the diesel powertrain fuel consumption rate in an endeavour to achieve the 1st objective in this research. The analytical model of diesel engine fuel consumption rate has been thus developed in Chapter 5 contributing to achieving the 1st objective of this research with respect to the analytical modeling of the diesel powertrain fuel consumption rate. With r_{COD} of 99.6% and ε_R of 4.3%, the average percentage of deviation of the steady speed-based simulated results from the corresponding field data on \dot{m}_{AFSS} is 3.7% for all Freeway cycles. With r_{COD} of 98% and ε_R of 1.2%, the average percentage of deviation of the acceleration-based simulated results from the corresponding field data under negative acceleration is 0.12 %. Under positive acceleration, the average percentage of deviation of the acceleration-based simulated results from the corresponding field data is 1.77 % with r_{COD} of 93.5% ε_R of 1.8%.

In Chapter 6 the analytical model of diesel powertrain exhaust system has been developed contributing to the implementation of the 1st and 2nd pillars of the research philosophy adopted in this study with respect to the analytical modeling of the diesel powertrain regulated emissions rate in an endeavour to achieve the 1st objective in this research. The analytical model of diesel engine regulated emissions rate has been thus developed in Chapter 6 contributing to achieving the 1st objective of this research with respect to the analytical modeling of the diesel powertrain regulated emissions rate. With r_{COD} of 99% and ε_R of 3%, the average percentage of deviation of the steady speed-based simulated results from the corresponding field data on R_{COSSST} , $R_{COSSCO+O_2}$, and $R_{COSSCO+H_2O}$ is 1.6% and 1.8% for all low speed Freeway cycles and for all high speed Freeway cycles, respectively. The study has pointed out with r_{COD}

of 99.9% and ε_R of 1.75% that the average percentage of deviation of the steady speed-based simulated results from the corresponding field data on $R_{NOx\text{ SST}}$, $R_{NO_2\text{ SS}}$, and $R_{NO\text{ SST}}$ is 2.2% and 1.67% for all low speed Freeway cycles and for all high speed Freeway cycles, respectively. With r_{COD} of 83% and ε_R of 2%, the average percentage of deviation of the steady speed-based simulated results from the corresponding field data on $R_{HC\text{ SS}}$ is 0% and 4% for all low speed Freeway cycles and for all high speed Freeway cycles, respectively.

Chapter 7 has presented based on the sensitivity analysis the simplified version of the analytical models developed in this study contributing to the implementation of the 3rd pillar of the research philosophy adopted in this study in an endeavour to achieve the 1st objective in this research. Chapter 7 has contributed to achieving the 1st objective of this research with respect to the analytical modeling of both the diesel powertrain fuel consumption rate and the diesel regulated emissions rate. In Chapter 8, the simulated results and experimental validation of the analytical models developed in this study have been pointed out achieving the 2nd objective of this research. In addition, the MATLAB programming code and the interface facility developed in this study on diesel fuel consumption rate, CO emission rate, NOx emission rate, unburned diesel hydrocarbon and HC emission rate which are provided in Appendix A, Appendix B, Appendix C, Appendix D and Appendix E have achieved the 3rd objective of this research. The models developed in this study are limited to supercharged diesel trucks and light duty vehicles fuelled by diesel fuel no. 2.

9.2. MAJOR CONTRIBUTIONS

The major contributions of this study are as follows:

- i. Unprecedented experimentally validated analytical model of diesel regulated emissions rate;
- ii. Unprecedented experimentally validated analytical model of diesel fuel consumption rate;
- iii. Instantaneous, gear-shifting-based and microscopic analytical models directly account for the individual vehicle characteristics and for the forces acting on the vehicle;
- iv. Widely valid models which are not restricted to a specific dataset unlike empirical models which are only valid for the set of data based on which they were built and unlike statistical models which need recalibration with each dataset;
- v. Mathematically explainable models so that they can be extended to other types of vehicle;
- vi. The average percentage of deviation of the developed models of fuel consumption and regulated emissions rates outperforms widely recognized models such as the CMEM and VT-Micro;
- vii. Unprecedented experimentally validated analytical models of engine brake power, supercharging compressor mechanical efficiency, and supercharged air density;
- viii. Unprecedented experimentally validated analytical models of the intake manifold gas speed dynamics, in-cylinder gas speed dynamics, and supercharging compressor power that address and correct flaws exist in

corresponding models presented in key references in this research area, such as (Heywood, 1988);

- ix. The study has suggested two new classifications of modeling of fuel consumption and emission rate: formulation approach-based modeling and main input variable-based modeling;
- x. The developed analytical models are an efficient tool for determining the fuel optimal control signals for each requested vehicle speed;
- xi. The developed analytical models are an efficient tool for quickly judging whether the corresponding experimental measurements make sense or not;
- xii. The developed analytical models show which chemical reaction within the powertrain kinetically influences significantly the regulated emissions rate;
- xiii. The developed models can help in cost-effectively estimating the actual rate of fuel consumption and therefore the exhaust emission rate for the environmentally sustainable development and assessment of diesel powertrains technologies and of diesel automotive pollution controls;
- xiv. The developed models quantify a source of air pollution that negatively affects the atmosphere helping in evaluating the relative risks associated therewith.

9.3. SUGGESTIONS FOR FUTURE WORK

The development of diesel powertrain technologies is a promising research area. Thus, this study suggests the following future work:

1. Extending the developed analytical models of diesel regulated emissions rate for the accelerating and decelerating modes of vehicle driving;

2. Conducting extensive sensitivity analysis on the developed simplified analytical models for further simplifying these developed models.

REFERENCES

- Aceves, S.M., Flowers, D.L., Westbrook, C.K., Smith, J.R., Pitz, W., Dibble, R., Christensen, M. and Johansson, B. (2000). A multi-zone model for prediction of HCCI combustion and emissions. *SAE 2000 World Congress, Detroit, MI, USA*, paper # 2000-01-0327.
- Aceves, S.M., Flowers, D.L., Martinez-Frias, J., Smith, J.R., Dibble, R., Au, M. and Girard, J. (2001). HCCI combustion: analysis and experiments. *SAE International*, paper # 2001-01-2077.
- Ahmed, S.A. (2010). An experimental investigation of the flow field between two radial plates. *Canadian Aeronautics and Space Journal*, vol. 65, no. 1.
- Ahn, K. (1998). *Microscopic Fuel Consumption and Emission Modelling*. Master of Science Thesis, Virginia Polytechnic Institute and State University.
- Ahn, K. (2002). *Modelling Light Duty Vehicle Emissions Based on Instantaneous Speed and Acceleration Levels*. PhD Dissertation, Virginia Polytechnic Institute and State University.
- Ahn, K. and Trani, A. (1999). Microscopic fuel consumption and emission modelling. In *Proceedings of the 78th Annual Meeting of the Transportation Research Board*, Washington, D.C.
- Ahn, K., Rakha, H., Trani, A. and Van Aerde, M. (2002). Estimating vehicle fuel consumption and emissions based on instantaneous speed and acceleration levels. *Journal of Transportation Engineering*, vol. 128, no. 2, pp. 182-190.
- Akcelik, R. (1985). An interpretation of the parameters in the simple average travel speed model of fuel consumption. *Australian Road Research*, vol. 15, pp. 46-49.
- An, F. and Barth, M. (1997). Development of a comprehensive Modal emissions model: operating under hot-stabilized conditions. *Transportation Research Record*, vol. 1587, pp. 52-62.
- Ang, B.W. (1990). The effects of maintenance on the fuel efficiency of public buses. *Energy*, vol. 15, no. 12, pp. 1099-1105.
- Arsie, I., Di Genova, F., Mogavero, A., Pianese, C., Rizzo, G., Caraceni, A., Cioffi, P. and Flauti, G. (2006). Multi-zone predictive modelling of common-rail multi-injection diesel engines. *SAE International*, paper # 2006-01-1384.
- Arsie, I., Di Genova, F., Pianese, C., Rizzo, G., Caraceni, A., Cioffi, P. and Flauti, G. (2005). Thermodynamic modelling of jet formation and combustion in common rail multi-jet diesel engines. *SAE International*, paper # 2005-01-1121.
- Arsie, I., Pianese, C. and Sorrentino, M. (2007). Control parameters optimization in automotive diesel engines via two zone modelling. In *Proceedings of the Fifth IFAC Symposium on Advances in Automotive Control*, Advances in Automotive Control, vol. 5, no. 1.
- Assanis, D., Delagrammatikas, G., Fellini, R., Filipi, Z., Liedtke, J., Michelena, N., Papalambros, P., Reyes, D., Rosenbaum, D., Sales, A. and Sasena, M. (1999). An optimization approach to hybrid electric propulsion system design. *Mechanics of Structures and Machines*, vol. 27, no. 4, pp. 393-421.

- Assanis, D.N., Filipi, Z.S., Gravante, S., Grohnke, D., Gui, X., Louca, L.S., Rideout, G.D., Stein, J.L. and Wang, Y. (2000). Validation and use of Simulink integrated, high fidelity, engine-invehicle simulation of the international class VI truck. In Proceedings of the SAE World Congress, 2000, SAE International, paper # 2000-01-0288.
- Autili, M. and Pelliccione, P. (2008). Towards a graphical tool for refining user to system requirements. *Electronic Notes in Theoretical Computer Science*, vol. 211, pp. 147-157.
- Bachman, W. and Sarasua, W. (1996). Geographic information framework for modelling mobile-source emissions. *Transportation Research Record*, vol. 1551, pp. 123-133.
- Bachman, W. and Sarasua, W. (2000). Modelling regional mobile source emissions in a geographic information system framework. *Transportation Research Part C: Emerging Technologies*, vol. 8, pp. 205-229.
- Bala showry, K., Sita Rama Raju, A.V. (2010). Simulation of injection angles on combustion performance using multiple injection strategy in HSDI diesel engine by CFD. *International Journal of Engineering and Technology*, vol. 2, no. 4, pp. 234-239.
- Barba, C., Burkhardt, C., Boulouchos, K. and Bargende, M. (2000). A phenomenological combustion model for heat release rate prediction in high-speed DI diesel engines with common rail injection. *SAE International*, paper # 2000-01-2933.
- Bar–Meir, G. (2002). *Fundamentals of compressible fluid mechanics*. Free Software Foundation, Inc.
- Barth, M., An, F., Norbeck, J. and Ross, M. (1996). Model emission modelling: a physical approach. *Transportation Research Record*, no. 1520.
- Barth, M., Norbeck, J. and Ross, M. (1998). National cooperative highway research program project 25-11: development of a comprehensive modal emissions model. In Proceedings of the 77th Annual Meeting of the Transportation Research Board, Washington, D.C.
- Bazari, Z. (1994). Diesel exhaust emissions prediction under transient operating conditions, *SAE International*, paper # 940666.
- Biteus, J. (2002). *Mean Value Engine Model of a Heavy Duty Diesel Engine*, Research Report, Linköping universitet, Sweden.
- Botros, K.K. and Ganesan, S.T. (2008). Dynamic instabilities in industrial compression systems with centrifugal compressors. Proceedings of the Thirty-Seventh Turbo-machinery Symposium, pp. 119-132.
- Boxill, S.A. and Yu, L. (2000). *An evaluation of traffic simulation models for supporting ITS development*. Technical Report # SWUTC/00/167602-1, Center for Transportation Training and Research, Texas Southern University.
- Bracco, F.V. (1985). Modelling of engine sprays. *SAE International*, paper # 850394.
- Bramston-Cook, R., Scensy, M. and Brittain, R.D. (2000) Determination of Hydrocarbons in diesel exhaust. International Symposium on the Measurement of Toxic and Related Air Pollutants, USA.
- Brown, T.L., LeMay, H.E., Bursten, B.E., Murphy, C.J. (2009). Chemistry: the central science. Pearson Prentice Hall.

- Brzezinski, D.J., Glover, E., and Enns, P. (1999). The determination of hot running emissions from FTP bag emissions. *MOBILE6 Stakeholder Review Document, Report # M6.STE.002*, US EPA, Ann Arbor, Michigan.
- Butler, K.L., Ehsani, M. and Kamath, P. (1999). A Matlab-based modelling and simulation package for electric and hybrid electric vehicle design. *IEEE Transactions on Vehicular Technology*.
- Butschek, M. (2000) *Modelling and diagnosis of leakages in the air intake path of an automotive diesel engine*. Master's Thesis, Fachhochschule Trier.
- Cacciari, A. and Piancastelli, L. (2001). Fuel consumption optimisation and power requirement reduction via multiple speed gearbox and automatic selection system for an automotive application. *XII Associazione Nazionale Disegno di Macchine (ADM) International Conference, Rimini, Italy*, pp. G144-G152.
- Canova, M., Chiara, F., Rizzoni, G. and Wang, Y. (2010). Model-based characterization and analysis of diesel engines with two-stage turbochargers. SAE 2010 World Congress & Exhibition, April 2010, Detroit, MI, USA, SAE International, paper # 2010-01-1220.
- Cappiello, A., Chabini, I., Lue, A., Zeid, M. and Nam, E.K. (2002). A statistical model of vehicle emissions and fuel consumption. *Ford-MIT Alliance Collection*.
- Ceccarelli, R., Canudas-de-Wit, C., Moulin, P. and Sciarretta, A. (2009). Model-based adaptive observers for intake leakage detection in diesel engines. In Proceedings of the IEEE American Control Conference, IEEE ACC'09, Missouri, USA.
- Chang, M. and Evans, L. (1981). Trip time versus stop time and fuel consumption characteristics in cities. *Transportation Science*, vol. 15, no. 3, pp. 183-209.
- Cho, D. and Hedrick, J.K. (1989). Automotive powertrain modelling for control. In Proceedings of the ASME Journal of Dynamic Systems, Measurement, and Control.
- Cook, J.A. and Powell, B.K. (1987). Modelling of an internal combustion engine for control analysis. In Proceedings of the American Control Conference, Minneapolis, Minnesota, USA.
- Cook, J.A., Sun, J., Buckland, J.H., Kolmanovsky, I.V., Peng, H. and Grizzle, J.W. (2006). Automotive powertrain control — a survey. *Asian Journal of Control*, vol. 8, no. 3, pp. 237-260.
- Davis, N., Lents, J., Osses, M., Nikkila, N. and Barth, M.J. (2005). Development and application of an international vehicle emissions model: attachment C: characterizing emission variations due to driving behavior from on-road vehicles. *Transportation Research Record: Journal of the Transportation Research Board*, no. 1939.
- Daw, C.S., Edwards, K.D., Finney, C.E.A. and Wagner, R.M. (2009). A simple model for exploring the cyclic dynamics of spark-assisted HCCI. In Proceedings of the 6th US National Combustion Meeting.
- De Nicolao, G., Scattolini, R. and Siviero, C. (1996). Modelling the volumetric efficiency of ic engines: parametric, non-parametric and neural techniques. *Control Engineering Practice*, vol. 4, no. 10, pp. 1405-1415.
- de Weille, J. (1966). Quantification of road user savings. World Bank Occasional Papers, No. 2, World Bank, Washington, D.C.
- Dean, A.M. and Bozzelli, J.W. (2000). *Chapter 2: Combustion Chemistry of Nitrogen*. In: *Gas-phase Combustion Chemistry*, Gardiner W C, (Editor), Springer, pp. 125-341.

- Dec, J.E. (2009). Advanced compression-ignition engines—understanding the in-cylinder processes. In *Proceedings of the Combustion Institute*, vol. 32, pp. 2727–2742.
- Demers, A., Gao, O., Gehrke, J., Koch, C., Vaz Salles, M. and White, W. (2009). Scaling transportation simulations through declarative processing. In *Proceedings of the Next Generation Data Mining Summit NGDM '09*, Columbia, USA.
- Ding, Y. (2000). Quantifying the Impact of Traffic-Related and Driver-related Factors on Vehicle Fuel Consumption and Emissions, Master Thesis, Virginia Polytechnic Institute and State University.
- Ding, Y. and Rakha, H. (2004). Trip-based explanatory variables for estimating vehicle fuel consumption and emission rates. *Journal of Water, Air, & Soil Pollution*.
- dSPACE GmbH. (2006). *Dynamic Models for Deutz Diesel Power*, dSPACE GmbH.
- Durrani, S., Zhou, X. and Chandra, A. (2010). Effect of vehicle mobility on connectivity of vehicular ad hoc networks. In *Proceedings of the IEEE Vehicular Technology Conference (VTC2010-Fall)*, Canada.
- Easley, W.L., Agarwal, A. and Lavoie, G.A. (2001). Modelling of HCCI combustion and emissions using detailed chemistry. *SAE 2001 World Congress, Detroit, MI, USA*, paper # 2001-01-1029.
- Eaton M90 Supercharger. Retrieved April 3, 2014.
http://www.eaton.com/Eaton/ProductsServices/Automotive/AutomotiveAftermarket/Superchargers/PCT_221790#tabs-1 .
- Edelbrock Pro-Flo XT EFI LS1 Chevy Intake Manifold Systems. Retrieved April 3, 2014.
http://www.edelbrock.com/automotive_new/mc/efi/pf-xt_ls1.shtml .
- Hendricks, E. (1997). Engine modelling for control applications: a critical survey. *Meccanica Journal*, vol. 32, pp. 387–396.
- Elmqvist, H., Mattsson, S.E., Olsson, H., Andreasson, J., Otter, M., Schweiger, C. and Brück, D. (2004). Realtime simulation of detailed vehicle and powertrain dynamics. *SAE International*, paper # 04AE-31.
- Environmental Protection Agency (EPA). (1996). High-tech I/M test procedures, emission standard, quality control requirements, and equipment specifications: IM240 and functional evaporative systems tests, revised technical guidance. Environmental Protection Agency.
- Eriksson, L. (2007). Modelling and control of turbocharged SI and DI engines. *Oil & Gas Science and Technology – Rev. IFP*, vol. 62, no. 4, pp. 523-538.
- Eriksson, L., Nielsen, L., Brugard, J., Bergstrom, J., Pettersson, F. and Andersson, P. (2002). Modelling and simulation of a turbo charged SI engine. *Annual Reviews in Control*, vol. 26, no. 1, pp. 129–137.
- Eriksson, L., Wahlström, J. and Klein, M. (2010). Automotive model predictive control. *Lecture Notes in Control and Information Sciences*, vol. 402, pp. 53-71.
- Esteves-Booth, A., Muneer, T., Kubie, J. and Kirby, H. (2002). A review of vehicular emission models and driving cycles. *Proceedings of the Institution of Mechanical Engineers, Part C: Journal of Mechanical Engineering Science*, vol. 216, no. 8.
- Evans L. and Herman, R. (1978). Automobile fuel economy on fixed urban driving schedules.

- Transportation Science*, vol. 12, no. 2, pp. 137-152.
- Evans, L. and Herman, L. (1976). Multivariate analysis of traffic factors related to fuel consumption in urban driving. *Transportation Science*, vol. 10, no. 2, pp. 205-215.
- Ewalds, R. (2003). *TNO DYNAMO – User Guide*. TNO Automotive internal report.
- Fabian, B. (2010). Freight and its impact on air pollution, greenhouse gas emissions, and fuel consumption in Asia. In Proceedings of the ESCAP Expert Group Meeting on Sustainable Transport Development: Eco-efficiency in Freight Transportation and Logistics, Bangkok.
- Fang, F.C. and Elefteriadou, L. (2008). Capability-enhanced microscopic simulation with real-time traffic signal control. *IEEE Transactions on Intelligent Transportation Systems*, vol. 9, no. 4, pp. 625-632.
- Feng, C. (2007). Transit Bus Load-Based Modal Emission Rate Model Development. PhD Dissertation, Georgia Institute of Technology.
- Filipi, Z.S. and Assanis, D.N. (2001). A nonlinear, transient, single-cylinder diesel engine simulation for predictions of instantaneous engine speed and torque. *Journal of Engineering Gas Turbines Power*, vol. 123, no. 4, pp. 951-959.
- Ford Essex V6 Engine. Retrieved April 3, 2014. [http://en.wikipedia.org/wiki/Ford_Essex_V6_engine_\(Canadian\)](http://en.wikipedia.org/wiki/Ford_Essex_V6_engine_(Canadian)) .
- Ford Motors. Retrieved April 3, 2014. <http://www.ford.com/> .
- Ford Parts. Retrieved April 3, 2014. <http://www.fordracingparts.com/download/charts/217.pdf> .
- Foster, D.E. (1985). An overview of zero-dimensional thermodynamic models for I.C. engine data analysis. *SAE International*, paper # 852070.
- Frey, H.C., Roupail, N.M., Zhai, H., Farias, T.L. and Gonçalves, G.A. (2007). Comparing real-world fuel consumption for diesel- and hydrogen-fueled transit buses and implication for emissions. *Transportation Research Part D: Transport and Environment*, vol. 12, no. 4, pp. 281-291.
- Froschhammer, F., Mathiak, D. and Rabenstein, F. (2006). Hochdynamische prüfstände — ein werkzeug für die insta-tionärapplikation. *ATZ/MTZ Konferenz — Motor; Motorenentwick-lung auf dynamischen Prüfständen, Wiesbaden*.
- Froschhammer, F., Schittenhelm, M. and Keppler, R. (2009). *BMW High-Dynamic Engine Test Benches using SIMPACK Real-Time Models*. SIMPACK.
- Ganesan, V. (2008). *Internal Combustion Engines*, Tata McGraw-Hill.
- Gao, D.W., Mi, C. and Emadi, A. (2007). Modelling and simulation of electric and hybrid vehicles. In Proceedings of IEEE.
- Gerdes, J.C. and Hedriek, J.K. (1997). Vehicle speed and spacing control via coordinated throttle and brake actuation. *Control Engineering Practice*, vol. 5, no. 11, pp. 1607-1614.
- Gilbert, T.R., Kirss, R.V., Foster, N., Davies, G. (2011). *Chemistry: the science in context*. 3rd edition, W. W. Norton & Company.
- Gissinger, G.L., Renard, R. and Hassenforder, M. (1989). Model based design and control of

- diesel engines. *SAE International*, paper # 890568.
- GM Powertrain. Retrieved April 3, 2014. <http://gmpowertrain.com>.
- Gning, A.C., Mihaylova, L. and Boel, R. (2011). Interval macroscopic models for traffic networks. *IEEE Transactions on Intelligent Transportation Systems*.
- Greenwood, I.D. (2003). A new approach to estimate congestion impacts for highway evaluation – effects on fuel consumption and vehicle emissions. PhD Thesis, The University of Auckland.
- Grossi, F., Palladino, A., Zanasi, R. and Fiengo, G. (2009). The power-oriented graphs technique for modelling engine dynamics based on electrical analogy. In Proceedings of the American Control Conference.
- Guensler, R., Yoon, S., Feng, C., Li, H., Jun, J. (2005). Heavy-duty diesel vehicle modal emission model (HDDV-MEM) volume I: modal emission modeling framework. US Environmental Protection Agency, Research report # EPA-600/R-05/090a.
- Guensler, R.L., Washington, S.P., Sperling, D. (1993). A Weighted Disaggregate Approach to Modelling Speed Correction Factors. Institute of Transportation Studies, University of California, Davis, Research Report # UCD-ITS-RR-93-06.
- Guzzella, L. and Amstutz, A. (October 1998). Control of diesel engines. *IEEE Control Systems*, pp. 53-71.
- Gupta, H.N. (2006). *Fundamentals of Internal Combustion Engines*, Prentice-Hall India.
- Hallmark, S.L., Fomunung, I., Guensler, R. and Bachman, W. (2000). Assessing impacts of improved signal timing as a transportation control measure using an activity-specific modelling approach. In Proceedings of the Annual Meeting of the Transportation Research Board.
- Harari, R. and Sher, E. (1995). Measurement of engine friction power by using inertia tests. In Proceedings of the SAE International Congress & Exposition, Detroit, USA, SAE paper # 950028.
- Harris, H.D. and Pearce, F. (1990). A universal mathematical model of diesel engine performance. *Journal of Agriculture Engineering Research*, vol. 47, pp. 165-176.
- Havstad, M.A., Aceves, S.M., McNenly, M.J., Piggott, W.T., Edwards, K.D., Wagner, R.M., Daw, C.S. and Finney, C.E.A. (2010). Detailed chemical kinetic modelling of Iso-octane SI-HCCI. In Proceedings of SAE 2010 World Congress, Detroit, MI, USA, paper # 10PEL-0840.
- Hellström, E. (2010). Look-ahead Control of Heavy Vehicles. PhD Dissertation, Linköpings universitet, Sweden.
- Hendricks, E. (1986). A compact, comprehensive model of large turbocharged, two-stroke diesel engines. *SAE International*, paper # 861190.
- Hendricks, E. (1989). Mean value modelling of large turbocharged two-stroke diesel engines. *SAE International*, paper, # 890564.
- Hendricks, E. (1997). Engine modelling for control applications: a critical survey. *Meccanica Journal*, Vol. 32, pp. 387–396.
- Hendricks, E. (2001). Isothermal vs. adiabatic mean value SI engine models. In Proceedings of the 3rd IFAC Workshop, Advances in Automotive Control, Preprints, Karlsruhe,

- Germany, pp. 373–378.
- Hendricks, E. and Sorenson, S.C. (1990). Mean value modelling of spark ignition engines. *SAE International*, paper # 900616.
- Hess, S.L. (1979). *Introduction to theoretical meteorology*. Krieger Publication Co.
- Heywood, J. (1988). *Internal combustion engine fundamentals*. McGraw Hill, New York.
- Hiellier, V., and Coomber, P. (2004). *Fundamentals of motor vehicle technology*. Nelson Thornes, p.121.
- Hill, P. and Peterson, C. (1992). *Mechanics and thermodynamics of propulsion*. Second Edition. Reading: Addison-Wesley Publishing Company.
- Hillion, M., Chauvin, J. and Petit, N. (2009). Combustion control of an HCCI diesel engine with cool flame phenomenon. In Proceedings of the European Control Conference 2009, Budapest, Hungary, paper # WeA10.5, pp. 3827-3832.
- Hillion, M., Chauvin, J., Grondin, O. and Petit, N. (2008). Active combustion control of diesel HCCI engine: combustion timing. *SAE International*, paper # 2008-01-0984.
- Hong, S., Wooldridge, M.S., Im, H.G. and Assanis, D.N. (2006). Modeling of diesel combustion soot and NO Emissions based on a modified eddy dissipation concept. *Combustion Science and Technology*.
- Holmgren, A. (2005). Mean value modelling of the intake manifold temperature. Master Thesis, Linkopings Universitet.
- Hrovat, D. and Sun, J. (1997). Models and control methodologies for IC engine idle speed control design. *Journal of Control Engineering Practice*.
- Hung, W., Tong, H. and Cheung, C. (2005). A modal approach to vehicular emissions and fuel consumption model development. *Journal of the Air and Waste Management Association*, vol. 55, no. 10, pp. 1431-1440.
- Ibrahim, A.H., and Dunn, P.F. (2006). Effects of temporal flow acceleration on the detachment of microparticles from surfaces. *Aerosol Science*, vol. 37, pp. 1258 – 1266.
- INRO Consultants (1996). *EMME/2 User's Manual, Release 8*. Montreal, CA, INRO Consultants.
- Int Panis, L., De Vlieger, I., Pelkmans, L. and Schrooten, L. (2007). Effect of speed reduction on emissions of heavy duty lorries. In Proceedings of the 8th Highway and Urban Environment Symposium, pp. 53–61, Springer.
- Ismail, A.F., Faris, W.F. and Mohyuddin, M.R. (2009). *Fundamentals of fluid mechanics*. International Islamic University Malaysia (IIUM) Press.
- Johnston, R. (1992). *Elements of applied thermodynamics*, Naval Institute Press.
- Joumard, R., Philippe, F. and Vidon, R. (1999). Reliability of the current models of instantaneous pollutant emissions. *The Science of the Total Environment*, vol. 235, no. 1-3, pp. 133-142.
- Jung, D. and Assanis, D.N. (2001). Multi-zone DI diesel spray combustion model for cycle simulation studies of engine performance and emissions. *SAE International*, paper # 2001-01-1246.

- Jung, M., and Glover, K. (2003). Control-oriented linear parameter-varying modelling of a turbocharged diesel engine. In Proceedings of IEEE.
- Kao, M. and Moskwa, J.J. (1995). Turbocharged diesel engine modelling for nonlinear engine control and state estimation. *ASME Transactions, Journal of Dynamic Systems, Measurement and Control*, vol. 117, no. 1, pp. 20-30.
- Kao, M. and Moskwa, J.J. (1994). Engine load and equivalence ratio estimation for control and diagnostics via nonlinear sliding observer. In Proceedings of the American Control Conference, Maryland. Paper # TM1 – 1:50, pp. 1574-1578.
- Karlsson, F. (2001). *Modelling the intake manifold dynamics in a diesel engine*. Master Thesis, Linkopings Universitet.
- Karmiggelt, R. (1998). Mean value modelling of a spark ignition engine. Research Report, Eindhoven University of Technology.
- Keller, G. (2012). *Statistics for Management and Economics*. South Western, Cengage Learning, 9th edition.
- Khayyam, H., Kouzani, A., Khoshmanesh, K., and Hu, E. (2008). Power analysis and simulation of a vehicle under combined loads. In Proceedings of the 4th International Green Energy Conference (IGEC-IV 2008), North China Electric Power University (NCEPU), Beijing, China, 855-871.
- Khummongkol, D., Pansri, M. and Arayaprane, W., (2004). Heat transfer between impinging air and impinged surface: a factorial design. In Proceedings of the Joint International Conference on Sustainable Energy and Environment (SEE), Hua Hin, Thailand, Paper # 4-003 (O).
- Killingsworth, N., Aceves, S., Flowers, D. and Krstic, M. (2006). A simple HCCI engine model for control. In Proceedings of the IEEE International Conference on Control Applications, Munich, Germany.
- Kim, H.M., Kokkolaras, M., Louca, L.S., Delagrammatikas, G.J., Michelena, N.F., Filipi, Z.S., Papalambros, P.Y., Stein, J.L. and Assanis, D.N. (2002). Target cascading in vehicle redesign: a class VI truck study. *International Journal of Vehicle Design*, vol. 29, no.3, pp. 199-225.
- Kim, K. and Kim, D. (1999). Improving the NO_x-BSFC Trade Off of a Turbocharged Large Diesel Engine Using Performance Simulation. Research Report, Hyundai Heavy Industries Co., Ltd.
- Kolmanovsky, I., Moraal, P., van Nieuwstadt, M. and Stefanopoulou, A. (1997). Issues in modelling and control of intake flow in variable geometry turbocharged engines. In Proceedings of the 18th IFIP Conference on System Modelling and Optimization, Detroit, USA.
- Komninos, N.P. and Hountalas, D.T. (2008). Improvement and validation of a multi-zone model for HCCI engine combustion concerning performance and emissions. *Energy Conversion and Management*, vol. 49, no. 10, pp. 2530-2537.
- Komninos, N.P., Hountalas, D.T. and Kouremenos, D.A. (2005). Description of in-cylinder combustion processes in HCCI engines using a multi-zone model. In Proceedings of the SAE World Congress & Exhibition, Detroit, MI, USA, paper # 2005-01-0171.
- Kottek, M., Grieser, J., Beck, C., Rudolf, B., and Rubel, F. (2006). World map of the Köppen–Geiger climate classification updated. *Meteorol. Z.*, vol. 15, no. 3, pp. 259–263.

- Kulkarni, M.M. Sinha, R.P. and Dhariwal, H.C. (1992). Reduced order model of turbo charged diesel engine. In *Proceedings of the American Control Conference, Green Valley*, vol. 2, pp. 927-931.
- Lansky, L. (2008). Diesel Engine Modelling and Control. Master Thesis, Czech Technical University in Prague.
- Lavoie, G.A. and Blumberg, P.N. (1980). A fundamental model for predicting fuel consumption, NO_x and HC emissions of the conventional spark-ignited engine. *Journal of Combustion Science and Technology*.
- Lavoie, G.A., Heywood, J.B. and Keck, J.C. (1970). Experimental and theoretical study of Nitric Oxide formation in internal combustion engines. *Combustion Science and Technology*, vol. 1, pp. 313-326.
- Leung, D.Y.C. and Williams, D.J. (2000). Modelling of motor vehicle fuel consumption and emissions using a power-based model. *Environmental Monitoring and Assessment*, vol. 65, no. 1-2.
- Li, K. and Ioannou, P. (2004). Modelling of traffic flow of automated vehicles. *IEEE Transactions on Intelligent Transportation Systems*, vol. 5, no. 2, pp. 99-113.
- Liao, T. and Machemehl, R.B. (1998). Development of an aggregate fuel consumption model for signalized intersections. *Transportation Research Record*, no. 1641, pp. 9-18.
- Lindhjem, C.E., Pollack, A.K., Slott, R.S. and Sawyer, R.F. (2004). Analysis of EPA's Draft Plan for Emissions Modelling in MOVES and MOVES GHG. Research Report # CRC Project E-68, ENVIRON International Corporation.
- Liu, Z. and Chen, R. (2009). A zero-dimensional combustion model with reduced kinetics for SI engine knock simulation. *Combustion Science and Technology*, vol. 181, no. 6, pp. 828 – 852.
- Livengood, J.C. and Wu, P.C. (1995). Correlation of auto ignition phenomena in internal combustion engines and rapid compression machine. In *Proceedings of the 5th International Symposium on Combustion*, pp. 347–356.
- Lloyd, V. and Rudd, C. (2007). Service design, The Stationary Office (TSO), p. 92.
- Louca, L.S., Stein, J.L. and Rideout, D.G. (2001). Integrated proper vehicle modelling and simulation using a bond graph formulation. In *Proceedings of the International Conference on Bond Graph Modelling*, Phoenix, AZ, 2001, published by the Society for Computer Simulation, San Diego, CA, ISBN 1-56555-221-0.
- Lysholm Supercharger LYS 2300 AX. Retrieved April 3, 2014.
http://www.lysholm.us/_2300ax.php .
- Marsden, G., Bell, M. and Reynolds, S. (2001). Towards a real-time microscopic emissions model. *Transportation Research Part D* 6, pp. 37-60.
- Masterton, W., Huley, C. (2009). *Chemistry: principles and reactions*, Brooks/Cole Cengage Learning.
- Metallidis, P., and Natsiavas, S. (2003). Linear and nonlinear dynamics of reciprocating engines. *Int J Non-Linear Mechanics*, vol. 38, pp. 723-738.
- Miller, R., Davis, G., Lavoie, G., Newman, C. and Gardner, T. (1998). A super-extended Zel'dovich mechanism for NO_x modelling and engine calibration. SAE paper # 980781.

- Moskwa, J.J. and Hedrick, J.K. (1992). Modelling and validation of automotive engines for control algorithm development. *Journal of Dynamic Systems, Measurements, Control*, vol. 114, no. 2, pp. 278-286.
- Mukherjee, A. and Karmakar, R. (2000). *Modelling and Simulation of Engineering Systems Through Bondgraphs*. CRC Press.
- National Research Council (NRC). (1995). Expanding Metropolitan Highways: Implications for Air Quality and Energy Use, Washington, D.C. Transportation Research Board National Research Council.
- Ni, D. and Henclewood, D. (2008). Simple engine models for vehicle infrastructure integration-enabled in-vehicle applications. *IEEE Trans. Vehicular Technology*, vol. 57, no. 5, pp. 2695-2702.
- Nieuwoudt, A., McCorquodale, M.S., Borno, R.T. and Massoud, Y. (2006). Accurate analytical spiral inductor modelling techniques for efficient design space exploration. *IEEE Electron Device Letters*, vol. 27, no. 12.
- Nyberg, M. and Sutte, T. (2004). Model based diagnosis of the air path of an automotive diesel engine. *Control Engineering Practice*, vol. 12, no. 5, pp. 513-525.
- Oberg, S. (2001). Identification and Improvements of an Automotive Diesel Engine Model purposed for Model Based Diagnosis. Research Report for DaimlerChrysler AG, M.Sc. Thesis, Linkopings Universitet.
- Obert, E.F. (1973). *Internal combustion engines and air pollution*, Harper & Row Publishers, Inc.
- Oliver, G. (2006). Computer simulation of air injection to inlet manifold on turbocharged engines. In Proceedings of the International Federation of Automotive Engineering Societies Congress, Paper # f2006sc35, 2006.
- Omran, R., Younes, R. and Champoussin, J. (2007). Neural networks for real-time nonlinear control of a variable geometry turbocharged diesel engine. *International Journal of Robust and Nonlinear Control*, DOI: 10.1002/rnc.1264.
- Organisation for Economic Co-operation and Development. (2002). Strategies to Reduce Greenhouse Gas Emissions from Road Transport: Analytical Methods. Research Report ITRD No. E109210, Organisation for Economic Co-operation and Development.
- Ouladsine, M., Bloch, G. and Dovifaaz, X. (2004). Neural Modelling and Control of a Diesel Engine with Pollution Constraints. Research Report, Domaine Universitaire de Saint-Jérôme.
- Panis, L.I., Broekx, S. and Liu, R. (2006). Modelling instantaneous traffic emission and the influence of traffic speed limits. *Science of the Total Environment*, vol. 371, no. 1-3, pp. 270-285.
- Park, J.Y., Noland, R.B. and Polak, J.W. (2001). A microscopic model of air pollutant concentrations: comparison of simulated results with measured and macroscopic estimates. *Transportation Research Record*, vol. 1750, pp. 64-73.
- Patterson, M.A., Kong, S.C., Hampson, G.J. and Reitz, R.D. (1994). Modelling the effects of fuel injection characteristics on diesel engine soot and NOx emissions. *SAE International*, paper # 940523.

- Polifke, W. (1995). A NO_x prediction scheme for lean-premixed gas turbine combustion based on detailed chemical kinetics. *Proceedings of ASME GT*, Paper # 95-GT-108.
- Powell, B.K., Bailey, K.E. and Cikanek, S.R. (1998). Dynamic modelling and control of hybrid electric vehicle powertrain systems, *IEEE Control Systems*, pp. 17-33.
- Rakha H., Ahn K., and Trani A. (2003). Comparison of Mobile5a, VT-Micro, and CMEM models for estimating hot-stabilized light duty gasoline vehicle emissions. *Canadian Journal of Civil Engineering*, vol. 30, no. 6, pp. 1010-1021.
- Rakha, H. and Ahn, K. (2004). Integration modelling framework for estimating mobile source emissions. *Journal of Transportation Engineering*, vol. 130, no. 2, pp. 183-193.
- Rakha, H. and Lucic, I. (2002). Variable power vehicle dynamics model for estimating maximum truck acceleration levels. *Journal of Transportation Engineering*, vol. 128, pp. 412-419.
- Rakha, H. and Van Aerde, M. (2000). Requirements for evaluating traffic signal control impacts on energy and emissions based on instantaneous speed and acceleration measurements. *Transportation Research Record: Journal of the Transportation Research Board*, no. 1738, pp. 56-67.
- Rakha, H., Ahn, K. and Trani, A. (2004a). Development of VT-Micro model for estimating hot stabilized light duty vehicle and truck emission. *Transportation Research Part D-Transport and Environment*, vol. 1, no. 9, pp. 49-74.
- Rakha, H., Van Aerde, M., Bloomberg, L. and Huang, X. (1998). Construction and Calibration of a Large-scale Micro-simulation Model of the Salt Lake Area. Research Report, Center for Transportation Research Virginia Polytechnic Institute & State University.
- Rakha, H.A., Ahn, K., Faris, W. and Moran, K. (2010). Simple vehicle powertrain model for use in traffic simulation software. In Proceedings of the 89th Transportation Research Board Annual Meeting.
- Rakha, H.A., Ahn, K., Moran, K., Saerens, B. and Van den Bulck, E. (2011). Simple comprehensive fuel consumption and CO₂ emission model based on instantaneous vehicle power. In Proceedings of the 90th Transportation Research Board Annual Meeting, USA.
- Rakha, H.A., Ahn, K., Faris, W., and Moran K.S. (2012). Simple vehicle powertrain model for modeling intelligent vehicle applications. *IEEE Trans. on Intelligent Transportation Systems*, vol. 13, no. 2.
- Rama, D.D., and Durgaiah, D.R. (2007). *Fluid mechanics and machinery*. New Age International, p.784.
- Ran, H., Thomas, R. and Mavris, D. (2007). A mean value based sizing and simulation model of a hydrogen fueled spark-ignition internal combustion engine. In Proceedings of the Society of Automotive Engineers SAE 2007 AeroTech Congress & Exhibition, USA, paper # 2007-01-3789.
- Rao, J.S., Suresh, S., Ratnakar, R. and Narayan, R. (2011). A procedure to predict influence of acceleration and damping of blades passing through critical speeds on fatigue life. Altair Engineering, Inc.
- RB Racing RSR Intercoolers. Retrieved April 3, 2014.
<http://rbracing-rsr.com/intercoolers.htm> .
- Rizzotto, G., Lo Presti, M., Di Marco, F., and Lanzafame, R. (1995). Road vehicle energy

- consumption model by using neuro-fuzzy approach, In Proceedings of the IEEE 1995 International Symposium on Industrial Electronics (ISIE '95), vol. 2, pp. 798 – 802.
- Rothery, R.W. (1975). *Chapter 4: Car Following Models, In: Traffic Flow Theory*, Edited by Gartner, N.H., Messer, C. and Rathi, A.K., United States Department of Transportation, Federal Highway Administration.
- Roy, S. and Liu, Z. (2008). Road vehicle suspension and performance evaluation using a two-dimensional vehicle model. *International Journal of Vehicle Systems Modelling and Testing*, vol. 3, no. 1/2, pp.68–93.
- Schmitt, J., Fremovici, M., Grondin, O. and Le Berr, F. (2009). Compression ignition engine model supporting powertrain development. In Proceedings of the IFAC Workshop on Engine and Powertrain Control, Simulation and Modelling, Engine and Powertrain Control, Simulation and Modelling, France.
- Seykens, X.L.J., Baert, R.S.G., Willems, F.P.T., Vink, W. and Van den Heuvel, I.T.M. (2006). Development of a dynamic engine brake model for control purposes. In Proceedings of the New Trends in Engine Control, Simulation and Modelling Conference, France.
- Shaver, G.M., Roelle, M.J. and Gerdes, J.C. (2006). Modelling cycle-to-cycle dynamics and mode transition in HCCI engines with variable valve actuation. *Control Engineering Practice*, vol. 14, no. 3, pp. 213-222.
- Shrivastava, R., Hessel, R. and Reitz, R.D. (2002). CFD optimization of DI diesel engine performance and emissions using variable intake valve actuation with boost pressure, EGR and multiple injections. In Proceedings of the SAE World Congress & Exhibition, March 2002, Detroit, MI, USA, paper # 2002-01-0959.
- Singh, S.P. (2007). *Physical Chemistry - States of Matter: Gaseous, Liquid and Solids*, Janta Vedic P.G. College, Baraut, Distt Meerut, India. Retrieved April 3, 2014.
<http://nsdl.niscair.res.in/bitstream/123456789/800/4/revised+STATES+OF+MATTER.pdf>.
- Silverlind, D. (2001). Mean Value Engine Modelling with Modelica. Master Thesis, Linköpings Universitet, Sweden.
- Smit, R., Smokers, R. and Rabe, E. (2007). A new modelling approach for road traffic emissions: VERSIT+. *Transportation Research Part D: Transport and Environment*, vol. 12, no. 6, pp. 414-422.
- Smits, J.J.M., (2006). Modeling of a fluid flow in an internal combustion engine. Research Report # WVT 2006.22, Eindhoven University of Technology.
- Sommer, C., German, R. and Dressler, F. (2011). Bidirectionally coupled network and road traffic simulation for improved IVC analysis. *IEEE Transactions on Mobile Computing*, vol. 10, no. 1, pp. 3-15.
- Song, G., Yu, L. and Wang, Z. (2009). Aggregate fuel consumption model of light-duty vehicles for evaluating effectiveness of traffic management strategies on fuels. *Journal of Transportation Engineering*, vol. 135, no. 9, pp. 611-618.
- Sonntag, R.E., Borgnakke, C., and Van Wylen, G.J. (2008). *Fundamentals of thermodynamics*. Wiley, 7th edition.
- Sorenson, S.C., Hendrick, E., Magnusson, S. and Bertelsen, A. (2005). Compact and accurate turbocharger modelling for engine control. *Electronic Engine Controls, SAE Special Collections 2005 (SP-1975)*, SAE International, paper # 2005-01-1942.

- Souder, J.S. (2002). Powertrain Modelling and Nonlinear Fuel Control. M.Sc. Thesis, University of California, Berkley.
- Spirig, M., Schmied, J., Jenckel, P. and Kanne, U. (2002). Three practical examples of magnetic bearing control design using a modern tool. *Journal of Engineering for Gas Turbines and Power - Transactions of The ASME*, vol. 124, no. 4, pp. 1025-1031.
- Stankovic, A. (2000). Modelling of Air Flows in Automotive Engines Using Modelica. Master Thesis, Linköping University.
- Streit, E.E. and Borman, G.L. (1971). Mathematical simulation of a large turbocharged two-stroke diesel engine. *SAE International*, paper # 710177.
- Sulaiman, S.A., Murad, S.H.M., Ibrahim, I. and Abdul Karim, Z.A. (2010). "Study of flow in air-intake system for a single-cylinder go-kart engine. *International Journal of Automotive and Mechanical Engineering*, vol. 1, pp. 91-104.
- Sun, J., Kolmanovsky, I., Cook, J.A. and Buckland, J.H. (2005). Modelling and control of automotive powertrain systems: a tutorial. In Proceedings of the American Control Conference, Portland, USA, paper # ThC14.1, pp. 3271-3283.
- Swan, K., Shahbakhti, M. and Koch, C. (2006). Predicting start of combustion using a modified knock integral method for an HCCI engine. In Proceedings of the SAE World Congress, paper # 2006-01-1086.
- Taklanti, A. and Delhay, B. (1999). Multi-dimensional modelling of the aerodynamic and combustion in diesel engines. *Oil & Gas Science and Technology – Rev. IFP*, vol. 54, no. 2, pp. 271-277.
- Tapani, A. (2005). Versatile model for simulation of rural road traffic. *Transportation Research Record: Journal of the Transportation Research Board*, no. 1934, pp. 169–178.
- Taylor, C.F. (1985). *The Internal-Combustion Engine in Theory and Practice*. The MIT Press.
- Taylor, N.B. (2003). The CONTRAM dynamic traffic assignment model. *Networks and Spatial Economics*, vol. 3, pp. 297-322.
- The MathWorks Inc. (2000). SIMULINK. Dynamic System Simulation for MATLAB. Version 4, The MathWorks Inc., Natick, MA.
- The Seider Group. (1997). MINUTP Technical User's Manual. Palo Alto, CA, The Seider Group.
- The Urban Analysis Group. (1992). TRANPLAN, Version 7.1. Danville, CA, The Urban Analysis Group.
- Tirkey, J.V., Gupta, H.N. and Shukla, S.K. (2010). Analytical study to minimize the engine exhaust emissions and safe knock limit of CNG powered four-stroke SI engine. *International Journal of Energy and Environment*, vol. 1, no. 1, pp.31-52.
- United Nations Economic and Social Council. (2009). Major Issues in Transport: Transport and Environment. United Nations Economic and Social Council.
- United States Environmental Protection Agency EPA. (2001). Process for conducting probabilistic risk assessment. APPENDIX A, RAGS Volume 3 Part A, Environmental Protection Agency EPA.
- Usan, M. (2005). Automotive component product development enhancement through multi-

- attribute system design optimization in an integrated concurrent engineering framework. Master Thesis, Massachusetts Institute of Technology.
- Varnavas, C. and Assanis, D.N. (1996). A high temperature and high pressure evaporation model for the KIVA-3 code. *SAE International*, paper # 960629.
- Velmurugan, A. and Loganathan, M. (2011). Performance and emission characteristics of a DI diesel engine fuelled with Cashew Nut Shell Liquid (CNSL) – Diesel blends. *Engineering and Technology*, World Academy of Science, vol. 58, pp. 889-894.
- Villarba, M. (2013). *CHEM 162: General Chemistry II – Course Notes*. Seattle Central Community College, Chapter 15.
- Whitten, K.W., Davis, R.E., Peck, M.L. and Stanley, G.G. (2004). *General Chemistry*. 7th edition, Thomson Brooks/Cole, p. 465,594,601.
- Wahlstrom, J. (2005). Modelling of a Diesel Engine with VGT and EGR. Technical report, Division of Vehicular Systems, Linkoping University, Linkoping, Sweden.
- Wahlstrom, J. and Eriksson, L. (2011). Modeling diesel engines with a variable-geometry turbocharger and exhaust gas recirculation by optimization of model parameters for capturing non-linear system dynamics. *Proc. the Institution of Mechanical Engineers, Part D, Journal of Automobile Engineering*, vol. 225, no. 7.
- Wang, H. and Zhang, J. (2006). Control oriented dynamic modelling of a turbocharged diesel engine. In Proceedings of the Sixth International Conference on Intelligent Systems Design and Applications (ISDA'06).
- Wang, H., Fu, L., Zhou, Y. and Li, H. (2008). Modelling of the fuel consumption for passenger cars regarding driving characteristics. *Transportation Research Part D: Transport and Environment*, vol. 13, no. 7, pp. 479-482.
- Waston, H.C. and Milkins, E.E. (1980). A simplified method for quantifying fuel consumption of vehicles in urban traffic. *SAE-Austria*, vol. 40, no. 1, pp. 6-13.
- Watson, N. (1984). Dynamic turbocharged diesel engine simulator for electronic control system development. *Journal of Dynamic Systems, Measurements, and Control*, vol. 106, pp. 27-45.
- Watson, N. and Janota, M.S. (1982). *Turbocharging the Internal Combustion Engine*. Wiley-Interscience Publications, John Wiley, New York.
- Watson, N., Pilley, A.D. and Marzouk, M. (1980). A combustion correlation for diesel engine simulation. *SAE International*, paper # 800029.
- Weeks, R.W. and Moskwa, J.J. (1995). Automotive engine modelling for real-time control using MATLAB/SIMULINK. In Proceedings of SAE 1995 International Congress and Exposition.
- West, B., McGill, R., Hodgson, J., Sluder, S., and Smith, D. (1997). Development of Data-Based Light-Duty Modal Emissions and Fuel Consumption Models. *SAE International*, paper No. 972910.
- Whitehouse, N. and Sareen, B.K. (1974). Prediction of heat release in a quiescent chamber diesel engine allowing for fuel/air mixing. *SAE International*, paper # 740084.
- Winge Vigild, C. (2001). The Internal Combustion Engine –Modelling, Estimation and Control Issues. PhD thesis, Technical University of Denmark.

- Winterbone, D.E., Thiruarooran, C. and Wellstead, P.E. (1977). A wholly dynamic model of a turbocharged diesel engine for transfer function evaluation. *SAE International*, paper # 770124.
- Wu, X. and Moin, P. (2008). Large-activation-energy theory for premixed combustion under the influence of enthalpy fluctuations in the oncoming mixture Part II: applications. Annual Research Briefs 2008, Center for Turbulence Research, Imperial College London, pp. 421-436.
- Xia, H. and Oh, P. (1999). A dynamic model for automotive torque converters. *International Journal of Vehicle Design*, vol. 21, no. 4-5, pp. 344-354.
- Yang, M. and Sorenson, S.C. (1992). Modelling of the dynamic processes in an electronic diesel fuel injection system, *SAE SP*, paper # 920240.
- Yildiz, Y., Annaswamy, A.M., Yanakiev, D. and Kolmanovsky, I. (2009). *Spark Ignition Engine Idle Speed Control: An Adaptive Control Approach*, MIT Press.
- Yue, H. (2008). Mesoscopic Fuel Consumption and Emission Modelling. Doctor of Philosophy Dissertation, Virginia Polytechnic Institute and State University.
- Zargari, S.A. and Khan, A.M. (2003). Fuel consumption model for bus rapid transit. *Journal of Advanced Transportation*, vol. 37, no. 2, pp. 139-157.
- Zhao, F.Q., Lai, M.C. and Harrington, D.L. (1997). A review of mixture preparation and combustion control strategies for spark-ignited direct injection gasoline engines. *SAE International*, paper # 970627.
- Zito, G. and Dor'e Landau, I. (2005). Narmax model identification of a variable geometry turbocharged diesel engine. In Proceedings of the American Control Conference 2005, Portland, USA.
- Zweiri, Y.H., Whidborne, J.F. and Seneviratne, L.D. (2001). Detailed analytical model of a single-cylinder diesel engine in the crank angle domain. *Proceedings of the Institution of Mechanical Engineers, Part D: Journal of Automobile Engineering*, vol. 215, no. 11, pp. 1197-1216.

APPENDIX A

DIESEL FUEL CONSUMPTION RATE INTERFACE FACILITY AND CODE

The screenshot shows a MATLAB GUI window titled "DieselFuelConsumptionRate". The window contains a light blue header bar. Below the header, there are ten input fields arranged vertically, each with a label to its left: "Equivalence Ratio", "Air Density (kg/m3)", "Volumetric Efficiency (%)", "Displaced Volume (m3)", "Vehicle Speed (m/s)", "Gear Ratio", "Final Drive Ratio", "Vehicle Tire Rolling Radius (m)", and "Vehicle Acceleration (m/s2) (-1.5 to +2)". At the bottom of the window is a button labeled "Diesel Fuel Consumption Rate (kg/s)".

```
function varargout = DieselFuelConsumptionRate(varargin)
% DIESELFUELCONSUMPTIONRATE M-file for DieselFuelConsumptionRate.fig
%   DIESELFUELCONSUMPTIONRATE, by itself, creates a new
DIESELFUELCONSUMPTIONRATE or raises the existing
%   singleton, i.e. one instance of GUI.
%
%   H = DIESELFUELCONSUMPTIONRATE returns the handle to a new
DIESELFUELCONSUMPTIONRATE or the handle to the existing singleton.
% DIESELFUELCONSUMPTIONRATE('CALLBACK',hObject,eventData,handles,...)
calls the local
```

```

%      function named CALLBACK in DIESELFUELCONSUMPTIONRATE.M with
the given input arguments.
%
%      DIESELFUELCONSUMPTIONRATE('Property','Value',...) creates a
new DIESELFUELCONSUMPTIONRATE or raises the
%      existing singleton. Starting from the left, property value
pairs are applied to the GUI before
DieselFuelConsumptionRate_OpeningFunction gets called. All inputs are
passed to DieselFuelConsumptionRate_OpeningFcn via varargin.

% Begin initialization code
gui_Singleton = 1;
gui_State = struct('gui_Name',       mfilename, ...
                  'gui_Singleton',   gui_Singleton, ...
                  'gui_OpeningFcn',  @DieselFuelConsumptionRate_OpeningFcn, ...
                  'gui_OutputFcn',  @DieselFuelConsumptionRate_OutputFcn, ...
                  'gui_LayoutFcn',  [], ...
                  'gui_Callback',    []);
if nargin && ischar(varargin{1})
    gui_State.gui_Callback = str2func(varargin{1});
end

if nargout
    [varargout{1:nargout}] = gui_mainfcn(gui_State, varargin{:});
else
    gui_mainfcn(gui_State, varargin{:});
end
% End initialization code

% --- Executes just before DieselFuelConsumptionRate is made visible.
function DieselFuelConsumptionRate_OpeningFcn(hObject, eventdata,
handles, varargin)
% This function has no output args.
% hObject    handle to figure
% handles     structure with handles and user data
% varargin    command line arguments to DieselFuelConsumptionRate (see
VARARGIN)

% Choose default command line output for DieselFuelConsumptionRate
handles.output = hObject;

% Update handles structure
guidata(hObject, handles);

% --- Outputs from this function are returned to the command line.
function varargout = DieselFuelConsumptionRate_OutputFcn(hObject,
eventdata, handles)
% varargout    cell array for returning output args
% hObject      handle to figure
% handles      structure with handles and user data

% Get default command line output from handles structure
varargout{1} = handles.output;

% Equivalence Ratio Edit Textbox

```

```

function ERet_Callback(hObject, eventdata, handles)
% hObject      handle to ERet (see GCBO)
% handles      structure with handles and user data

% --- Executes during object creation, after setting all properties.
function ERet_CreateFcn(hObject, eventdata, handles)

%       See ISPC and COMPUTER.
if ispc && isequal(get(hObject,'BackgroundColor'),
get(0,'defaultUiControlBackgroundColor'))
    set(hObject,'BackgroundColor','white');
end

% Air Density Edit Textbox
function ADet_Callback(hObject, eventdata, handles)

% --- Executes during object creation, after setting all properties.
function ADet_CreateFcn(hObject, eventdata, handles)

% Volumetric Efficiency Edit Textbox
function VEet_Callback(hObject, eventdata, handles)

% --- Executes during object creation, after setting all properties.
function VEet_CreateFcn(hObject, eventdata, handles)
% hObject      handle to VEet (see GCBO)
% handles      empty - handles not created until after all CreateFcns
called

% Displaced Volume Edit Textbox
function DVet_Callback(hObject, eventdata, handles)

% --- Executes during object creation, after setting all properties.
function DVet_CreateFcn(hObject, eventdata, handles)

% Vehicle Speed Edit Textbox
function VSet_Callback(hObject, eventdata, handles)

% --- Executes during object creation, after setting all properties.
function VSet_CreateFcn(hObject, eventdata, handles)

% Gear Ratio Edit Textbox
function GRet_Callback(hObject, eventdata, handles)

% --- Executes during object creation, after setting all properties.
function GRet_CreateFcn(hObject, eventdata, handles)

% Final Drive Ratio Edit Textbox
function FDRet_Callback(hObject, eventdata, handles)

% --- Executes during object creation, after setting all properties.

```



```

function FDRet_CreateFcn(hObject, eventdata, handles)

% Vehicle Tire Rolling Radius Edit Textbox
function VTRRet_Callback(hObject, eventdata, handles)

% --- Executes during object creation, after setting all properties.
function VTRRet_CreateFcn(hObject, eventdata, handles)

% Vehicle Linear Acceleration Edit Textbox
function VLAet_Callback(hObject, eventdata, handles)

% --- Executes during object creation, after setting all properties.
function VLAet_CreateFcn(hObject, eventdata, handles)

% Diesel Fuel Consumption Rate Push Button
% --- Executes on button press in DFCRpb.
function DFCRpb_Callback(hObject, eventdata, handles)

aFC=str2num(get(handles.ERet,'string'))
cFC=str2num(get(handles.ADet,'string'))
dFC=str2num(get(handles.VEet,'string'))
eFC=str2num(get(handles.DVet,'string'))
fFC=str2num(get(handles.VSet,'string'))
gFC=str2num(get(handles.GRet,'string'))
hFC=str2num(get(handles.FDRet,'string'))
iFC=str2num(get(handles.VTRRet,'string'))
jFC=str2num(get(handles.VLAet,'string'))

if jFC==0    % i.e. Accelration=0
set(handles.DFCRtext,'string',num2str(((aFC*0.069588*cFC*(dFC/100)*(eF
C/10)*fFC*gFC*hFC*2)/(iFC*2*3.14))) % Actual Mass Flow Rate of Fuel
at Steady Speed , i.e. Acceleration=0 , Equivalence Ratio = 0.7

elseif jFC>-1.6 & jFC<0 & fFC<=13.9 % i.e. -1.6 m/s2 <Accelration<
0 and Speed<= 50 km/h, Equivalence Ratio = 0.6

set(handles.DFCRtext,'string',num2str((((aFC*0.069588*cFC*(dFC/100)*(e
FC/10)*fFC*gFC*hFC*(2^1.19))/(iFC*2*3.14))*(exp(jFC*(fFC/(2^4.8))))))

elseif jFC>-1.6 & jFC<0 & fFC>13.9 % i.e. -1.6 m/s2 <Accelration< 0
and Speed> 50 km/h, Equivalence Ratio = 0.6

set(handles.DFCRtext,'string',num2str((((aFC*0.069588*cFC*(dFC/100)*(e
FC/10)*fFC*gFC*hFC*(2^1.19))/(iFC*2*3.14))*(exp(jFC*(fFC/(2^5.2))))))

elseif jFC>0 & jFC<=0.9 & fFC<=13.9 % i.e. 0 <Accelration< 0.9 m/s2
and Speed<= 50 km/h, Equivalence Ratio = 0.8

set(handles.DFCRtext,'string',num2str((((aFC*0.069588*cFC*(dFC/100)*(e
FC/10)*fFC*gFC*hFC*(2^0.78))/(iFC*2*3.14))*(exp(jFC+0.25))))

elseif jFC>0 & jFC<=0.9 & fFC>13.9 % i.e. 0 <Accelration< 0.9 m/s2
and Speed> 50 km/h, Equivalence Ratio = 0.8

```

```

set(handles.DFCRtext,'string',num2str(((aFC*0.069588*cFC*(dFC/100)*(e
FC/10)*fFC*gFC*hFC*(2^0.78))/(iFC*2*3.14))*(exp(jFC+0.5))))

elseif jFC>0.9 & jFC<=2 & fFC<=13.9 % i.e. 0.9 <Accelration< 2 m/s2
and Speed<= 50 km/h, Equivalence Ratio = 0.8

set(handles.DFCRtext,'string',num2str(((aFC*0.069588*cFC*(dFC/100)*(e
FC/10)*fFC*gFC*hFC*(2^0.78))/(iFC*2*3.14))*(exp(jFC))))

elseif jFC>0.9 & jFC<=2 & fFC>13.9 % i.e. 0.9 <Accelration< 2 m/s2
and Speed> 50 km/h, Equivalence Ratio = 0.8

set(handles.DFCRtext,'string',num2str(((aFC*0.069588*cFC*(dFC/100)*(e
FC/10)*fFC*gFC*hFC*(2^0.78))/(iFC*2*3.14))*(exp(jFC*(2^0.25))))))

end

```

APPENDIX B

DIESEL CO EMISSIONS RATE INTERFACE FACILITY AND CODE

The screenshot shows a MATLAB GUI window titled "DieselCOEmissionsRate". The window has a light gray background and a blue title bar with standard MATLAB window controls. At the top, there is a solid cyan rectangular bar. Below this, there are ten input fields, each preceded by a label. The labels and their corresponding units are: "Equivalence Ratio", "Air Density (kg/m3)", "Volumetric Efficiency (%)", "Displaced Volume (m3)", "Vehicle Speed (m/s)", "Gear Ratio", "Final Drive Ratio", "Vehicle Tire Rolling Radius (m)", "Vehicle Acceleration (m/s2)", and "Unburned Hydrocarbon (ppm) (1ppm=0.0001%)". Each input field is a white rectangle with a thin gray border. At the bottom of the window, there is a large, light blue button with a gradient and a black border, labeled "Diesel CO Emission Rate (g/s)".

```
function varargout = DieselCOEmissionsRate(varargin)

% Begin initialization code
gui_Singleton = 1;
gui_State = struct('gui_Name',       mfilename, ...
                  'gui_Singleton',   gui_Singleton, ...
                  'gui_OpeningFcn',  @DieselCOEmissionsRate_OpeningFcn, ...
                  'gui_OutputFcn',   @DieselCOEmissionsRate_OutputFcn, ...
                  'gui_LayoutFcn',   [], ...
                  'gui_Callback',    []);
```

```

if nargin && ischar(varargin{1})
    gui_State.gui_Callback = str2func(varargin{1});
end

if nargin
    [varargout{1:nargout}] = gui_mainfcn(gui_State, varargin{:});
else
    gui_mainfcn(gui_State, varargin{:});
end
% End initialization code

% --- Executes just before DieselCOEmissionsRate is made visible.
function DieselCOEmissionsRate_OpeningFcn(hObject, eventdata,
handles, varargin)
% This function has no output args.
% hObject    handle to figure
% handles     structure with handles and user data
% varargin    command line arguments to DieselCOEmissionsRate

% Choose default command line output for DieselCOEmissionsRate
handles.output = hObject;

% Update handles structure
guidata(hObject, handles);

% --- Outputs from this function are returned to the command line.
function varargout = DieselCOEmissionsRate_OutputFcn(hObject,
eventdata, handles)
% varargout    cell array for returning output args;
% hObject     handle to figure
% handles     structure with handles and user data

% Get default command line output from handles structure
varargout{1} = handles.output;

% Equivalence Ratio Edit Text Box
function ERet_Callback(hObject, eventdata, handles)

% --- Executes during object creation, after setting all properties.
function ERet_CreateFcn(hObject, eventdata, handles)

%         See ISPC and COMPUTER.
if ispc && isequal(get(hObject,'BackgroundColor'),
get(0,'defaultUiControlBackgroundColor'))
    set(hObject,'BackgroundColor','white');
end

% Air Density Edit Text Box
function ADet_Callback(hObject, eventdata, handles)

% --- Executes during object creation, after setting all properties.
function ADet_CreateFcn(hObject, eventdata, handles)

% Volumetric Efficiency Edit Text Box
function VEet_Callback(hObject, eventdata, handles)

```

```

% --- Executes during object creation, after setting all properties.
function VEet_CreateFcn(hObject, eventdata, handles)

% Displaced Volume Edit Text Box
function DVet_Callback(hObject, eventdata, handles)

% --- Executes during object creation, after setting all properties.
function DVet_CreateFcn(hObject, eventdata, handles)

% Vehicle Speed Edit Text Box
function VSet_Callback(hObject, eventdata, handles)

% --- Executes during object creation, after setting all properties.
function VSet_CreateFcn(hObject, eventdata, handles)

% Gear Ratio Edit Text Box
function GRet_Callback(hObject, eventdata, handles)

% --- Executes during object creation, after setting all properties.
function GRet_CreateFcn(hObject, eventdata, handles)

% Final Drive Ratio Edit Text Box
function FDRet_Callback(hObject, eventdata, handles)

% --- Executes during object creation, after setting all properties.
function FDRet_CreateFcn(hObject, eventdata, handles)

% Vehicle Tire Rolling Radius Edit Text Box
function VTRet_Callback(hObject, eventdata, handles)

% --- Executes during object creation, after setting all properties.
function VTRet_CreateFcn(hObject, eventdata, handles)

% Vehicle Acceleration Edit Text Box
function VAet_Callback(hObject, eventdata, handles)

% --- Executes during object creation, after setting all properties.
function VAet_CreateFcn(hObject, eventdata, handles)

% Unburned Hydrocarbon Edit Text Box
function UHet_Callback(hObject, eventdata, handles)

% --- Executes during object creation, after setting all properties.
function UHet_CreateFcn(hObject, eventdata, handles)

% Diesel CO Emission Rate Push Button
% --- Executes on button press in DCOERpb.
function DCOERpb_Callback(hObject, eventdata, handles)

aCO=str2num(get(handles.ERet,'string')) % Equivalence Ratio
bCO=str2num(get(handles.ADet,'string')) % Air Density
cCO=str2num(get(handles.VEet,'string')) % Volumetric Efficiency
dCO=str2num(get(handles.DVet,'string')) % Displaced Volume
eCO=str2num(get(handles.VSet,'string')) % Vehicle Speed
fCO=str2num(get(handles.GRet,'string')) % Gear Ratio
gCO=str2num(get(handles.FDRet,'string')) % Final Drive Gear Ratio

```

```

hCO=str2num(get(handles.VTRRet,'string')) % Vehicle Tire Rolling
Radius
iCO=str2num(get(handles.VAet,'string')) % Vehicle Acceleration
jCO=str2num(get(handles.UHet,'string')) % Unburned Hydrocarbon

Rcrosscoo2=((((aCO*0.069588*bCO*(cCO/100)*(dCO/10)*eCO*fCO*gCO*(2^(-
12.2)))/(hCO*2*3.14))*1000)*(0.028*(1-
(jCO*0.000001))*0.0002*0.0197)*eCO)/(0.0137*(1)))*1000 % Rate of
steady state-based CO emission for CO+O2 reaction (g/s)

Rcrosscoh2ols=((((aCO*0.069588*bCO*(cCO/100)*(dCO/10)*eCO*fCO*gCO*(2^
(-((log(eCO))/(log(3.33)))-1.70)))/(hCO*2*3.14))*1000)*(0.028*(1-
(jCO*0.000001))*(2.25^2)*0.008*0.008)*eCO*hCO)/(0.0137*(1)*eCO*fCO*gC
O))*1000 % Rate of steady state-based CO emission for CO+H2O
reaction (g/s) for Low Speed Cycles

Rcrosscoh2ohs=((((aCO*0.069588*bCO*(cCO/100)*(dCO/10)*eCO*fCO*gCO*(2^
-2.57))/(hCO*2*3.14))*1000)*(0.028*(1-
(jCO*0.000001))*(2.25^2)*0.008*0.008)*eCO*hCO)/(0.0137*(1)*eCO*fCO*gC
O))*exp(eCO/(2^5.01))*1000 % Rate of steady state-based CO emission
for CO+H2O reaction (g/s) for High Speed Cycles

if iCO==0 & eCO<=13.9 % i.e. Acceleration = 0 and Speed<= 50 km/h

    Rcross=Rcrosscoo2+Rcrosscoh2ols
    set(handles.DCOERtext,'string',num2str(Rcross))

elseif iCO==0 & eCO>13.9 % i.e. Acceleration = 0 and Speed> 50 km/h

    Rcross=Rcrosscoo2+Rcrosscoh2ohs
    set(handles.DCOERtext,'string',num2str(Rcross))

```

APPENDIX C

DIESEL NO_x EMISSIONS RATE INTERFACE FACILITY AND CODE

The screenshot shows a MATLAB GUI window titled "DieselNOxEmissionsRate". The window contains a series of input fields for various parameters: Equivalence Ratio, Air Density (kg/m³), Volumetric Efficiency (%), Displaced Volume (m³), Vehicle Speed (m/s), Gear Ratio, Final Drive Ratio, Vehicle Tire Rolling Radius (m), Vehicle Acceleration (m/s²), and Unburned Hydrocarbon (ppm) (1ppm=0.0001%). A button at the bottom is labeled "Diesel NO_x Emission Rate (g/s)".

```
function varargout = DieselNOxEmissionsRate(varargin)

% Begin initialization code
gui_Singleton = 1;
gui_State = struct('gui_Name',       mfilename, ...
                  'gui_Singleton',   gui_Singleton, ...
                  'gui_OpeningFcn',  @DieselNOxEmissionsRate_OpeningFcn, ...
                  'gui_OutputFcn',   @DieselNOxEmissionsRate_OutputFcn, ...
                  'gui_LayoutFcn',   [], ...
                  'gui_Callback',    []);
if nargin && ischar(varargin{1})
```

```

        gui_State.gui_Callback = str2func(varargin{1});
    end

    if nargout
        [varargout{1:nargout}] = gui_mainfcn(gui_State, varargin{:});
    else
        gui_mainfcn(gui_State, varargin{:});
    end
    % End initialization code

    % --- Executes just before DieselNOxEmissionsRate is made visible.
    function DieselNOxEmissionsRate_OpeningFcn(hObject, eventdata,
handles, varargin)

    % Choose default command line output for DieselNOxEmissionsRate
handles.output = hObject;

    % Update handles structure
guidata(hObject, handles);

    % --- Outputs from this function are returned to the command line.
    function varargout = DieselNOxEmissionsRate_OutputFcn(hObject,
eventdata, handles)

    % Get default command line output from handles structure
varargout{1} = handles.output;

    % Equivalence Ratio Edit Text Box
    function ERet_Callback(hObject, eventdata, handles)

    % --- Executes during object creation, after setting all properties.
    function ERet_CreateFcn(hObject, eventdata, handles)

    %         See ISPC and COMPUTER.
    if ispc && isequal(get(hObject,'BackgroundColor'),
get(0,'defaultUicontrolBackgroundColor'))
        set(hObject,'BackgroundColor','white');
    end

    % Air Density Edit Text Box
    function ADet_Callback(hObject, eventdata, handles)

    % --- Executes during object creation, after setting all properties.
    function ADet_CreateFcn(hObject, eventdata, handles)

    % Volumetric Efficiency Edit Text Box
    function VEet_Callback(hObject, eventdata, handles)

    % --- Executes during object creation, after setting all properties.
    function VEet_CreateFcn(hObject, eventdata, handles)

    % Displaced Volume Edit Text Box
    function DVet_Callback(hObject, eventdata, handles)

    % --- Executes during object creation, after setting all properties.

```



```

function DVet_CreateFcn(hObject, eventdata, handles)

% Vehicle Speed Edit Text Box
function VSet_Callback(hObject, eventdata, handles)

% --- Executes during object creation, after setting all properties.
function VSet_CreateFcn(hObject, eventdata, handles)

% Gear Ratio Edit Text Box
function GRet_Callback(hObject, eventdata, handles)

% --- Executes during object creation, after setting all properties.
function GRet_CreateFcn(hObject, eventdata, handles)

% Final Drive Ratio Edit Text Box
function FDRet_Callback(hObject, eventdata, handles)

% --- Executes during object creation, after setting all properties.
function FDRet_CreateFcn(hObject, eventdata, handles)

% Vehicle Tire Rolling Radius Edit Text Box
function VTRRet_Callback(hObject, eventdata, handles)

% --- Executes during object creation, after setting all properties.
function VTRRet_CreateFcn(hObject, eventdata, handles)

% Vehicle Acceleration Edit Text Box
function VAet_Callback(hObject, eventdata, handles)

% --- Executes during object creation, after setting all properties.
function VAet_CreateFcn(hObject, eventdata, handles)

% Unburned Hydrocarbon Edit Text Box
function UHet_Callback(hObject, eventdata, handles)

% --- Executes during object creation, after setting all properties.
function UHet_CreateFcn(hObject, eventdata, handles)

% Diesel NOx Emission Rate Push Button
% --- Executes on button press in DNOxERpb.
function DNOxERpb_Callback(hObject, eventdata, handles)

aNOx=str2num(get(handles.ERet,'string'))
bNOx=str2num(get(handles.ADet,'string'))
cNOx=str2num(get(handles.VEet,'string'))
dNOx=str2num(get(handles.DVet,'string'))
eNOx=str2num(get(handles.VSet,'string'))
fNOx=str2num(get(handles.GRet,'string'))
gNOx=str2num(get(handles.FDRet,'string'))
hNOx=str2num(get(handles.VTRRet,'string'))
iNOx=str2num(get(handles.VAet,'string'))
jNOx=str2num(get(handles.UHet,'string'))

mDotSS=((aNOx*0.069588*bNOx*(cNOx/100)*(dNOx/10)*eNOx*fNOx*gNOx*2)/(h
NOx*2*3.14))*1000 % Steady state fuel mass flow rate (g/s)

```

```

Rnosszmls=((mDotSS*((0.030)*(1-
(jNOx*0.000001))*((0.00001)^2)*(0.799)*(0.199))*(hNOx/(fNOx*gNOx)))/
(0.0137*(1)))*(2^-3.82)*(exp(eNOx/(2^3.7)))*1000 % Zeldovich
Mechanism for Steady Speed-based NO emission rate (g/s) for Low Speed
Cycles

Rnosszmhs=((mDotSS*((0.030)*(1-
(jNOx*0.000001))*((0.00001)^2)*(0.799)*(0.199))*(hNOx/(fNOx*gNOx)))/
(0.0137*(1)))*(2^-4.97)*(exp(eNOx/(2^3.55)))*1000 % Zeldovich
Mechanism for Steady Speed-based NO emission rate (g/s) for High
Speed Cycles

Rnossezmls=((mDotSS*((0.030)*(1-
(jNOx*0.000001))*((0.015)^2)*(0.356)*(0.356))*(hNOx/(fNOx*gNOx)))/(0.
0137*(1)))*(2^-3.65)*(exp(eNOx/(2^3.90)))*1000 % Extended Zeldovich
Mechanism for Steady Speed-based NO emission rate (g/s) for Low Speed
Cycles

Rnossezmhs=((mDotSS*((0.030)*(1-
(jNOx*0.000001))*((0.015)^2)*(0.356)*(0.356))*(hNOx/(fNOx*gNOx)))/(0.
0137*(1)))*(2^-4.85)*(exp(eNOx/(2^3.55)))*1000 % Extended Zeldovich
Mechanism for Steady Speed-based NO emission rate (g/s) for High
Speed Cycles

Rnosssezmls=((mDotSS*((0.030)*(1-
(jNOx*0.000001))*((0.018)^2)*(0.0176)*(0.0176))*(hNOx/(fNOx*gNOx)))/
(0.0137*(1)))*(2^-3.82)*(exp(eNOx/(2^3.7)))*1000 % Super Extended
Zeldovich Mechanism for Steady Speed-based NO emission rate (g/s) for
Low Speed Cycles

Rnosssezmhs=((mDotSS*((0.030)*(1-
(jNOx*0.000001))*((0.018)^2)*(0.0176)*(0.0176))*(hNOx/(fNOx*gNOx)))/
(0.0137*(1)))*(2^-4.97)*(exp(eNOx/(2^3.55)))*1000 % Super Extended
Zeldovich Mechanism for Steady Speed-based NO emission rate (g/s) for
High Speed Cycles

Rno2ssls=((mDotSS*((0.046)*(1-
(jNOx*0.000001))*(6^1.5)*(0.0066)*((0.0034)^0.5))*((hNOx/(fNOx*gNOx))
^0.5)*(eNOx^0.5))/((0.0137)*(1)))*(2^-
16.15)*(exp(eNOx/(2^3.85)))*1000 % for Steady Speed-based NO2
emission rate (g/s) for Low Speed Cycles

Rno2sshs=((mDotSS*((0.046)*(1-
(jNOx*0.000001))*(6^1.5)*(0.0066)*((0.0034)^0.5))*((hNOx/(fNOx*gNOx))
^0.5)*(eNOx^0.5))/((0.0137)*(1)))*(2^-
17.95)*(exp(eNOx/(2^3.55)))*1000 % for Steady Speed-based NO2
emission rate (g/s) for High Speed Cycles

if iNOx==0 & eNOx<=13.9 % i.e. Acceleration = 0 and Vehicle Speed <=
50 km/h

set(handles.DNOxERtext,'string',num2str(Rno2ssls+(Rnosszmls+Rnossezml
s+Rnosssezmls)))

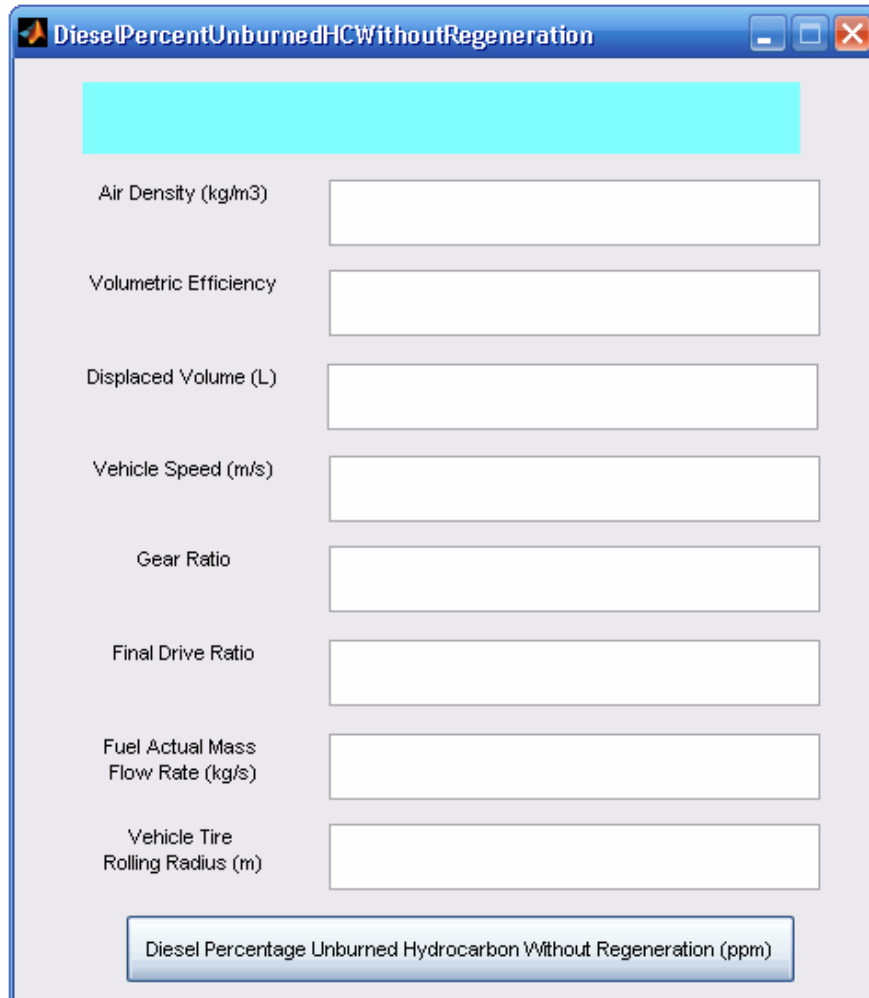
elseif iNOx==0 & eNOx>13.9 % i.e. Acceleration = 0 and Vehicle Speed
> 50 km/h

```

```
set(handles.DNOxERtext,'string',num2str(Rno2sshs+(Rnosszmhs+Rnossezmh  
s+Rnossezmhhs)))
```

APPENDIX D

DIESEL PERCENT UNBURNED HC WITH REGENERATION INTERFACE FACILITY AND CODE



```
function varargout =  
DieselPercentUnburnedHCWithoutRegeneration(varargin)  
  
% Begin initialization code  
gui_Singleton = 1;  
gui_State = struct('gui_Name',       mfilename, ...  
                  'gui_Singleton',  gui_Singleton, ...  
                  'gui_OpeningFcn', @DieselPercentUnburnedHCWithoutRegeneration_OpeningFcn, ...  
                  'gui_OutputFcn',  @DieselPercentUnburnedHCWithoutRegeneration_OutputFcn, ...  
                  'gui_LayoutFcn',  [], ...  
                  'gui_Callback',   []);  
  
if nargin && ischar(varargin{1})  
    gui_State.gui_Callback = str2func(varargin{1});  
end  
  
if nargout  
    [varargout{1:nargout}] = gui_mainfcn(gui_State, varargin{:});  
end
```

```

else
    gui_mainfcn(gui_State, varargin{:});
end
% End initialization code

% --- Executes just before DieselPercentUnburnedHCWithoutRegeneration
is made visible.
function
DieselPercentUnburnedHCWithoutRegeneration_OpeningFcn(hObject,
eventdata, handles, varargin)

% Choose default command line output for
DieselPercentUnburnedHCWithoutRegeneration
handles.output = hObject;

% Update handles structure
guidata(hObject, handles);

% --- Outputs from this function are returned to the command line.
function varargout =
DieselPercentUnburnedHCWithoutRegeneration_OutputFcn(hObject,
eventdata, handles)

% Get default command line output from handles structure
varargout{1} = handles.output;

function ADet_Callback(hObject, eventdata, handles)

% --- Executes during object creation, after setting all properties.
function ADet_CreateFcn(hObject, eventdata, handles)

%       See ISPC and COMPUTER.
if ispc && isequal(get(hObject,'BackgroundColor'),
get(0,'defaultUiControlBackgroundColor'))
    set(hObject,'BackgroundColor','white');
end

function VEet_Callback(hObject, eventdata, handles)

% --- Executes during object creation, after setting all properties.
function VEet_CreateFcn(hObject, eventdata, handles)

function DVet_Callback(hObject, eventdata, handles)

% --- Executes during object creation, after setting all properties.
function DVet_CreateFcn(hObject, eventdata, handles)

function VSet_Callback(hObject, eventdata, handles)

% --- Executes during object creation, after setting all properties.
function VSet_CreateFcn(hObject, eventdata, handles)

function GRet_Callback(hObject, eventdata, handles)

```

```

% --- Executes during object creation, after setting all properties.
function GRet_CreateFcn(hObject, eventdata, handles)

function FDRet_Callback(hObject, eventdata, handles)

% --- Executes during object creation, after setting all properties.
function FDRet_CreateFcn(hObject, eventdata, handles)

function FAMFRet_Callback(hObject, eventdata, handles)

% --- Executes during object creation, after setting all properties.
function FAMFRet_CreateFcn(hObject, eventdata, handles)

function VTRRet_Callback(hObject, eventdata, handles)

% --- Executes during object creation, after setting all properties.
function VTRRet_CreateFcn(hObject, eventdata, handles)

% --- Executes on button press in DPUHWRpb.
function DPUHWRpb_Callback(hObject, eventdata, handles)
% hObject      handle to DPUHWRpb (see GCBO)
% eventdata    reserved - to be defined in a future version of MATLAB
% handles      structure with handles and user data (see GUIDATA)

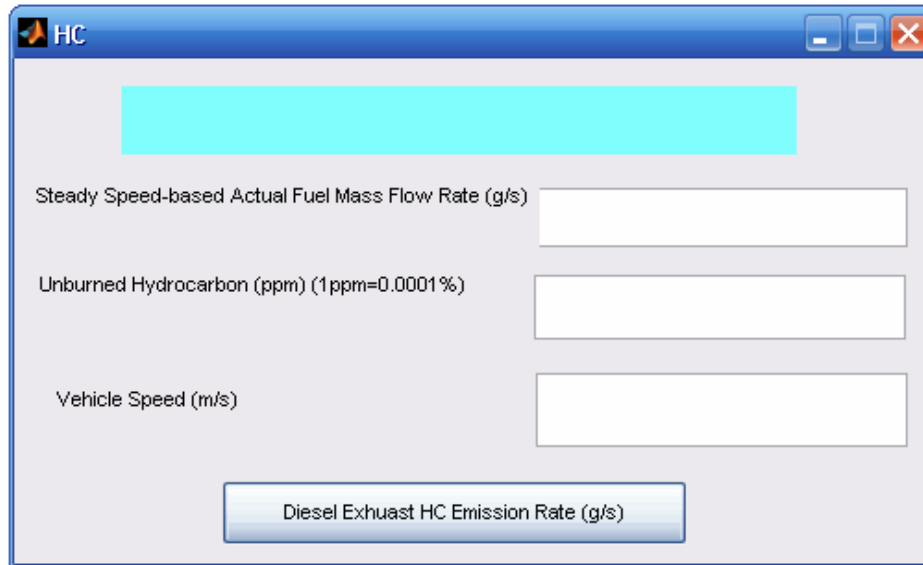
aPUHWR=str2num(get(handles.ADet,'string'))
bPUHWR=str2num(get(handles.VEet,'string'))
cPUHWR=str2num(get(handles.DVet,'string'))
dPUHWR=str2num(get(handles.VSet,'string'))
ePUHWR=str2num(get(handles.GRet,'string'))
gPUHWR=str2num(get(handles.FDRet,'string'))
iPUHWR=str2num(get(handles.FAMFRet,'string'))
jPUHWR=str2num(get(handles.VTRRet,'string'))

set(handles.PUHWRtext,'string',num2str(4*(2^5)*( 1- (0.01*(( (
(aPUHWR* bPUHWR* (cPUHWR/10000)* dPUHWR* ePUHWR* gPUHWR*
2)/(2*pi*jPUHWR*iPUHWR) )+1) * ( ((1*(-
454.5e3))+(22.8*(0))+(85.82*(0)))-((16*(-393.5e3))+(13.6*(-
241.8e3))+(85.82*(0))))/(42.8e6) )))))

```

APPENDIX E

DIESEL HC EMISSIONS RATE INTERFACE FACILITY AND CODE



```
function varargout = HC(varargin)

% Begin initialization code
gui_Singleton = 1;
gui_State = struct('gui_Name',       mfilename, ...
                  'gui_Singleton',   gui_Singleton, ...
                  'gui_OpeningFcn', @HC_OpeningFcn, ...
                  'gui_OutputFcn',  @HC_OutputFcn, ...
                  'gui_LayoutFcn',  [], ...
                  'gui_Callback',    []);
if nargin && ischar(varargin{1})
    gui_State.gui_Callback = str2func(varargin{1});
end

if nargout
    [varargout{1:nargout}] = gui_mainfcn(gui_State, varargin{:});
else
    gui_mainfcn(gui_State, varargin{:});
end
% End initialization code

% --- Executes just before HC is made visible.
function HC_OpeningFcn(hObject, eventdata, handles, varargin)

% Choose default command line output for HC
handles.output = hObject;

% Update handles structure
guidata(hObject, handles);

% --- Outputs from this function are returned to the command line.
function varargout = HC_OutputFcn(hObject, eventdata, handles)
```

```

% Get default command line output from handles structure
varargout{1} = handles.output;

function edit1_Callback(hObject, eventdata, handles)

% --- Executes during object creation, after setting all properties.
function edit1_CreateFcn(hObject, eventdata, handles)

%       See ISPC and COMPUTER.
if ispc && isequal(get(hObject,'BackgroundColor'),
get(0,'defaultUiControlBackgroundColor'))
    set(hObject,'BackgroundColor','white');
end

function edit2_Callback(hObject, eventdata, handles)

% --- Executes during object creation, after setting all properties.
function edit2_CreateFcn(hObject, eventdata, handles)

function edit3_Callback(hObject, eventdata, handles)

% --- Executes during object creation, after setting all properties.
function edit3_CreateFcn(hObject, eventdata, handles)

% --- Executes on button press in pushbutton1.
function pushbutton1_Callback(hObject, eventdata, handles)

aHCER=str2num(get(handles.edit1,'string')) % Actual steady state fuel
mass flow rate
bHCER=str2num(get(handles.edit2,'string')) % Unburned Hydrocarbon
cHCER=str2num(get(handles.edit3,'string')) % Vehicle Speed

HCRls= ( (aHCER*(2^-10.46)) * (exp(bHCER*0.000001)) ) % i.e.
Speed<= 50 km/h and steady speed so that Accelration=0

HCRhs= ( (aHCER*(2^-9.97)) * (exp(bHCER*0.000001)) ) % i.e. Speed>
50 km/h and steady speed so that Accelration=0

if cHCER<=13.9 % i.e. Speed<= 50 km/h and steady speed so
Accelration=0
set(handles.text1,'string',num2str(HCRls))

elseif cHCER>13.9 % i.e. Speed> 50 km/h and steady speed so that
Accelration=0
set(handles.text1,'string',num2str(HCRhs))

end

```


APPENDIX F

COMPARISONS BETWEEN THE SUBCATEGORIES OF EACH OF THE MODELLING CLASSIFICATIONS

F.I COMPARISON OF ASSUMPTIONS AND LIMITATIONS IN SUBCATEGORIES OF MODELLING

In modelling, assumptions play a key role to tell how robust the developed model is. The limitations of modelling as well help the model users to grasp to what extent this model can be used efficiently and help the model developers to better understand how this model can be extended and further developed. Therefore, this section elucidates the key assumptions and limitations in the five classifications of modelling presented in this study as shown in Table F.I, Table F.II, Table F.III, Table F.IV, and Table F.V, respectively.

Table F.I
The main assumptions and limitations in the scale of the input variable-based modelling classification

Modelling type	Assumptions	Limitations
Microscopic vehicle fuel consumption and emissions models	1. Assuming a constant emissions rate (Rakha, et al., 2004a).	1. Relatively expensive and time-consuming (Yue, 2008; Rakha, 2011); 2. The requirements of a validated microscopic model for large-scale modelling are: (a) the model must be capable of modelling Origin-Destination demand tables, (b) the model must be capable of modelling dynamic traffic routing, and (c) the model must be capable of modelling the dynamic interaction of freeway/arterial facilities (Rakha, 1998).
Macroscopic vehicle fuel consumption and emissions models	1. Assuming all vehicles maintain a constant speed while on the highway and no overtaking is allowed (Durrani, 2010). Vehicles follow each other with the same speed. If a vehicle is below the desired speed it will accelerate to that speed using the maximum possible acceleration for the given speed and vehicle type; 2. All vehicles pollute similarly for the same average speed and vehicle-miles traveled (An and Barth, 1997); 3. Variations in driver's behavior can be neglected (An and Barth, 1997).	1. Are based on statistical analysis of publicly available data and engine maps (Yue, 2008; Rakha, 2011); 2. Do not adequately take into account aerodynamic drag resistance at high speeds, and thus they should only be used for average speeds of less than 55 km/h in most cases (Akcelik, 1985).
Mesoscopic vehicle fuel consumption and emissions models	1. Assuming a constant emissions rate (Rakha, et al., 2004a).	1. Relatively expensive and time-consuming (Yue, 2008; Rakha, 2011).

Table F.II
The main assumptions and limitations in the formulation approach-based modelling classification

Modelling type	Assumptions	Limitations
Analytical models	<ol style="list-style-type: none"> 1. Each cylinder undergoes the same thermodynamic cycle (Streit and Borman, 1971); 2. Volumetric efficiency is assumed to be constant (Souder, 2002); 3. The ideal gas law applies in the intake manifold, engine, and exhaust manifold (Sun et al., 2005). 4. Combustion is modeled as a uniformly distributed heat release process (Kim et al., 2002); 5. Constant temperature of exhaust manifold (Ceccarelli, 2009); 6. Air is an ideal gas (Ni and Henclewood, 2008). 	<ol style="list-style-type: none"> 1. Since they usually are not simple models, they can not be easily integrated into modern automobile control systems without simplification which in turn may lead to modelling errors (Organisation for Economic Co-operation and Development, 2002).
Empirical models	<ol style="list-style-type: none"> 1. Emission rates can be approximated as a linear function of fuel rate (Cappiello et al., 2002); 2. The variables that govern emission rates are the same variables that govern fuel rate (Cappiello et al., 2002); 3. The ideal gas law holds in the intake manifold (Gerdes and Hedrick, 1997). 	<ol style="list-style-type: none"> 1. Simplification of a model leads to some modelling errors (Organisation for Economic Co-operation and Development, 2002); 2. They sometimes do not describe the physical phenomena associated with vehicle operation and emissions productions comprehensively with explainable mathematical trends and rationally-accepted results (Ni and Henclewood, 2008; Cook et al., 2006; Barth et al., 1996; Barth et al., 1998; Ahn, 1998); 3. In evaluating fuel consumption and exhaust emissions models, vehicle-to-vehicle correlation is impossible due to the well-known high variability of emissions between nominally identical vehicles (Leung and Williams, 2000).

Table F.II – Continued

Statistical models	<ol style="list-style-type: none"> 1. Assuming the data are a representative sample of the facility traffic (Rothery, 1975); 2. Average vehicle fuel efficiency (Ang, 1990); 3. Average driver's behaviour (Ang, 1990); 4. Average trip characteristics (Ang, 1990). 	<ol style="list-style-type: none"> 1. Available data are often not sufficiently detailed (in terms of key variables such as hourly traffic, freight vehicle shares, fuel consumption per vehicle, average annual distance travelled) (Organisation for Economic Co-operation and Development, 2002); 2. Although emission maps are relatively easy to be generated and to be used, emission maps are sometimes not satisfactory because emission maps can be highly sensitive to the driving cycle (Cappiello et al., 2002); 3. Emission maps are also sparse and not flexible enough to account for such factors as road grade, loading condition such as accessory use, or history effects (Cappiello et al., 2002).
Graphical models	<ol style="list-style-type: none"> 1. The processor is sufficiently fast to run the model (Weeks and Moskwa, 1995); 2. Air and EGR are homogeneously mixed and have the same molecular weight and temperature (Weeks and Moskwa, 1995). 	<ol style="list-style-type: none"> 1. Generate estimates of relatively low prediction accuracy (Smit and McBroom, 2009).

Table F.III
The main assumptions and limitations in the main input variable-based modelling classification

Modelling type	Assumptions	Limitations
Average speed models	<ol style="list-style-type: none"> 1. Assuming all vehicles maintain a constant speed while on the highway and no overtaking is allowed (Durrani et al., 2010). 2. All vehicles pollute similarly for the same average speed and vehicle-miles traveled (An and Barth, 1997); 3. Variations in driver's behavior can be neglected (An and Barth, 1997). 	<ol style="list-style-type: none"> 1. Should only be used for average speeds of less than 55 km/h in most cases (Akcelik, 1985); 2. Are based on statistical analysis of publicly available data and engine maps (Rakha, 2011).
Instantaneous speed models	<ol style="list-style-type: none"> 1. Vehicles are not operating under cold start conditions (Park et al., 2001); 2. Vehicles follow each other with the same speed (Park et al., 2001). 	<ol style="list-style-type: none"> 1. Relatively expensive and time-consuming (Rakha, 2011).
Specific power models	<ol style="list-style-type: none"> 1. Most alternative fueled vehicles were assumed to have the same corrections as their gasoline counterparts (Davis et al., 2005). 	<ol style="list-style-type: none"> 1. The use of vehicle specific power usually results in a bang-bang control (i.e. the optimum fuel consumption results from a full throttle acceleration) (Durrani et al., 2010).

Table F.IV
The main assumptions and limitations in the state variable value-based modelling classification

Modelling type	Assumptions	Limitations
Crank-angle resolution-based models	<ol style="list-style-type: none"> 1. A constant intercooler temperature (Guzzella and Amstutz, 1998); 2. The engine is assumed to be nominally operated at the constant set-point (e.g. angular speed, mass flow rate, and temperature) (Guzzella and Amstutz, 1998). 	<ol style="list-style-type: none"> 1. Require relatively long computational time for their complexity (Guzzella and Amstutz, 1998).
Mean value-based models	<ol style="list-style-type: none"> 1. All cylinders and all strokes have the same crank-angle phase difference (Guzzella and Amstutz, 1998); 2. The intake manifold and cylinders are modeled as mass and internal energy reservoirs in the usual "emptying and filling" approach (Winterbone, 1977); 3. No heat-losses in the compressor walls (Guzzella and Amstutz, 1998). 	<ol style="list-style-type: none"> 1. Do not account for delays (Guzzella and Amstutz, 1998).

Table F.V
The main assumptions and limitations in the number of dimensions-based modelling classification

Modelling type	Assumptions	Limitations
Zero/one dimensional /single zone models	1. The cylinder charge is uniform in both composition and temperature, at all time during the cycle (Jung and Assanis, 2001; Foster, 1985).	1. Do not account for the spatial variation in mixture composition and temperature in the cylinder charge (Jung and Assanis, 2001; Foster, 1985).
Quasi dimensional models	1. There is a degree of spatial variation in mixture composition and temperature in the cylinder charge (Jung and Assanis, 2001).	1. Do not account for large spatial variations in mixture composition and temperature in the cylinder charge (Jung and Assanis, 2001).
Multi dimensional /multi zone models	1. There is spatial variation in mixture composition and temperature in the cylinder charge (Jung and Assanis, 2001; Bracco, 1985); 2. The control volume of each zone is treated as an open system, and mass and energy equations are solved for each zone (Jung and Assanis, 2001; Bracco, 1985).	1. Require relatively long computational time and therefore are less suitable for control applications (Jung and Assanis, 2001; Bracco, 1985).

The merits and drawbacks of these subcategories of powertrain modelling classifications are elucidated in the next subsection.

F.II COMPARISON OF MERITS AND DRAWBACKS OF SUBCATEGORIES OF MODELLING

Since modelling types vary with respect to strengths and weaknesses, this section presents how different the presented modelling subcategories are with respect to these aspects. Thus, the merits and drawbacks of the five classifications of modelling

presented in this study are presented in Table F.VI, Table F.VII, Table F.VIII, Table F.IX, and Table F.X, respectively.

Table F.VI
The merits and drawbacks of the scale of the input variable-based modelling classification

Modelling type	Merits	Drawbacks
Microscopic vehicle fuel consumption and emissions models	<ol style="list-style-type: none"> 1. Capture transient changes in a vehicle speed and acceleration level as it travels on a highway network (Marsden et al., 2001); 2. Capture the impact of intelligent transportation system strategies such as traffic signal coordination (Marsden et al., 2001; Fang and Elefteriadou, 2008); 3. More accurate in estimating vehicle emissions than macroscopic models in terms of both their absolute magnitude and their relative trends than of average speed-based models (Hallmark, 2000; Rakha and Van Aerde, 2000; Fang and Elefteriadou, 2008). 	<ol style="list-style-type: none"> 1. The calibration of a microscopic model of a large-scale network is an extensively time consuming task (Rakha et al., 1998). 2. Microscopic models are very labour intensive in conducting inventory analysis given that they need very detailed information which may not be available (Yue, 2008).
Macroscopic vehicle fuel consumption and emissions models	<ol style="list-style-type: none"> 1. Are helpful in estimating aggregate emissions inventories (Rakha, et al., 2004a; Rakha and Ahn, 2004; Gning, 2011). 	<ol style="list-style-type: none"> 1. Ignore transient changes in a vehicle speed and acceleration level as it travels on a highway network (Yue, 2008); 2. Less accurate in estimating vehicle emissions than microscopic models (Hallmark et al., 2000).
Mesoscopic vehicle fuel consumption and emissions models	<ol style="list-style-type: none"> 1. Mesoscopic models utilize link-by-link input parameters to construct a synthetic drive cycle and to compute average link fuel consumption and emission rates while utilizing instantaneous speed and instantaneous acceleration inputs (Yue, 2008; Li and Ioannou, 2004); 2. Can be used for computing average fuel consumption and emission rates for a specific facility type (Yue, 2008; An and Barth, 1997). 	<ol style="list-style-type: none"> 1. Can not be used alone to estimate emissions inventory (Yue, 2008).

Table F.VII

The merits and drawbacks of the formulation approach-based modelling classification

Modelling type	Merits	Drawbacks
Analytical models	<ol style="list-style-type: none"> 1. Describe the physical phenomena associated with vehicle operation and emissions productions and with explainable mathematical trends (Barth et al., 1996; Barth et al., 1998; Ahn, 1998); 2. Result in reasonable and rationally-accepted results (Barth et al., 1996; Barth et al., 1998; Ahn, 1998); 3. Most accurate type of formulation approach-based modelling (Hendricks, 1986; Ni and Henclewood, 2008). 	<ol style="list-style-type: none"> 1. More calculation intensive which may result in reduced computational efficiency in case of implementation (Lindhjem et al., 2004); 2. The model may be more complicated and thus require additional training for users in case of implementation (Lindhjem et al., 2004).
Empirical models	<ol style="list-style-type: none"> 1. Simple model that can be easily integrated into vehicle control systems (Lindhjem et al., 2004). 	<ol style="list-style-type: none"> 1. A lot of experimental/field data must be taken (Lindhjem et al., 2004); 2. They are valid only for the range of data based on which they are built (Lindhjem et al., 2004); 3. They sometimes do not describe the physical phenomena associated with vehicle operation and emissions productions comprehensively with explainable mathematical trends and rationally-accepted results (Ni and Henclewood, 2008; Cook et al., 2006; Barth et al., 1996; Barth et al., 1998; Ahn, 1998).
Statistical models	<ol style="list-style-type: none"> 1. Relatively easy to be made (Lindhjem et al., 2004); 2. Uncertainty can be quantified (Lindhjem et al., 2004). 	<ol style="list-style-type: none"> 1. Data-driven and thus their prediction can be relatively inaccurate (Lindhjem et al., 2004); 2. Require recalibration with each dataset (Lindhjem et al., 2004); 3. Difficult to interpolate gaps in the dataset and to extrapolate data beyond the bounds of the dataset (Lindhjem et al., 2004).
Graphical models	<ol style="list-style-type: none"> 1. Easy to be recognised and understood visually (Al-qaimari et al., 1995; Autili and Pelliccione, 2008). 	<ol style="list-style-type: none"> 1. Least accurate type of formulation approach-based modelling since they are simplification based on analytical models (Lloyd and Rudd, 2007).

Table F.VIII
The merits and drawbacks of the main input variable-based modelling classification

Modelling type	Merits	Drawbacks
Average speed models	1. Are helpful in estimating aggregate emissions inventories (Rakha, et al., 2004a; Rakha and Ahn, 2004; Gning, 2011).	1. Ignore transient changes in a vehicle's speed and acceleration level as it travels on a highway network (Yue, 2008); 2. Less accurate in estimating vehicle emissions than instantaneous speed models (Hallmark, 2000); 4. Do not adequately take into account aerodynamic drag resistance at high speeds (Akcelik, 1985).
Instantaneous speed models	1. Capture transient changes in a vehicle speed and acceleration level as it travels on a highway network (Marsden, 2001); 2. Capture the impact of intelligent transportation system strategies such as traffic signal coordination (Marsden, 2001); 3. More accurate in estimating vehicle emissions than average speed models in terms of both their absolute magnitude and their relative trends (Hallmark, 2000; Rakha and Van Aerde, 2000).	1. Are labour intensive in conducting inventory analysis given that they need very detailed information which may not be available (Yue, 2008).
Specific power models	1. More suitable for heavy duty diesel vehicle engines and more accurate than average speed models (Feng, 2007).	1. Need availability of relevant specific power data (Frey, 2007).

Table F.IX
The merits and drawbacks of the state variable value-based modelling classification

Modelling type	Merits	Drawbacks
Crank-angle resolution-based models	1. Accurate (Guzzella and Amstutz, 1998).	1. Require relatively long computational time for their complexity (Guzzella and Amstutz, 1998).
Mean value-based models	1. Less complicated than Crank-angle resolution-based models so that they require only short computational time (Guzzella and Amstutz, 1998; Eriksson et al., 2002); 2. Suitable for control applications (Guzzella and Amstutz, 1998; Eriksson et al., 2002).	1. Less accurate than the crank-angle resolution-based models (Guzzella and Amstutz, 1998; Eriksson et al., 2002).

Table F.X
The merits and drawbacks of the number of dimensions-based modelling classification

Modelling type	Merits	Drawbacks
Zero/one dimensional /single zone models	<ol style="list-style-type: none"> 1. Simplicity (Killingsworth, 2006; Jung and Assanis, 2001); 2. High computational efficiency (Killingsworth, 2006; Jung and Assanis, 2001); 3. Suitable for modelling and powertrain control applications (Jung and Assanis, 2001). 	<ol style="list-style-type: none"> 1. Low accuracy (Jung and Assanis, 2001).
Quasi dimensional models	<ol style="list-style-type: none"> 1. Require a moderate amount of computational time (Jung and Assanis, 2001). 	<ol style="list-style-type: none"> 1. Are not suitable for modelling large spatial variation in mixture composition and temperature in the cylinder charge (Jung and Assanis, 2001).
Multi dimensional /multi zone models	<ol style="list-style-type: none"> 1. High accuracy (Jung and Assanis, 2001). 	<ol style="list-style-type: none"> 1. Require relatively long computational time (Jung and Assanis, 2001); 2. Their usually included phenomenological sub-models that result in having results which may vary according to the assumed initial or boundary conditions in these submodels (Jung and Assanis, 2001).

The characteristic parameters and data collection techniques in these subcategories of powertrain modelling classifications are elucidated in the next subsection.

F.III COMPARISON OF CHARACTERISTIC PARAMETERS AND DATA COLLECTION TECHNIQUE IN SUBCATEGORIES IF MODELIING

Characteristic parameters are key to implement models. They reflect the inputs to and deliverables of the model. The technique of data collection is crucial as well in

making the models developed using these data valid. Therefore, the characteristic parameters of and data collection technique in the five classifications of modelling presented in this study are elucidated in this section as shown in Table F.XI, Table F.XII, Table F.XIII, Table F.XIV, and Table F.XV, respectively.

Table F.XI
The characteristic parameters of and data collection technique in the scale of the input variable-based modelling classification

Modelling type	Characteristic parameters	Data collection technique
Microscopic vehicle fuel consumption and emissions models	<ol style="list-style-type: none"> 1. Instantaneous crankshaft speed (Rakha and Van Aerde, 2000; Ahn, 2002; De Nicolao, 1996; Rakha, 2011); 2. Instantaneous crankshaft acceleration (Rakha and Van Aerde, 2000; Ahn, 2002; De Nicolao, 1996; Rakha, 2011). 	<ol style="list-style-type: none"> 1. Field data collection (Yildiz et al., 2009; Rakha, et al., 2004a; Sorenson et al., 2005); 2. Lab dynamometer (Yildiz et al., 2009; Rakha, et al., 2004a; Sorenson et al., 2005).
Macroscopic vehicle fuel consumption and emissions models	<ol style="list-style-type: none"> 1. Vehicle average speed (Rakha, 2011); 2. Vehicle average acceleration (Rakha, 2011). 	<ol style="list-style-type: none"> 1. Field data collection (Rakha, 2011; Rakha, 2004; Rakha and Ahn, 2004); 2. Engine maps (Rakha, 2011; Rakha, et al., 2004a; Rakha and Ahn, 2004).
Mesosopic vehicle fuel consumption and emissions models	<ol style="list-style-type: none"> 1. Instantaneous engine speed (De Nicolao et al., 1996; Yue, 2008; Rakha and Van Aerde, 2000; Ahn, 2002); 2. Instantaneous engine acceleration (Yue, 2008; Rakha and Van Aerde, 2000; Ahn, 2002). 	<ol style="list-style-type: none"> 1. Field data collection (Rakha, 2011; Rakha, et al., 2004a; Rakha and Ahn, 2004; Yue, 2008); 2. Engine maps (Rakha, 2011; Rakha, et al., 2004a; Rakha and Ahn, 2004; Yue, 2008).

Table F.XII
The characteristic parameters of and data collection technique in the formulation
approach-based modelling classification

Modelling type	Characteristic parameters	Data collection technique
Analytical models	<ol style="list-style-type: none"> 1. Instantaneous crankshaft speed (Rakha and Van Aerde, 2000; Ahn, 2002; De Nicolao et al., 1996; Rakha, 2011); 2. Instantaneous crankshaft acceleration (Rakha and Van Aerde, 2000; Ahn, 2002; De Nicolao et al., 1996; Rakha, 2011); 3. Engine torque (De Nicolao et al., 1996; Rakha, 2011); 4. Intake manifold pressure (DeNicolao et al., 1996; Rakha, 2011); 5. Engine displacement volume (Frey et al., 2007). 	No data are required to be collected.
Empirical models	<ol style="list-style-type: none"> 1. Vehicle average speed (Rakha, 2011); 2. Vehicle average acceleration (Rakha, 2011); 3. Engine torque (De Nicolao, 1996; Rakha, 2011). 	<ol style="list-style-type: none"> 1. Field data collection (Rakha, 2011; Rakha, et al., 2004a; Rakha and Ahn, 2004; Joumard et al., 1999); 2. Engine maps (Rakha, 2011; Rakha, et al., 2004a; Rakha and Ahn, 2004; Joumard et al., 1999).
Statistical models	<ol style="list-style-type: none"> 1. Vehicle average speed (Rakha, 2011); 2. Vehicle average acceleration (Rakha, 2011); 3. Engine torque (De Nicolao et al., 1996; Rakha, 2011); 4. Road grade (Lindhjem et al., 2004); 5. Vehicle weight (Lindhjem et al., 2004); 6. Loading condition, such as accessory use (e.g. air conditioning) (Yue, 2008). 	<ol style="list-style-type: none"> 1. Remote sensing-based field data collection with the aid of Global Positioning System (GPS) in case of expected high emission rates (Rakha, 2011; Rakha, et al., 2004a; Rakha and Ahn, 2004; Joumard et al., 1999; Lindhjem et al., 2004); 2. On-vehicle portable dynamometer with on-vehicle data-processing unit-based field data collection in case of expected low emission rates (Rakha, 2011; Rakha, et al., 2004a; Rakha and Ahn, 2004; Joumard et al., 1999; Lindhjem et al., 2004); 3. Engine maps (Rakha, 2011; Rakha, et al., 2004a; Rakha and Ahn, 2004; Joumard et al., 1999).
Graphical models	<ol style="list-style-type: none"> 1. Vehicle average speed (Rakha, 2011); 2. Vehicle average acceleration (Rakha, 2011). 	<ol style="list-style-type: none"> 1. Field data collection (Rakha, 2011; Rakha, et al., 2004a; Rakha and Ahn, 2004; Joumard et al., 1999); 2. Engine maps (Rakha, 2011; Rakha, et al., 2004a; Rakha and Ahn, 2004; Joumard et al., 1999).

Table F.XIII
The characteristic parameters of and data collection technique in the main input
variable-based modelling classification

Modelling type	Characteristic parameters	Data collection technique
Average speed models	<ol style="list-style-type: none"> 1. Vehicle average speed (Rakha, 2011; Rakha, 2004; Rakha and Ahn, 2004; Joumard et al., 1999); 2. Vehicle average acceleration (Rakha, 2011; Rakha, et al., 2004a; Rakha and Ahn, 2004; Joumard et al., 1999). 	<ol style="list-style-type: none"> 1. Field data collection (Rakha, 2011; Rakha, et al., 2004a; Rakha and Ahn, 2004; Joumard et al., 1999); 2. Engine maps (Rakha, 2011; Rakha, et al., 2004a; Rakha and Ahn, 2004; Joumard et al., 1999).
Instantaneous speed models	<ol style="list-style-type: none"> 1. Crankshaft instantaneous speed (De Nicolao et al., 1996; Joumard et al., 1999; Rakha and Van Aerde, 2000; Ahn, 2002); 2. Crankshaft instantaneous acceleration (De Nicolao et al., 1996; Joumard et al., 1999; Rakha and Van Aerde, 2000; Ahn, 2002). 	<ol style="list-style-type: none"> 1. Field data collection (Rakha, 2011; Rakha, et al., 2004a; Rakha and Ahn, 2004; Joumard et al., 1999); 2. Lab dynamometer (Rakha, 2011; Rakha, et al., 2004a; Rakha and Ahn, 2004; Joumard et al., 1999).
Specific power models	<ol style="list-style-type: none"> 1. Engine torque (De Nicolao et al., 1996; Rakha, 2011); 2. Crankshaft speed (De Nicolao et al., 1996; Rakha, 2011); 3. Intake manifold pressure (De Nicolao et al., 1996; Rakha, 2011). 4. Engine displacement volume (Frey et al., 2007). 	<ol style="list-style-type: none"> 1. Field data collection (Rakha, 2011; Rakha, et al., 2004a; Rakha and Ahn, 2004); 2. Engine maps (Rakha, 2011; Rakha, et al., 2004a; Rakha and Ahn, 2004); 3. Portable emissions measurement instrument (Wang et al., 2008).

Table F.XIV
The characteristic parameters of and data collection technique in the state variable
value-based modelling classification

Modelling type	Characteristic parameters	Data collection technique
Crank-angle resolution-based models	<ol style="list-style-type: none"> 1. Crank angle (Guzzella and Amstutz, 1998); 2. Crank shaft angular speed (Guzzella and Amstutz, 1998); 3. Fluid mass flow rate (Guzzella and Amstutz, 1998); 4. Fluid temperature (Guzzella and Amstutz, 1998). 	<ol style="list-style-type: none"> 1. For models validation, published data of real engines are used, such as manufacturer's turbine data sheets (Guzzella and Amstutz, 1998). 2. For models validation, measured data from real engines are used (Guzzella and Amstutz, 1998).
Mean value-based models	<ol style="list-style-type: none"> 1. Intake manifold temperature (Guzzella and Amstutz, 1998; Eriksson et al., 2002); 2. Intake manifold pressure (Guzzella and Amstutz, 1998; Eriksson et al., 2002); 3. Exhaust manifold temperature (Guzzella and Amstutz, 1998; Eriksson et al., 2002); 4. Exhaust manifold pressure (Guzzella and Amstutz, 1998; Eriksson et al., 2002); 5. Fluid mass flow rate (Guzzella and Amstutz, 1998; Eriksson et al., 2002). 	<ol style="list-style-type: none"> 1. For models validation, measured data from real engines are used (Guzzella and Amstutz, 1998; Eriksson et al., 2002).

Table F.XV
The characteristic parameters of and data collection technique in the number of
dimensions-based modelling classification

Modelling type	Characteristic parameters	Data collection technique
Zero/one dimensional/ single zone models	<ol style="list-style-type: none"> 1. Temperature of the zone (Jung and Assanis, 2001; Foster, 1985); 2. Volume of the zone (Jung and Assanis, 2001; Foster, 1985). 	<ol style="list-style-type: none"> 1. Data for validation are experimental data collected from representative engines (Jung and Assanis, 2001; Foster, 1985).
Quasi dimensional models	<ol style="list-style-type: none"> 1. Temperature of the zone (Jung and Assanis, 2001); 2. Volume of the zone (Jung and Assanis, 2001). 	<ol style="list-style-type: none"> 1. Data for validation are experimental data collected from representative engines (Jung and Assanis, 2001).
Multi dimensional/ multi zone models	<ol style="list-style-type: none"> 1. Start of injection timing (Jung and Assanis, 2001; Bracco, 1985); 2. Injection pressure (Jung and Assanis, 2001; Bracco, 1985); 3. Density of the mixture (Jung and Assanis, 2001; Bracco, 1985); 4. The mass fraction of fuel vapor (Jung and Assanis, 2001; Bracco, 1985); 5. The mass fraction of oxygen (Jung and Assanis, 2001; Bracco, 1985); 6. Temperature of the zone (Jung and Assanis, 2001; Bracco, 1985); 7. Volume of the zone (Jung and Assanis, 2001; Bracco, 1985); 8. Engine average speed (Jung and Assanis, 2001; Bracco, 1985); 9. Average fuel/air equivalence ratio (Jung and Assanis, 2001; Bracco, 1985). 	<ol style="list-style-type: none"> 1. Data for validation are experimental data collected from representative engines (Jung and Assanis, 2001; Bracco, 1985).

The accuracy and relevance to road traffic in these subcategories of powertrain modelling classifications are elucidated in the next subsection.

F.IV COMPARISON OF ACCURACY AND RELEVANCE TO ROAD TRAFFIC IN SUBCATEGORIES OF MODELLING

Models vary in terms of accuracy. They vary as well in their relevance to

transportation applications. This section identifies how accurate and how relevant to transportation applications is each subcategory in the presented modelling classifications. Table F.XVI, Table F.XVII, Table F.XVIII, Table F.XIX, and Table F.XX, illustrate the accuracy and relevance to road traffic of the scale of the five classifications of modelling presented in this study.

Table F.XVI
The accuracy and relevance to road traffic in the scale of the input variable-based modelling classification

Modelling type	Accuracy	Relevance to road traffic
Microscopic vehicle fuel consumption and emissions models	1. Most accurate (Ding, 2000; Hallmark et al., 2000).	1. High (Yue, 2008).
Macroscopic vehicle fuel consumption and emissions models	1. Less accurate than microscopic models (Ding, 2000; Hallmark et al., 2000).	1. Low (Yue, 2008).
Mesoscopic vehicle fuel consumption and emissions models	1. More accurate than macroscopic models (Yue, 2008).	1. Moderate (Yue, 2008).

Table F.XVII
The accuracy and relevance to road traffic in the scale of the formulation approach-based modelling classification

Modelling type	Accuracy	Relevance to road traffic
Analytical models	1. Most accurate type of formulation approach-based modelling (Ni and Henclewood, 2008; Hendricks, 1986).	1. High (Hellström, 2010; Biteus, 2002; Hendricks, 1997; Silverlind, 2001; Karmiggelt, 1998).
Empirical models	1. Less accurate than analytical models (Nieuwoudt et al., 2006; Karmiggelt, 1998).	1. High (Rakha, et al., 2004a; Rakha and Ahn, 2004).
Statistical models	1. Less accurate than empirical models (Nieuwoudt et al., 2006; Karmiggelt, 1998).	1. High (Rakha, et al., 2004a; Rakha and Ahn, 2004).
Graphical models	1. Least accurate type of formulation approach-based modelling since they are simplification based on analytical models (Nieuwoudt et al., 2006; Karmiggelt, 1998).	1. Moderate (Cho and Hedrick, 1989; Grossi et al., 2009).

Table F.XVIII

The accuracy and relevance to road traffic in the main input variable-based modelling classification

Modelling type	Accuracy	Relevance to road traffic
Average speed models	1. Were validated against field data with modelling errors of 57% (Joumard et al., 1999); 2. The use of average speed as a sole explanatory variable is inadequate for estimating vehicle fuel consumption and emissions, and the addition of speed variability as an explanatory variable results in better models (Ding, 2000).	1. High (Yue, 2008; Esteves-Booth et al., 2002).
Instantaneous speed models	1. More accurate in estimating vehicle emissions than average speed models (Hallmark et al., 2000).	1. Moderate (Yue, 2008; Esteves-Booth et al., 2002).
Specific power models	1. Were validated against field data with modelling errors of 57% (Joumard et al., 1999).	1. Moderate (Rakha, 2011).

Table F.XIX

The accuracy and relevance to road traffic in the state variable value-based modelling classification

Modelling type	Accuracy	Relevance to road traffic
Crank-angle resolution-based models	1. High (Guzzella and Amstutz, 1998).	1. Moderate (Guzzella and Amstutz, 1998).
Mean value-based models	1. Moderate (Guzzella and Amstutz, 1998; Eriksson et al., 2002).	1. High (Guzzella and Amstutz, 1998; Eriksson et al., 2002).

Table F.XX
The accuracy and relevance to road traffic in the number of dimensions-based
modelling classification

Modelling type	Accuracy	Relevance to road traffic
Zero/one dimensional/single zone models	1. Low (Jung and Assanis, 2001; Foster, 1985).	1. High (Jung and Assanis, 2001; Foster, 1985).
Quasi dimensional models	1. Moderate (Jung and Assanis, 2001).	1. Moderate (Jung and Assanis, 2001).
Multi dimensional/multi zone models	1. High (Jung and Assanis, 2001; Bracco, 1985).	1. Moderate (Jung and Assanis, 2001; Bracco, 1985).

APPENDIX G

THE FOUNDATION OF A PROPOSED LAW OF THERMODYNAMICS ON THE ENTHALPY OF GASEOUS PURE SUBSTANCES IN THERMODYNAMIC EQUILIBRIUM

Although enthalpy is the preferred expression of energy in many chemical and physical analyses because it greatly simplifies many descriptions of energy transfer, there has been as yet no thermodynamics law for enthalpy such that enthalpy can be evaluated from its fundamental definition. The need for establishing an absolute scale for the enthalpy content of a substance has been emphasized in a key reference in Thermodynamics authored by a key research authority in the Thermodynamics research area (Obert, 1973). This key reference (Obert, 1973) states on page 80: *'Table VB in the appendix yields the absolute values of entropy for each constituent. Unfortunately, there is no thermodynamics law for the property of enthalpy, so that tables of relative enthalpies must be consulted'*. The combination of the words *"unfortunately there is no thermodynamics law for the property of enthalpy"* with the word *"must"* gives the obviously dominant implication that the world renowned authority in thermodynamics research Professor Edward Obert, whose name is commemorated by an international annual ASME award on thermodynamics research, wished that had not been the case. This is particularly true since having an absolute scale of enthalpy is more convenient than having these different tables. This appendix presents the foundation of a proposed thermodynamics law that enables enthalpy to be evaluated from its fundamental definition. It shows that the enthalpy of a monatomic gaseous pure substance as well as of ideal gases in complete thermodynamic equilibrium becomes zero at the absolute zero of temperature. This conclusion has been validated analytically through Van der Waals' equation of state and experimentally through experimental measurements. This conclusion can help transform the tables of thermodynamic data defining absolute zero on the enthalpy scale so that replacing the column of enthalpy of formation H_{fo} with a column of absolute enthalpy H_o .

The infinitesimal internal energy of a system can be formulated based on the principle of the Second Law of Thermodynamics for any reversible non-flow process as follows (Obert, 1973):

$$du = T ds - \delta w \quad (\text{G.I})$$

The internal energy of a system can be as well formulated differentially based on the principle of the First Law of Thermodynamics for any flow process as well as for any non-flow process following from equation (3.42) as follows (Obert, 1973):

$$du = dh - dw \quad (\text{G.II})$$

Thus, following from the fundamental definition of work and from equations (G.I) and (G.II) the enthalpy of substances can now be infinitesimally evaluated as follows:

$$dh = T ds + v dP \quad (\text{G.III})$$

In an endeavour to investigate how temperature can affect the enthalpy of pure substances in gaseous phase, let us recall Van der Waals' equation of state that is valid for all gases (Whitten et al., 2004):

$$p = \frac{n_{mol} RT}{v - n_{mol} b_{VW}} - \frac{n_{mol}^2 a_{VW}}{v^2} \quad (\text{G.IV})$$

The Van der Waal's equation of state is explained by the Kinetic Theory of Gases according to which the molecules in a gas are in the state of rapid random motion colliding each other (Singh, 2007); But under complete thermodynamic equilibrium the intermolecular forces vanish for a monatomic molecule and for a diatomic molecule, in case a molecule rather than an atom is the most stable form of the substance considered. This is particularly true since under complete thermodynamic equilibrium the attraction equalizes repulsion in the diatomic molecule due to the fact that the size of these atoms is the same. Thus, the term that represents the attraction/repulsion forces between atoms and that includes Van der Waal's constant " a_{vw} " vanishes under complete thermodynamic equilibrium at least for ideal gases and for real gaseous monatomic pure substances. This should not be surprising in light of the fact that the value of the Van der Waal's constant " a_{vw} " varies with pressure and temperature that are different from those at which Van der Waal's constant " a_{vw} " was originally measured. For ideal gases and monatomic gaseous pure substances in complete thermodynamic equilibrium the term that represents the attraction/repulsion forces between atoms on the right hand side of equation (G.IV) vanishes. Therefore, combining equations (G.III) and (G.IV) leads to the following:

$$h = \int_{s_{ref}}^{s_1} T ds + n_{mol} R \int_{ref}^1 v d \left(\frac{T}{v - n_{mol} b_{vw}} \right) + h_{ref} \quad (G.V)$$

The term h_{ref} indicated in equation (G.V) represents the enthalpy of formation of the element under consideration at the temperature (T_{ref}) at which the element is in its most thermodynamically stable state in reacting systems. The term " h_{ref} " thus vanishes for pure elements in complete thermodynamic equilibrium (Whitten, 2004). It is note worthy this is not an assumption in this regard but rather a fact confirmed by authorities in this research area such as (Whitten, 2004). Hence, For pure elements in complete thermodynamic equilibrium, the absolute enthalpy at the state of T_1 equals thus the enthalpy change which represents the energy required to change temperature from T_{ref} to T_1 . For isothermal reversible non-flow processes, equation (G.V) can therefore be rewritten as follows:

$$h = T \left[\int_{s_{ref}}^{s_1} ds + n_{mol} R \int_{ref}^1 v d \left(\frac{1}{v - n_{mol} b_{vw}} \right) \right] \quad (G.VI)$$

Hence, following from equation (G.VI), it is evident that the enthalpy of ideal gases and monatomic pure substances in gaseous phase undergo isothermal processes in complete thermodynamic equilibrium becomes zero at 0K. In an endeavour to further validate this conclusion, experimental validation is presented in the next section.

APPENDIX H

LIST OF SPOTTED FLAWS IN CORRESPONDING MODELS DEVELOPED IN KEY REFERENCES

No.	Reference	Page	Point of Spotted Flaw
1	[Heywood, J. (1988). <i>Internal combustion engine fundamentals</i> , McGraw Hill, New York.]	261	Missed square on the term U_2 at the right hand side of equation (6.59) on the centrifugal compressor model
2	[Heywood, J. (1988). <i>Internal combustion engine fundamentals</i> , McGraw Hill, New York.]	757	Incorrect terms in equation (14.15) on gas dynamics models: unsteady one-dimensional gas flow analysis, which is called Navier-Stokes equation
3	[Heywood, J. (1988). <i>Internal combustion engine fundamentals</i> , McGraw Hill, New York.]	758	A missed term of p/p to be included as an added term into the enclosed parenthesis in the third equation on that page on the rate of change of energy in gas dynamics models: unsteady one-dimensional gas flow analysis
4	[Heywood, J. (1988). <i>Internal combustion engine fundamentals</i> , McGraw Hill, New York.]	45	There is a missed term in the right hand side of equation (2.11) on the relation between piston speed and the geometrical properties of the reciprocating internal combustion engines
5	[Taylor, C.F. (1985). <i>The internal-combustion engine in theory and practice</i> , The MIT Press.]	363	In equation (10-3) on the modelling of ideal compressors, i.e. based on reversible processes, p_2 has to be p_{2s} (i.e. isentropic pressure) in order to differentiate it from p_2 (i.e. pressure in a real process)

APPENDIX I

LIST OF PUBLICATIONS

1	Faris, W.F., Rakha, H.A., Kafafy, R.M., Idres, M. and Elmoselhy, S.A.M., "Vehicle fuel consumption and emission modelling: an in-depth literature review," Int. J. Vehicle Systems Modelling and Testing, vol. 6, nos. 3/4, pp. 318-395, 2011. (SCOPUS-indexed)
2	Faris, W.F., Rakha, H.A. and Elmoselhy, S.A.M., "Supercharged Diesel Powertrain Intake Manifold Analytical Model," Int. J. Vehicle Systems Modelling and Testing, vol. 9, no. 1, 2014. (SCOPUS-indexed)
3	Faris, W.F., Rakha, H.A. and Elmoselhy, S.A.M., "Impact of Intelligent Transportation Systems on Vehicle Fuel Consumption and Emission Modelling: An Overview," SAE Transactions: International Journal of Materials and Manufacturing, vol. 7, no. 1, SAE Paper # 12JMM-0032/2013-01-9094, 2014. (Expected to be ISI-indexed in 2014)
4	Faris, W.F., Rakha, H.A. and Elmoselhy, S.A.M., "Analytical model of diesel engines exhaust NOx emission rate," Int. J. Vehicle Systems Modelling and Testing, vol. 9, no. 3/4, 2014. (SCOPUS-indexed)
5	Elmoselhy, S.A.M., Faris, W.F., and Rakha, H.A., "Experimentally Validated Analytical Modeling of Diesel Exhaust HC Emission Rate," Journal of Mechanical Science and Technology, Forthcoming 2014. (ISI-indexed)
6	Elmoselhy, S.A.M., Faris, W.F., and Rakha, H.A., "Analytical Modelling of Diesel Powertrain Intake Manifold With Flexible Crankshaft," submitted to SAE Transactions: International Journal of Materials and Manufacturing, SAE Paper # 15JMM-0019. (Expected to be ISI-indexed in 2014)
7	Faris, W.F., Rakha, H.A. and Elmoselhy, S.A.M., "Experimentally validated analytical model of diesel engine regulated exhaust CO emission rate," submitted to SAE Transactions: International Journal of Materials and Manufacturing, SAE Paper # 15JMM-0022. (Expected to be ISI-indexed in 2014)
8	Faris, W.F., Rakha, H.A. and Elmoselhy, S.A.M., "Analytical modelling of diesel powertrain fuel system and consumption rate," SAE Transactions: International Journal of Materials and Manufacturing, SAE Paper # 13JMM-0049, 2014 (Forthcoming). (Expected to be ISI-indexed in 2014)
9	Elmoselhy, S.A.M., Faris, W.F., and Rakha, H.A., "Experimentally validated analytical modeling of supercharging diesel radial centrifugal compressors with vanes-based diffuser," submitted to the International Journal of Heavy Vehicle Systems. (ISI-indexed)
10	Elmoselhy, S.A.M., Faris, W.F., and Rakha, H.A., "Experimentally validated analytical modeling of diesel engine power and in-cylinder gas speed dynamics," submitted to Journal of Mechanical Science and Technology. (ISI-indexed)
11	Elmoselhy, S.A.M., Faris, W.F., and Rakha, H.A., "The Foundation of a proposed law of thermodynamics on the enthalpy of gaseous pure substances in thermodynamic equilibrium," submitted to journal of physics. (SCOPUS-indexed)